DYNAMIC STATE ESTIMATION BASED TRANSMISSION LINE PROTECTION

A Dissertation
Presented to
The Academic Faculty

by

Zhenyu Tan

In Partial Fulfillment
Of the Requirements for the Degree
Doctor of Philosophy in the
School of Electrical and Computer Engineering

Georgia Institute of Technology
December 2016

DYNAMIC STATE ESTIMATION BASED TRANSMISSION LINE PROTECTION

Approved by:

Dr. A.P. Meliopoulos, Advisor
School of Electrical and Computer Engineering
Georgia Institute of Technology

Dr. Fumin Zhang
School of Electrical and Computer Engineering
Georgia Institute of Technology

Dr. Ronald G. Harley
School of Electrical and Computer Engineering
Georgia Institute of Technology

Dr. Andy Sun
School of Industrial and Systems Engineering
Georgia Institute of Technology

Dr. David Taylor
School of Electrical and Computer Engineering
Georgia Institute of Technology

Date Approved: November 04, 2016

ACKNOWLEDGEMENTS

The doctoral study at Georgia Tech is a long-distance adventure. This journey would not have been accomplished without the inspiration, encouragement, and help from many people. I would like to express my heartfelt gratitude to all of them at this time.

First of all, I would like to owe my most sincere thanks to my advisor, Dr. A. P. Sakis Meliopoulos. I could not imagine having a better advisor and mentor in the pursuit of Ph.D career. It is due to his patience, motivation, inspiration, and immense knowledge that I have gained a deeper understanding of engineering and mathematics. His careful guidance on solving problems, writing reports and professional communication skills rewards my entire research life and the life afterwards. Without his illuminating instruction, consistent encouragement, and confidence in my capability, this thesis work could not be completed in the present form. I am deeply grateful for his guidance and support during my Ph. D. career.

I would also like to extend my sincere gratitude to Dr. Ronald G. Harley, Dr. Fumin Zhang, Dr. David Taylor and Dr. Andy Sun for serving as my dissertation committee and for their valuable time contribution in reviewing the drafts. Their insightful comments and suggestions have also made considerable contribution to the completion of this work.

I am also grateful to Dr. George J. Cokkinides for his valuable support and practical contributions towards completion of my work. His professional expertise in theory and instinct in practice was always excellent and admirable.

The members of the Power Systems Control and Automation Laboratory (PSCAL) have contributed generously to my personal and research time at Georgia Tech. The people

in the group are encouraging and always offer me good advice and collaboration. I would specially thank Dr. Renke Huang for his unwavering support, insightful suggestions, and kind advice. We cooperated on several research projects during our Ph. D researches, and Dr. Renke Huang generously shared with me his valuable experience and sharp insight with power system analysis experience, practical problem solving, coding skills, and report and paper writing. I would also like to thank Liangyi Sun, Rui Fan, Yu Liu, Dongbo Zhao, Wenlu Fu, and Boqi Xie for their friendship and support.

Most of all, I owe my loving thanks to my family. My parents' encouragement and support kept me focused and motivated. With their unflagging love, encouragement, and understanding, I eventually reached the final stages of this doctoral degree.

TABLE OF CONTENTS

LIST OF TABLES

LIST OF FIGURES

SUMMARY

As the guardian of power system network, protective relays are ubiquitous, assuring power system operation by reliably and selectively isolating faulty power system

components in minimum possible time. During the past three decades, the introduction of microprocessor-based relays and the advancement of communication technology has enriched both the functionality and computational capability of numerical protective relays in many folds. Yet, despite the fact that research effort in this field leads to more sophisticated protection functions that overcome many dependability and security issues brought by the protection functions that were once simple, such sophistication also introduces unpredictable human errors in setting for a single relay and coordinating an entire protection system. Meanwhile, protection gaps still exist in many ways. The two causes contribute to protective relay mis-operations that may result into system wide disturbances or even blackouts. The November 1965 blackout was initiated by a line relay mis-operation. Moreover, most sub-causes from the relay mis-operations can be associated with transmission line protection.

This thesis proposes a dynamic state estimation based protection algorithm for the transmission line to 1) eliminate complex protection settings in order to prevent human error, 2) fulfill the protection gaps caused by legacy protection functions, and as a result, reduce relay mis-operations. The dynamic model of the line is first converted into an equivalent algebraic companion form by quadratic integration (if the current transformer is also modeled then quadratization process is also needed). Then three dynamic state estimation algorithms and the protection logic based on the estimation results are introduced for the protection purpose. The proposed algorithm is compared with legacy protection functions in numerous test cases.

Chapter 1 introduces the scope, background and motivation of the problem; Chapter 2 summarizes the traditional protection algorithms, requirements, advantages and

disadvantages, as well as state of the art fault detection algorithms; Chapter 3 presents the overall approach and conceptual design of the proposed algorithm in this thesis in order to address the issues brought by traditional algorithms; Chapter 4 derives the mathematical model needed for the proposed approach; Chapter 5 describes the underlying dynamic state estimation algorithm for the mathematical model and corresponding protection logic; Chapter 6 describes the laboratory setup for demonstration; Chapter 7 presents numeral test cases against traditional methods, all cases can be demonstrated via the laboratory setup; Chapter 8 summarizes the thesis and discusses future work.

CHAPTER 1 INTRODUCTION

1.1 Problem Statement

As the guardian of power system transmission network, transmission line protective relays are ubiquitous, assuring power system operation by reliably and selectively isolating faulty power system components or regions in minimum possible time. During the past three decades, the introduction of microprocessor-based relays and the advancement of communication technology has enriched both the functionality and computational capability of numerical transmission line protective relays in many folds. Yet, despite the fact that research effort in this field leads to more sophisticated protection functions that overcome many dependability and security issues brought by the line protection functions that were once simple, 1) such sophistication also complicates the commissioning process and introduces unpredictable human errors in setting a single relay and coordinating an entire transmission network protection system. Improper settings and coordination of protective relays comes from the fact that traditional line protection schemes are based on limited information, i.e., they monitor limited number of quantities (for example just three voltages and three currents of the transmission line) and act when the quantities enter a pre-specified locus (settings). While present day line protection engineers have many analytical tools, settings and coordination rely heavily on engineer's experiences. The coordinated settings exhibit limitations for two reasons: (a) limited relay information and (b) there are typically competing factors. An example is the stepped distance protection for a long transmission line with series compensated capacitor. The distance element has no information on the status of the capacitor, so once the capacitor is put into service, the

distance protection would overreach the line if settings are not correctly adjusted according to the status of the capacitor. 2) Meanwhile, protection gaps still exist in line protection in many ways. The two causes contribute to transmission line protective relay mis-operations that may result into 1) system wide disturbances or 2) even blackouts.

In 2012, North American Electric Reliability Corporation (NERC) outlined a preliminary set of high priority reliability issues, ranking relay mis-operations as top priority concern [1]. As a result, Protection System Mis-operations Task Force (PSMTF) was formed to investigate system disturbances caused by relay mis-operations. Of 1500 mis-operation records analyzed, 28% were categorized as incorrect setting/logic/design errors [2]. Specific causes associated with transmission line protection include improper zone timers and time overcurrent coordination, overreaching zone 1, instantaneous overcurrent elements, improper coordination of directional comparison blocking trip and block elements, improper modeling, and others. 20% of the 1500 mis-operations were due to relay failures (calibration issue, internal failure, firmware issue, and so on), 17% were due to communication failures, 12% unexplainable, 9% personnel error (wrong wiring), 8% AC system error (failures that include instrument transformer failure and VT or CT secondary circuit failures), 5% DC system error (failures to a station's dc system such as station battery), 1% others.

The November 9, 1965 Blackout, which occurred in the Northeastern United States and Ontario, originated from a relay mis-operation. The event began when 230 kV transmission lines from a hydro generating facility were heavily loaded due to high power transfer from the hydro facility to a major load center which was hit by a cold weather while coupled with outage of a nearby steam plant. The zone 3 backup relay were set at a

power level well below the capacity of the line to detect the fault beyond the next switching point from the generating plant. From the time the relays were initially set, the settings remained unchanged while the loads on the lines steadily increased. Under the heavy load circumstance, the plant operator attempted to increase the power transfer on one of the 230 kV lines in order to support the major load center, without awareness of the relay limitation. As a result, the load impedance entered the zone 3 operating characteristics and the relay tripped the circuit breaker. Consequently, the load on the tripped line redistributed to the rest of the five lines. As a result, each line breaker was tripped within 2.7 seconds. With all lines tripped, the hydro generators were disconnected from the loads and started accelerating. This resulting drop in generation at the hydro plant and the rapid build-up of generation in the interconnected system resulted in large power swings that resulted in a loss of synchronism between two portions of the system. The massive outage lasted a few days in some area and directly affected 30 million people [3].

The problem associated with transmission line relay mis-operation stems from 1) the complexity of protective relay setting. The relay engineers have to manage 100-150 protective relays in a modern substation, 2) the natural disadvantages of the traditional protection functions. The directional elements are vulnerable with close faults, the overcurrent element under-reaches the full transmission line (or overreaches), the stepped distance element does not work well with series compensation, the current differential has to increase its security during CT saturation, etc.

1.2 Research Objectives

The dissertation objectives are: 1) to avoid setting and coordination errors, and 2) to fulfill numerous protection gaps. An approach is proposed that does not require coordination and simplify the settings, and that demonstrates better dependability, security, and sensitivity in simulation environment. Towards this goal, the proposed approach is to exploit dynamic state estimation that monitor the operating condition of a protection zone and use this information to protect the zone. Specifically, the mathematical model of any protection zone is first expressed in object oriented format by quadratizing the differential algebraic equations of the zone (if the model has nonlinear order higher than two), and performing quadratic integration over the differential equations. Secondly dynamic state estimation algorithms for the object oriented model are described, and probability of whether the measurements match the model, i.e., confidence level, is developed over the estimation results. The protection logic examines the average of the confidence level over an integration window and issues a tripping command if the average drops below a certain threshold. Compared with legacy protection functions, this proposed approach requires no coordination, and the only settings are the integration window size and confidence level threshold. 3) to propose an infrastructure of data acquisition module and data processing module for the proposed transmission line protective relay that takes advantage of the prototype IEC 61850 compliant sensor, and implement laboratory setup for demonstration. 4) to investigate the performance of the DSE based protection in numerous test cases, 5) to investigate several practical issues (such as modeling error) for the DSE based protection.

1.3 Thesis Outline

The outline of the remaining parts of this dissertation is as follows.

In Chapter 2, background information is provided on the origin of the transmission line protection topic along with presently available technologies that are being used. In addition, a thorough literature survey is presented that summarizes related research work efforts. In particular, the survey starts with a summary of the current line protection functions. The presently utilized technology for line protection along with its limitations are presented. Synchronizing technology (GPS and IRIG-B) and how it can be utilized for the development of modern protection functions is also presented. Next the state-of-art fault detection, identification technology for general engineering systems is summarized.

Chapter 3 presents the overall approach and the conceptual design of the infrastructure of data acquisition systems, which provides the necessary information for an automated transmission line protective relay.

Chapter 4 presents the general and detailed methodology for the derivation of an object-oriented, interoperable, and unified model for components in the power system. The model is named as the state and control algebraic quadratic companion form (SCAQCF). Transmission lines as an example for how to derive the SCAQCF model from the original differential and algebraic equations of the component is also given. Both single and multi-section models are included.

Chapter 5 presents in detail the mathematical formulation and the solution methodology of the developed dynamic state estimator. The mathematical model and the categorization of the DSE measurements are also presented. The DSE solution algorithm and performance evaluation follow.

Chapter 6 discusses the detailed implementation for the proposed line protective relay in laboratory environment, including the infrastructure of data acquisition system that take advantage of the merging unit technology, the communication workflow between the proposed line protective relay and the IEC 61850 compliant sensors (merging units), the new human machine interface for relay settings, and the laboratory setup for numerical experiments.

Chapter 7 presents numerous test cases in evaluating the performance of the proposed approach in metrics of dependability, security and sensitivity with current state-of-art protection functions, and also investigates several practical issues including CT/PT error.

Finally, Chapter 8 summarizes the research work and outlines the results and contributions of this dissertation.

CHAPTER 2 LITERATURE REVIEW

2.1 Overview

This chapter provides the background information of existing technologies related to the proposed research along with a literature review of the research efforts on these topics. Section 2.2 starts with the evolution and a summary of the technologies for protective relays and the current architecture of a modern relay. Section 2.3 then summarizes the currently utilized technology in transmission line protection functions in the modern architecture. Lastly Section 2.4 provides a literature review on the state-of-the-art fault detection, identification (diagnosis) algorithms utilized for general engineering systems from a broader context that treats the power system as a specific example.

2.2 The Evolution of Protective Relays

Originally electromechanical relays were used to protect power systems. Most relays used either electromagnetic attraction or electromagnetic induction principle for their operation. Plunger type relays formed instantaneous units for detecting overcurrent or over-voltage conditions. Balanced-beam relays provided differential protection, distance protection as well as low burden overcurrent units. These relays operated when the magnitude of an operating signal was larger than the magnitude of the restraining signal. These relays were classified as amplitude comparators. Single input induction type relays provided operations with time delays – such as induction disk from Westinghouse and induction cup from GE. Two input induction type relays provided directional protection. The operation of these relays depended on the phase displacement between the applied electrical inputs. These relays were classified as phase comparators.

The invention of the transistor in the late 1940s and the subsequent advancement of solid state technology in the early 1960s made it possible to replace bulky electromechanical relays with solid state relays. The major advantage of these relays was that no moving parts were needed for performing their intended functions. The operating speeds of these relays were also more than the speed of their electro-mechanical counterparts and, their reset times were less than the reset times of their electromechanical counterparts [4].

Solid-state relays appeared to be the technology poised to replace the electromechanical counterparts in late 1960s when researchers ventured into the use of computers for power system protection. The first computer relay was developed in 1970 with a trial implementation in a substation in California. Later the attempts and the advances in the Very Large Scale Integrated technology and software techniques in the 1970s led to the development of microprocessor-based relays (numerical relays) that were first offered as commercial devices in 1979. Early designs use the fundamental approaches that were previously used in the electromechanical relays. In spite of the developments of complex algorithms for implementing protection functions, the numerical relays in those days did not incorporate them. The major advantage is that it allows multiple protection functions in a very small package (space) and at a low cost (economy). Specifically, the protection of a transmission line required several single function electromechanical relays taking several racks in a substation control house. Now the entire set of microprocessor-based relays is typically housed in a 19 inch by 8 inch device. Meanwhile electromechanical relays had no significant drawbacks in their protection functions, but the additional features offered by the microprocessor technologies encouraged the evolution

of relays that introduced many changes to the industry. These features include 1) customized logic schemes, 2) much less burden on instrument transformers than the burden placed by the relays of the previous technologies, 3) microprocessor-based relays can be programmed to detect saturation of instrument transformers for minimizing incorrect operations, 4) fewer instrument transformer connections as some quantities such as zero sequence can be internally computed, 5) sequence of events and oscillography, 6) self-monitoring and self-testing, and 7) numerical relays are equipped with communication ports and allow engineers to access the relay from the comfort of their office, review settings, enter new settings, etc. At the same time, several trends are emerging. These include common hardware platforms, configuring the software to perform different functions, integrating protection with substation control, and substituting cables carrying voltages and currents with fiber optic lines carrying signals in the form of polarized light.

The evolution of microprocessor-based protection systems has not been without its challenges. The industry has, however, come to the conclusion that the benefits far outweigh the shortcomings. This has gradually increased the acceptance of numerical relays during the previous twenty years. The current architecture for a modern relay is a device containing a central processing unit (CPU) that handles multiple types of input and output signals, see Figure 2.1. The voltage and current transformers reduced the level of voltage and current signals typically to 67 V and 5 A nominal value respectively. The outputs of instrument transformers are applied to the analog input subsystem of the relay. This subsystem electrically isolates the relay from the power system. The analog inputs are applied to analog filters, amplifiers, sample and hold, multiplexers and analog-to-digital converters.

A relaying algorithm, which is a part of the software, processes the acquired information. The algorithm uses signal-processing techniques to estimate the magnitudes and angles of voltages and current phasors, and also frequency. These measurements are used to calculate other quantities, such as impedances. The computed quantities are then compared with pre-specified threshold (settings) to decide whether the power system is experiencing a fault/abnormal operating condition or not. If it is, the relay sends a command to open one or more circuit breakers for isolating the minimum faulted zone of the power system. The trip output is transmitted to the circuit breaker through the digital output subsystem by energizing the trip coil.

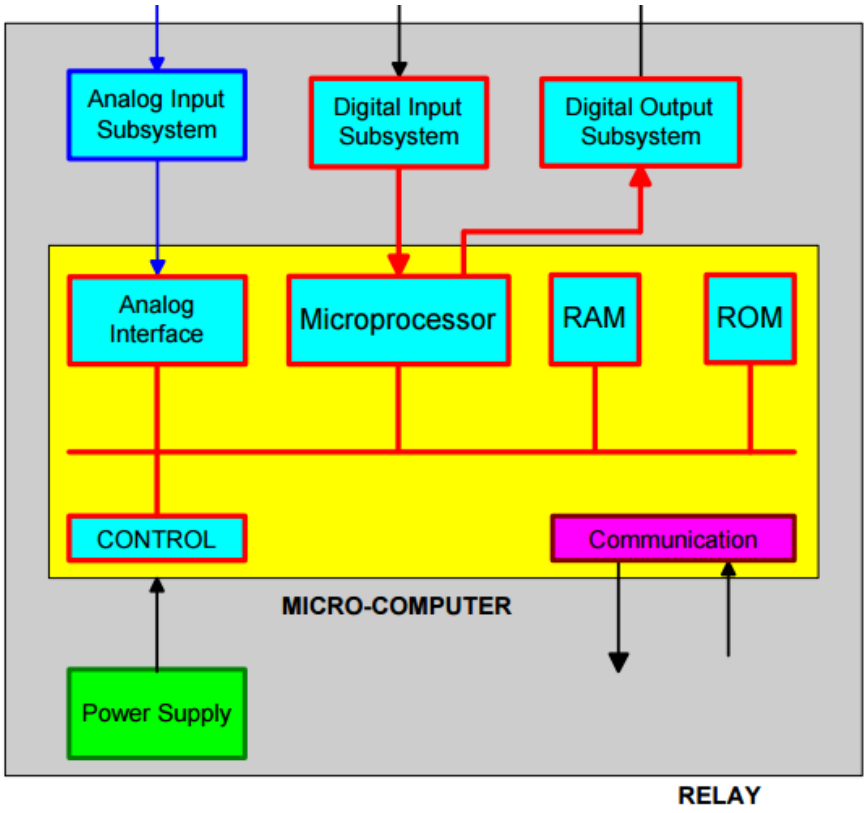

Figure 2-1 Modern Relay Architecture [4]

2.3 Survey of Legacy Protection Functions

A transmission line is mainly protected by the following protection functions in a multi-function relay: (1) directional instantaneous overcurrent (2) directional time overcurrent, (3) stepped distance, (4) pilot scheme, and (5) current differential. These functions are reviewed next. As an example, see the General Electric L90 current differential protection system in Figure 2.2 [5], both the instantaneous overcurrent (50P/50G) and time overcurrent (51P/51G) are supervised by directional element (67P), and distance protection (21P), phase segregated current differential (87L/87LG), and pilot scheme via dedicated communication in the assistance of distance element. For full line protection, all these functions are applied as in a multi-function numerical relay and it is expected that at least one will trip the line for any fault that may occur in the line and will not operate for any faults outside the line. While this is true for the majority of faults, it is also true that there are fault events on the line that these schemes may miss, see Chapter 7 where none of the legacy methods detect the high impedance fault, or they may trip the line for some faults outside the protected line (mis-operations), see Chapter 7 where directional time overcurrent, distance and pilot elements may trip for external fault.

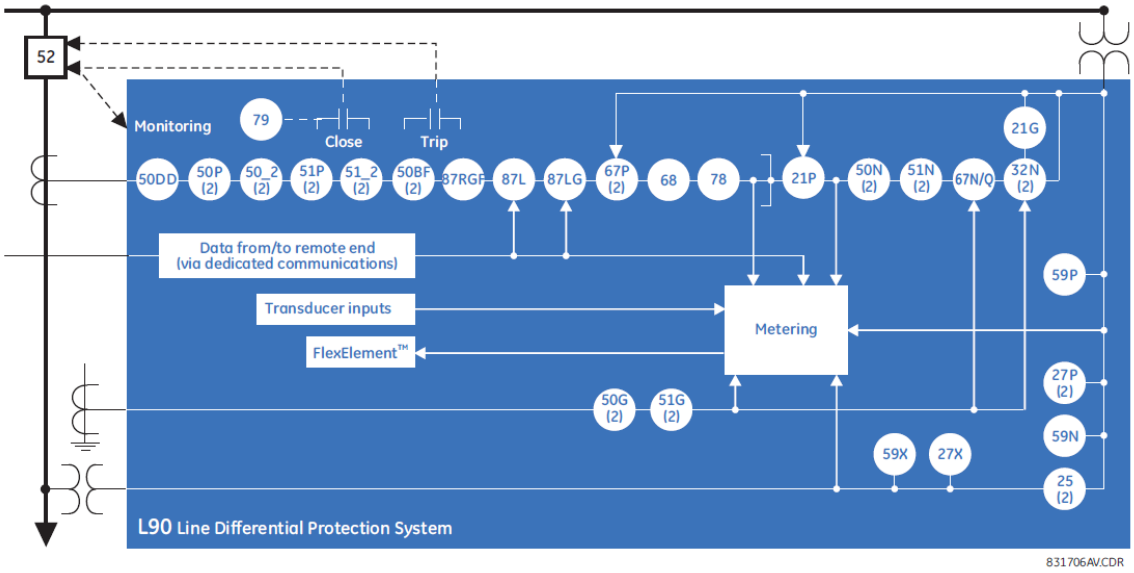

Figure 2-2 General Electric L90 Current Differential Protection System [5]

2.3.1 Directional Instantaneous Overcurrent Protection

The directional instantaneous overcurrent relay, one of the first and simplest protective relays, developed around 60-70 years ago, is still used in transmission line protection [6]. The relay monitors the electric current in the secondary of the current transformer and when this current exceeds a threshold and the direction of the fault is forward, relay bit is activated which eventually may operate a contact that is integrated with the tripping system of a breaker.

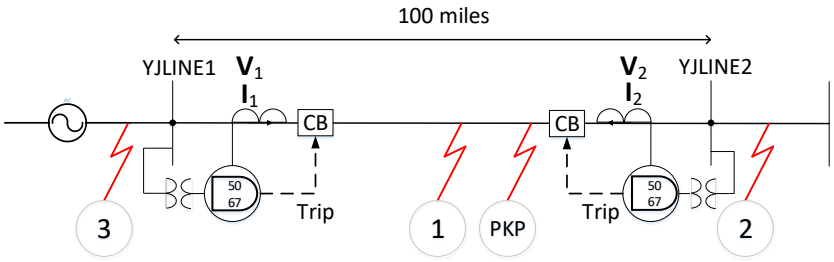

Figure 2-3 Directional Instantaneous Overcurrent Line Protection

For transmission lines where loop system is dominant, a directional element indicating whether the fault direction is forward or reverse to the tripping zone is necessary to supervise the overcurrent element (and also distance element). There are several ways to design the directional element [7]-[8]. 1) Directional element responds to the phase shift between a polarizing quantity and an operate quantity. For forward faults, the measured current lags the measured voltage by the fault loop impedance angle, for reverse faults the measured current leads the measured voltage by 180 degrees minus the fault loop impedance angle. The options for selecting polarizing and operating signals vary and include voltage or current signals (Va, Ia), phase pairs (Vab, Iab), or symmetrical components (V1, I1). Before numerical relays, the operating quantity and polarizing quantity are applied to induction cup electromechanical relays via two individual windings. The relay was designed such that no rotational movement or torque occurred when the magnetic fluxes of the two coils were in phase (zero torque angle), and maximum torque when they were certain degrees apart (maximum torque angle). Usually negative or zero sequence quantities are preferred over quadrature quantities as Warrington first identified a security weakness of the quadrature-polarized phase directional element. When the source behind the relay is strong, the voltage measured at the relay location for a remote fault can be too small to overcome the minimum torque requirement of a torque-product directional element, thus 2) rather than the product, another approach to use the ratio of negative sequence voltage and current, or negative sequence impedance was used. For a fault in front of the relay, the measured negative sequence impedance equals minus source impedance behind the relay, for a fault behind the relay, the measured impedance equals

the line impedance plus the remote source impedance. Thus by comparing the measured value with thresholds, this element also yields the fault direction.

While this function is very simple, the disadvantages stem from the fact that the pickup setting must have sufficient margin (under reach the full length of line) to avoid operation for external fault [9]: 1) for a short transmission line the fault current level (for both phase and ground element) at local end and remote end can be approximately the same, thus it is difficult to set a pickup value to differentiate internal and external fault. 2) the appropriate setting for both phase and ground element is affected by variations in system conditions (source impedance), and it's difficult to obtain adaptive settings based on system conditions. For transmission lines, if the number of generating units on line changes due to maintenance outage, the source impedance varies as well as the fault current level. Several other protection challenges exist for ground element, 1) the mutual coupling from a parallel line can result in incorrect direction determination as well as increased or reduced sensitivity [9], 2) single phase tripping on remote end, adjacent lines or mutually coupled lines can result in zero sequence current that cause a false trip [10]-[11], 3) weak source (when strong source out of service) may contribute relatively low current magnitude undetected by overcurrent element [12].

2.3.2 Directional Time Overcurrent Protection

Different from directional instantaneous overcurrent element, the directional time overcurrent element trips the line after a time delay. It extends the protection coverage (overreach the full length of line) of the directional instantaneous overcurrent element by coordinating with the protection functions at the remote bus on the basis of operating time.

For any external fault the operating time of remote relay is set less than the operating time of local directional time overcurrent element so that the fault is cleared before the local relay operates.

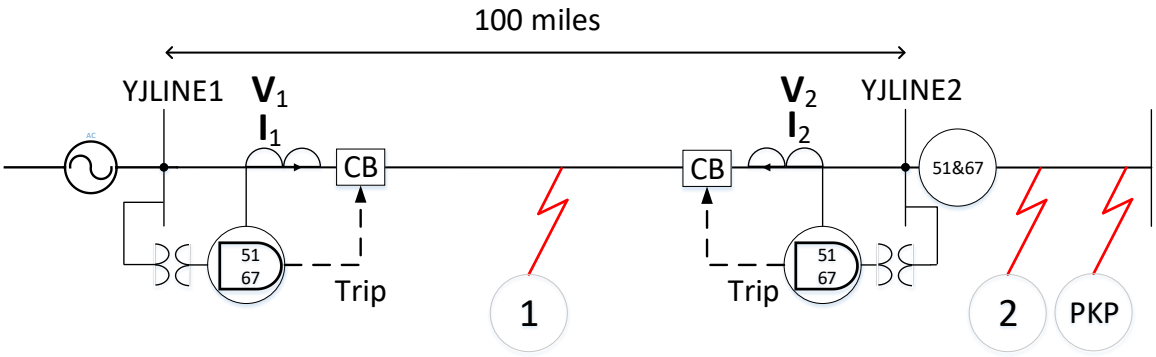

Figure 2-4 Directional Time Overcurrent Line Protection

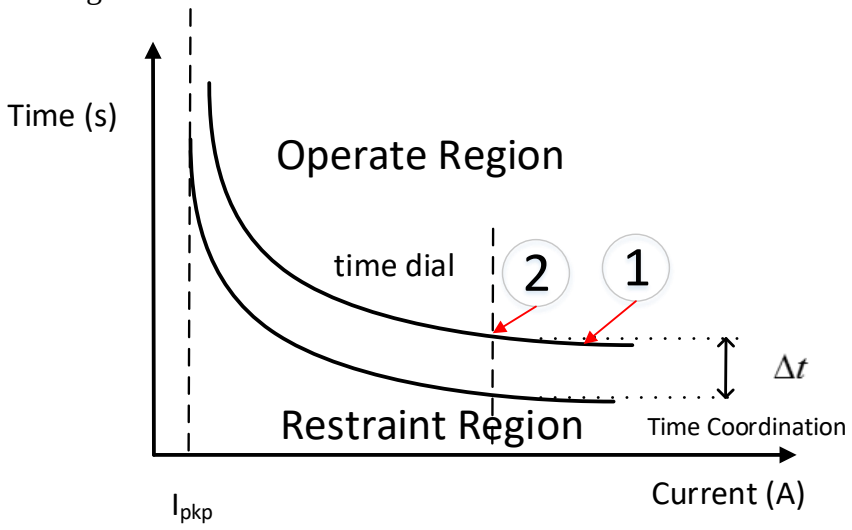

Figure 2-5 Directional Time Overcurrent Characteristic

However the disadvantages still stem from the setting and coordination: 1) for long transmission lines, as the relay reaches further into the remote end, the closer the fault current magnitude approaches maximum load current, thus it is difficult to set a pickup value to differentiate fault and heavy load for phase element [9], and the closer the fault

current magnitude approaches maximum unbalanced load, thus it is difficult to set a pickup value to differentiate fault and heavy load with non-transposed line for ground element. 2) if the remote bus has a load, then the current measured at local relay would be higher than that of remote relay, making it extremely difficult to coordinate. 3) variations in system operating conditions can affect both the settings and coordination.

2.3.3 Stepped Distance Protection

The major advantage of distance relays compared to direction IOC/TOC relays is its ability to operate for fault currents near or less than maximum load current and relative immune to system operating conditions and fault current levels. Distance relays track the apparent impedance looking into a transmission line, and operate when the impedance enters a pre-specified locus. A standardized distance relay is designed such that when a fault occurs, the apparent impedance is approximately equal to the positive sequence impedance of the circuit per unit length times the distance to the fault. The most classical electromechanical relay being balanced beam type where the operating region is a circle on the R-X diagram, and microprocessor based relays either mimic the behavior, or better shape the operating region, such as Mho, lenticular, quadrilateral shapes that are implemented by major manufacturers (ABB [13], SEL [14], and GE [15]). Six elements are needed for phase-phase faults and phase-ground faults. For typical step distance protection practices, three zones are usually used. Zone 1 covers 80% of the line (the apparent impedance reach is set as 80% of the positive sequence impedance of the total line) so that transients and CT/PT errors would not overreach the protected zone. There is no intentional delay for the trip logic so that zone 1 uses instantaneous tripping. Zone 2 covers 125% of the line and 20 cycles of delay is used to coordinate with other fast tripping

relays. Zone 3 is set to reach 100% of the line plus 150% of the next line with 30 cycles delay.

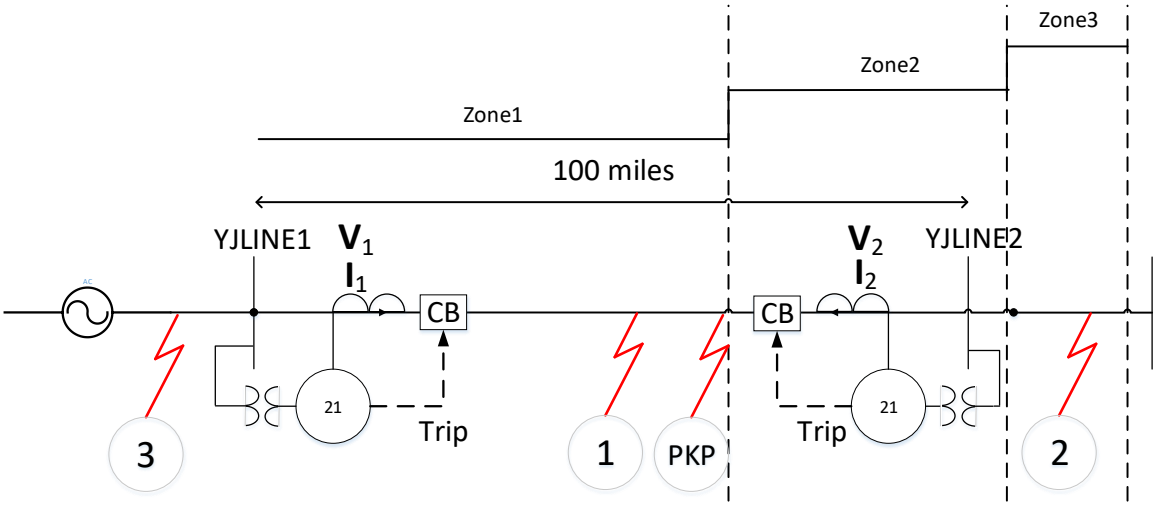

Figure 2-6 Stepped Distance Line Protection

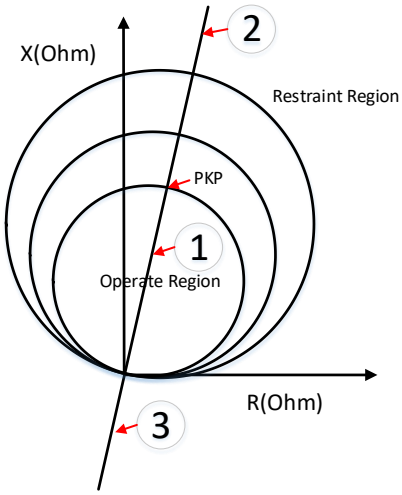

Figure 2-7 Stepped Distance Protection Operating Characteristic

The disadvantages of distance relays are that 1) it's likely that for an internal fault the relays at the two ends see the impedance in different zones and thus will not trip simultaneously, 2) for close-in faults where the voltage is very small, a self-polarized mho function may operate incorrectly, and for a three phase fault even cross-polarized functions

will be jeopardized [16]. Currently major manufacturers use memorized voltage for this issue. 3) it's difficult to apply this function to long transmission lines where series capacitor compensation is used, since a) faults in close vicinity of series capacitor where the reactance from relay to the fault is capacitive can create voltage and current inversion that lead to false direction discrimination, b) the series capacitor modifies the line impedance that the relay measures and it's likely to make mho element overreach, c) the subharmonic-frequency oscillations cause the impedance estimation to oscillate [17]. Other practical issues include a) load encroachment where a heavy load with low power factor may encroach zone 3 element, a load encroachment logic is usually implemented by further shaping the operating region [13]-[15], b) mutual coupling induces voltages on the faulted and unfaulted lines zero sequence network and may alter the relay reach on ground elements—if the currents in both lines are in same direction the ground distance element would under reach, if the currents are in opposite direction the ground distance element would overreach. The first solution is to modify the compensation factor that consider mutual coupling effect, however the factor should be different values when the coupled healthy line is either in service, out of service but not grounded, and out of service but grounded [18]. Another solution is to use the zero-sequence current from the coupled line, however the current information may not be available when the coupled line is out of service [18]. c) tapped lines that are common in sub-transmission lines due to economic reasons provide in-feed current that would under reach, or out-feed current that would overreach when source of generation or grounded neutral wye-delta transformer exist behind the tap [19]. d) fault resistance introduces an error in the distance estimation, and a popular solution is to use quadrilateral tripping zone to obtain a better fault resistance

coverage and arc compensation [20], however the fault resistance coverage is limited by the maximum line loading, which may cause relay misoperation for faults with high-fault resistance value [21]. e) during power swings the measured positive sequence impedance trajectory may traverse the operating region of a distance element and cause a misoperation. Traditional power swing blocking logic uses dual-blinder characteristics that measures the time it takes for the positive sequence impedance to cross the outer and inner blinders, or concentric dual-quadrilateral characteristics [22], however long and heavily loaded line make it difficult to set the blinders.

2.3.4 Pilot Protection

Neither directional instantaneous overcurrent, directional time overcurrent nor distance relay provides the possibilities of high-speed simultaneous clearing of the fault at the two ends of transmission line protected zone. They require zone 2 coordination for 100% cover of the protected zone. Pilot relaying are introduced for such purpose. It is an alternative to differential protection for which the limited or processed information at the remote terminal are brought to the local relay by a communication channel, and comparison is made with local information. By information compared, pilot schemes can be categorized into 1) directional (power flow) comparison type as most widely used [22], 2) unit type by using current information only. Direction comparison systems compare the direction of fault current flow at the two line terminals, and declare internal fault if there is no agreement in flow direction between the line terminals. By tripping logic, pilot schemes can be categorized into 1) blocking mode, 2) tripping mode. A blocking mode is one in which the presence of a transmitted signal prevents tripping of a circuit breaker and a tripping mode is one in which the signal initiates tripping a circuit breaker. The

communication media includes 1) pilot wires for 50 or 60 Hz transmission, typically a 15kV twisted pair of telephone cables, AWG#19 and appropriated shielded. The problems experienced is induction from lightning or parallel power circuit [6]. 2) audio frequency tones (telephone line) in the range of 1000-3000 Hz from leased telephone facilities, 3) power line carrier, where radio frequencies between 30 and 300 kHz were superimposed on the power lines. The line tuner cancels the coupling capacitance and provides a low-impedance path for efficient transfer of RF signals to and from the other terminal. PLC were originally used in an on-off mode and as time progressed frequency-shift mode became available. In the United States phase-to-ground coupling is most commonly used. 4) microwave in the range of 150 MHz and 20 GHz, and 5) digital channel usually in optic fiber that's becoming the communication link of choice.

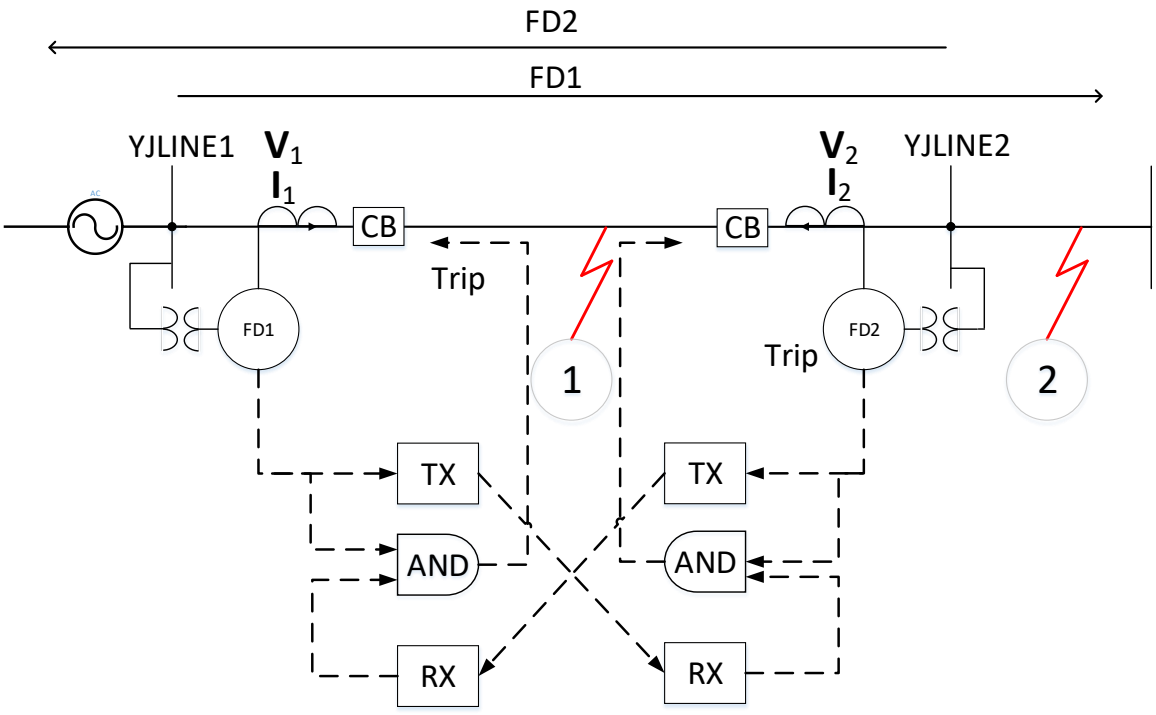

Figure 2-8 Permissive Overreaching Transfer Trip Line Protection

Traditionally, pilot schemes were designed to operate over a specific media. It is illustrated in the following.

Directional Comparison Blocking by power line carrier in on/off mode – is the most widely used pilot scheme [23], the main reason being the low communication channel requirements. The relays at two terminals compare the direction of the power flow, and the blocking signal is transmitted only when a fault occurs in reverse direction at one terminal. DCB favors dependability over security because it does not depend on channel for tripping for internal fault, but it risks overtripping for external faults when block signal is delayed or lost. Another disadvantage is that the communication channel is normally off so periodic checking is required.

Directional Comparison Unblocking was developed when power line carrier on frequency-shift mode became available. Relays at both terminals only key the transmitters to unblocking mode (or transfer tripping) when forward fault is 'seen', or otherwise stay at blocking mode (or guard). It resolves the security issue from DCB scheme because a monitoring signal is continuously sent over the channel during normal operation, so relays at both terminals would be locked out if channel is lost [6]. Another advantage is that if the unblocking signal is delayed during internal fault, the relay can still trip. The disadvantage being it requires a duplex communications channel.

A tripping scheme is a viable option when communication channel is independent of the power line, such as audio tones and microwave. Permissive schemes are inherently more secure but less dependable than blocking schemes. Direct Underreach Transfer Trip scheme is the simplest application of tripping scheme. During normal operation guard signal is transmitted, and the relay at each terminal will directly trip when it 'sees' a

forward fault (and sends trip signal to the other end), or will trip upon arrival of trip signal from the other end. Such system is not in general use because of the very high security requirements of the channels, as any transient or spurious operation of the receiver will result in incorrect operation [6]. As a consequence, an overreaching fault detector is added to supervise the channel to provide more security, as known as the Permissive Underreach Transfer Trip scheme. Both underreach schemes share a common disadvantage such that when the remote terminal is open, or has weak infeed, then the local terminal is not able to protect the full line.

Permissive Overreach Transfer Trip uses overreach fault detectors. Similar to DCUB, relays at both terminals only key the transmitters to transfer trip mode when forward fault is 'seen', or otherwise stay at guard mode. It would trip only if both fault detector is asserted and trip signal is received. The only difference is DCUB also has logic when both guard and trip signal are not received, i.e. channel lost that deals specifically with PLC.

The inherent disadvantage for overreach fault detectors in POTT, DCB and DCUB is current reversal that result in a sequential trip operation [6]. A typical solution by manufacturers (ABB [13]) is current reversal logic where a reverse element (zone 3) is used to detect when the fault is initially seen behind the relay, and a dropout delay prevents the relay from keying permission upon a transition from reverse to forward [24]. The inherent disadvantage for pilot schemes except DCB is weak-infeed source when the relay at the weak source terminal will not operate due to insufficient energy until the breaker at the other terminal opens, and also open terminal scenario. A typical solution by manufacturers (ABB [13]) is weak-end infeed logic that echo back the received signal when no fault is 'seen' in both forward and reverse direction. Lastly, all directional

comparison schemes require voltage information, that may subject to loss of voltage for close-in fault, blown fuses, ferroresonance problems in voltage transformers, and transient response problems associated with capacitive-coupled voltage transformers [25].

2.3.5 Line Differential Protection

Compared to pilot schemes, unit type protection uses current information only and does not rely on voltage information to decide directionality [26]. Phase comparison scheme was mostly used for short lines. PC can be implemented on both pilot wires where analog information is transmitted, or on audio tones where digital information is transmitted. PC compares the phase angle of local current and remote current, where in-phase represents load flow or through fault, and out-of-phase represents internal fault. For pilot wires, it transmits an analog signal that is a mix of sequence current to save channel capacity [27], the restraint coil carries the local current and tends to prevent relay trip, while the operating coil carries the differential current and tends to produce relay operation. For audio tones, it transmits only two of states: either the sending waveform is in positive half cycle, or in negative half cycle. The relay coincides the local states with remote states. With increased communication capacity, segregated phase comparison and dual phase comparison are also available. Other schemes include charge comparison [28] and wave comparison. The advantage is that they do not require synchronization of individual relays. However, the disadvantage is that channel delay has to be precisely compensated.

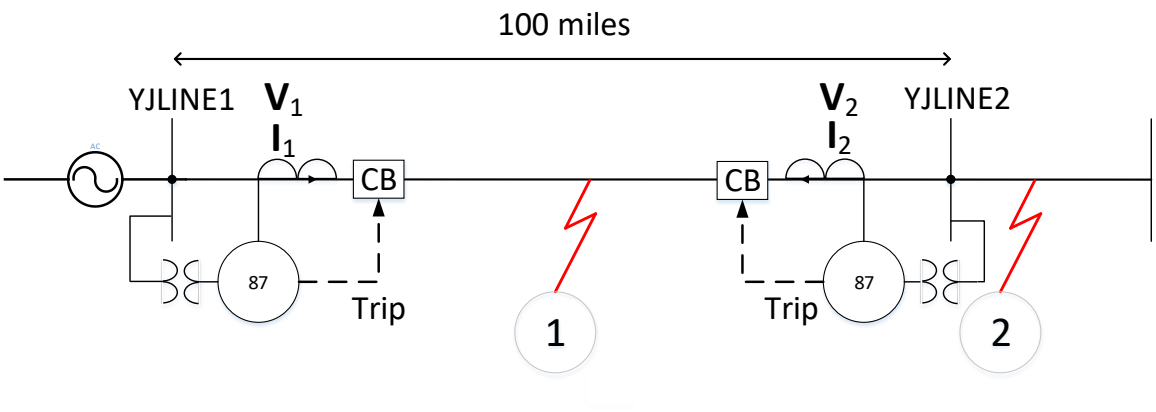

Figure 2-9 Current Differential Line Protection

The true current differential protection scheme compares both magnitude and phase. Here all the electric current quantities entering and leaving the protected zone are compared by the protection function. If the net current between all the various circuits is zero, it is assumed no internal fault exists, otherwise the associated relays would be operated [6]. Specifically, two major types of algorithms (with various forms) are implemented by major vendors. The first type works with operating/restraint current and the trip characteristic is a dual slope line, the restraint region is under the line while the operating region is above the line Figure **2-10**. The operating current is defined as the net current entering the protection zone from all terminals for each phase. Ideally the operating current is zero except internal fault. However, it may also be generated during external fault conditions due to CT saturation. To provide stability for through fault conditions, the restraint current is used to distinguish between fault currents and measurement errors in current transformers. The first variation of restraint current is defined as the measured phase current of the largest magnitude in any line end [29] by ABB, and the second variation is defined as the average of measured current at each line end [30] by Alstom. Both variations

would trigger trip element if the operating condition falls into the operating region. However, this algorithm does not reflect the magnitude error (from CT saturation) and phase error (from CT saturation, channel asymmetry) respectively. The second type works with complex ratio of remote/local current on alpha plane [31] by SEL. If the vector ratio falls outside the restraint region and the differential current exceeds a threshold, the relay operates. The setting of radius reflects the magnitude error and the setting of angle reflects the phase error. Both algorithms are implemented on segregated phase elements (Alstom [30]), while some vendors also implement sequence elements to allow phase element to be set more sensitive (above load) for multi-phase faults. Specifically, GE [5] and Siemens [32] implements zero sequence element, ABB [29] implements negative sequence element, while SEL [31] do both.

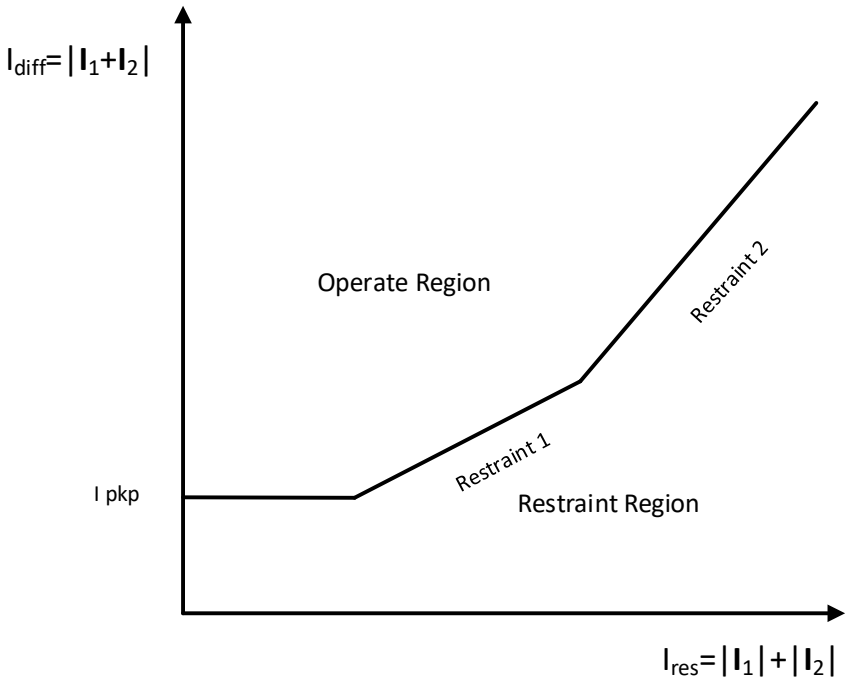

(a)

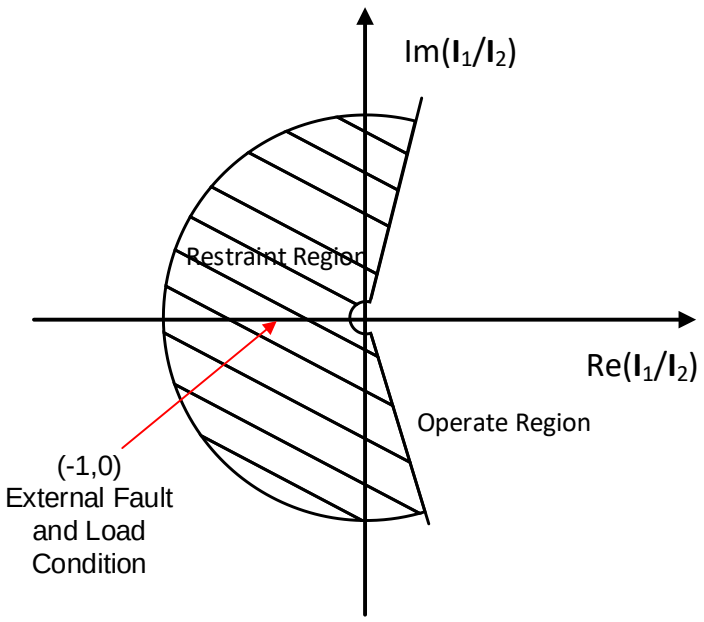

(b)

Figure 2-10 Two Popular Current Differential Algorithms (a) dual slope (b) alpha plane [29]-[31]

Differential protection is advantageous such that it doesn't require coordination between relays, it's also superior to other protection functions in terms of selectivity and speed. However, from application perspective, a proper restraining technique (setting) is required to ensure security against sensitivity, i.e., the many sources of error for ultra-sensitive operating signals, such errors include CT saturation (particularly in dual breaker application where both CTs become differently saturated) and line charging current. The steady state line charging current can be compensated by using voltage information. The CT saturation effect on operating current can be counteracted by increasing restraint current dynamically on phase elements [5] ,[32]. However such restraining also reduce the sensitivity to high resistance faults which draw small fault currents that blend with load currents. A typical solution is to use sequence element to provide more sensitivity while letting phase elements to provide more security, since the sequence element can provide

infinite sensitivity for resistive ground faults. However, the sequence element is much less stable than phase element so that it has to be blocked during CT saturation, and high resistive multi-phase fault may not be picked up by any element.

Also from relay design perspective, the geographically dispersed differential element brings challenge on data synchronization and the amount of data exchanged (channels are usually limited by bandwidth for 64kbps, and therefore only limited data can be exchanged) [33]. To facilitate the line differential function, the local current data must be sent to the remote terminals, each relay that receives a full set of data from its remote peers can time align the data and perform differential trip equations. Some relays exchange samples of currents [29], [31], some relays exchange current phasors [5],[30],[32]. When exchanging current samples, the system can collect at a rate that is high enough for accurate interpolation (1kHZ), the data synchronization can be achieved by measuring the data latency between the remote and local relays and interpolating the remote current samples to align them with local current samples. Traditionally, a channel-based synchronization known as ping-pong algorithm is used to estimate clock offset between two relays working via a communications channel, the relay sample clock does not have to be synchronized, but it resamples (interpolation) based on calculated clock offset. However, clock offset can only be calculated if the channel is symmetrical, which would not be the case when dedicated channel (direct fiber) is too expensive, and multiplexed channel (SONET, SDH) is used. When exchanging current phasors, twice the bandwidth is needed for real and imaginary part of the phasor, such that exchanging rate may not be high enough for interpolation, in that case the relay sampling clocks must be synchronized. A time drift of 1 microsecond correspond to 0.02 degree, and typical requirement for time alignment is

within 1 microsecond. The typical solution to both problems is external GPS or IRIG-B synchronization.

In modern substation architecture where external synchronization is used, typically one GPS antenna/receiver is used, and intelligent electronic devices (IED) such as SEL 2407 satellite clock, can be synchronized via the GPS signal, and redistribute IRIG-B (both modulated and unmodulated) and PPS signal into other IEDs such as protective relays that needs synchronization. With the advancement of synchronization technology, a computer network based protocol, namely as Precision Time Protocol, or IEEE 1588 version 2, is also picking up the steam. It achieves the clock accuracy in the sub-microsecond (typically 500 nanoseconds) range, that describes a hierarchical master-slave architecture for clock distribution. An ordinary clock is a device with a single network connection and it acts as either source (grandmaster) clock or destination (slave) clock. A boundary clock has multiple network connections and it accurately synchronize the network segments it connected to. A transparent clock modifies the PTP messages as they pass through the device.

2.4 Survey of Fault Detection and Identification Algorithms

The process fault detection based on state estimation methods applied to a general engineering system is first described in early 1980s and summarized in [35]. Previous supervision of technical processes was restricted to checking directly measurable variables for upward or downward transgression of fixed limits or trends, similar to the five protection functions described above. Other than that, the fault detection methods can be

divided as being mainly based on the following quantities 1) non-measurable state variables, see Figure 2-11, 2) non-measurable process parameters, see Figure 2-12, by assuming that faults in the system would be reflected in a change of the parameters in the system model, an example is the slow degradation of system components, 3) non-measurable characteristic quantities. A survey on failure detection by 1) was given by Willsky [36], the problem of failure detection is concerned with the detection of abrupt changes in a system, as modeled in state space. Such abrupt changes can arise in a number of ways. For example, in aerospace applications, one is concerned with the failure of control actuators and surfaces. Such abrupt changes can manifest themselves as shifts in the control gain matrix, increased process noise, or as a bias, all categorized as actuator failure, and also there might be sensor failure. As a matter of fact, any model changes in observed system may be considered as actuator or sensor failure even though they have nothing to do with actuator or sensor. There are four failure detection methods with non-measurable state variables:

1) fault sensitive filter, where the feedback matrix H is chosen so that particular fault modes manifest themselves as residuals in a fixed direction, or in a fixed plane, which is a deterministic approach. A class of detector filters was developed by Beard [37] and Jones [38]. Consider the continuous time, time-invariant, deterministic system model

$$\dot{x}(t) = Ax(t) + Bu(t) \tag{2.1}$$

$$z(t) = Cx(t) \tag{2.2}$$

and design a filter of the system

$$\frac{d}{dt}\hat{x}(t) = A\hat{x}(t) + D(z(t) - C\hat{x}(t)) + Bu(t) \tag{2.3}$$

and the primary criterion in the choice of gain matrix D is not that (2.3) provide is good estimate of x, as it is with observers or optimal estimators, but rather that effect of certain failures is accentuated in the filter residual

$$r(t) = z(t) - C\hat{x}(t) \tag{2.4}$$

The basic idea is to choose D so that particular failure modes for the system manifest themselves as residuals which remain in a fixed direction or in a fixed plane. Suppose we wish to detect a failure of the ith actuator. If we assume the failure takes the form of a constant bias, our state equation becomes

$$\dot{x}(t) = Ax(t) + B[u(t) + ve_i] = Ax(t) + Bu(t) + vb_i \tag{2.5}$$

where e_i is the ith standard basis vector, b_i is the ith column of B. Suppose we consider the case of full state measurement, i.e., C = I, in this case we obtain a differential equation of the residual

$$\dot{r}(t) = [A - D]r(t) + vb_i \tag{2.6}$$

If we choose $D = \sigma I + A$ we obtain

$$r(t) = e^{-\sigma t} r(0) + \frac{v[1 - e^{-\sigma t}]}{\sigma} b_i \tag{2.7}$$

Thus, as the effect of the initial condition dies out, r(t) maintains a fixed direction b_i with magnitude proportional to failure size v. If we increase σ, the initial condition dies out faster, but the magnitude of the steady state value of r decreases. In his thesis, Jone [38] described a procedure in which one first chooses the structure of D for failure detection purposes and then chooses the remaining free parameters in order to minimize the estimation error covariance, although this yields a suboptimal filter design.

2) Whiteness or chi-square test of the residuals of the normal Kalman filter, in this case the noises are assumed Gaussian distributed, and so are the residuals, and the sum of

square of the normalized residuals would follow chi square distribution. A test of the chi square value is performed to test whether the hypothesis of non-fault model is rejected or not.

3) A finite bank of Kalman filters with a standard multiple hypothesis testing that the systems most likely respond to one of the assumed models with hypothesized faults included. Filters for each of the models are constructed, and the innovations from the various filters are used to compute the conditional probability that each system model is the correct one.

4) A generalized likelihood ratio test which results in a correlation of the observed residuals with the precomputed filter responses due to certain faults. It is motivated by the shortcomings of the simpler chi-squared procedure. The GLR approach, which can be applied to a wide range of actuator and sensor failures, makes an attempt to isolate different failures by using knowledge of the different effects such failures have on the system innovations. The method provides an statistically optimum decision rule for failure detection and provides useful failure identification information.

Descriptions of the last two statistical methods is given by [39]-[40].

A more recent survey paper includes all the research efforts within the latest two decades, the analytical redundancy approach can be divided into quantitative model based methods and qualitative model based methods. The qualitative methods include artificial intelligence to capture discrepancies between observed behavior and that predicted by a model. A general quantitative method includes residual generation and residual evaluation. A robust residual generation is to design a robust filter that generates residuals which are insensitive to noise and uncertainties, and at the same time sensitive to faults. Examples of

this approach are a) full-state observer based method, b) unknown input observer method, c) parity relations approach, d) optimization-based approach, e) Kalman filter based approach. Based on the fundamental works from [37], [38], detailed algorithms have been developed by White and Speyer [42], Park et al [43],[44]. The basic idea of unknown input observer approach is to generate state estimation errors which are decoupled from the unknown input disturbance, this approach was introduced by Watanabe and Himmelblau [45]. The concept of parity relation-based fault detection approach is to form residuals as the difference between the system and model outputs. These residuals are then subject to a linear transformation. The residual generation should be designed to enhance fault isolation so that they exhibit directional or structural properties in response to a particular fault. The residual generation problem can also be formulated as optimization problem, as to minimizing the sensitivity of the residuals with respect to noise or unknown disturbances, and maximizing their sensitivity with respect to faults, see survey paper [46]. The Kalman filter approach can be considered as a special case of stochastic optimization minimizing the covariance matrix using linear quadratic optimization techniques. It was first introduced in [46] to use innovations generated by Kalman filter and the faults are diagnosed by statistical testing on whiteness, mean and covariance of the residuals.

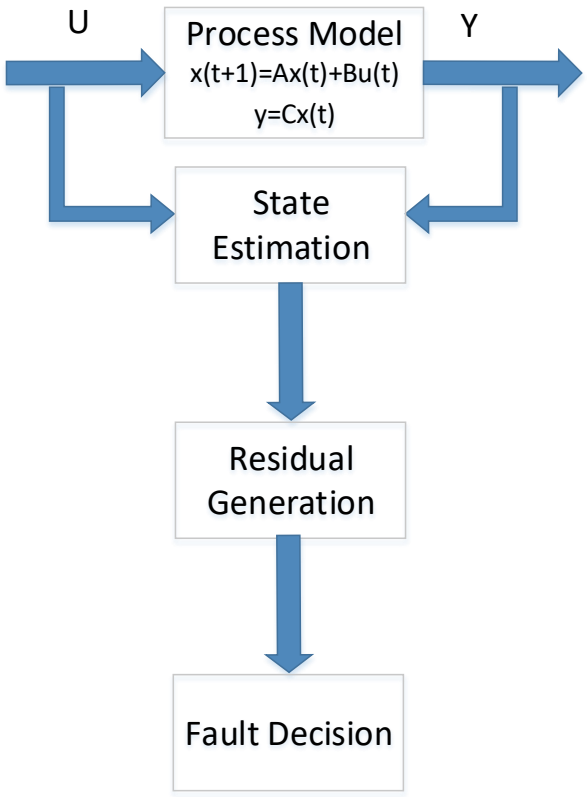

Figure 2-11 Fault Detection Based on State Variable Estimation

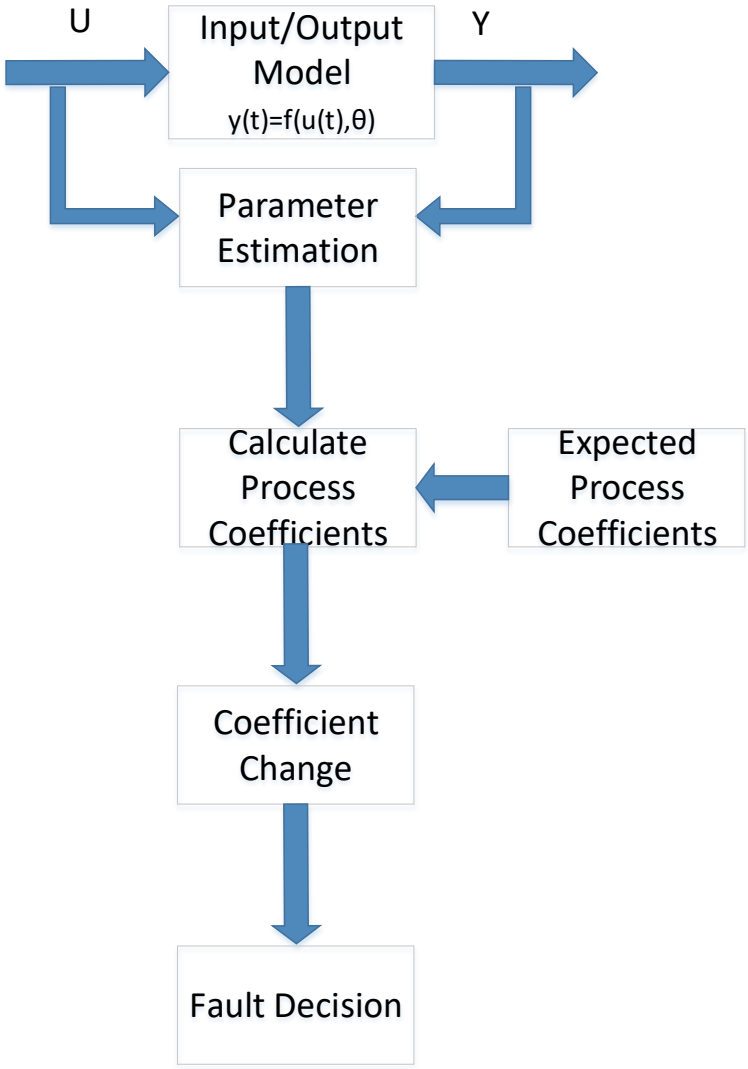

Figure 2-12 Fault Detection Based on Parameter Estimation (assuming faults in the system would be reflected in a change of the parameters in the system model)

2.5 Summary

This chapter presented an overall description and related work on the research topics of this dissertation. In particular, Section 2.2 gives a summary of the evolution of protective relays, current architecture, technologies. Section 2.3 summarizes the present practices on

protection functions. The GPS technology is also introduced and it is discussed how it can contribute to eliminate the asymmetry channel delay in the current differential protection. Section 2.4 provides a literature review of the fault detection and identification methods that have been used in many engineering systems besides power system. In general, there are advantages and shortcomings for each method, engineers have to fit a certain method with a specific engineering problem.

CHAPTER 3 THE OVERALL APPROACH

3.1 Description of Overall Approach

In this chapter, an overview of the proposed approach is first introduced, and then the necessary data infrastructure is presented.

Due to the fact that 1) traditional protection functions cause many coordination and setting errors, 2) gaps exist such that there is no reliable protection for a number of scenarios, and 3) disadvantages of each protection function as discussed in Chapter 2, a new method is proposed. The method has been inspired from the fact that differential protection is one of the most secure protection schemes, and it does not require coordination with other protection functions. Differential protection simply monitors the validity of KCL in a device, i.e. the sum of the currents going into a healthy device must be equal to zero. This concept can be generalized into monitoring the validity of all other physical laws that a healthy device must satisfy, such as Kirchoff's voltage law, Faraday's law, etc. This monitoring can be achieved in a systematic way by the use of dynamic state estimation. Specifically, all the physical laws that a component must obey are expressed in the state space dynamic model of the component, i.e., device model, in an object oriented approach. The measurement from each instrumentation channel is also defined as a function of states. Dynamic state estimation is directly applied to the measurements to estimate states, assuming no modeling error.

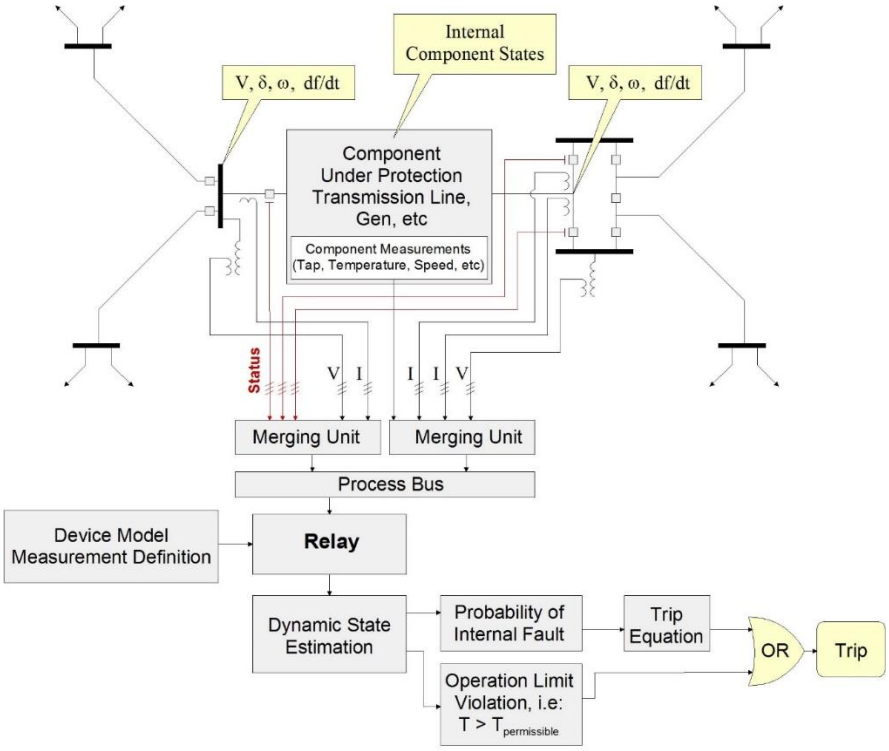

Figure 3-1 Illustration of Dynamic State Estimation based Protection Scheme [47]

After estimating the states, the well-known chi-square test and confidence level is applied [47] to calculate the probability that the measurement data are consistent with the component model, i.e., the physical laws that govern the operation of the component under healthy condition. A high confidence level indicates a good fit between the measurements and the model, or a low probability that the protection zone has an internal fault. A low confidence level indicates a very poor fit between the measurement and the component model, or a high probability that the protection zone has an internal fault. Figure 3-1 shows the concept of entire proposed protection scheme [47].

This proposed method is general enough to be applied to any power system component, such as synchronous machines, transformers, transmission lines, capacitor banks, induction machines, etc. However the transmission line is a very unique component worth studying

separately, the main reasons being 1) it's a geographically dispersed component, such that the lumped model may be inaccurate, and it's desired to analyze the effect of modeling error, 2) the protection of the line requires synchronization of multiple data acquisition systems, thus the effect of synchronization accuracy needs to be considered, 3) transmission line is a linear model and the estimation error can be directly analyzed, 4) transmission line faults are unique.

In general, the proposed method can identify any internal abnormality of the component within a cycle and trip the component immediately, unless the fault is extremely trivial (see case study for high impedance fault). Furthermore, it does not degrade the security because a relay does not trip in the event of normal behavior of the component, for example in case of line energization, transformer energization, since in those cases the energization currents are consistent with the transient behavior of the component as long as that's accurately modeled in the differential algebraic equations, the method will produce a high confidence level.

It is important to note that the proposed scheme will perform best when: a) the measurements are as accurate as possible – depending on the type of instrument transformer used, i.e., potential transformer, current transformer, etc. and the instrument channel, i.e., control cable, and b) the accuracy of the dynamic model of the component under protection. These issues would be discussed in Chapter 7.

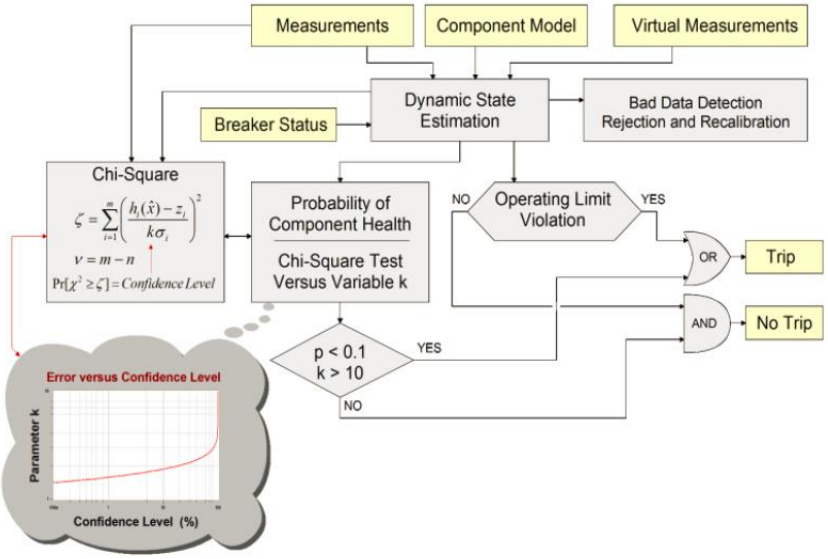

Figure 3-2 Illustration of the protection logic through chi square test [48]

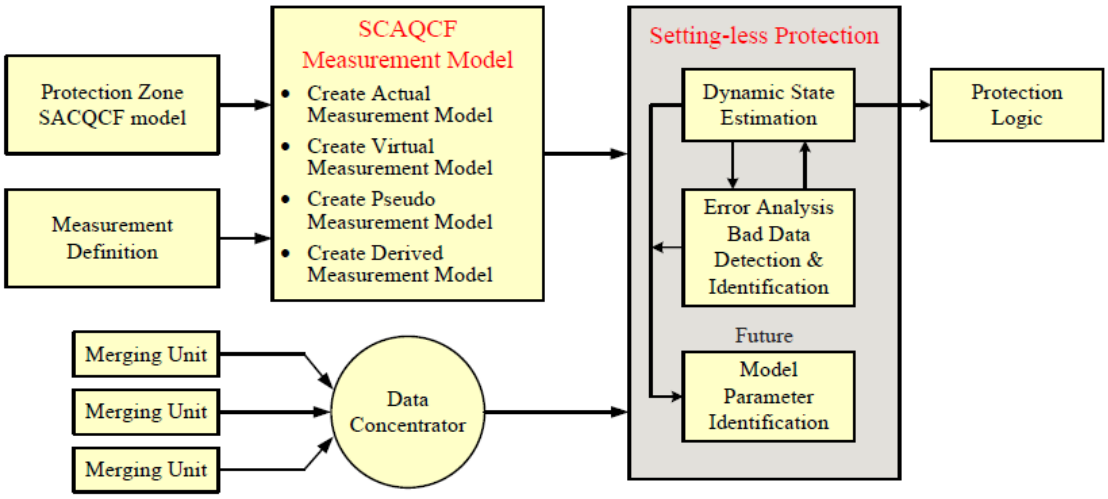

Figure 3-3 Dynamic State Estimation Based Protective Relay Organization

The proposed logic is briefly illustrated in Figure 3-2. The trip equation is based on average of the confidence level, the reason to average the confidence level is 1) filter out transients caused by external faults, circuit breaker operations, etc., 2) make correct

tripping when the internal fault is small (see Appendix A). As a side benefit of the proposed method, since the model must be high fidelity, we can foresee the possibility that this model used for protective relaying can also be used as the main repository of the model for other applications, for example in energy management system (EMS) applications, a positive sequence model can be computed from the three phase transmission line model and send to the EMS database for optimal power flow, voltage stability monitoring and contingency analysis applications, the advantage is that the EMS will use a field validated model.

The implementation of the dynamic state estimation based protective relay has been approached from an object orientation point of view, see overview of the relay organization in Figure 3-3, the approach requires the following objects: 1) the mathematical device model of the protection zone, 2) the physical measurements that may consist of analog and digital data. 3) the mathematical model of the physical measurements, 4) the mathematical model of the virtual measurements, 5) the mathematical model of the derived measurements, 6) the mathematical model of the pseudo measurements, 7) the dynamic state estimation algorithms, 8) the bad data detection and identification algorithm, 9) the protection logic and trip signals, 10) online parameter identification method. Items would be described individually in following chapters. The last task has not been addressed but it is an integral part of the overall approach as in many cases it will be necessary to fine tune the model of the protection zone via online parameter identification methods.

In order to implement the algorithm in practice, the algorithm needs to be integrated with data acquisition module. In next chapter, a geographically dispersed infrastructure of data acquisition systems that provide the necessary information for an automated protective relaying algorithms is described.

3.2 Proposed Data Infrastructure for Transmission Line Protection

The overall proposed data infrastructure for a two terminal transmission line is shown in Figure **3-4**. The potential transformers and current transformers presents a duplicate of the voltages across the different phases of the line and the currents through different phase of the line, and transform them from primary level to secondary level. The merging unit, synchronized with external GPS, samples and digitizes (details would be described in Chapter 6) and the process bus gathers the data. The relay at the local terminal would collect the data on the process bus, and the data from the remote terminal through fiber optic link. Today most current differential systems work with 64 kbps channels, which is equivalent to 1067 bits per power system cycle, or 14 bits per each of 80 samples in a 60 HZ power cycle. Considering the communication link. Each measurement would need a 16bit data storage type, and a measurement set typically contains 6 measurements, together with GPS timestamp and Cyclic Redundancy Code (CRC). This is far more than the 14 bits per time stamp requirement. As a result, the communication is the bottleneck here. Dedicated fiber optic allows bandwidths in the range of tens of megabits per second, and multiplexed channels can be requested with a bandwidth of Nx64kbps, as a result dedicated fiber optic is needed for the proposed protection scheme.

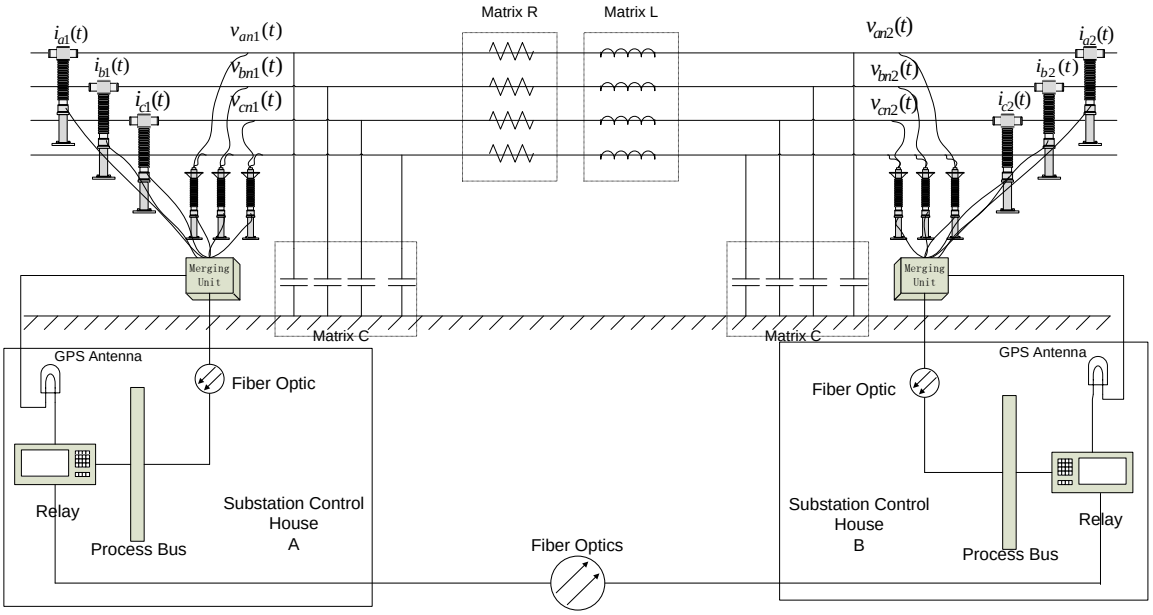

Figure 3-4 Transmission Line Dynamic State Estimation Based Protection Data Infrastructure

3.3 Summary

This chapters provided an overview of the proposed approach, each part within the proposed approach would be described in later chapters. An infrastructure of data acquisition systems that provide the necessary information for two terminal transmission line protection is also proposed in this chapter.

CHAPTER 4 MODELLING – THE STATE AND CONTROL ALGEBRAIC QUADRATIC COMPANION FORM

4.1 Overview

The implementation of the dynamic state estimation based protection has been approached from an object orientation point of view. For this purpose, the constituent parts of the approach have been evaluated and have been abstracted into a number of objects. Specifically, the approach requires the following objects:

1) the mathematical model of the protection zone

2) the physical measurements that may consist of analog and digital data

3) the mathematical model of the physical measurements

4) the mathematical model of the derived measurements

5) the mathematical model of the virtual measurements

6) the mathematical model of the pseudo measurements

In this chapter, an object-oriented, interoperable, and unified algebraic quadratic companion form (SCAQCF) for the transmission line model in the power system is proposed and the methodology for obtaining this SCAQCF model is presented. The proposed SCAQCF model can be universally applied to various protective relays protecting different components.

Section 4.2 gives the general and detailed methodology for the derivation of the SCAQCF model of a component from the original model of the component, which is described by a set of dynamic and algebraic equations. To illustrate the implementation of

this methodology, section 4.3 and section 4.4 give examples of the derivation of the AQCF model for the single section and multi section transmission line in the time domain respectively.

4.2 The Derivation of the SCAQCF Device and Measurement Model

In this section, an object-oriented, interoperable, and unified SCAQCF model is proposed and the methodology for obtaining this SCAQCF model is presented. First of all, the quadratized device model is used to represent the physical model and it is a preliminary step to obtain the State and Quadratic Companion Form SCAQCF device model. All the terms in quadratized model are at most second order. The model can be developed in several forms. The specific model we use has been developed under the following requirements: (a) list all the linear equations for through variables first; (b) list all the remaining linear equations; (c) all differential terms only appear in the linear equations; (d) list all the remaining quadratic equations; (e) the state and control variables should be so selected as to make any functional measurement linear; (f) the interface states must be listed at the beginning of the states and the interface states' order should be the same as terminals; (f) the highest order of the model is second order. The requirements are always easily met by introduction of additional state variables.

4.2.1 The Derivation of SCAQCF Device Model

The standard time domain quadratized model is shown below:

$$
\begin{aligned}
i(t) &= Y_{eqx1}\mathbf{x}(t) + D_{eqxd1}\frac{d\mathbf{x}(t)}{dt} + C_{eqc1} \\
0 &= Y_{eqx2}\mathbf{x}(t) + D_{eqxd2}\frac{d\mathbf{x}(t)}{dt} + C_{eqc2} \\
0 &= Y_{eqx3}\mathbf{x}(t) + Y_{equ3}\mathbf{u}(t) + \left\{ \begin{array}{c} \vdots \\ \mathbf{x}(t)^T \left\langle F^i_{eqxx3} \right\rangle \mathbf{x}(t) \\ \vdots \end{array} \right\} + C_{eqc3}
\end{aligned}
\tag{4.1}
$$

$$
\mathbf{h}(\mathbf{x}) = Y_{feqx}\mathbf{x} + \left\{ \begin{array}{c} \vdots \\ \mathbf{x}^T \left\langle F^i_{feqxxx} \right\rangle \mathbf{x} \\ \vdots \end{array} \right\} + C_{feqc} \tag{4.2}
$$

Connectivity: *TerminalNodeName*

Normalization Factors: StateNormFactor, ThroughNormFactor

$$
\begin{aligned}
\textit{subject to:} \qquad & \mathbf{h}_{\min} \le \mathbf{h}(\mathbf{x}) \le \mathbf{h}_{\max} \\
& \mathbf{x}_{\min} \le \mathbf{x} \le \mathbf{x}_{\max}
\end{aligned}
$$

where:

$i(t)$: the through variables of the device model

$\mathbf{x}(t)$: external and internal state variables of the device model

Y_{eqx1}: matrix defining the linear part for state variables in linear through variable equations,

D_{eqxd1}: matrices defining the differential part for state variables in linear through variable equations,

C_{eqc1}: constant vector of the device model in linear through variable equations,

Y_{eqx2}: matrix defining the linear part for state variables in linear virtual equations,

D_{eqxd2} : matrices defining the differential part for state variables in linear virtual equations,

C_{eqc2} : constant vector of the device model in linear virtual equations,

Y_{eqx3} : matrix defining the linear part for state variables in the remaining quadratic equations,

C_{eqc3} : constant vector of the device model in the remaining quadratic equations,

F_{eqxx} : matrices defining the quadratic part for state variables in the remaining quadratic equations,

TerminalNodeName : terminal names defining the connectivity of the device model,
StateNormFactor: Normalization Factors for the states
ThroughNormFactor: Normalization Factors for the through and zero variables
ControlNormFactor: Normalization Factors for the controls
$\mathbf{h}_{\min} \le \mathbf{h}(\mathbf{x}) \le \mathbf{h}_{\max}$: functional constraints,

$\mathbf{x}_{\min}, \mathbf{x}_{\max}$: lower and upper bounds for the state variables.

Y_{feqx} : constraint matrix defining the linear part for state variables,

F_{feqx} : constraint matrices defining the quadratic part for state variables,

C_{feqc} : constraint history dependent vector of the device model.

Each device mathematical model should be also expressed in the generalized State and Control Algebraic Quadratic Companion Form (SCAQCF). The advantage of this SCAQCF device model is that it does not contain differential terms, and the highest order is second order so that it is easy for computers to perform simulation and computation.

This SCAQCF model is derived by applying the quadratic integration method to the differential equation in the previous quadratized model.

The quadratic integration method is applied to every set of equations separately in the quadratized device model. Since there are three sets of equations, each one is analyzed below to show how they can be transferred to SCAQCF model. Quadratic integration is by assuming any variable vary quadratically over the integration period. See Figure 4-1 [49]. Note that the three points $x(t-h)$, x_m and $x(t)$ fully define the quadratic function in the interval [t-h, t]. The general integration results over time intervals [t-h, t_m] and [t-h, t] are listed as follows:

$$\int_{t-h}^{t_m} x(\tau)d\tau = \frac{5h}{24}x(t-h) + \frac{h}{3}x_m - \frac{h}{24}x(t),$$
$$\int_{t-h}^{t} x(\tau)d\tau = \frac{h}{6}x(t-h) + \frac{2h}{3}x_m + \frac{h}{6}x(t). \tag{4.3}$$

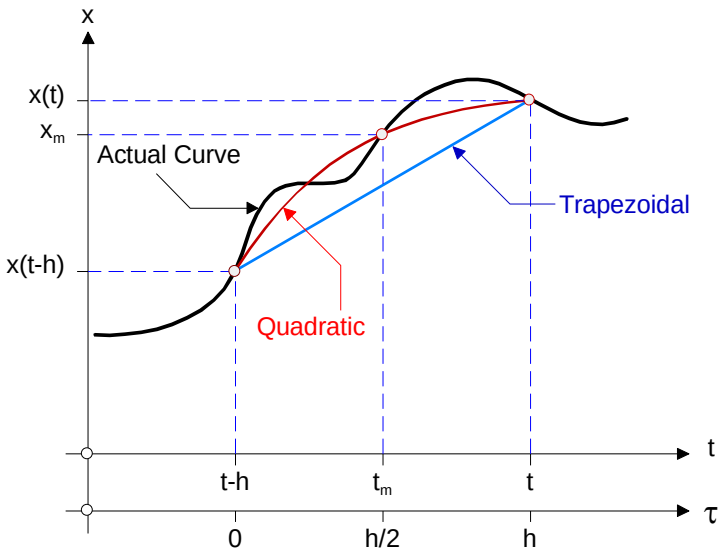

Figure 4-1. Illustration of the quadratic-integration method [49].

1) Through variable equations:

$$i(t) = Y_{eqx1}\mathbf{x}(t) + Y_{equ1}\mathbf{u}(t) + D_{eqxd1}\frac{d\mathbf{x}(t)}{dt} + C_{eqc1}$$

After applying quadratic integration, we have

From time t-h to t,

$$i(t) = (\frac{4}{h}D_{eqxd1} + Y_{eqx1})\mathbf{x}(t) - \frac{8}{h}D_{eqxd1}\mathbf{x}(t_m) + (\frac{4}{h}D_{eqxd1} - Y_{eqx1})\mathbf{x}(t-h) + i(t-h)$$

From time t-h to tm,

$$i(t_m) = \frac{1}{2h}D_{eqxd1}\mathbf{x}(t) + (\frac{2}{h}D_{eqxd1} + Y_{eqx1})\mathbf{x}(t_m) + (\frac{1}{2}Y_{eqx1} - \frac{5}{2h}D_{eqxd1})\mathbf{x}(t-h) - \frac{1}{2}i(t-h) + \frac{3}{2}C_{eqc1}$$

2) Linear virtual equations:

$0 = Y_{eqx2}\mathbf{x}(t) + D_{eqxd2}\frac{d\mathbf{x}(t)}{dt} + C_{eqc2}$ After applying quadratic integration, we have

From time t-h to t,

$$0 = (D_{eqxd2} + \frac{h}{6}Y_{eqx2})\mathbf{x}(t) + \frac{2h}{3}Y_{eqx2}\mathbf{x}(t_m) + (\frac{h}{6}Y_{eqx2} - D_{eqxd2})\mathbf{x}(t-h) + hC_{eqc2}$$

From time t-h to tm,

$$0 = -\frac{h}{24}Y_{eqx2}\mathbf{x}(t) + (D_{eqxd2} + \frac{h}{3}Y_{eqx2})\mathbf{x}(t_m) + (\frac{5h}{24}Y_{eqx2} - D_{eqxd2})\mathbf{x}(t-h) + \frac{h}{2}C_{eqc2}$$

3) Nonlinear equations

$$0 = Y_{eqx3}\mathbf{x}(t) + \left\{ \begin{array}{c} \vdots \\ \mathbf{x}(t)^T \left\langle F^i_{eqxx3} \right\rangle \mathbf{x}(t) \\ \vdots \end{array} \right\} + C_{eqc3}$$

These equations are the same under time t and time tm

$$0 = Y_{eqx3}\mathbf{x}(t) + \left\{ \begin{array}{c} \vdots \\ \mathbf{x}(t)^T \left\langle F^i_{eqxx3} \right\rangle \mathbf{x}(t) \\ \vdots \end{array} \right\} + C_{eqc3}$$

$$0 = Y_{eqx3}\mathbf{x}(t_m) + \left\{ \begin{array}{c} \vdots \\ \mathbf{x}(t_m)^T \left\langle F^i_{eqxx3} \right\rangle \mathbf{x}(t_m) \\ \vdots \end{array} \right\} + C_{eqc3}$$

By restructuring and stacking the above three sets of equations into one matrix form, the standard time domain SCAQCF device model is obtained:

$$\left\{ \begin{array}{c} i(t) \\ 0 \\ 0 \\ i(t_m) \\ 0 \\ 0 \end{array} \right\} = Y_{eqx}\mathbf{x} + \left\{ \begin{array}{c} \vdots \\ \mathbf{x}^T \left\langle F^i_{eqx} \right\rangle \mathbf{x} \\ \vdots \end{array} \right\} - B_{eq} \tag{4.4}$$

$$B_{eq} = -N_{eqx}\mathbf{x}(t-h) - M_{eq}i(t-h) - K_{eq} \tag{4.5}$$

$$\mathbf{h}(\mathbf{x}) = Y_{feqx}\mathbf{x} + \left\{ \begin{array}{c} \vdots \\ \mathbf{x}^T \left\langle F^i_{feqxxx} \right\rangle \mathbf{x} \\ \vdots \end{array} \right\} + C_{feqc}$$

Connectivity: *TerminalNodeName*

Normalization Factors: StateNormFactor, ThroughNormFactor, ControlNormFactor

$$\textit{subject to}: \qquad \mathbf{h}_{\min} \le \mathbf{h}(\mathbf{x}) \le \mathbf{h}_{\max}$$
$$\mathbf{x}_{\min} \le \mathbf{x} \le \mathbf{x}_{\max}$$

The normalization factors, functional constraints and variable limits are the same as the time domain quadratized device model.

where:

$$Y_{eqx} = \begin{bmatrix} \frac{4}{h} D_{eqxd1} + Y_{eqx1} & -\frac{8}{h} D_{eqxd1} \\ D_{eqxd2} + \frac{h}{6} Y_{eqx2} & \frac{2h}{3} Y_{eqx2} \\ Y_{eqx3} & 0 \\ \frac{1}{2h} D_{eqxd1} & \frac{2}{h} D_{eqxd1} + Y_{eqx1} \\ -\frac{h}{24} Y_{eqx2} & D_{eqxd2} + \frac{h}{3} Y_{eqx2} \\ 0 & Y_{eqx3} \end{bmatrix}$$

$$Y_{equ} = \begin{bmatrix} Y_{equ1} & 0 \\ \frac{h}{6} Y_{equ2} & \frac{2h}{3} Y_{equ2} \\ Y_{equ3} & 0 \\ 0 & Y_{equ1} \\ -\frac{h}{24} Y_{equ2} & \frac{h}{3} Y_{equ2} \\ 0 & Y_{equ3} \end{bmatrix}$$

$$F_{eqx} = \begin{bmatrix} 0 & 0 \\ 0 & 0 \\ F_{eqxx3} & 0 \\ 0 & 0 \\ 0 & 0 \\ 0 & F_{eqxx3} \end{bmatrix}$$

$$F_{equ} = \begin{bmatrix} 0 & 0 \\ 0 & 0 \\ F_{equu3} & 0 \\ 0 & 0 \\ 0 & 0 \\ 0 & F_{equu3} \end{bmatrix}$$

$$F_{equx} = \begin{bmatrix} 0 & 0 \\ 0 & 0 \\ F_{equx3} & 0 \\ 0 & 0 \\ 0 & 0 \\ 0 & F_{equx3} \end{bmatrix}$$

$$N_{eqx} = \begin{bmatrix} -Y_{eqx1} + \frac{4}{h} D_{eqxd1} \\ \frac{h}{6} Y_{eqx2} - D_{eqxd2} \\ 0 \\ \frac{1}{2} Y_{eqx1} - \frac{5}{2h} D_{eqxd1} \\ \frac{5h}{24} Y_{eqx2} - D_{eqxd2} \\ 0 \end{bmatrix}$$

$$N_{equ} = \begin{bmatrix} -Y_{equ1} \\ \frac{h}{6} Y_{equ2} \\ 0 \\ \frac{1}{2} Y_{equ1} \\ \frac{5h}{24} Y_{equ2} \\ 0 \end{bmatrix}$$

$$N_{equ} = \begin{bmatrix} I_{size(i(t))} \\ 0 \\ 0 \\ \frac{1}{2} I_{size(i(t))} \\ 0 \\ 0 \end{bmatrix}$$

$$K_{eq} = \begin{bmatrix} 0 \\ hC_{eqc2} \\ C_{eqc3} \\ \frac{3}{2} C_{eqc1} \\ \frac{1}{2} hC_{eqc2} \\ C_{eqc3} \end{bmatrix}$$

$i(t)\ and\ i(t_m)$: the through variables of the device model

$\mathbf{x}$: external and internal state variables of the device model, $\mathbf{x} = [\mathbf{x}(t), \mathbf{x}(t_m)]$

Y_{eqx}: matrix defining the linear part for state variables,

F_{eqx}: matrices defining the quadratic part for state variables,

B_{eq}: history dependent vector of the device model,

N_{eqx}: matrix defining the last integration step state variables part,

M_{eq}: matrix defining the last integration step through variables part,

K_{eq}: constant vector of the device model,

TerminalNodeName: terminal names defining the connectivity of the device model,

StateNormFactor: Normalization Factors for the states

ThroughNormFactor: Normalization Factors for the through and zero variables

$\mathbf{h}_{\min} \le \mathbf{h}(\mathbf{x}) \le \mathbf{h}_{\max}$: functional constraints,

$\mathbf{x}_{\min}, \mathbf{x}_{\max}$: lower and upper bounds for the state variables

Y_{feqx} : constraint matrix defining the linear part for state variables,

F_{feqx} : constraint matrices defining the quadratic part for state variables,

C_{feqc} : constraint history dependent vector of the device model.

4.2.2 The Derivation of SCAQCF Measurement Model

Any measurement, i.e., current, voltage, temperature, etc. can be viewed as an object that consists of the measured value and a corresponding function that expresses the measurement as a function of the state of the component. This function can be directly obtained (autonomously) from the State and Control Algebraic Quadratic Companion Form of the component. Because the algebraic companion form is quadratic at most, the measurement model will be also quadratic at most. Thus, the object-oriented measurement model can be expressed as the following standard equation:

$$z_k(t) = \sum_i a^k_{i,t} \cdot x_i(t) + \sum_i a^k_{i,tm} \cdot x_i(t_m) + \sum_{i,j} b^k_{i,j,t} \cdot x_i(t) \cdot x_j(t) + \sum_{i,j} b^k_{i,j,tm} \cdot x_i(t_m) \cdot x_j(t_m) + c_k(t) + \eta_k \tag{4.6}$$

where *z* is the measured value, *t* the present time, *tm* the midpoint between the present and previous time, *x* the state variables, *a* the coefficients of linear terms, b the coefficients of nonlinear terms, c the constant term, and η the measurement error.

The measurements can be identified as: (a) actual measurements, (b) virtual measurements, (c) derived measurements, (d) pseudo measurements. The types of measurements will be discussed next.

Actual Measurements: In general, the actual measurements can be classified as across and through measurements. Across measurements are measurements of voltages or other physical quantities at the terminals of a protection zone such as speed on the shaft of a generator/motor. These quantities are typically states in the model of the component. For this reason, the across measurements has a simple model as follows:

$$z_i = x_i \pm x_j + \eta_i$$

Through measurements are typically currents at the terminals of a device or other quantities at the terminals such as torque on the shaft of a generator/motor. The quantity of a through measurement is typically a function of the state of the device. For this reason, the through measurement model is extracted from the algebraic companion form, i.e., the measurement model is simply one equation of the SCAQCF model, as follow:

$$z_k = \sum_i Y^k_{eqx,i} \cdot x_i + \sum_{i,j} F^k_{eqx,i,j} \cdot x_i \cdot x_j - \sum_i b^k_{eq,i}$$

where the superscript k means the k^{th} row of the matrix or the vector.

Virtual Measurements: The virtual measurements represent a physical law that must be satisfied. For example, we know that at a node the sum of the currents must be zero by Kirchoff's current law, or the voltage drop across any closed loop must be zero by Kirchoff's voltage law. In this case we can define a measurement (sum of current, or

voltage across a loop); note that the value of the measurement (zero) is known with certainty. This is a virtual measurement.

The model can provide virtual measurements in the form of equations that must be satisfied. Consider for example the k^{th} SCAQCF model equation below:

$$0 = \sum_i Y^k_{eqx,i} \cdot x_i + \sum_{i,j} F^k_{eqx,i,j} \cdot x_i \cdot x_j - \sum_i b^k_{eq,i}$$

This equation is simply a relationship among the states of the component that must be satisfied. Therefore, we can state that the zero value is a measurement that we know with certainty. We refer to this as a virtual measurement.

Derived Measurements: A derived measurement is a measurement that can be defined for a physical quantity by utilizing physical laws. An example derived measurement is shown in Figure 4-2 where in order to protect the transmission line, the currents through the line is requires as actual measurements. However, since there's no current transformer on the line such measurement is not available. On the other hand, the two circuit breakers on the bus measures the current going into the line, as a result, the current through the line could be measured as sum of the two currents. See Figure 4-3 for another example, the figure illustrates a series compensated power line with actual measurements on the line side only. Then derived measurements are defined for each capacitor section. Note that the derived measurements enable the observation of the voltage across the capacitor sections.

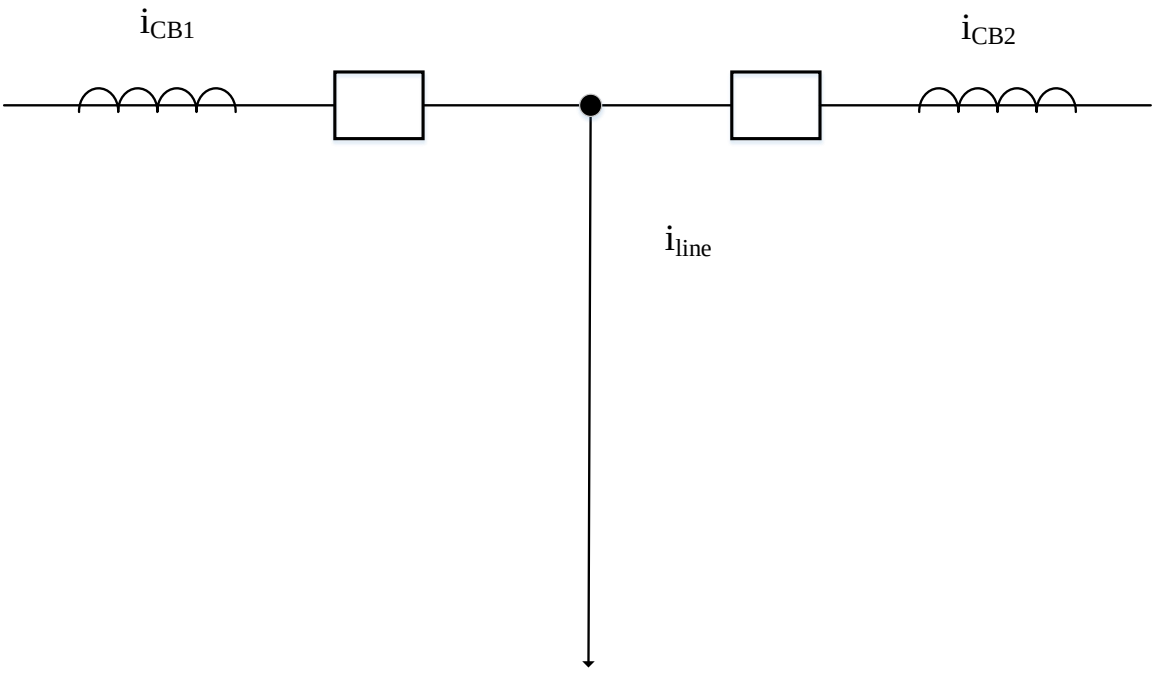

Figure 4-2 Illustration of derived measurement – transmission line breaker and a half case

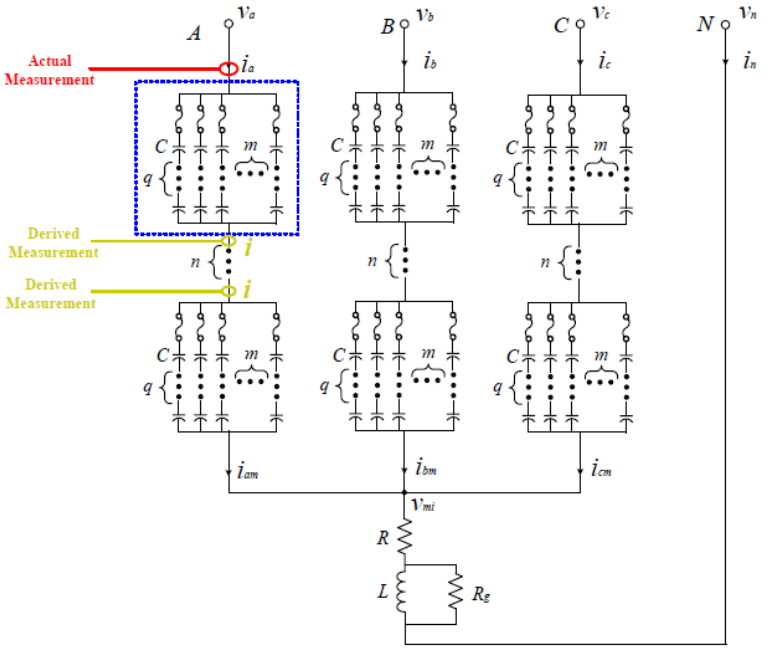

Figure 4-3 Illustration of derived measurement – series compensated capacitor bank along transmission line case

Pseudo Measurements: Pseudo measurements are hypothetical measurements for which we may have an idea of their expected values but we do not have an actual measurement. For example, a pseudo measurement can be the voltage at the neutral; we know that this voltage will be very small under normal operating conditions. In this case we can define a measurement of value zero but with a very high uncertainty.

Summary: Eventually, all the measurement objects have the following measurement format:

$$z = h(x,t,t_m) + \eta = a^T x(t) + b^T x(t_m) + \begin{bmatrix} x^T(t) & x^T(t_m) \end{bmatrix} F \begin{bmatrix} x(t) \\ x(t_m) \end{bmatrix} + \eta$$

The time domain SCAQCF measurement model is the matrix expression for each measurement in SCAQCF. The primary data that define a measurement are pointers and the measurement error. This model is also created by the computer program automatically.

The time domain SCAQCF measurement model comes from two parts: 1) time domain SCAQCF device model; 2) quadratic integration of time domain quadratized device model.

If the measurement equation is derived from time domain SCAQCF device model, it just pulls equation from the time domain SCAQCF device model.

If the measurement equation comes from the time domain quadratized device model, the quadratic integration algorithm should be applied to this equation. The procedure is the same as deriving the time domain SCAQCF device model from time domain quadratized device model.

The above two steps are processed for each measurement. Then all the equations are stacked into the following standard time domain SCAQCF measurement model:

$$\mathbf{z} = h(x, t, t_m) = Y_{m,x}\mathbf{x} + \left\{ \begin{array}{c} \vdots \\ \mathbf{x}^T F^i_{m,x} \mathbf{x} \\ \vdots \end{array} \right\} + C_m \tag{4.7}$$

$$C_m = N_{m,x}\mathbf{x}(t-h) + M_m i(t-h) + K_m \tag{4.8}$$

Measurement noise error: dMeterScale, dMeterSigmaPU

where:

$\mathbf{z}$: measurement variables at both time t and time t_m, $\mathbf{z} = [\mathbf{z}(t), \mathbf{z}(t_m)]$

$\mathbf{x}$: external and internal state variables of the measurement model, $\mathbf{x} = [\mathbf{x}(t), \mathbf{x}(t_m)]$

$Y_{m,x}$: matrix defining the linear part for state variables,

$F_{m,x}$: matrices defining the quadratic part for state variables,

C_m : history dependent vector of the measurement model,

$N_{m,x}$: matrix defining the last integration step state variables part,

M_m : matrix defining the last integration step through variables part,

K_m : constant vector of the measurement model,

dMeterScale : the scale that meters use (in metric units),

dMeterSigmaPU : the standard deviation for the measurements (in per. unit),

Detailed examples of the formulation of the SCAQCF model for the transmission line in time-domain are given in the following two sections.

4.3 The SCAQCF Model for a Single Section Transmission Line in Time Domain

In many power system applications, the model of transmission lines is of fundamental importance, including 1) power flow (optimal power flow and state estimation) analysis, 2) fault analysis, 3) harmonic analysis, 4) transient stability analysis. The conditions involved in these analysis problems range from the steady-state fundamental frequency to switching surges or lightning-induced transients. If certain phenomenon involves the earth path, then the earth path would have to be modeled as well. Depending on the actual application, the transmission line models can be drastically different.

The basis of all widely used models for transmission line is included in Appendix A. For the application of protection, the model is simplified to a pi equivalent model which is described in this Chapter.

This section presents the SCAQCF for the single section transmission line model. First the compact model is presented and then the SCAQCF model is presented by applying model quadratization and quadratic integration.

4.3.1 Transmission Line in Time Domain – Compact & Quadratized Form

Figure 4.2 illustrates the diagram of the transmission line lump model.

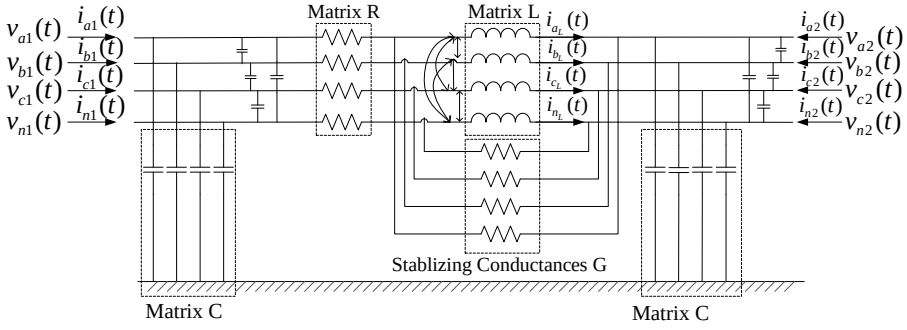

Figure 4-4. Transmission line model- single section.

The differential algebraic equations ruling the transmission line are derived from KCL, KVL, and written in compact form:

$$i_1(t) = C\frac{dv_1(t)}{dt} + i_L(t) + GL\frac{di_L(t)}{dt} \tag{4.9}$$

$$i_2(t) = C\frac{dv_2(t)}{dt} - i_L(t) - GL\frac{di_L(t)}{dt} \tag{4.10}$$

$$0 = -v_1(t) + v_2(t) + R\left(i_L(t) + GL\frac{di_L(t)}{dt}\right) + L\frac{di_L(t)}{dt} \tag{4.11}$$

where,

R, L, C, G: 4×4 resistance, inductance, capacitance and stabilizing conductance matrices.

$i_1(t)$: all through variables on left side of pi equivalent model at time t

$i_2(t)$: all through variables on right side of pi equivalent model at time t

$v_1(t)$: all across variables on left side of pi equivalent model at time t

$v_2(t)$: all across variables on right side of pi equivalent model at time t

$x(t) = [v_1(t) \quad v_2(t) \quad i_L(t)]$

Since the transmission line is a linear model, no quadratization is needed, the quadratized form is same as the compact form.

4.3.2 Transmission Line in Time Domain – Single Section SCAQCF Device Model

Quadratic integration of the above linear model from time t-h to t:

$$\frac{h}{6}i(t)+\frac{2h}{3}i(t_m)+\frac{h}{6}i(t-h)=\left(\frac{h}{6}Y_{eqx1}+D_{eqxd1}\right)x(t)+\frac{2h}{3}Y_{eqx1}x(t_m)+\left(\frac{h}{6}Y_{eqx1}-D_{eqxd1}\right)x(t-h) \tag{4.12}$$

$$0=\left(\frac{h}{6}Y_{eqx2}+D_{eqxd2}\right)x(t)+\frac{2h}{3}Y_{eqx2}x(t_m)+\left(\frac{h}{6}Y_{eqx2}-D_{eqxd2}\right)x(t-h) \tag{4.13}$$

Quadratic integration of the above linear model from time t-h to tm:

$$-\frac{h}{24}i(t)+\frac{h}{3}i(t_m)+\frac{5h}{24}i(t-h)=-\frac{h}{24}x(t)+\left(\frac{h}{3}Y_{eqx1}+D_{eqxd1}\right)x(t_m)+\left(\frac{5h}{24}Y_{eqx1}-D_{eqxd1}\right)x(t-h) \tag{4.14}$$

$$0=-\frac{h}{24}x(t)+\left(\frac{h}{3}Y_{eqx2}+D_{eqxd2}\right)x(t_m)+\left(\frac{5h}{24}Y_{eqx2}-D_{eqxd2}\right)x(t-h) \tag{4.15}$$

The integration yields the AQCF according to (4.4):

$$Y_{eqx}=\begin{bmatrix} \frac{4}{h}C & 0 & I_4+\frac{4}{h}GL & -\frac{8}{h}C & 0 & -\frac{8}{h}GL \\ 0 & \frac{4}{h}C & -I_4-\frac{4}{h}GL & 0 & -\frac{8}{h}C & \frac{8}{h}GL \\ -I_4 & I_4 & R+\frac{4}{h}(RGL+L) & 0 & 0 & -\frac{8}{h}(RGL+L) \\ \frac{1}{2h}C & 0 & \frac{1}{2h}GL & \frac{2}{h}C & 0 & I_4+\frac{2}{h}GL \\ 0 & \frac{1}{2h}C & -\frac{1}{2h}GL & 0 & \frac{2}{h}C & -I_4-\frac{2}{h}GL \\ 0 & 0 & \frac{1}{2h}(RGL+L) & -I_4 & I_4 & R+\frac{2}{h}(RGL+L) \end{bmatrix}$$

$F_{eqxx}=0\ \ K_{eq}=0$

$$N_{eqx}=\begin{bmatrix} \frac{8}{h}C & 0 & I_4-\frac{4}{h}GL \\ 0 & \frac{8}{h}C & -I_4+\frac{4}{h}GL \\ -I_4 & I_4 & R-\frac{4}{h}(RGL+L) \\ \frac{5}{2h}C & 0 & -\frac{1}{2}I_4+\frac{5}{2h}GL \\ 0 & \frac{5}{2h}C & \frac{1}{2}I_4-\frac{5}{2h}GL \\ \frac{1}{2}I_4 & -\frac{1}{2}I_4 & -\frac{1}{2}R+\frac{5}{2h}(RGL+L) \end{bmatrix} \qquad M_{eq}=\begin{bmatrix} I_4 & 0 & 0 \\ 0 & I_4 & 0 \\ 0 & 0 & 0 \\ -\frac{1}{2}I_4 & 0 & 0 \\ 0 & -\frac{1}{2}I_4 & 0 \\ 0 & 0 & 0 \end{bmatrix}$$

where I_4 means identity matrix with 4 rows and 4 columns.

The definition of the external state, internal state, and through variables are listed in Table 4.1 to Table 4.3, respectively.

Table 4.1. External states of the four phase transmission line – single section.

Index	Variable	Description
0	$v_{a1}(t)$	voltage of phase A to ground on left terminal
1	$v_{b1}(t)$	voltage of phase B to ground on left terminal
2	$v_{c1}(t)$	voltage of phase C to ground on left terminal
3	$v_{n1}(t)$	voltage of phase N to ground on left terminal
4	$v_{a2}(t)$	voltage of phase A to ground on right terminal
5	$v_{b2}(t)$	voltage of phase A to ground on right terminal
6	$v_{c2}(t)$	voltage of phase A to neutral on right terminal
7	$v_{b2}(t)$	voltage of phase A to neutral on right terminal

Table 4.2. Internal states of the four phase transmission line – single section.

Index	Variable	Description
8	$i_{aL}(t)$	current through the inductance of phase A
9	$i_{bL}(t)$	current through the inductance of phase B
10	$i_{cL}(t)$	current through the inductance of phase C
11	$i_{nL}(t)$	current through the inductance of phase N

Table 4.3. Through variables of the four phase transmission line – single section.

Index	Variable	Description
0	$i_{a1}(t)$	current through transmission line phase a left terminal
1	$i_{b1}(t)$	current through transmission line phase b left terminal
2	$i_{c1}(t)$	current through transmission line phase c left terminal
3	$i_{n1}(t)$	current through transmission line phase n left terminal
4	$i_{a2}(t)$	current through transmission line phase a right terminal
5	$i_{b2}(t)$	current through transmission line phase b right terminal
6	$i_{c2}(t)$	current through transmission line phase c right terminal
7	$i_{n2}(t)$	current through transmission line phase n right terminal

4.3.3 Transmission Line in Time Domain – Single Section SCAQCF Measurement Model

In this thesis, the transmission line protective relay needs access to the voltages and currents on both terminals of the line, so the 24 actual measurements are: 1) Three phase currents at both left and right sides at time t, t_m – extracted from device model; 2) Three phase-to-neutral voltages at both left and right sides at time t, t_m – linear combination of external states; 3) The 4 pseudo measurements are neutral voltages on left and right sides at time t, t_m – linear combination of external states; 4) The 8 virtual measurements are zero values from KVL at each phase at time t, t_m – extracted from device model; There are in total 36 measurements and 24 states, with a redundancy of 50%.

$$Y_{mx} = \begin{bmatrix} \frac{4}{h}C_{1:3,1:4} & 0_{3,4} & I_{3,4}+\frac{4}{h}GL_{1:3,1:4} & -\frac{8}{h}C_{1:3,1:4} & 0_{3,4} & -\frac{8}{h}GL_{1:3,1:4} \\ 0_{3,4} & \frac{4}{h}C_{1:3,1:4} & -I_{3,4}-\frac{4}{h}GL_{1:3,1:4} & 0_{3,4} & -\frac{8}{h}C_{1:3,1:4} & \frac{8}{h}GL_{1:3,1:4} \\ -I_4 & I_4 & R+\frac{4}{h}(RGL+L) & 0_4 & 0_4 & -\frac{8}{h}(RGL+L) \\ K & 0_4 & 0_4 & 0_4 & 0_4 & 0_4 \\ 0_4 & K & 0_4 & 0_4 & 0_4 & 0_4 \\ \frac{1}{2h}C_{1:3,1:4} & 0_{3,4} & \frac{1}{2h}GL_{1:3,1:4} & \frac{2}{h}C_{1:3,1:4} & 0_{3,4} & I_{3,4}+\frac{2}{h}GL_{1:3,1:4} \\ 0_{3,4} & \frac{1}{2h}C_{1:3,1:4} & -\frac{1}{2h}GL_{1:3,1:4} & 0_{3,4} & \frac{2}{h}C_{1:3,1:4} & -I_{3,4}-\frac{2}{h}GL_{1:3,1:4} \\ 0_4 & 0_4 & \frac{1}{2h}(RGL+L) & -I_4 & I_4 & R+\frac{2}{h}(RGL+L) \\ 0_4 & 0_4 & 0_4 & K & 0_4 & 0_4 \\ 0_4 & 0_4 & 0_4 & 0_4 & K & 0_4 \end{bmatrix}$$

$$F_{mxx} = 0$$

$$N_{mx} = \begin{bmatrix} \frac{8}{h}C_{1:3,1:4} & 0_{3,4} & I_3 - \frac{4}{h}GL_{1:3,1:4} \\ 0_{3,4} & \frac{8}{h}C_{1:3,1:4} & -I_3 + \frac{4}{h}GL_{1:3,1:4} \\ -I_4 & I_4 & R - \frac{4}{h}(RGL + L) \\ 0_4 & 0_4 & 0_4 \\ 0_4 & 0_4 & 0_4 \\ \frac{5}{2h}C_{1:3,1:4} & 0_{3,4} & -\frac{1}{2}I_3 + \frac{5}{2h}GL_{1:3,1:4} \\ 0_{3,4} & \frac{5}{2h}C_{1:3,1:4} & \frac{1}{2}I_3 - \frac{5}{2h}GL_{1:3,1:4} \\ \frac{1}{2}I_4 & -\frac{1}{2}I_4 & -\frac{1}{2}R + \frac{5}{2h}(RGL + L) \\ 0_4 & 0_4 & 0_4 \\ 0_4 & 0_4 & 0_4 \end{bmatrix}$$

$$M_m = \begin{bmatrix} I_{3,4} & 0_{3,4} & 0_{3,4} \\ 0_{3,4} & I_{3,4} & 0_{3,4} \\ 0_4 & 0_4 & 0_4 \\ 0_4 & 0_4 & 0_4 \\ 0_4 & 0_4 & 0_4 \\ -\frac{1}{2}I_{3,4} & 0_{3,4} & 0_{3,4} \\ 0_{3,4} & -\frac{1}{2}I_{3,4} & 0_{3,4} \\ 0_4 & 0_4 & 0_4 \\ 0_4 & 0_4 & 0_4 \\ 0_4 & 0_4 & 0_4 \end{bmatrix}$$

where any submatrix with subscripts such as 1:3,1:4 means the first three rows and the first four columns of that matrix, and

$$K = \begin{bmatrix} 1 & 0 & 0 & -1 \\ 0 & 1 & 0 & -1 \\ 0 & 0 & 1 & -1 \\ 0 & 0 & 0 & 1 \end{bmatrix}$$

4.4 The SCAQCF Model for a Multi Section Transmission Line in Time Domain

When the transmission line is long, the equivalent pi circuit parameters in Appendix A are functions of the frequency and no longer proportional to the length of the line. Or put in other words, the RLC elements which are proportional to the length of the line must be corrected in order to get an exact line model at a specified frequency. For a more accurate representation of a long transmission line, the multi-section model is desired. The model is derived by combining multiple single section models, as in Figure 4-5.

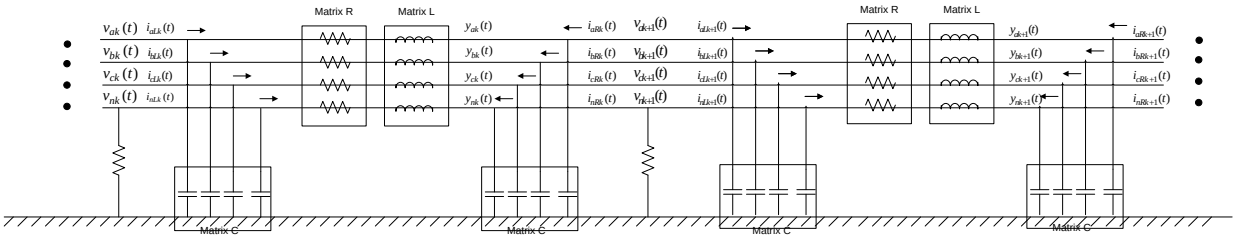

Figure 4-5 Transmission Line Model – Multi Section

4.4.1 Transmission Line in Time Domain - Compact & Quadratized Form

The transmission line is divided into N sections, the right terminal of k^{th} single section and the left terminal of the $k+1^{th}$ single section part are electrically connected. Let the states be defined as:

$$x^T = \left[v_1, v_2, \ldots v_N, v_{N+1}, i_{L1}, \ldots i_{LN}\right]^T$$

where:

v_k : (k=1,…,N+1)the voltage on the left hand side of kth section or the right hand side of the k-1th section (since they're connected)

i_{Lk} : (k=1,…,N) the inductance current of the kth section.

For the through variables $i_1 = [i_{a1}, i_{b1}, i_{c1}, i_{n1}]^T$ on the left terminal of the multi-section line,

$$i_1(t) = C_1 \frac{dv_1(t)}{dt} + i_{L1}(t) \tag{4.16}$$

For the through variables $i_2 = [i_{a2}, i_{b2}, i_{c2}, i_{n2}]^T$ on the right terminal of the multi-section line,

$$i_2(t) = C_N \frac{dv_{N+1}(t)}{dt} - i_{LN}(t) \tag{4.17}$$

For the intersection between the kth line and k+1th line, the law of KCL holds (k=1,…N-1):

$$0_{KCL,k,k+1} = C_k \frac{dv_{k+1}(t)}{dt} - i_{Lk}(t) + C_{k+1} \frac{dv_{k+1}(t)}{dt} + i_{Lk+1}(t) \tag{4.18}$$

For the kth line, the law of KVL holds (k=1,…N):

$$0_{KVL,k} = -v_k + v_{k+1} + R_k i_{Lk}(t) + L_k \frac{di_{Lk}(t)}{dt} \tag{4.19}$$

where R_k, L_k, C_k are four-phase resistance, inductance, and capacitance of the kth line (k=1,…N).

By stacking all the individual equations into matrices, the above model can be written into compact form:

$$\begin{bmatrix} i_1(t) \\ i_2(t) \\ 0_{KCL,k,k+1}(t) \\ 0_{KVL,k}(t) \end{bmatrix} = Ax + B\frac{dx}{dt} \tag{4.20}$$

where,

$$A = \begin{bmatrix} 0 & \cdots & \cdots & 0 & I_4 & 0 & \cdots & 0 \\ 0 & \cdots & \cdots & 0 & 0 & \cdots & 0 & -I_4 \\ 0 & \cdots & \cdots & 0 & -I_4 & I_4 & \cdots & 0 \\ \vdots & \vdots & \vdots & \vdots & \vdots & \vdots & \vdots & \vdots \\ 0 & \cdots & \cdots & 0 & 0 & \cdots & -I_4 & I_4 \\ -I_4 & I_4 & \cdots & 0 & R_1 & \cdots & \cdots & 0 \\ \vdots & \vdots & \vdots & \vdots & \vdots & \vdots & \vdots & \vdots \\ 0 & \cdots & -I_4 & I_4 & 0 & \cdots & \cdots & R_N \end{bmatrix}$$

$$B = \begin{bmatrix} C_1 & \cdots & \cdots & 0 & 0 & \cdots & \cdots & 0 \\ 0 & \cdots & \cdots & C_N & 0 & \cdots & \cdots & 0 \\ 0 & C_1 + C_2 & \cdots & 0 & 0 & \cdots & \cdots & 0 \\ \vdots & \vdots & \vdots & \vdots & \vdots & \vdots & \vdots & \vdots \\ 0 & \cdots & C_{N-1} + C_N & 0 & 0 & \cdots & \cdots & 0 \\ 0 & \cdots & \cdots & 0 & L_1 & \cdots & \cdots & 0 \\ \vdots & \vdots & \vdots & \vdots & \vdots & \vdots & \vdots & \vdots \\ 0 & \cdots & \cdots & 0 & 0 & \cdots & \cdots & L_N \end{bmatrix}$$

Since this model is also linear, no quadratization process is needed, the quadratized model is same as compact model.

4.4.2 Transmission Line in Time Domain – Multi Section SCAQCF Device Model

The algebraic companion form model is derived after quadratic integration similarly as in Section 4.3.2.

$$A_1\begin{bmatrix} i_1(t) \\ i_2(t) \\ 0_{KCL}(t) \\ 0_{KVL}(t) \\ i_1(t_m) \\ i_2(t_m) \\ 0_{KCL}(t_m) \\ 0_{KVL}(t_m) \end{bmatrix} = \begin{bmatrix} \frac{h}{6}A+B & \frac{2h}{3}A \\ -\frac{h}{24}A & \frac{h}{3}A+B \end{bmatrix}\begin{bmatrix} x(t) \\ x(t_m) \end{bmatrix} - \begin{bmatrix} B-\frac{h}{6}A \\ B-\frac{5h}{24}A \end{bmatrix} x(t-h) - A_2\begin{bmatrix} i_1(t-h) \\ i_2(t-h) \\ 0_{KCL}(t-h) \\ 0_{KVL}(t-h) \end{bmatrix} \tag{4.21}$$

where:

$$A_1 = \begin{bmatrix} \frac{h}{6}I_4 & 0_4 & 0_{4\times 4(N-1)} & 0_{4\times 4N} & \frac{2h}{3}I_4 & 0_4 & 0_{4\times 4(N-1)} & 0_{4\times 4N} \\ 0_4 & \frac{h}{6}I_4 & 0_{4\times 4(N-1)} & 0_{4\times 4N} & 0_4 & \frac{2h}{3}I_4 & 0_{4\times 4(N-1)} & 0_{4\times 4N} \\ 0_{4(N-1)\times 4} & 0_{4(N-1)\times 4} & 0_{4(N-1)\times 4(N-1)} & 0_{4(N-1)\times 4N} & 0_{4(N-1)\times 4} & 0_{4(N-1)\times 4} & 0_{4(N-1)\times 4(N-1)} & 0_{4(N-1)\times 4N} \\ 0_{4N\times 4} & 0_{4N\times 4} & 0_{4N\times 4(N-1)} & 0_{4N\times 4N} & 0_{4N\times 4} & 0_{4N\times 4} & 0_{4N\times 4(N-1)} & 0_{4N\times 4N} \\ -\frac{h}{24}I_4 & 0_4 & 0_{4\times 4(N-1)} & 0_{4\times 4N} & \frac{h}{3}I_4 & 0_4 & 0_{4\times 4(N-1)} & 0_{4\times 4N} \\ 0_4 & -\frac{h}{24}I_4 & 0_{4\times 4(N-1)} & 0_{4\times 4N} & 0_4 & \frac{h}{3}I_4 & 0_{4\times 4(N-1)} & 0_{4\times 4N} \\ 0_{4(N-1)\times 4} & 0_{4(N-1)\times 4} & 0_{4(N-1)\times 4(N-1)} & 0_{4(N-1)\times 4N} & 0_{4(N-1)\times 4} & 0_{4(N-1)\times 4} & 0_{4(N-1)\times 4(N-1)} & 0_{4(N-1)\times 4N} \\ 0_{4N\times 4} & 0_{4N\times 4} & 0_{4N\times 4(N-1)} & 0_{4N\times 4N} & 0_{4N\times 4} & 0_{4N\times 4} & 0_{4N\times 4(N-1)} & 0_{4N\times 4N} \end{bmatrix}$$

$$A_2 = \begin{bmatrix} \frac{h}{6}I_4 & 0_4 & 0_{4\times 4(N-1)} & 0_{4\times 4N} \\ 0 & \frac{h}{6}I_4 & 0_{4\times 4(N-1)} & 0_{4\times 4N} \\ 0_{4(N-1)\times 4} & 0_{4(N-1)\times 4} & 0_{4(N-1)\times 4(N-1)} & 0_{4(N-1)\times 4N} \\ 0_{4N\times 4} & 0_{4N\times 4} & 0_{4N\times 4(N-1)} & 0_{4N\times 4N} \\ \frac{5h}{24}I_4 & 0_4 & 0_{4\times 4(N-1)} & 0_{4\times 4N} \\ 0 & \frac{5h}{24}I_4 & 0_{4\times 4(N-1)} & 0_{4\times 4N} \\ 0_{4(N-1)\times 4} & 0_{4(N-1)\times 4} & 0_{4(N-1)\times 4(N-1)} & 0_{4(N-1)\times 4N} \\ 0_{4N\times 4} & 0_{4N\times 4} & 0_{4N\times 4(N-1)} & 0_{4N\times 4N} \end{bmatrix}$$

Let

$$E=\begin{bmatrix} \frac{4}{h}I_8 & 0_{8\times 4(2N-1)} & -\frac{8}{h}I_8 & 0_{8\times 4(2N-1)} \\ 0_{4(2N-1)\times 8} & I_{4(2N-1)\times 4(2N-1)} & 0_{4(2N-1)\times 8} & 0_{4(2N-1)\times 4(2N-1)} \\ \frac{1}{2h}I_8 & 0_{8\times 4(2N-1)} & \frac{2}{h}I_8 & 0_{8\times 4(2N-1)} \\ 0_{4(2N-1)\times 8} & 0_{4(2N-1)\times 4(2N-1)} & 0_{4(2N-1)\times 8} & I_{4(2N-1)\times 4(2N-1)} \end{bmatrix}$$

$$F_1=\begin{bmatrix} \frac{h}{6}A+B & \frac{2h}{3}A \\ -\frac{h}{24}A & \frac{h}{3}A+B \end{bmatrix}$$

$$F_2=\begin{bmatrix} B-\frac{h}{6}A \\ B-\frac{5h}{24}A \end{bmatrix}$$

Then in the format of (4.9), (4.21) becomes

$$\begin{Bmatrix} i(t) \\ 0 \\ 0 \\ i(t_m) \\ 0 \\ 0 \end{Bmatrix} = Y_{eqx}\mathbf{x}+\begin{Bmatrix} \vdots \\ \mathbf{x}^T\left\langle F_{eqx}^i\right\rangle\mathbf{x} \\ \vdots \end{Bmatrix}-B_{eq} \tag{4.22}$$

$$\boldsymbol{B}_{eq}=-\boldsymbol{N}_{eqx}\mathbf{x}(t-h)-\boldsymbol{M}_{eq}\boldsymbol{i}(t-h)-\boldsymbol{K}_{eq} \tag{4.23}$$

where,

$Y_{eqx}=-E\times F_1$

$F_{eqx}=0$

$N_{eqx}=-E\times F_2$

$M_{eq}=E\times A_2$

$K_{eq}=0$

The definition of the external state, internal state, and through variables are listed in Table 4.4 to Table 4.6, respectively.

Table 4.4. External states of the four phase transmission line – multi section.

Index	Variable	Description
0	$v_{a1}(t)$	voltage of phase A to ground on left terminal
1	$v_{b1}(t)$	voltage of phase B to ground on left terminal
2	$v_{c1}(t)$	voltage of phase C to ground on left terminal
3	$v_{n1}(t)$	voltage of phase N to ground on left terminal
4*N	$v_{a(N+1)}(t)$	voltage of phase A to ground on right terminal
4*N+1	$v_{b(N+1)}(t)$	voltage of phase A to ground on right terminal
4*N+2	$v_{c(N+1)}(t)$	voltage of phase A to neutral on right terminal
4*N+3	$v_{n(N+1)}(t)$	voltage of phase A to neutral on right terminal

Table 4.5. Internal states of the four phase transmission line – multi section.

Index	Variable	Description
4*1	$v_{a2}(t)$	voltage of phase A to ground on right terminal of the first section
4*1+1	$v_{b2}(t)$	voltage of phase B to ground on right terminal of the first section
4*1+2	$v_{c2}(t)$	voltage of phase C to ground on right terminal of the first section
4*1+3	$v_{n2}(t)$	voltage of phase N to ground on right terminal of the first section
…		…
4*k	$v_{ak}(t)$	Voltage of phase A to ground on right terminal of the k^{th} section (k=1,2…N-1)
4*k+1	$v_{bk}(t)$	Voltage of phase B to ground on right terminal of the k^{th} section (k=1,2…N-1)
4*k+2	$v_{ck}(t)$	Voltage of phase C to ground on right terminal of the k^{th} section (k=1,2…N-1)
4*k+3	$v_{nk}(t)$	Voltage of phase N to ground on right terminal of the k^{th} section (k=1,2…N-1)
…		
4*(N+1)	$i_{La1}(t)$	current through the inductance of phase A at the first section
4*(N+1)+1	$i_{La1}(t)$	current through the inductance of phase B at the first section

4*(N+1)+2	$i_{La1}(t)$	current through the inductance of phase C at the first section
4*(N+1)+3	$i_{La1}(t)$	current through the inductance of phase N at the first section
…		…
4*(N+1+k)	$i_{La1}(t)$	current through the inductance of phase A at the k^{th} section
4*(N+1+k)+1	$i_{La1}(t)$	current through the inductance of phase B at the k^{th} section
4*(N+1+k)+2	$i_{La1}(t)$	current through the inductance of phase C at the k^{th} section
4*(N+1+k)+3	$i_{La1}(t)$	current through the inductance of phase N at the k^{th} section
…		…

Table 4.6. Through variables of the four phase transmission line – multi section.

Index	Variable	Description
0	$i_{a1}(t)$	current through transmission line phase a left terminal
1	$i_{b1}(t)$	current through transmission line phase b left terminal
2	$i_{c1}(t)$	current through transmission line phase c left terminal
3	$i_{n1}(t)$	current through transmission line phase n left terminal
4	$i_{a2}(t)$	current through transmission line phase a right terminal
5	$i_{b2}(t)$	current through transmission line phase b right terminal
6	$i_{c2}(t)$	current through transmission line phase c right terminal
7	$i_{n2}(t)$	current through transmission line phase n right terminal

4.4.3 Transmission Line in Time Domain –Multi Section SCAQCF Measurement Model

In this thesis, the transmission line protective relay needs access to the voltages and currents on both terminals of the line, so the actual measurements are: 1) Three phase currents at left and right sides at time t, t_m – extracted from device model; 2) Three phase-to-neutral voltages at left and right sides at time t, t_m – linear combination of external states; 3) The 4 pseudo measurements are neutral voltages on left and right sides at time t, t_m – linear combination of external states; 4) The 8*(2N-1) virtual measurements are 8*(N-1)

zero values from KCL at intersection of each neighboring single sections, and 8*N zeros values from KVL for the loop at each phase for each single section at time t, t_m – extracted from device model; There are in total 8*(2*N+1)+12 measurements and 8*(2*N+1) states, with a redundancy of 3/(2*(2*N+1))%.

4.5 Summary

The mathematical formulation and derivation of the SCAQCF model for power system components were presented in this chapter. Detailed examples for the derivation of the SCAQCF models of the transmission line for both single section and multi section have been presented in this chapter to illustrate the procedure of obtaining the SCAQCF model for a component.

CHAPTER 5 DYNAMIC STATE ESTIMATION AND PROTECTION LOGIC

5.1 Overview

Given the measurement model in (4.6), the dynamic state estimation problem is formulated as the estimation of the present state from measured values and past history. Three algorithms are described for performing the dynamic state estimation. The unconstrained weighted least square method is referred in [47].

The first algorithm treats the virtual measurement as high fidelity measurement with small standard deviation, the problem is formulated as unconstraint optimization problem; The second algorithm treats the virtual measurements as hard constraints, the problem is formulated as constraint optimization problem; The third algorithm uses the widely accepted Kalman Filter for linear model.

5.2 Unconstraint Weighted Least Square Method

The first proposed dynamic state estimation algorithm is a weighted least square (WLS) that minimizes the objective function consisting of the squared normalized residuals of all measurements including virtual measurements:

$$\text{Min } J_1(x(t,t_m)) = \left[z(t,t_m) - h(x(t,t_m))\right]^T W \left[z(t,t_m) - h(x(t,t_m))\right] \qquad (5.1)$$

where $z(t,t_m) = \left[z_m(t) \quad z_m(t_m)\right]$ is combination of all available measurements including 1) actual measured value, derived value, pseudo value and 2) virtual value.

Here the past history $\hat{C}(t-h)$ uses estimated state and measured value at t-h:

$$\hat{C}_m(t-h) = N_{mx}\hat{x}(t-h) + M_m i(t-h) + K_m \tag{5.2}$$

The weight matrix W reflects modeling of the noise statistics of the measurements. In this thesis squared value of the standard deviation of each measurement is used as reciprocal of the diagonal entries of the weight matrix. Firstly, the standard deviations of the residuals from physical or derived quantities are modeled directly from instrumentation channels. Secondly, pseudo measurements are only hypothetical measurements that we have an idea of their expected value, i.e., first moment, but not their standard deviation, i.e., second moment, they're assigned a large standard deviation that they can reach, for example 0.1pu. Virtual measurements are assigned a very small standard deviation, for example 0.001pu.

Given that the measurement models are at most quadratic, the objective function is nonconvex. The Karush-Kuhn-Tucker (KKT) necessary condition to the local optima point is the gradient equals zero:

$$\nabla J_1(x) = 0 \tag{5.3}$$

The gradient can be computed in the following way:

$$\begin{aligned} \nabla J_1(x) &= \left[\frac{\partial J_1}{\partial x_1} \quad \cdots \quad \frac{\partial J_1}{\partial x_n}\right]^T = \left[\sum_{j=1}^{m}\frac{\partial J_1}{\partial h_j}\frac{\partial h_j(x)}{\partial x_1} \quad \cdots \quad \sum_{j=1}^{m}\frac{\partial J_1}{\partial h_j}\frac{\partial h_j(x)}{\partial x_n}\right]^T \\ &= \left(\nabla J_1(h)\cdot\frac{dh(x)}{dx}\right)^T = \left(\nabla J_1(h)\cdot H\right)^T = 2\left((h(x)-z)^T WH\right)^T \end{aligned} \tag{5.4}$$

And the solution of:

$$\nabla J_1(x)^T = f(x) = 2H^T W(h(x)-z) = 0 \tag{5.5}$$

can be solved by Newton Raphson's iterative method:

$$x_{j+1} = x_j - \left(\frac{\partial f}{\partial x}\right)^{-1} f(x)|_{x_j} = x_j - \left(H^T WH\right)^{-1} H^T W\left(h(x_j)-z\right) \tag{5.6}$$

Specifically, let $\hat{x}_j(t,t_m)$ be the estimated states at iteration j from time t and tm, then the solution is updated by Newton's iterative method at each iteration:

$$\hat{x}_{j+1}(t,t_m) = \hat{x}_j(t,t_m) + \left(H^T W H\right)^{-1} H^T W \left(z(t,t_m) - h\left(\hat{x}_j(t,t_m)\right)\right) \tag{5.7}$$

Where $\hat{x}_j(t,t_m)$ is the estimated state at j[th] iteration. $H = \frac{\partial h(x(t,t_m))}{\partial x}|_{x=\hat{x}_j(t,t_m)}$ is the Jacobian matrix of $h(x)$. The past history $\hat{C}_m$ uses $\hat{x}(t-h)$ which is the best estimate of previous time step. The algorithm terminates when $|\hat{x}_{j+1} - \hat{x}_j| < \xi$, let $\hat{x}(t,t_m) = \hat{x}_{j+1}(t,t_m)$ where $\hat{x}(t,t_m) = \left[\hat{x}(t) \quad \hat{x}(t_m)\right]$ is the best estimate of states at time t and t_m.

The initialization of the states at time t and tm are the best estimate of the states at time t-h, i.e., $\hat{x}_0(t,t_m) = \hat{x}(t-h)$. The detailed algorithm is in Figure 5-1 for nonlinear case.

Since the transmission line model is linear (both single section and multi section), the unconstraint optimization problem becomes a convex problem, and the necessary condition for the local optima is also the necessary condition for global optima:

$$0 = H^T W(h(x) - z) = H^T W(Hx + \hat{C}_m - z) = H^T WHx - H^T W(z - \hat{C}_m) \tag{5.8}$$

where the Jacobian matrix is a constant matrix regardless of x,

$$h(x) = Y_{mx}x + \hat{C}_m$$

$$H = \frac{\partial h(x)}{\partial x} = Y_{mx}$$

The solution of (5.8) is straightforward, since the matrix $H^T WH$ is non-singular (as a matter of fact it is positive semidefinite):

$$\hat{x}(t,t_m) = \left(H^T WH\right)^{-1} H^T W\left(z - \hat{C}_m\right) \tag{5.9}$$

The detailed algorithm for linear case is in Figure 5-2.

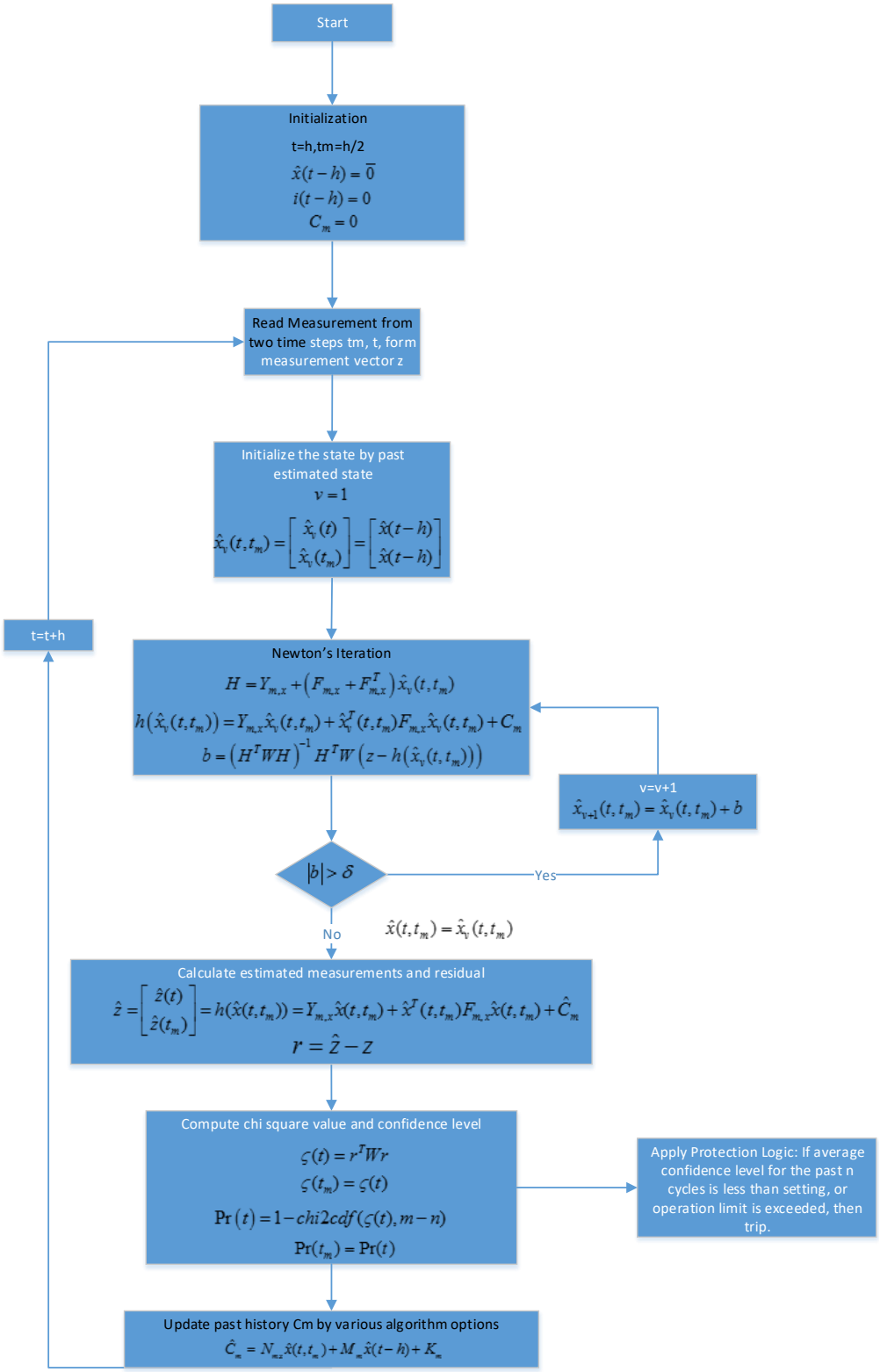

Figure 5-1 Dynamic State Estimation Algorithm – Unconstraint Optimization, Nonlinear Case

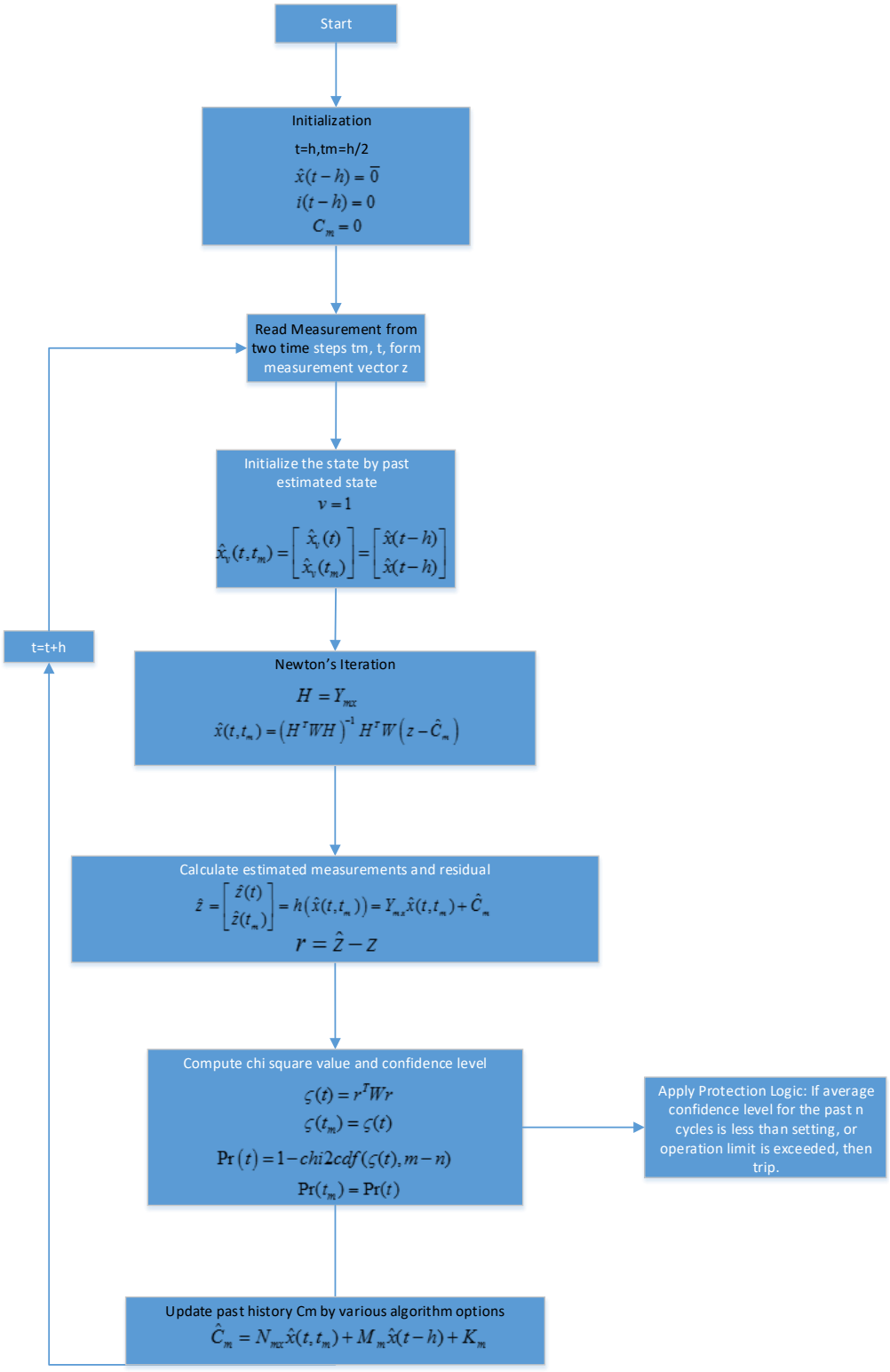

Figure 5-2 Dynamic State Estimation Algorithm – Unconstraint Optimization, Linear Case

5.3 Constraint Weighted Least Square Method

The unconstraint weighted least square method is particularly useful when there is modelling error: such that the measured value for KVL on each phase is not exactly zero, in single section models. Whereas in some other models, if the model is accurate enough, then the hard constraints might apply. In this case, the estimation problem is converted to a constraint optimization problem to minimize the objective function consisting of the squared normalized residuals of all measurements excluding virtual measurements:

$$\begin{aligned} \text{Min } J_2(x,t,t_m) &= \left[z(t,t_m) - h(x,t,t_m))\right]^T W \left[z(t,t_m) - h(x,t,t_m))\right] \\ \text{s.t. } g(x,t,t_m)) &= 0 \end{aligned} \tag{5.10}$$

whereas in this case, $z(t,t_m) = \left[z_m(t) \;\; z_m(t_m)\right]$ is combination of all available measurements including actual measured value, derived value, and pseudo value. Notice that virtual value is not included in the objective function, but it appears in the constraints $g(x,t,t_m) = 0$, so h(x) is only the set of measurement functions containing actual measurement, derived measurement and pseudo measurement.

The solution of this optimization problem starts with defining the Lagrangian function:

$$L(x,\lambda,t,t_m) = J_2(x,t,t_m) + 2\lambda^T g(x,t,t_m) \tag{5.11}$$

Where λ is called the KKT multiplier or Lagrangian multiplier.

The Karush-Kuhn-Tucker (KKT) necessary condition to the local optima point is the gradient equals zero:

$$\nabla_{x,\lambda} L(x,\lambda,t,t_m) = \left[\frac{\partial J_2(x,t,t_m)}{\partial x} + 2\lambda^T \frac{\partial g(x,t,t_m)}{\partial x} \quad g(x,t,t_m)\right] = 0 \tag{5.12}$$

where the partial derivative of L to x is:

$$\frac{\partial L(x,\lambda,t,t_m)}{\partial x} = -2\left(z(t,t_m) - h(x,t,t_m)\right)^T W \frac{\partial h(x,t,t_m)}{\partial x} + 2\lambda^T \frac{\partial g(x,t,t_m)}{\partial x} = 0 \tag{5.13}$$

Or equivalently:

$$\left(\frac{\partial h(x)}{\partial x}\right)^T Wh(x) + \left(\frac{\partial g(x)}{\partial x}\right)^T \lambda = \left(\frac{\partial h(x)}{\partial x}\right)^T Wz \tag{5.14}$$

where $h(x,t,t_m)$ and $g(x,t,t_m)$ are shortened as $h(x)$ and $g(x)$.

Thus the optimization problem is equivalent to solving the following equation:

$$f = \begin{bmatrix} f_1(x,\lambda) \\ f_2(x,\lambda) \end{bmatrix} = \begin{bmatrix} \left(\frac{\partial h(x)}{\partial x}\right)^T Wh(x) + \left(\frac{\partial g(x)}{\partial x}\right)^T \lambda - \left(\frac{\partial h(x)}{\partial x}\right)^T Wz \\ g(x) \end{bmatrix} = 0 \tag{5.15}$$

Such problem can again be solved through Newton Raphson's iterative method:

$$\begin{aligned} \begin{bmatrix} x_{j+1} \\ \lambda_{j+1} \end{bmatrix} &= \begin{bmatrix} x_j \\ \lambda_j \end{bmatrix} - \begin{pmatrix} \frac{\partial f_1(x,\lambda)}{\partial x} & \frac{\partial f_1(x,\lambda)}{\partial \lambda} \\ \frac{\partial f_2(x,\lambda)}{\partial x} & \frac{\partial f_2(x,\lambda)}{\partial \lambda} \end{pmatrix}^{-1} \begin{bmatrix} f_1(x_j,\lambda_j) \\ f_2(x_j,\lambda_j) \end{bmatrix}_{x_j,\lambda_j} \\ &= \begin{bmatrix} x_j \\ \lambda_j \end{bmatrix} - \begin{pmatrix} \left(\frac{\partial h(x)}{\partial x}\right)^T W \frac{\partial h(x)}{\partial x} + \left(\frac{\partial^2 g}{\partial x^2}\right)^T \lambda - \left(\frac{\partial^2 h}{\partial x^2}\right)^T W(h(x)-z) & G^T \\ G & 0 \end{pmatrix}^{-1} \begin{bmatrix} \left(\frac{\partial h(x)}{\partial x}\right)^T W(h(x)-z) + \left(\frac{\partial g}{\partial x}\right)^T \lambda \\ g(x) \end{bmatrix}_{x_j,\lambda_j} \end{aligned} \tag{5.16}$$

Specifically, let $\hat{x}_j(t,t_m)$ be the estimated states and $\hat{\lambda}_j(t,t_m)$ be the estimated multiplier at iteration j from time t and tm, then the solution is updated by Newton's iterative method at each iteration:

$$\begin{bmatrix} \hat{x}_{j+1}(t,t_m) \\ \hat{\lambda}_{j+1}(t,t_m) \end{bmatrix} = \begin{bmatrix} \hat{x}_j(t,t_m) \\ \hat{\lambda}_j(t,t_m) \end{bmatrix} - \begin{pmatrix} H^T WH & G^T \\ G & 0 \end{pmatrix}^{-1} \begin{bmatrix} H^T W(h(\hat{x}_j(t,t_m)) - z) + G^T \hat{\lambda}_j(t,t_m) \\ g(\hat{x}_j(t,t_m)) \end{bmatrix} \tag{5.17}$$

Where $\hat{x}_j(t,t_m)$ is the estimated state and $\hat{\lambda}_j(t,t_m)$ at j[th] iteration. $H = \frac{\partial h(x(t,t_m))}{\partial x}|_{x=\hat{x}_j(t,t_m)}$ is the Jacobian matrix of $h(x)$, $G = \frac{\partial g(x(t,t_m))}{\partial x}|_{x=\hat{x}_j(t,t_m)}$ is the Jacobian matrix of g(x). The past history $\hat{C}_m$ uses $\hat{x}(t-h)$ which is the best estimate of previous time step. The algorithm

terminates when $|\hat{x}_{j+1}-\hat{x}_j|<\xi$, let $\hat{x}(t,t_m)=\hat{x}_{j+1}(t,t_m)$ where $\hat{x}(t,t_m)=\left[\hat{x}(t)\quad \hat{x}(t_m)\right]$ is the best estimate of states at time t and t_m.

The initialization of the states at time t and tm are the best estimate of the states at time t-h, i.e., $\hat{x}_0(t,t_m)=\hat{x}(t-h)$. The detailed algorithm is in for nonlinear case is illustrated in Figure **5-3**.

Since the transmission line model is linear (both single section and multi section), the constraint optimization problem has a convex objective function, and since the constraint becomes linear, the optimization problem becomes a convex optimization problem. The necessary condition for the local optima is also the necessary condition for global optima:

$$0=\begin{bmatrix}\left(\frac{\partial h(x)}{\partial x}\right)^T Wh(x)+\left(\frac{\partial g(x)}{\partial x}\right)^T\lambda-\left(\frac{\partial h(x)}{\partial x}\right)^T Wz\\ g(x)\end{bmatrix}=\begin{bmatrix}H^TW\left(Hx-\hat{C}_m^1\right)+G^T\lambda-H^TWz\\ Gx-\hat{C}_m^2\end{bmatrix} \tag{5.18}$$

where the Jacobian matrix is a constant matrix regardless of x,

$$h(x)=Y_{mx}^1x+\hat{C}_m^1$$

$$g(x)=Y_{mx}^2x+\hat{C}_m^2$$

$$H=\frac{\partial h(x)}{\partial x}=Y_{mx}^1$$

$$G=\frac{\partial g(x)}{\partial x}=Y_{mx}^2$$

The solution of (5.18) is straightforward, since the matrix H^TWH is non-singular (as a matter of fact it is positive semidefinite):

$$\begin{bmatrix}\hat{x}(t,t_m)\\ \hat{\lambda}(t,t_m)\end{bmatrix}=\begin{bmatrix}H^TWH & G^T\\ G & 0\end{bmatrix}^{-1}\begin{bmatrix}H^TW\left(z-\hat{C}_m^1\right)\\ -\hat{C}_m^2\end{bmatrix} \tag{5.19}$$

The detailed algorithm for linear case is in Figure **5-4**.

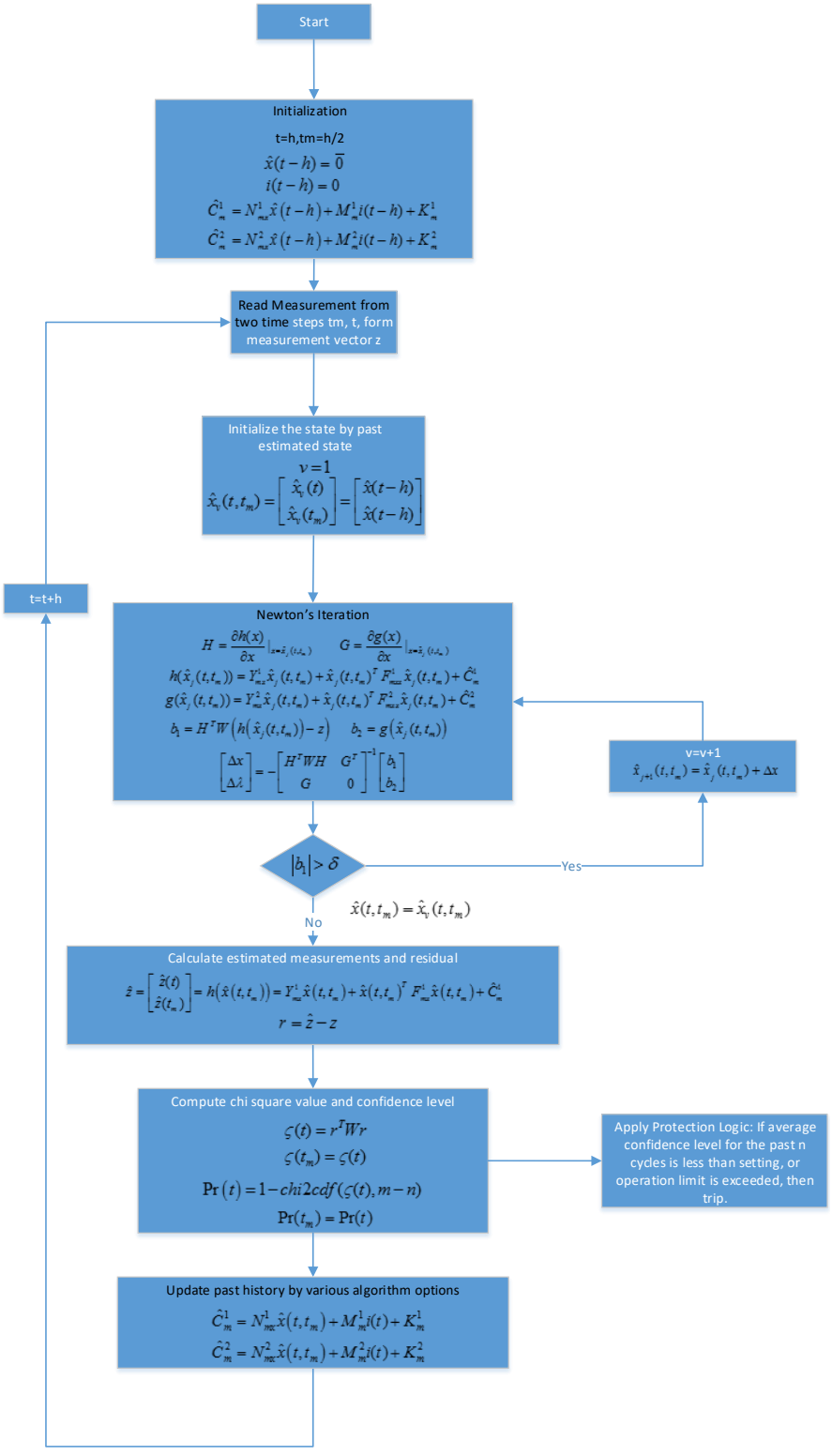

Figure 5-3 Dynamic State Estimation Algorithm – Constraint Optimization, Nonlinear Case

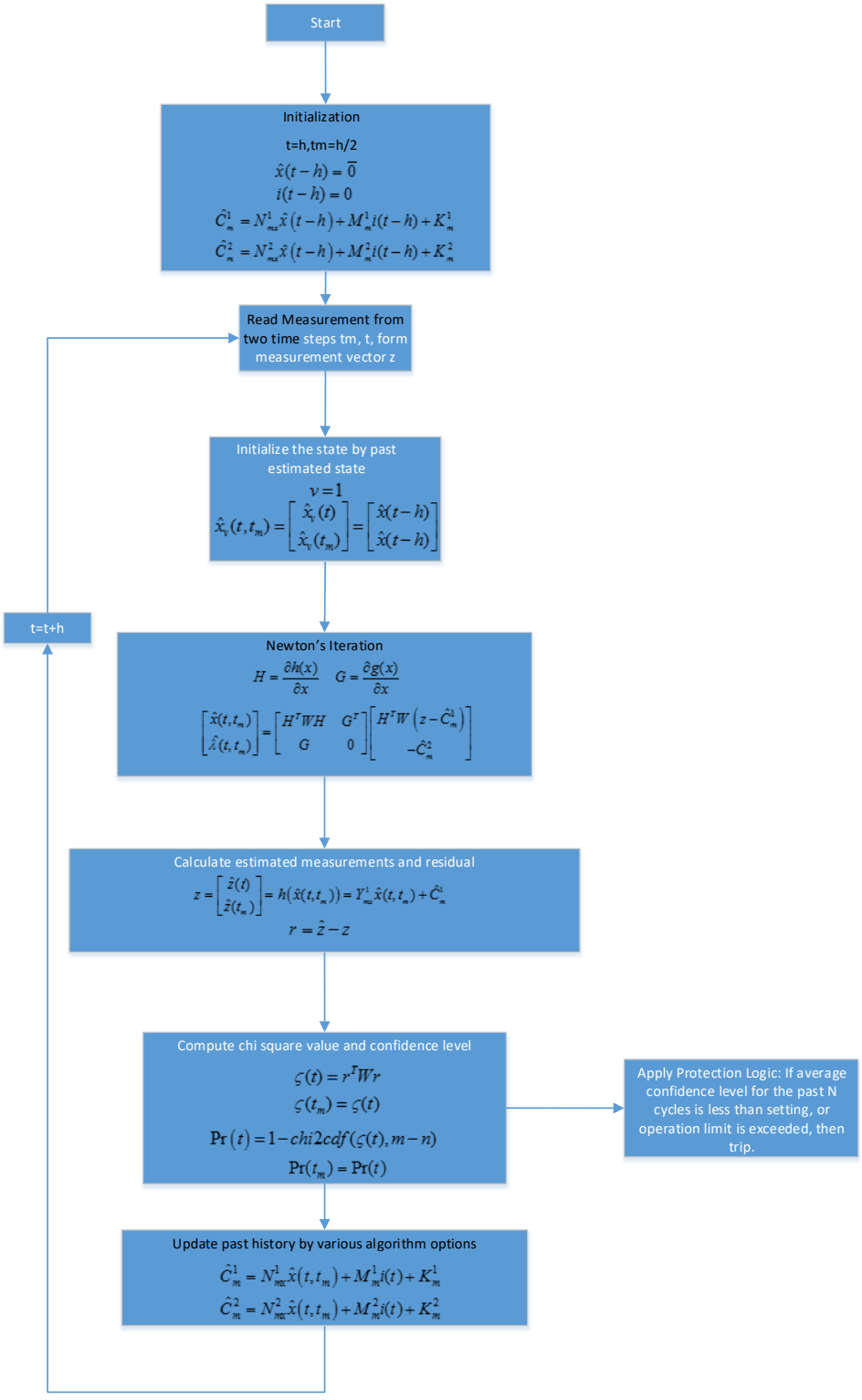

Figure 5-4 Dynamic State Estimation Algorithm – Constraint Optimization, Linear Case

5.4 Kalman Filtering for Linear SCAQCF Models

For linear models, Kalman Filter has long been recognized as the optimal estimator given that 1) the model is highly accurate and 2) the probability distribution of the noises is Gaussian [51]. The algorithm uses the system's dynamic model, known control inputs to that system, and a series of measurements observed over time, containing statistical noise and other inaccuracies, and produce estimates of unknown variables. The Kalman filtering has had numerous applications in technologies mostly for guidance, navigation and control of vehicles particularly aircraft and spacecraft, robotic motion control, trajectory optimization, etc. For power system applications, such techniques (Extended Kalman Filter) have recently caught attention mainly for synchronous generator monitoring. Transmission lines models described in Chapter 4 as linear time-invariant systems, however, may carry modeling error. Possible modeling errors include 1) temperature is a factor that influences resistance of the transmission line. In practice, the conductor temperature varies in the range of 0^{o} to 60^{o}. The resistance varies linearly with temperature within that range. Only by gathering the temperature data along the line would the algorithm be able to change the parameters of the system model in real-time. 2) the lines along towers may have line sags such that the height of the conductors is not evenly distributed, that affects the modeling of both resistance and inductance, and in this case the parameters of the model (resistance and inductance) would vary nonlinearly with the height. Another factor that influences the Kalman filter on the dynamic state estimation of transmission line is that measurement error does not always conform to Gaussian distribution due to the potential transformer and current transformer: sometimes the measurement error may even be biased. Due to the many reasons above, Kalman filter may not be the optimal estimator in field test, and future

work would need to investigate the performance of the three algorithms described here from any field gathered data.

This section includes the formulation of the Kalman filter to the linear transmission line model.

For Kalman filter to be applied to the transmission line model, the SCAQCF linear model (where $F_{eqx}=0$) should be converted in the way such that the states at time t (and tm) is a function of the states at time t-h. Refer to the SCAQCF device model in (4.5):

$$\begin{Bmatrix} i(t) \\ 0 \\ 0 \\ i(t_m) \\ 0 \\ 0 \end{Bmatrix} = Y_{eqx}\mathbf{x} + \begin{Bmatrix} \vdots \\ \mathbf{x}^T \left\langle F_{eqx}^i \right\rangle \mathbf{x} \\ \vdots \end{Bmatrix} - B_{eq} \tag{5.20}$$

$$\boldsymbol{B}_{eq} = -\boldsymbol{N}_{eqx}\mathbf{x}(t-h) - \boldsymbol{M}_{eq}\boldsymbol{i}(t-h) - \boldsymbol{K}_{eq} \tag{5.21}$$

where $x = \begin{bmatrix} x(t) & x(t_m) \end{bmatrix}^T$, when the model is linear and Y_{eqx} is full rank, this is equivalent to:

$$\begin{bmatrix} x(t) \\ x(t_m) \end{bmatrix} = -Y_{eqx}^{-1}N_{eqx}x(t-h) + Y_{eqx}^{-1}\left(\begin{bmatrix} i(t) \\ 0 \\ 0 \\ i(t_m) \\ 0 \\ 0 \end{bmatrix} - M_{eq}i(t-h) - K_{eq} \right) \tag{5.22}$$

(5.22) gives the system model needed to update the *a priori* states at time *t* or *tm* from the *posteriori* states at time t-h, from SCAQCF model. And the SCAQCF measurement model gives the measurement function for correcting the *posteriori* states at time t or tm from the *a priori* states at time t or tm:

$$\begin{bmatrix} x(t) \\ x(t_m) \end{bmatrix} = -Y_{eqx}^{-1} N_{eqx} x(t-h) + Y_{eqx}^{-1} \left(\begin{bmatrix} i(t) \\ 0 \\ 0 \\ i(t_m) \\ 0 \\ 0 \end{bmatrix} - M_{eq} i(t-h) - K_{eq} \right)$$
$$z = \begin{bmatrix} z(t) \\ z(t_m) \end{bmatrix} = Y_{mx} \begin{bmatrix} x(t) \\ x(t_m) \end{bmatrix} + N_{mx} x(t-h) + M_m i(t-h) + K_m \tag{5.23}$$

The above equations neglect the nonlinear terms (F_{eqxx}).

As a result the Kalman filter could be applied. Specifically, there are prediction step and correction step:

Prediction of the *a priori* states and computation of the covariance of the *a priori* states:

a priori states:

$$\begin{bmatrix} \hat{x}(t \mid t-h) \\ \hat{x}(t_m \mid t-h) \end{bmatrix} = -Y_{eqx}^{-1} N_{eqx} \hat{x}(t-h \mid t-h) + Y_{eqx}^{-1} \left(\begin{bmatrix} i(t) \\ 0 \\ 0 \\ i(t_m) \\ 0 \\ 0 \end{bmatrix} - M_{eq} i(t-h) - K_{eq} \right) \tag{5.24}$$

Covariance of *a priori* states:

$$P(t, t_m \mid t-h) = \left(Y_{eqx}^{-1} N_{eqx} \right) P(t-h \mid t-h) \left(Y_{eqx}^{-1} N_{eqx} \right)^T \tag{5.25}$$

Correction of the *a priori* states into *posteriori* states:

Innovation:

$$\begin{aligned} \begin{bmatrix} \tilde{y}(t) \\ \tilde{y}(t_m) \end{bmatrix} &= \begin{bmatrix} z(t) \\ z(t_m) \end{bmatrix} - Y_{mx} \begin{bmatrix} \hat{x}(t \mid t-h) \\ \hat{x}(t_m \mid t-h) \end{bmatrix} - \hat{C}_m \\ &= \begin{bmatrix} z(t) \\ z(t_m) \end{bmatrix} - Y_{mx} \begin{bmatrix} \hat{x}(t \mid t-h) \\ \hat{x}(t_m \mid t-h) \end{bmatrix} - N_m \hat{x}(t-h \mid t-h) - M_m i(t-h) - K_m \end{aligned} \tag{5.26}$$

Innovation Covariance:

$$S(t,t_m) = HP(t,t_m \mid t-h)H^T + R_k \tag{5.27}$$

Optimal Kalman Gain:

$$K(t,t_m) = P(t,t_m \mid t-h)H^T S^{-1}(t,t_m) \tag{5.28}$$

Update *posteriori* state estimate:

$$\hat{x}(t,t_m \mid t,t_m) = \hat{x}(t,t_m \mid t-h) + K(t,t_m)\cdot\begin{bmatrix}\tilde{y}(t)\\ \tilde{y}(t_m)\end{bmatrix} \tag{5.29}$$

Update *posteriori* state estimate covariance:

$$P(t,t_m \mid t,t_m) = (I - K(t,t_m)H)P(t,t_m \mid t-h) \tag{5.30}$$

where,

$\hat{x}(t \mid t-h)$: a priori state estimate for time t given the measurements up to t-h

$\hat{x}(t_m \mid t-h)$: a priori state estimate for time tm given the measurements up to t-h

$P(t,t_m \mid t-h)$: covariance matrix of the a priori state estimates at both time t and tm given the measurements up to t-h

$P(t-h \mid t-h)$: covariance matrix of the posteriori state estimates at time t-h given the measurements up to t-h

$\tilde{y}(t)$: innovation at time t

$\tilde{y}(t_m)$: innovation at time tm

$S(t,t_m)$: the covariance matrix of the innovations at both time t and tm

$K(t,t_m)$: the computed Kalman gain for both time t and tm

$\hat{x}(t \mid t,t_m)$: posteriori state estimate for time t given the measurements up to t

$\hat{x}(t_m \mid t,t_m)$: posteriori state estimate for time tm given the measurements up to tm

$P(t,t_m \mid t,t_m)$: covariance matrix for the posteriori state estimates at both time t and tm given the measurements up to t

5.5 Hypothesis Testing and Protection Logic

The solution of the dynamic state estimation provides the best estimate of the dynamic states of the component. The fault detection is divided into two steps: 1) hypothesis testing (chi square test and confidence level computation), 2) protection logic.

1): Specifically, substitution of the estimated state values into the measurement model generates the estimated measurements:

$$\hat{z} = \begin{bmatrix} \hat{z}(t) \\ \hat{z}(t_m) \end{bmatrix} = Y_{mx} \begin{bmatrix} \hat{x}(t) \\ \hat{x}(t_m) \end{bmatrix} + \begin{bmatrix} \hat{x}^T(t) & \hat{x}^T(t_m) \end{bmatrix}^T F_{mxx} \begin{bmatrix} \hat{x}(t) \\ \hat{x}(t_m) \end{bmatrix} + \hat{C}_m \tag{5.31}$$

Residuals are differences between measurements and estimated measurements:

$$r = \begin{bmatrix} r(t) \\ r(t_m) \end{bmatrix} = \hat{z} - z \tag{5.32}$$

And the normalized residuals being computed as:

$$s_i = \frac{r_i}{\sigma_i} \tag{5.33}$$

where r_i is the i^{th} element of r, σ_i is the standard deviation for the i^{th} measurement, thus the vector of normalized residual is represented as:

$$s = \sqrt{W} \cdot r$$

After the normalized residual vector is computed, the chi square value is a direct result. It is clear that when the modeling is accurate and there is no fault, and the measurements are following Gaussian distribution, then the sum of the square of the normalized residuals is following chi square distribution. Thus a chi square test would allow the protective relay to perform a statistical test on whether the protection zone has an internal fault (by the assumption that modeling is accurate and noise is Gaussian distributed). If there is no fault the computed value should follow chi square distribution. If there is an internal fault then

the computed value would not follow chi square distribution. In general, the computed chi square value does not have an explicit and analytical form under fault condition, Appendix B presents an analytical example of the distribution of the computed value for an internal fault given a simple linear model.

The chi-square test requires two parameters: the degree of freedom (v) and the chi-square value at the estimate (ζ). In order to express the probability with one single variable, we introduce the variable k in the definition of the chi-square expression:

$$v = m - n,\ \zeta = \sum_{i=1}^{m} \left(\frac{h_i(\hat{x}) - z_i}{k\sigma_i} \right)^2 \tag{5.34}$$

where m is the number of measurements. After the chi square value computation, then, the goodness of fit, or confidence level, is expressed as:

$$\Pr(\chi^2 \geq \zeta) = 1.0 - \Pr(\chi^2 \leq \zeta) = 1.0 - \Pr(\zeta, v) \tag{5.35}$$

This expresses the confidence level that the measurements fit the model given that the computed value follows chi square distribution. If the protected zone does not experience any internal fault, the measurements are expected to match the model, statistically the confidence level should be close to 100% (less than 100% would indicate measurement noise).

On the other hand, if the protected zone is experiencing an internal fault, then the healthy device model would be mismatched with the measurements inherently. As a consequence, the confidence level should be close to 0%.

2): The protection logic consists of two test: 1) if the operating limits are exceeded (for example, temperature above allowable limit) the component is tripped. and 2) if the average value of the confidence level over a sliding window exceeds a threshold. The window size

and threshold can be set by users. Such tripping model effectively filters any transients caused by external faults, while also sensitive and faster enough to detect high resistance fault. The mathematical description of this tripping equation is:

$$trip(t) = \begin{cases} 1 & \frac{1}{Nf_s / f} \sum_{1 \le i \le Nf_s / f} confidence\_level(t - \frac{N}{f} + \frac{i}{f_s}) < confidence\_level\_threshold \\ 0 & Otherwise \end{cases} \quad (5.36)$$

Where N is the number of cycles in the integration window, f_s is the sampling rate and f is the frequency of the system. The average of the confidence level is given by summation of the confidence level over an integration window and divided by the number of samples in that window.

5.6 Summary

The mathematical formulation and solution algorithm for unconstraint WLS, constraint WLS and Kalman filter have been presented in this chapter. Emphasis is given on the object-oriented modeling approach of the DSE.

CHAPTER 6 LABORATORY DEMONSTRATION OF DYNAMIC ESTIMATION BASED PROTECTION

6.1 Overall Description

In Chapter 3 the infrastructure for the data acquisition for the dynamic state estimation based protection is described. In laboratory environment however, building an actual transmission line with operating voltage of 115 or 230 kV equipped with potential transformer and current transformer is not a viable option, and simulating a fault is less realistic. Consequently, alternative options are being sought to test the proposed algorithm on transmission lines in laboratory environment. The laboratory setup described in this chapter simulates the test systems and instrumentation channel, and depends on actual data acquisition systems to perform real time dynamic state estimation, [48].

In this laboratory setup, there are two subsystems 1) power system simulator, 2) data acquisition system and proposed dynamic state estimation based relay. A power system simulator is used to replace an actual power system component with instrument transformers. See Figure 6-1, the simulator consists of a desktop that generates digital test waveforms. In the transmission line case, three phase voltages and currents on both sides of the line need to be generated. The power system simulator is general such that it could generate any fault simulated from any power system simulation software, or playback any fault happened in field that has been recorded by digital fault recorders (DFR), through COMTRADE files.

In this chapter, the power system simulator is briefly described, and the communication between relay and data acquisition system is explained in detail, finally the design of the relay module is presented.

Digital to Analog converter: the digital waveform from the desktop passes through the Ethernet and enters the D/A converter. The National Instrument D/A converter (NI9264) contains 32 channels with a maximum sampling rate of 25 kbps. The outputs of the D/A converter drive the inputs of 3 Omicron voltage and current amplifiers.

Omicron Amplifier: the three amplifiers are 2 CMS 156 that have three channels of voltages and three channels of currents, and 1 CMA 156 that has six channels of currents. The amplifier raises the inputs to voltage and current levels required by the merging units. Specifically, voltage amplify channels peak output voltage is 250 volts, and current amplify channels peak output current is 25A (for short duration transients) and 5A continuously.

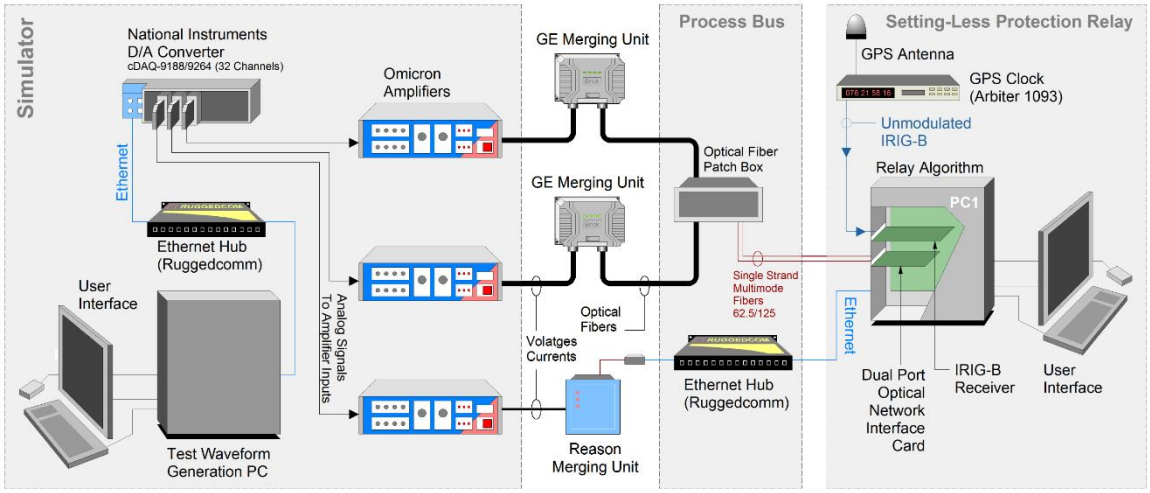

Figure 6-1. Illustration of laboratory setup.

The data acquisition system consists of merging units for each amplifier output. The data goes through the process bus and finally be collected and gathered by the Georgia Tech desktop. The dynamic state estimation based relay was implemented in the Windows operating system for performance evaluation and visualization purposes.

Merging Unit: A merging unit is a device that allows synchronized sampling of multiple instrumentation channels and collect the sampled values to the IEDs, in this laboratory setup the GE Brick, REASON MU320 and SIEMENS 7SC805 are used. Details included in Section 6.2.

Process Bus: the process bus is a device put in the process level that exchanges the data between merging units and other IEDs. In this laboratory setup the GE Cross Connect Panel and RuggedComm 2100 is used.

Dynamic State Estimation Based Relay: the relay has separate module that communicates with the merging units, and time aligns the data from different merging units (in the line case, 2 MUs) into a circular buffer module, and central processing module that retrieves the data from the circular buffer and performs dynamic state estimation and protection logic. Details included in Section 6.3. A desktop is used as a relay for implementing the algorithm instead of dedicated hardware for the reason of easy modification of the algorithm, real-time visualization of the data traffic, and animation of the performance of the algorithm.

Section 6.2 provides the detailed description of the communication flow between merging units and protective relays. Section 6.3 provides the design of the dynamic state estimation based protective relay in a desktop.

6.2 Merging Unit Communication Flow

The international standard IEC 61850 enables the migration to a fully digitalized substation. The standard describes the modeling of the electrical substation and the communication protocols that uses the modeling. The IEC 61850 models the objects in electrical substations in terms of logical devices and logical nodes, and the data associated with it in terms of data objects and data attributes in object-oriented way, and provides mapping to a number of protocols to allow the contents of the objects to be transmitted. For any manufacturer to support the IEC 61850 it needs to model the IED using the data models from the standard or inherited from it. Current mappings in the standard are Manufacturing Message Specification (MMS) in IEC 61850-6-1, Generic Object Oriented Substation Event (GOOSE) in IEC 61850-7-2, and Sampled Measured Values (SMV) in IEC 61850-9-2. These mapping are designed for different purposes and based on different communication layers, see Figure 6-2. The MMS protocols are designed for system operators to monitor and configure the settings of each intelligence electronic devices (IED) at the bay level through substation configuration language (SCL), it is based on TCP/IP layer, the GOOSE protocols are designed for the transmission of critical substation events between IEDs at the bay level and process level, and the SMV protocols are designed for the distribution of measurements from merging units to different IEDs at the process level, they are based on link layer.

The SMV protocol provides guidelines and details of the frame structure on the transmission of the sampled values, however 1) the detailed payload of the frame is left for user defined content. Because the IEC 61850-9-2 was a protocol largely open to the future that should not restrict any possible applications, there were many parameters that are not

fixed and are subject to different technical choices. The most flexible choice lies in the design of application service data unit (ASDU). Currently there are two versions, the manufacturer either uses self-defined content in ASDU and other IEDs are only able to interpret the payload after extracting the model from the merging unit through MMS first, or the manufacturer uses a light edition of IEC 61850-9-2 which specifically defined the ASDU payload. 2) the workflow of the communication between MUs and IEDs is not defined. Currently there are two versions of communication flow implemented by MUs on the market 1) master/slave mode, and 2) publisher/subscriber mode, and the laboratory demonstration contains both of them, which are described next. The advantages and disadvantages of each of them would be discussed.

6.2.1 Master/Slave Communication

The General Electric released its KEMA certified HardFiber system in 2009. It includes 1) a merging unit (GE Brick), 2) process bus (Cross Connect Panel), and 3) process card that communicates with the merging unit. See Figure 6-3 for graphical explanation. A compliant relay or IED sends a stream of GOOSE messages to facilitate the sampling process at the Brick. A point in time 100 us prior to the tail end of the Ethernet packet envelope is interpreted by the Brick as a sample and hold signal for the IED. The Brick digital core samples its data at this instant or by interpolation. The IED can apply any sampling rate and can sample freely at constant sampling intervals, variable sampling intervals, asynchronously with the absolute time, or in synchronism with the absolute time.

In this case, for time stamping purposes, the compliant IED is expected to keep track of timing of the tail end of the GOOSE Ethernet packet envelope so that samples can be correlated with the absolute time. Each GOOSE message carries a sample number

(smpNum). This number is used by the compliant IED to correlate samples with absolute time. GOOSE messages containing a Virtual LAN tag also “poll” for a set of eight samples to be returned to the compliant IED in a sampled value frame. When the poll frame is received, the Brick responds with the SV payload. The SV data set contains one sample number corresponding to the newest sample in the set of 8. This sample number is equal to the sample number in the initiating GOOSE frame. The detailed payloads for GOOSE and SMV envelopes are described in Appendix C.

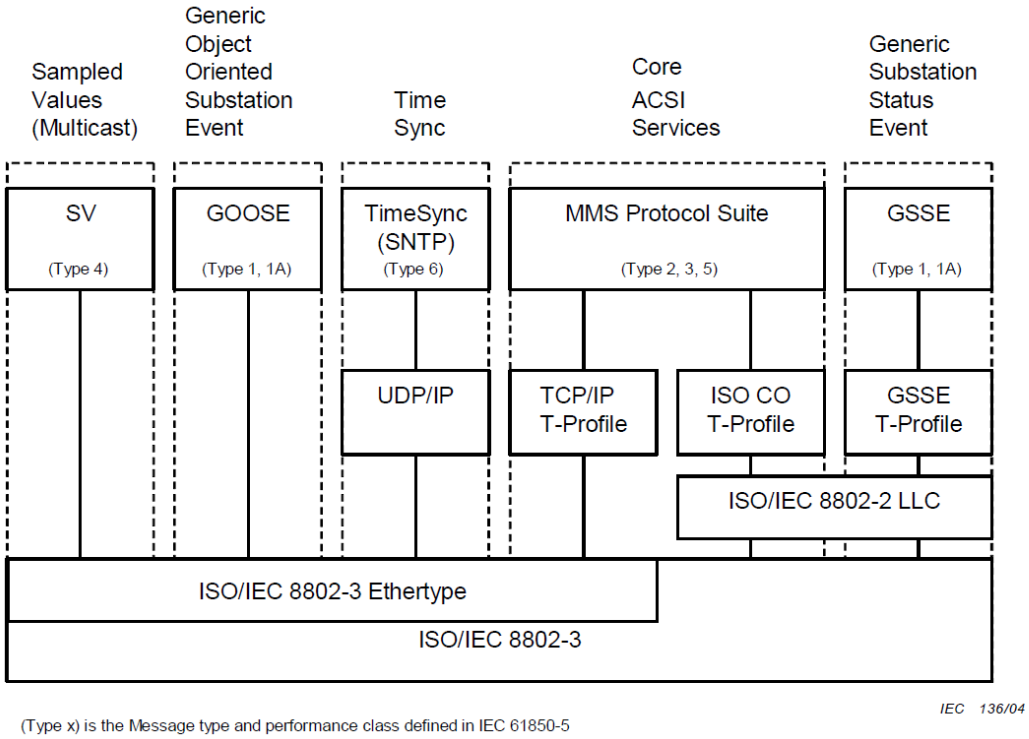

Figure 6-2 IEC 61850 communication stack – overview [53]

Each merging unit has one analog core and four digital cores, the analog core converts analog signals to digital signals and presents copies of these signals independently to each of the four digital cores using four independent digital data links. Each digital core transmits the data acquired from the analog core to the control house via an optical fiber

Ethernet link. In the control house, each digital core can be cross-connected to a different relay; A single merging unit can operate with up to four relays, and each digital core is completely independent of the other digital cores, thus each relay can sample at a different rate, can run different firmware versions, and can even be by a different manufacturer with different process bus implementations.

The merging units are usually placed nearby the instrument transformers and fiber optics are needed to transmit the sampled data back to the process bus housed within the substation room. The GE Cross Connect Panels is the corresponding dedicated process bus where outdoor and indoor fiber cables come together physically, and the optical paths between Bricks and relays are completed with patch cords. Each Cross Connect Panel contains sixteen receptacles for up to sixteen outdoor and indoor fiber cables in any combination. Standard LC 50/125 um multi-mode optical patch cords are used to make the required cross connections.

In the laboratory setup, since a desktop is used to implement the algorithm, the desktop would be required to initiate the communication with the Brick through fiber optic and meanwhile keep track of the time accurately (within 1 microsecond). The startech PEX100SFP network interface card (NIC) is chosen to be inserted to the PCI express slot in the motherboard of the desktop. The small form-factor pluggable (SFP) is a compact, hot-pluggable optical transceiver used for data communication. The Optoway 3702 is chosen as the SFP to be plugged into the NIC, since the Brick internally uses Optoway 3602 for transmitting 1310 nm and receiving 1550 nm wavelength bidirectional single-fiber multi-mode optics, and the Optoway 3702 transmits 1550 nm and receive 1310 nm as pair. 100 Mbps is the bandwidth for the communication. On the other hand, the

Microsemi bc635PCIe network interface card is chosen to be inserted to the PCI express slot in the mother board of the desktop, this time and frequency processor (TFP) model is high performance plug-in cards used for precise time synchronization of the host computer over the PCIe bus. The TFP is synchronized via GPS or IRIG-B. Within the TFP a programmable periodic output (heartbeat output) is provided. The output frequency is programmable and may be synchronized to the 1 PPS signal. This signal is capable of creating interrupts, such that the desktop could choose it as external interrupt and every time the interrupt comes a GOOSE message is sent by the desktop. The IRIG-B is converted from GPS antenna via an Arbiter satellite clock (Arbiter 1093).

This architecture implies a dedicated point-to-point communication between the MU and IED. The compliant IED would be required to initiate the communication. As aided by the process bus (Cross Connect Panel), each relay would be able to communicate with eight merging units. Since the data is transmitted point-to-point, it provides higher cyber security over the second implementation. Another advantage is that this design allows different protective relays to sample at their own needs. However, the disadvantages are 1) the relays would be required to timestamp the tail end of the GOOSE message when it leaves the relay (or the desktop in this thesis). This is usually a strict requirement. 2) the design is not horizontally scalable, which means if more than four relays need access to the same merging unit (Brick), the HardFiber system would not be able to meet its requirement. Figure **6-3** illustrates the communication process for the HardFiber system. The compliant relay is named HardFiber relay by General Electric, and the merging unit is named the Brick in this case.

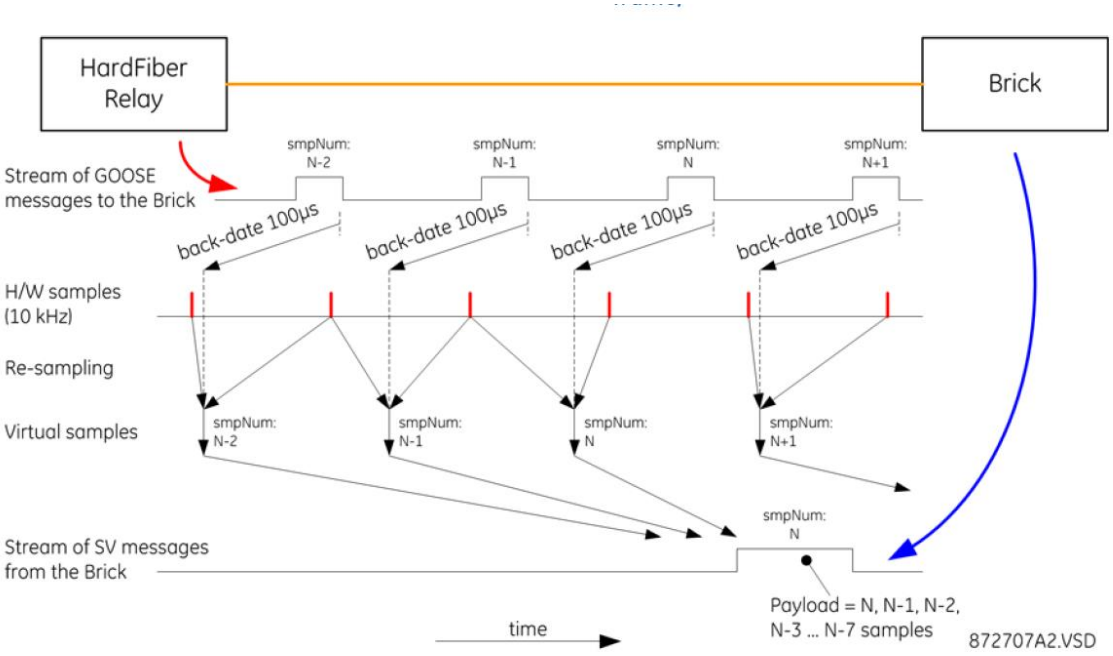

Figure 6-3 Example of Master/Slave Communication Mode (HardFiber relay is any relay compliant with the HardFiber system communication)

6.2.2 Publisher/Subscriber Communication

As described in Section 6.2.1, the compliant relay would need access to the model (as defined in IEC 61850) through MMS protocol first if the master/slave mode is used, otherwise it would not be able to interpret the data set transmitted by the merging unit. As another option, the publisher and subscriber mode is easier to implement, as it does not require the compliant relay to initiate the communication. Because the IEC 61850-9-2 was a protocol largely open to the future that should not restrict any possible applications, there were many parameters that are not fixed and are subjected to different technical choices. This supports the required flexibility of the standard that makes it future-proof. However, it introduces an interoperability issue that had to be resolved. The joint efforts of several major manufacturers under the umbrella of the UCA International Users Group resulted in

the publication of implementation guidelines for substation applications, which is the IEC 6180-9-2 light edition. Interoperability between merging units and protection, control and monitoring devices is ensured through this document by fixing all the flexible parameters and fixing the models of the merging units as described by IEC 61850. See Appendix C for the detailed model description and detailed message format. For protection applications, the merging units publish 80 samples/cycle or 4800 HZ to the process bus (broadcast, the destination MAC address is unique and does not change with device), each Ethernet frame has a single set of four voltage and four current samples. A timestamp is added to the values, so that the subscriber can check the timeliness of the values and use them to align the samples for further processing. However, since the timestamp is only optional in the guideline, most manufacturers such as REASON and Siemens do not implement that. As a result, the SV streamed by the merging unit are therefore not based on time-stamping the samples, but rather on the sample count which is a required field in the message protocol. The merging unit from REASON (MU320) uses the PPS information (pulse per second) from the IRIG-B to make sure that the first sample with sample count being 1 is always synchronized with the 1 second rollover. The subsequent samples are evenly spread in 208 microsecond intervals, summing up to the 4800 samples per second for protection application. See Figure 6-4. The sampling rate is guaranteed by hardware, as it runs on an independent FPGA soft-core, and the timestamps in the payload are neglected to reduce processing overhead at such transmission rates. As a matter of fact, MU320 supports timestamping in the much slower GOOSE message.

The process bus is a simple Ethernet switch in which case by receiving the sampled value messages it simply broadcasts to all available ports. Any compliant IED that needs

to subscribe to the target merging unit simply need to filter the incoming messages by the source MAC address of the target merging unit. And if timestamps are needed it can derive them by multiplying the sample count by the 208 microsecond interval of the current second, assuming the computer device is also synchronized.

In this thesis, either 1) network interface card is used for the desktop to communicate with the merging units through fiber optic cable, where the SFP is chosen as Avago 5750APZ SFP for 850 nm transmit and receive, or 2) a fiber optic to electric converter is first used to convert the fiber optic signals to electric signals transmitted by copper cable, and an Ethernet switch is used for broadcasting the sampled values, where the RuggedComm 2100 is chosen as industrial Ethernet network.

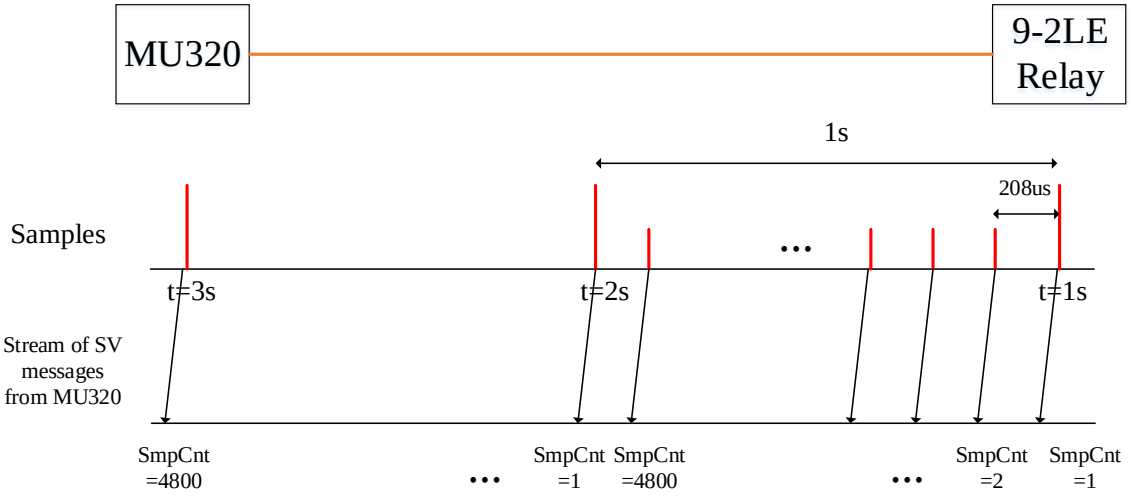

Figure 6-4 Example of Publisher/Subscriber Mode

The broadcast methodology has been adopted by many vendors such as REASON, Siemens and SEL. The advantage is that it is truly scalable – any IED that needs subscribe to the merging unit can do so by being connected to the Ethernet switch. And the IED does not need to keep track of the time since the merging unit is already time synchronized and

the sampled values contains time information. However, the disadvantage is also clear: 1) The sampling rate in the merging unit is fixed, because the samples/cycle are defined at the nominal frequency of the system. This is fundamentally different than the master/slave mode implemented by the HardFiber system where the IED tracks the power system frequency and adjust the sampling rate accordingly. At the same time, the protection algorithms in most cases are based on frequency tracking with a fixed number of samples per cycle at the current frequency of the power system, and as a matter of fact many devices that are used both as conventional IEDs and IEDs with process bus interface capabilities have sampling rate different from the 80 samples/cycle. This will require re-sampling in order to run the different protection and other algorithms. 2) The data is publicly broadcasted through the Ethernet switch such that any other devices can eavesdrop the data and compromise the cyber security requirements of the digital substation, and most importantly any other device can block the original sampled data, and emulate the malicious sampled data to the listening IEDs and consequently alter the protection logic and trip the circuit breaker that may endanger the whole network. Currently many research efforts focus on detecting the emulating data based on data signatures. 3) the concentration of the sampled data from different merging unit can be difficult if there is a data congestion in the Ethernet switch, such that the time delay of the sampled value messages is more than one second, then the IED would not be able to time align sampled values from two different merging units. This is a rare scenario.

6.3 Design of Dynamic State Estimation Based Relay

Figure 6-5 illustrates the overall design of the dynamic state estimation based protection user interface. The included modules are 1) MU Simulator, 2) MU Data Concentrator, 3) Circular Buffer, 4) COMTRADE data, 5) Device and Measurement Model Input, 6) EBP Relay processing, 7) Reports. This thesis contributes to the detailed technical implementation of the first two modules. The working sequence is to first input the device and measurement model, and setup the measurement channels from the merging units where the data would be coming from, or the COMTRADE file where the data would be generated from. If the data are coming from multiple merging units, the merging unit data concentrator would concentrate/time align the data based on the sample number as in GE Brick or sample count as in REASON MU. The circular buffer receives data from either the MU module or COMTRADE module. The next step is to choose the desired dynamic state estimation algorithm (protection logic involved) to start processing the data, and finally read the visualization results from the report.

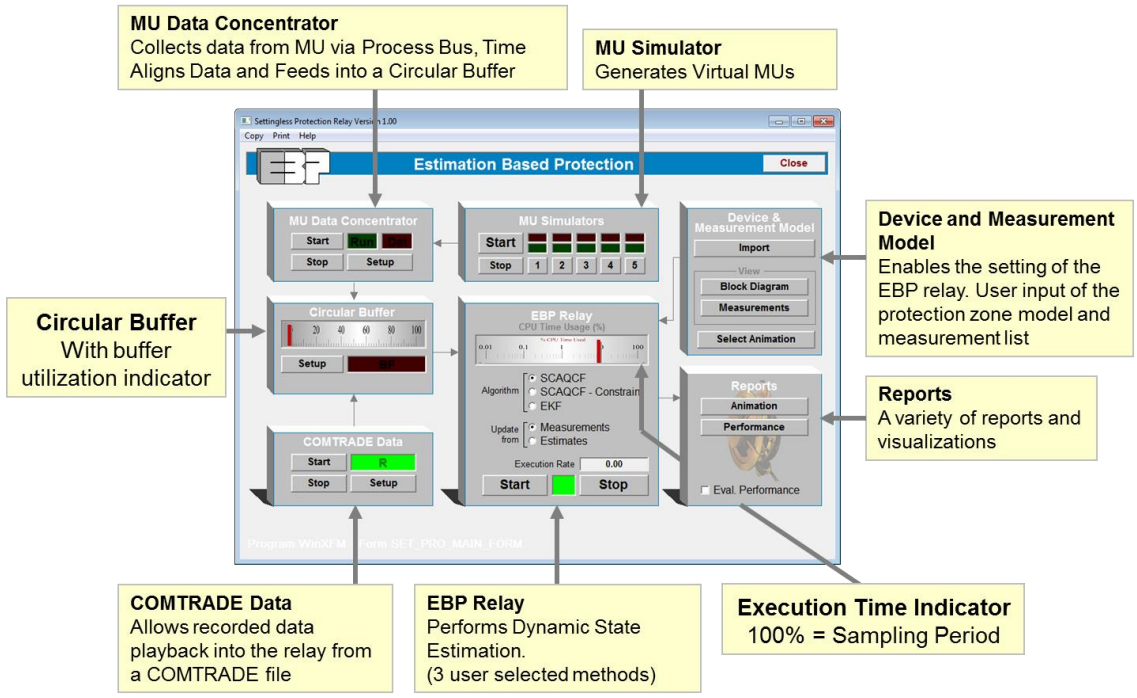

Figure 6-5 Dynamic State Estimation Based Protection User Interface (@Copyright of Power System Control and Automation Laboratory)

Specifically, the design of the MU simulator is shown in Figure 6-6, the user could define the original MAC address and name for the virtual merging unit, configuration revision, sampling rate, and to generate the actual data the relative phase angle would also be needed. These fields consist of the IEC 61850-9-2 light edition Ethernet message.

The design of the merging unit data concentrator module is shown in Figure 6-7. The relay would need access to the following parameters: sampling rate, base frequency, maximum latency, and buffer size. The user could select this module to plot raw data (in the main WINXFM frame), output packet reports and error reports. The sampling rate allows the relay to create the timestamp for the data. The maximum latency is a parameter for concentration. If the concentrator is receiving data from two merging units, and one packet with a certain sample count is received while the other packet with the same sample

count is still in the transmission path, the maximum latency tells the concentrator to wait for a certain number of consecutive samples before it claims that the packet would never be received and mark the data as invalid. The idea is illustrated in Figure 6-11, the first two samples are already time aligned, the current incoming sample carries sample count of 3, if after maximum latency (which is 8 in this case) the concentrator still does not receive the required sample from merging unit 2, it would declare the slot 2 as invalid and increase the late packet number in the error count area. Also within the error count area the sample count field means the new incoming sample count has a leap from the previous sample count, for example if the first two samples are time aligned and the current incoming sample has sample count being 4, then there is a leap of the sample count. The sample rate in the error count field means the number of sampled data which carries a different sampling rate than expected, the unknown MU means the number of sampled data which carries an unknown origin MAC address that is not defined in the measurement list, and the bad packet means the number of packets that claims in accordance to IEC 61850-9-2 but has a different format. The program is designed to listen only to the targeted merging units and filter out all packets in the network that is not relevant.

The assignment of the measurements in the concentrator is illustrated in Figure **6-8**, the merging unit list is shown in Figure **6-9**, and the merging unit property is shown in Figure 6-10. First of all, the user has to define which merging units in the network should this program target to by creating a new merging unit in the merging unit list interface and entering the merging unit property interface. Here the user first has to choose the network adaptor, since the desktop is installed with two NICs in the PCIe board there would be multiple network adaptors, then the program can see all the origin MAC addresses that is

uploading IEC 81850-9-2 compliant sampled value data and choose one that the program needs. If the merging unit is a GE Brick, this program also allows the user to send the GOOSE messages as indicated in the left down corner. After defining all the merging unit in the merging unit list interface, the program allows the assignment of the measurements in the measurement assignment interface. The program allows to map the measurement with a certain merging unit first, and then define which order in the sampled value set is the desired measurement, for example in the 9-2 light edition the first four samples are AC phase currents and the last four samples are AC phase voltages, in the GE Brick the AC input is mixed with the DC input as well. Also note that the order of the measurement assignment list should be in coincidence with the measurement definitions in the measurement model in order for the dynamic state estimator to process automatically.

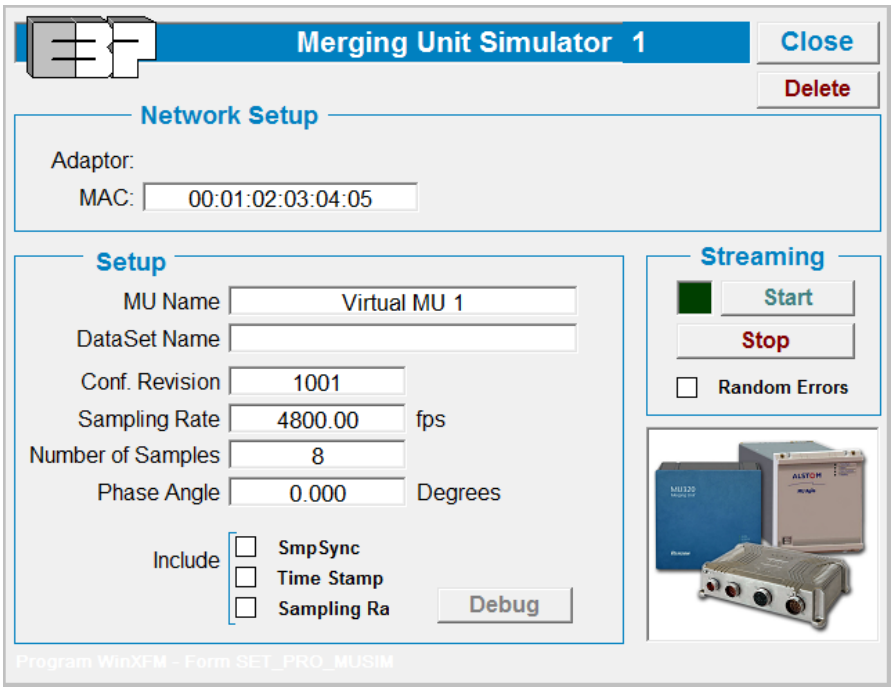

Figure 6-6 Merging Unit Simulator module

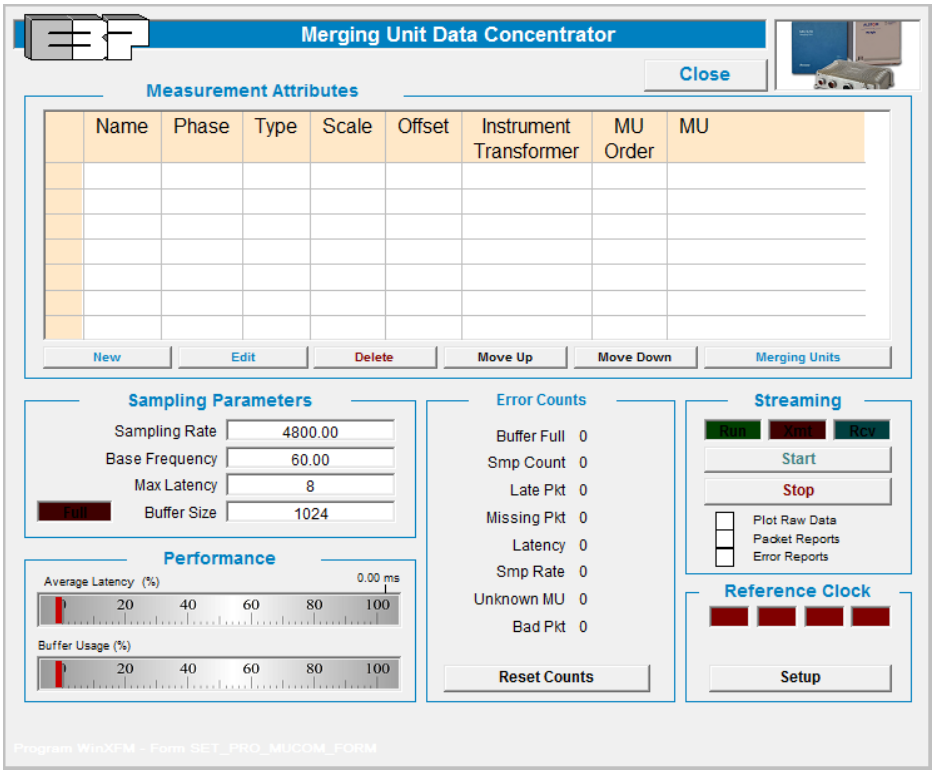

Figure 6-7 Merging Unit Data Concentrator module

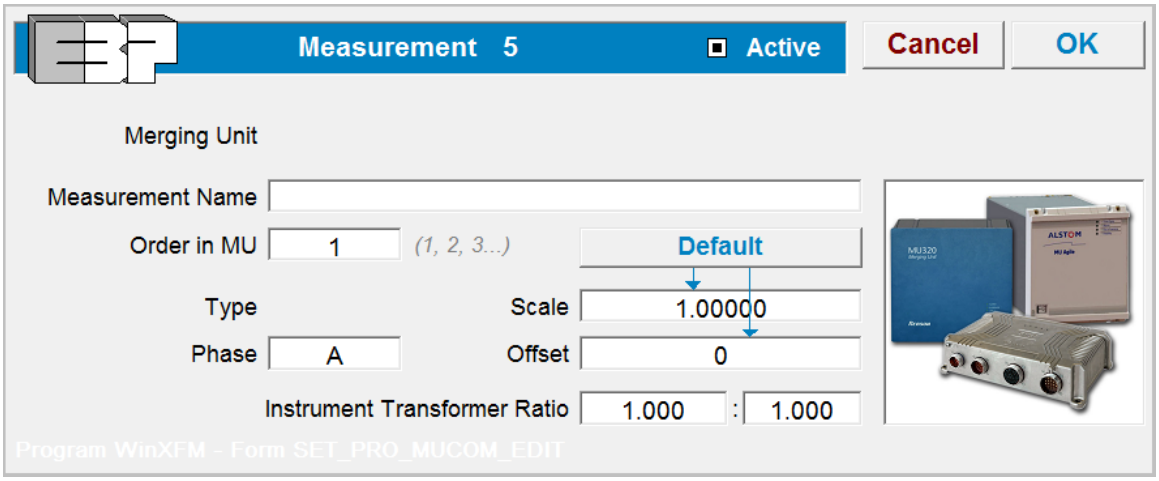

Figure 6-8 Merging Unit Data Concentrator module – measurement assignment

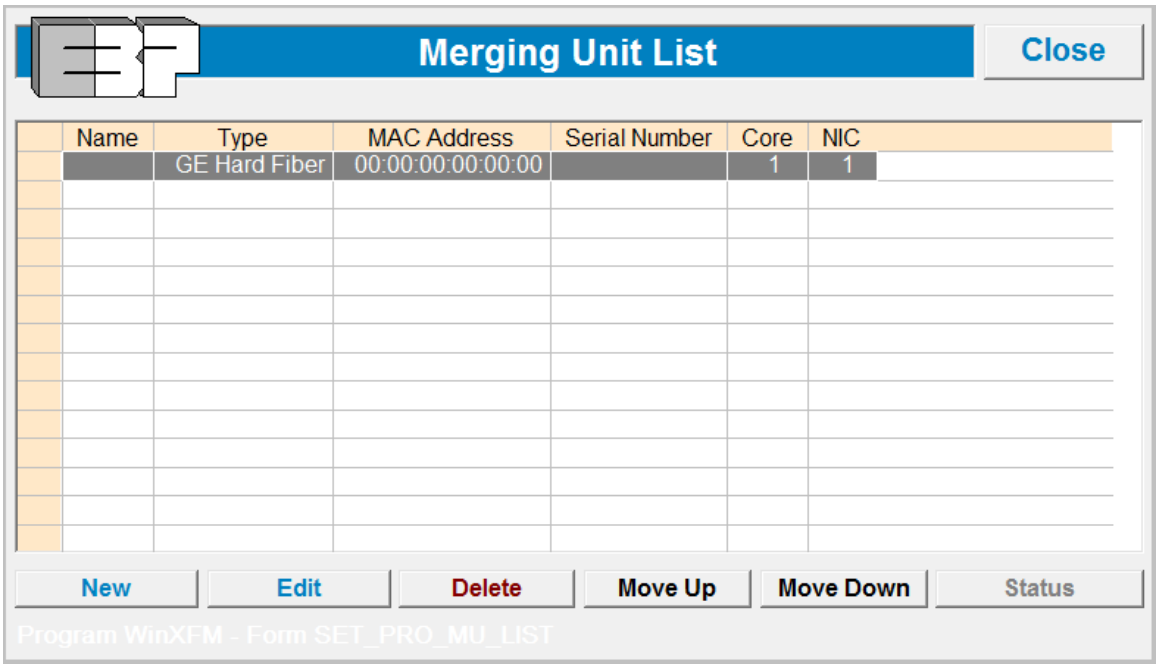

Figure 6-9 Merging Unit Data Concentrator module – merging unit list

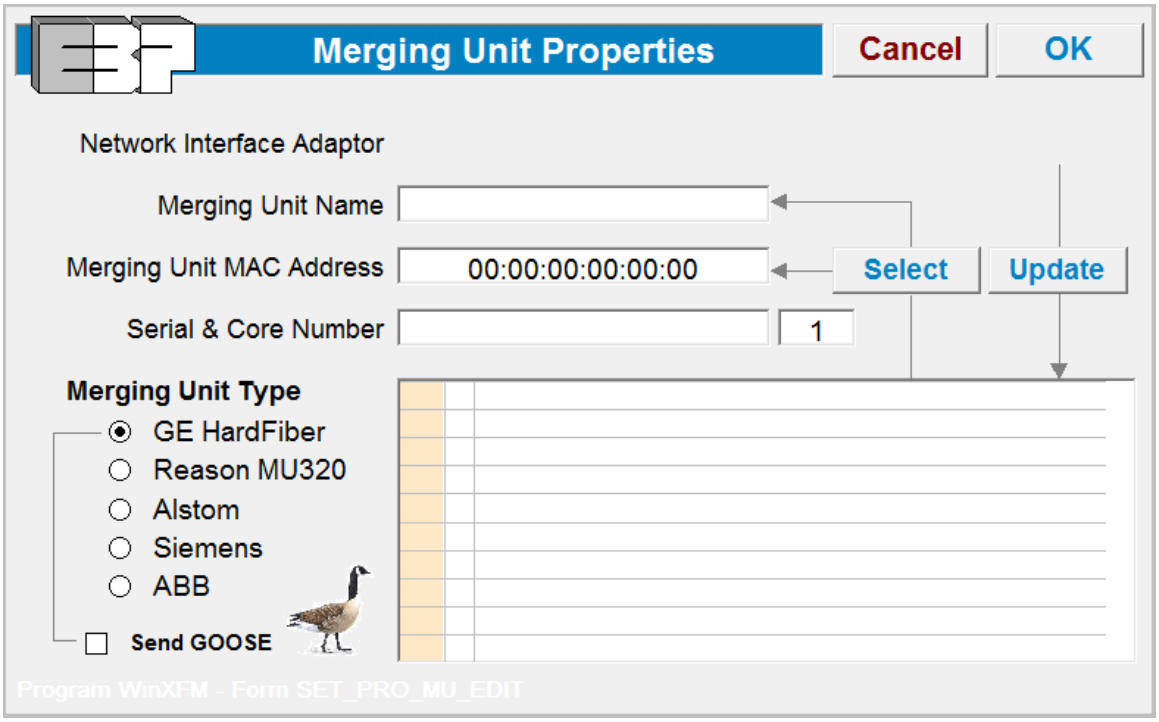

Figure 6-10 Merging Unit Data Concentrator module – merging unit properties

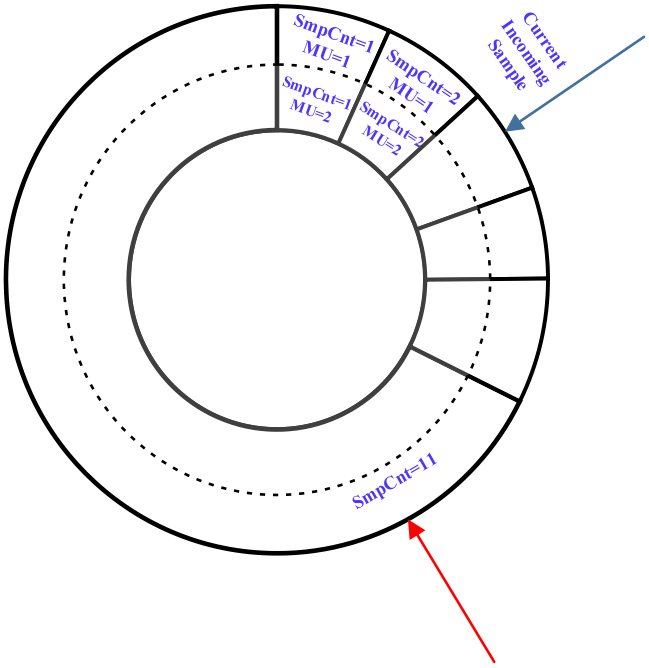

Figure 6-11. Merging Unit Data Concentrator – time alignment.

6.4 Summary

This chapter described the communication workflow between protective relay and merging unit. It also described the separate modules in the dynamic state estimation based protective relay. This thesis contributes to the MU simulator and MU concentrator module. The rest of the modules belong to the copyright of the protection and control lab of Georgia Tech.

CHAPTER 7 NUMERIC TEST CASES

7.1 Overview

In order to quantify the performance of the proposed methodology in this thesis, numerous test cases are conducted for the dynamic state estimation based protection and other legacy protection functions. The covariance matrices are used to compare the three different dynamic state estimation algorithms under normal operating condition in Section 7.2, and also the estimation results are compared by injecting noises into the measurements. The comparison shows that none of the three algorithms has significantly better performance over the other two. Subsequently the unconstraint optimization algorithm is used for the following test cases. Firstly, the dynamic state estimation based protection is compared with the combination of all the legacy protection functions in two test cases including 1) in Section 7.3 internal high impedance fault, all other legacy protection functions were not able to see the small fault while the DSE based protection is sensitive enough to a large fault resistance, and the limitation of the DSE based protection is also investigated. 2) in Section 7.4 external bus fault, many legacy functions would have a hard time determining the direction of the fault thus making incorrect decisions. These two cases compare the dynamic state estimation based protection with the combination of all legacy protection functions, and illustrates the major advantages of the DSE based protection, i.e. its sensitivity and security. Secondly, the dynamic state estimation based protection is compared with each one of the legacy protection functions to demonstrate the advantage of the DSE based protection over the weakness or disadvantages of the legacy protection functions described in Literature Review of Chapter 2 from Section 7.5 to Section 7.9. Lastly, the specific issues involved with the DSE based protection is presented in Section

7.10, including 1) PT/CT measurement errors, 2) modeling error for the resistance, inductance and capacitance of the transmission line, 3) synchronization error.

7.2 Covariance Matrices for three Dynamic State Estimation Algorithms

First the mathematical formulation of the covariance matrices is introduced. Note that the covariance matrix for Kalman filer is already described in Section 5.4.

For the **unconstraint optimization** DSE algorithm, the covariance matrix is computed by referring to (5.5)

$$H^T W h(\hat{x}) = H^T W z = H^T W (h(x^*) + \eta) \tag{7.1}$$

where x=x(t,t_m) represents the states at time t and tm. The hat symbol represents the estimated value, while the star symbol represents the

And the Tylor expansion of h(x^*) around the estimated state $\hat{x}$ gives the following:

$$\begin{aligned} &H^T W (h(x^*) + \eta) \approx H^T W (h(\hat{x}) + H \times (x^* - \hat{x}) + \eta) \\ &= H^T W h(\hat{x}) + H^T W H \times (x^* - \hat{x}) + H^T W \eta \end{aligned} \tag{7.2}$$

Here the Jacobian matrix should be computed at x^* but it's approximated by the Jacobian matrix at $\hat{x}$.

Substituting (7.2) back into (7.1) gets:

$$H^T W H \times (\hat{x} - x^*) = H^T W \eta \tag{7.3}$$

So that the covariance matrix is computed by:

$$Cov(x^*) = E\left[(x^* - \hat{x})(x^* - \hat{x})^T\right] = \left(H^T W H\right)^{-1} \tag{7.4}$$

For the **constraint optimization** algorithm, the covariance matrix is computed in a similar manner by Taylor expansion:

$$Cov\left(\begin{bmatrix} x(t,t_m) \\ \lambda(t,t_m) \end{bmatrix}\right) = E\left\{\begin{bmatrix} H^T WH & G^T \\ G & 0 \end{bmatrix}^{-1}\begin{bmatrix} H^T W\eta + G^T\lambda \\ 0 \end{bmatrix}\begin{bmatrix} \eta^T W^T H + \lambda^T G & 0 \end{bmatrix}\begin{bmatrix} H^T WH & G^T \\ G & 0 \end{bmatrix}^{-T}\right\}$$

$$= \begin{bmatrix} H^T WH & G^T \\ G & 0 \end{bmatrix}^{-1}\begin{bmatrix} H^T W\{E(\eta\eta^T)\}W^T H + H^T W\{E(\eta)\}\lambda^T G + G^T\lambda\{E(\eta^T)\}W^T H + G^T\lambda\lambda^T G & 0 \\ 0 & 0 \end{bmatrix}\begin{bmatrix} H^T WH & G^T \\ G & 0 \end{bmatrix}^{-T}$$

$$= \begin{bmatrix} H^T WH & G^T \\ G & 0 \end{bmatrix}^{-1}\begin{bmatrix} H^T W^T H + G^T\lambda\lambda^T G & 0 \\ 0 & 0 \end{bmatrix}\begin{bmatrix} H^T WH & G^T \\ G & 0 \end{bmatrix}^{-1}$$

And by matrix inversion lemma, the above equation can be simplified to:

$$Cov(x) = \left(H^T WH\right)^{-1} - \left(H^T WH\right)^{-1} G^T\left(G\left(H^T WH\right)^{-1} G^T\right)^{-1} G\left(H^T WH\right)^{-1} \qquad (7.5)$$

where only the covariance of x is of interest.

The covariance matrix for Kalman filter is dynamically computed for each time step. However, after the estimated states stabilize the covariance matrix for Kalman filter would also be fixed. In order to compare the performance of algorithms in this section, only the covariance matrix after the estimated states have been stabilized are analyzed. In this case, the posteriori covariance matrix is used for the comparison.

The test system is running in normal operation, the description of the test system can be referred to Section 7.3 and Figure 7-2. In normal operation the loading currents for all three phases are 400A.

The standard deviation for actual measurements are set at 0.01pu, for pseudo measurements are set at 0.1pu, for virtual measurements are set at 0.001pu (for unconstraint optimization method).

The square root of diagonal elements from the covariance matrices for all three algorithms are listed in Table 7.1. The algorithms for the accuracy on voltage states are similar with each other. The constraint optimization and Kalman filter are more accurate

on the internal states than the unconstraint optimization, and the reason is straightforward: 1) the internal states cannot be directly measured so that the accuracy for estimating internal states is generally worse than the accuracy for estimating external states, 2) the unconstraint optimization assumes 0.001 p.u. standard deviation on the virtual measurements which is the only equation that includes the internal states, while the constraint optimization and Kalman filter assumes exactly 0 p.u. standard deviation on the virtual measurements. If the standard deviation for the virtual measurements from unconstraint optimization is set smaller, then the accuracy for internal states would be improved.

Table 7.1 Square root of diagonal elements from covariance matrices – per unit

$\sqrt{variance}$ (p.u)	Unconstraint Opt	Constraint Opt	Kalman Filter
Va1	0.009721	0.009347	0.009390
Vb1	0.009623	0.009104	0.009164
Vc1	0.009616	0.009089	0.009151
Vn1	0.09161	0.0805	0.0812
Va2	0.009721	0.009347	0.009390
Vb2	0.009623	0.009104	0.009164
Vc2	0.009616	0.009089	0.009151
Vn2	0.09610	0.0805	0.0812
iLa	0.013530	0.001215	0.002592
iLb	0.010596	0.001091	0.002463
iLc	0.009482	0.001008	0.002337
iLn	0.021016	0.003028	0.005373

On the other hand, the estimation results on the phase A voltage and current measurement for the three algorithms during normal operation is illustrated in Figure **7-1**. From the table and figure it can be concluded the estimation results are close to each other.

Based on the fact that all three algorithms behave similarly, the following test cases only use the estimation results from the unconstraint optimization method.

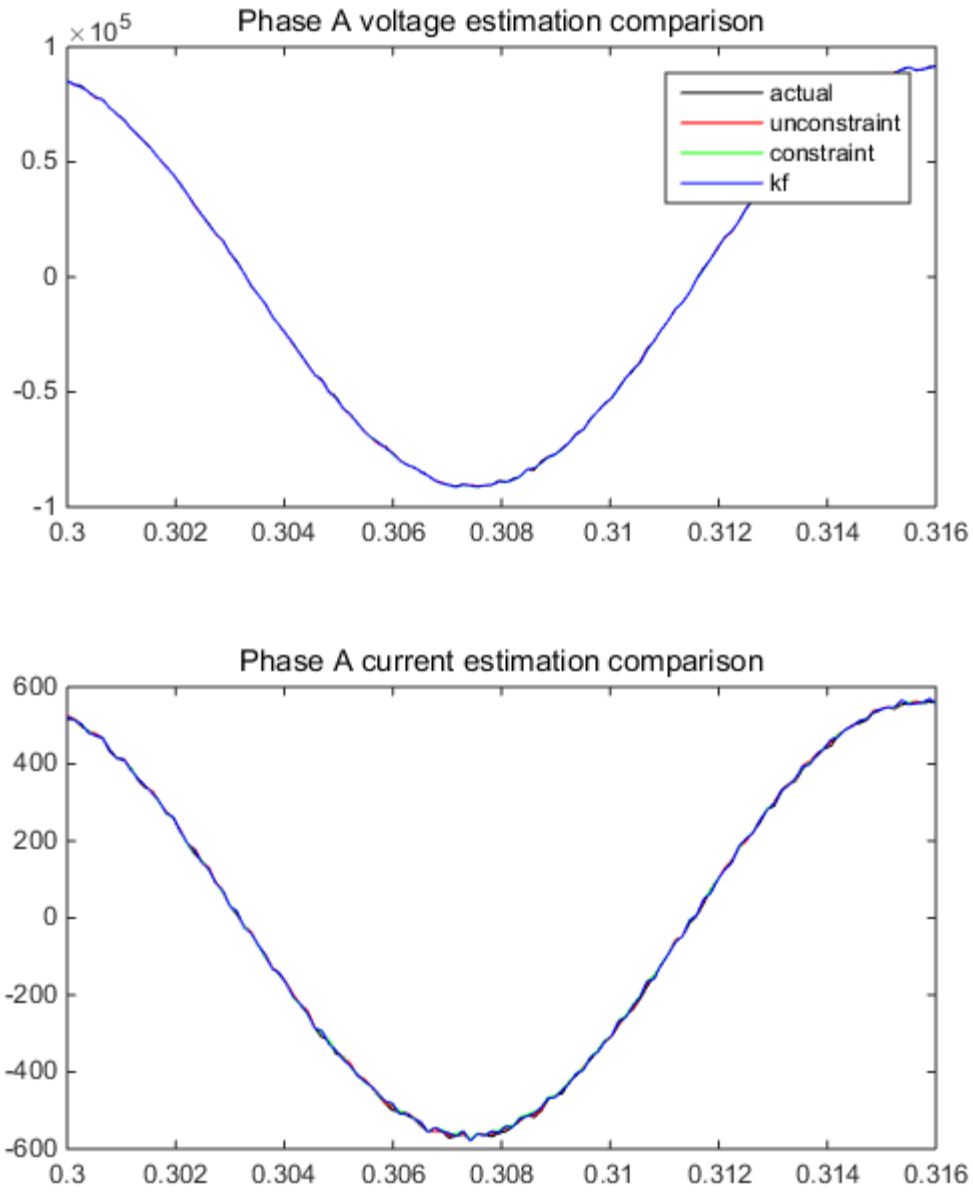

Figure 7-1 Estimation results for three DSE algorithms – test system in normal operation with Gaussian measurement noise, x axis is time (s), y axis is voltage (v) or current (A) – demonstrating the estimation difference between different algorithms

7.3 Scenario 1 – High Impedance Fault

This section presents a transmission line example by comparing the proposed DSE protection on high impedance fault scenario with legacy protection functions based on dependability and sensitivity. The protected zone is a 115kV 80 miles line from node YJLINE1 to YJLINE2, as shown in Figure 7-2. The sampling rate is 128 samples/cycle.

The event sequence is as follows: an internal high impedance fault (1000 Ohms) between phase A to ground at the middle of the transmission line (Node LINETEE) is initiated at t=0.6 s and cleared at t=0.8 s, the current magnitude at phase A at both terminals increase slightly from 400A to 425A; Subsequently an external low impedance three phase bus fault (0.001Ohms) at YJLINE2 is initiated at t=1.0 s and cleared at t=1.2 s, the phase currents on both terminals increase to 1000A. Unconstrained WLS is applied in both events. Only event 1 is studied here.

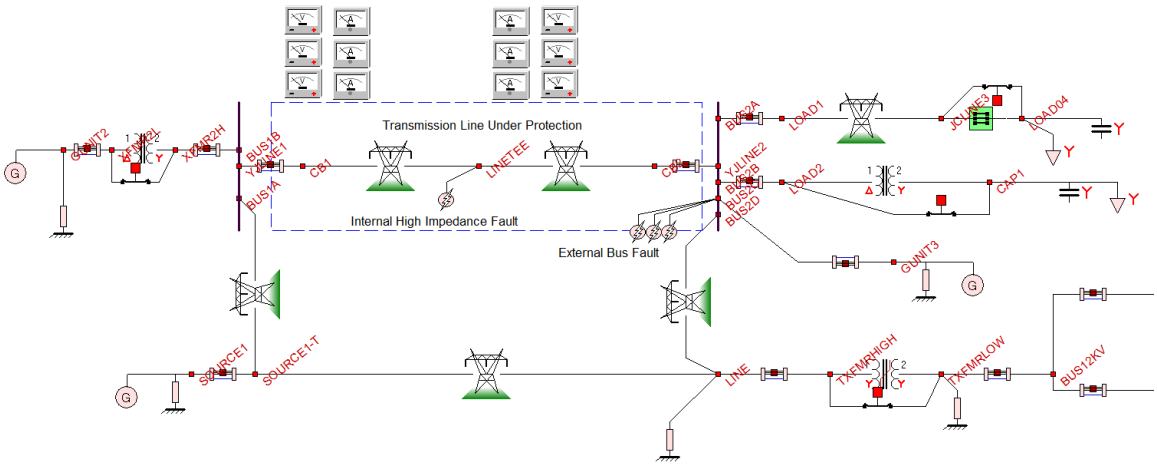

Figure 7-2 Test System with Protected Zone, Node YJLINE1 to YJLINE2, for High Impedance Fault

The compared protection functions and their settings are listed below:

Table 7.2 Protection Settings for High Impedance Fault Case

Protection Functions	Settings
Directional Instantaneous Overcurrent	50P PKP: 1400A 50G PKP: 600A 67Forward: <0Ohm 67Reverse: > 0Ohm
Directional Time Overcurrent	51P PKP: 600A 51G PKP: 30A 67Forward: <0Ohm 67Reverse: >0Ohm Time Dial: 0.1 Moderately Inverse
Stepped Distance	Z1PKP: 42.63 ∠ 84.42 Z2PKP: 63.95 ∠ 84.42 Z3PKP: 85.26∠84.42 compensation factor m: 3.03∠-6.28
Permissive Overreaching Transfer Trip	Forward Reaching Element: Z2 Communication Time Delay: 0ms Reverse Reaching Element: None
Percentage Current Differential	87 PKP: 45A Restraint 1: 15% Restraint 2: 40% Break Point: 1600A
Dynamic State Estimation Based	Integration Windows Size: 1 cycle Confidence Level Threshold: 50%

The POTT is designed as in Figure 7-3 where zone 2 elements are used for overreaching.

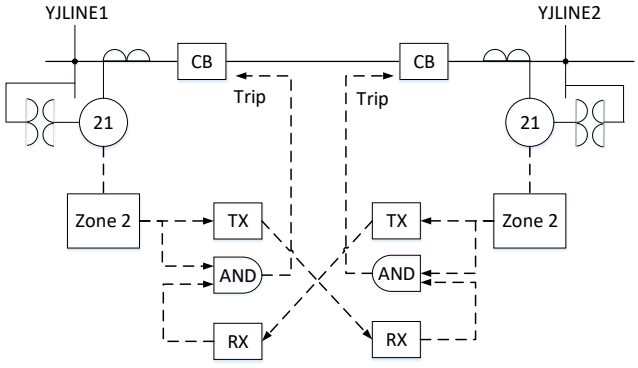

Figure 7-3 Permissive Overreaching Transfer Trip Scheme Design

Figure 7-4 is a summary of the relay performance for each protection function: 1) in -a) and b) the black and magenta traces are pickup settings for directional IOC and TOC, red/green/blue traces are measured three phase currents, cyan trace is computed ground current, since both phase currents and ground current are below pickup values, so they would not operate. 2) in Fig. 7.3-c) the relay characteristic superimposed with operating points are plotted for stepped distance protection, and 7.3-d) presents the POTT relay bits. Since the apparent impedances are outside the Mho zones, the POTT zone 2 element is not picked up and permission signal is not sent, both protection functions would not operate. 3) in Fig. 7.3-e) the relay characteristic superimposed with operating points are plotted for current differential, since the operating points are in the restraint zone, the protection function would not operate. 4) in Fig. 7.3-f) the estimation results, confidence level and protection logic are presented, since the fault is small, the confidence level oscillates, but the protection function still detects the fault and issues trip signal in about 0.8 cycle. More analysis shows that the current differential would operate when the fault resistance is less than 500 Ohms, while the DSE method can detect fault up to 3000 Ohms.

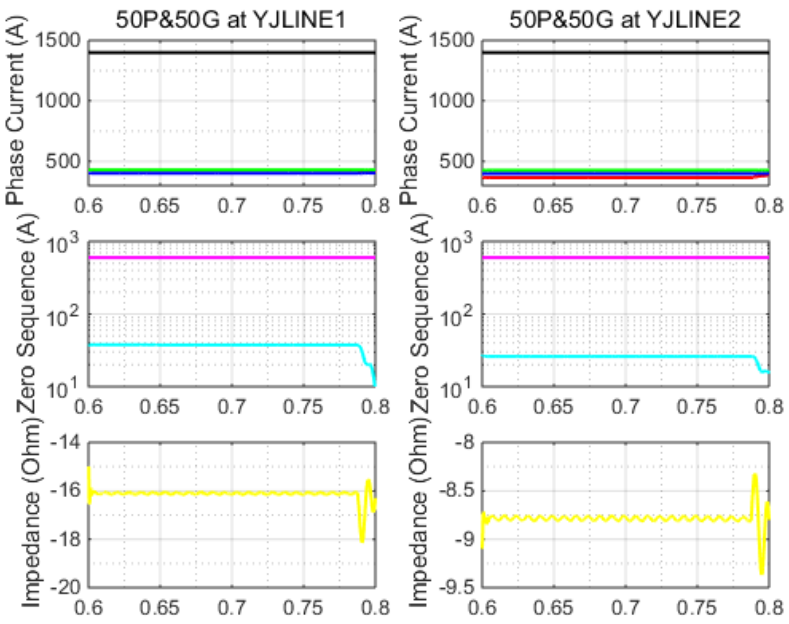
50P&50G at YJLINE1
50P&50G at YJLINE2
Phase Current (A)
Zero Sequence (A)
Impedance (Ohm)

(a)

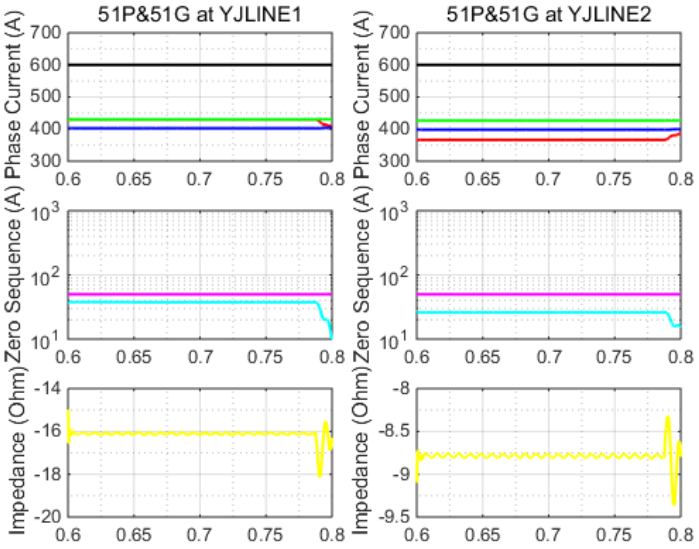
51P&51G at YJLINE1
51P&51G at YJLINE2
Phase Current (A)
Zero Sequence (A)
Impedance (Ohm)

(b)

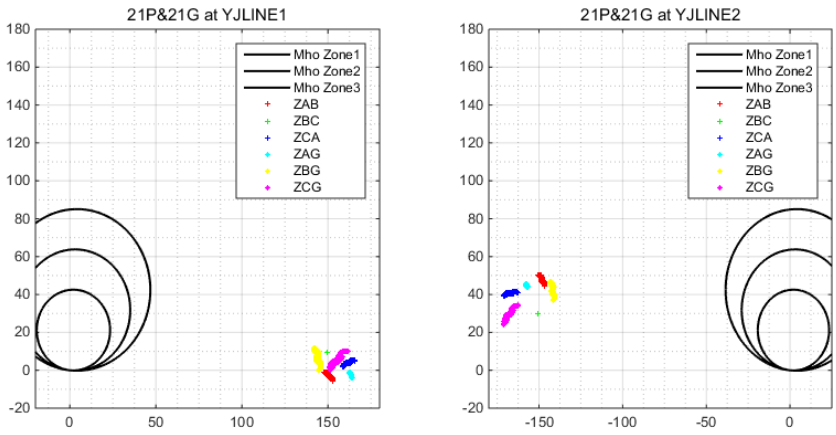
21P&21G at YJLINE1
21P&21G at YJLINE2
Mho Zone1
Mho Zone2
Mho Zone3
ZAB
ZBC
ZCA
ZAG
ZBG
ZCG

(c)

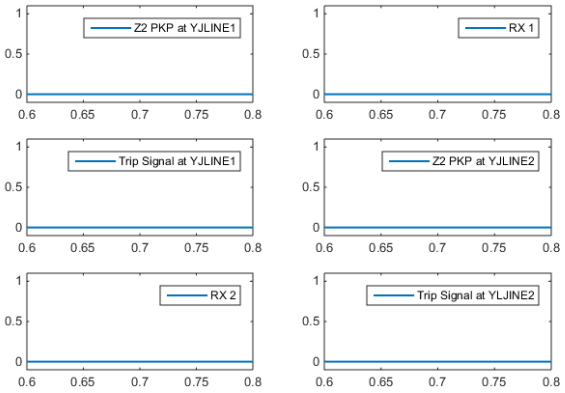
Z2 PKP at YJLINE1
RX 1
Trip Signal at YJLINE1
Z2 PKP at YJLINE2
RX 2
Trip Signal at YLJINE2

(d)

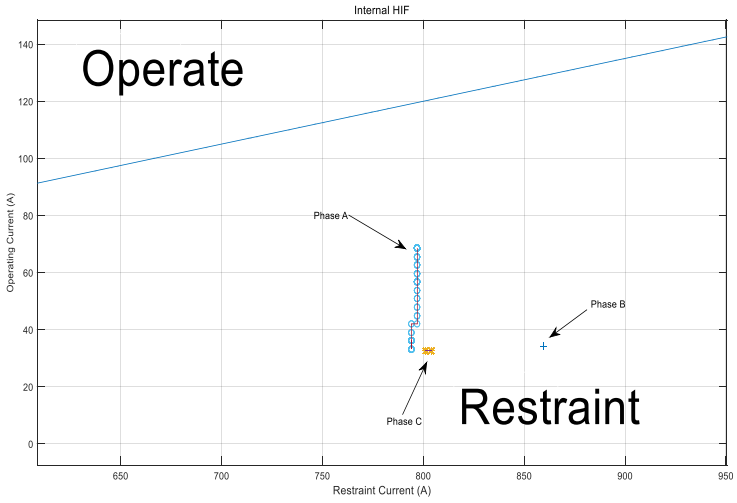
Internal HIF
Operate
Restraint
Phase A
Phase B
Phase C
Operating Current (A)
Restraint Current (A)

(e)

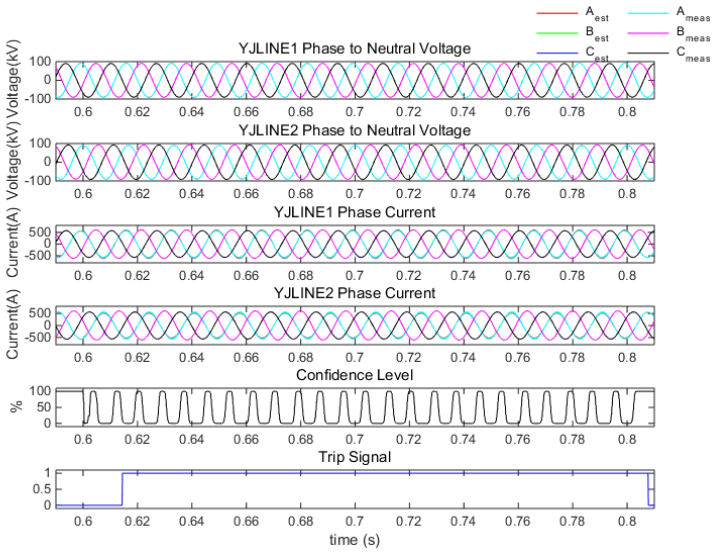

(f)

Figure 7-4 Relay Performance during Internal HIF, a) directional IOC, b) directional TOC, c) stepped distance, d) POTT, e) percentage differential, f) DSE protection

7.4 Scenario 2 – External Bus Fault

This section presents a transmission line example by comparing the proposed DSE protection on external low impedance bus fault scenario with legacy protection functions based on security. The protected zone is a 115kV 80 miles line from node YJLINE1 to YJLINE2, as shown in Figure 7-2. The sampling rate is 128 samples/cycle.

The event sequence is as follows: an internal high impedance fault (1000 Ohms) between phase A to ground at the middle of the transmission line (Node LINETEE) is initiated at t=0.6 s and cleared at t=0.8 s, the current magnitude at phase A at both terminals increase slightly from 400A to 425A; Subsequently an external low impedance three phase bus fault (0.001Ohms) at YJLINE2 is initiated at t=1.0 s and cleared at t=1.2 s, the phase currents on both terminals increase to 1000A. Unconstrained WLS is applied in both events. Only event 2 is studied here.

Figure 7-5 is a summary of the results for each protection function: 1) in Fig. 7.4-a) both phase currents and ground currents are below pickup value, so directional IOC would not operate. In Fig. 7.4-b) the phase currents are above pickup value and the directional element at YJLINE2 cannot determine the fault direction, so directional TOC would operate after $t = 0.1*\left(\frac{0.0515}{(1000/600)^{0.02}-1}+0.114\right) = 0.513s$. 2) in Fig. 7.4-c) the apparent impedances enter Mho zone 2 at YJLINE1 and enters zone 1 at YJLINE2 after 80 samples, the function would operate after 10ms. In Fig. 7.4-d) since the zone 2 is picked up on both terminals, the permission signals are transmitted, and the protection functions would operate after 10ms since no communication delay. 3) in Fig. 7.4-e) since the operating points are in the restraint zone, the protection function would not operate. 4) in Fig. 7.4-f) the confidence level drops to 0% temporarily since the fault causes non-differentiable change of the states, but the protection function filters out the transient and it does not operate.

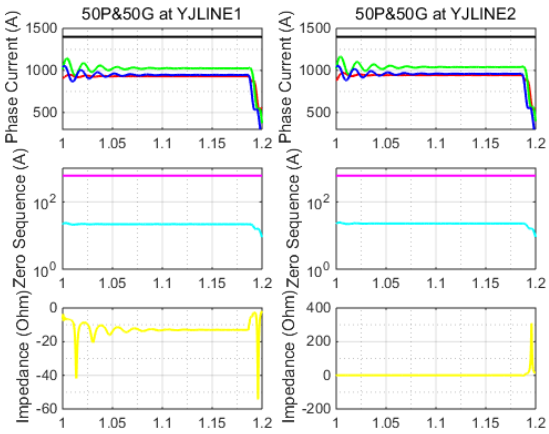

(a)

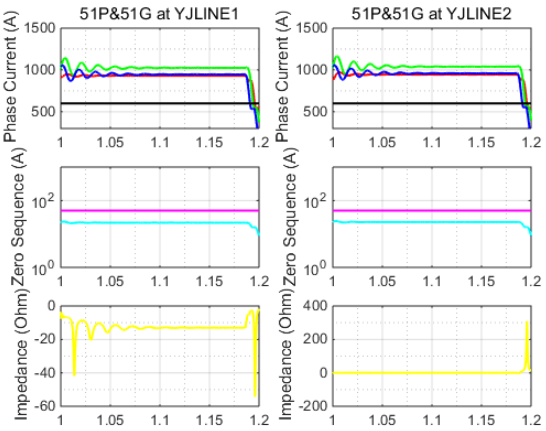
51P&51G at YJLINE1
51P&51G at YJLINE2
Phase Current (A)
Zero Sequence (A)
Impedance (Ohm)

(b)

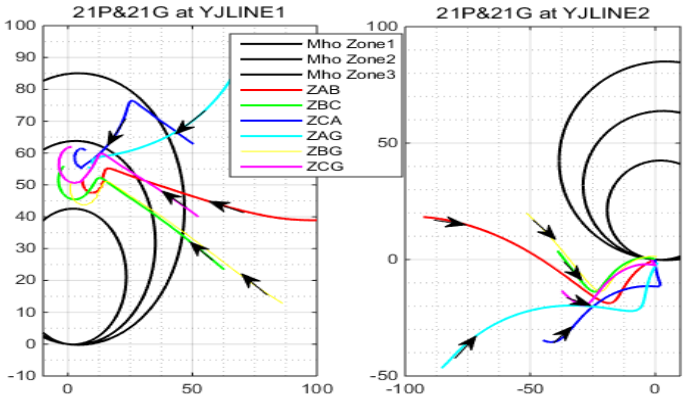
21P&21G at YJLINE1
21P&21G at YJLINE2
Mho Zone1
Mho Zone2
Mho Zone3
ZAB
ZBC
ZCA
ZAG
ZBG
ZCG

(c)

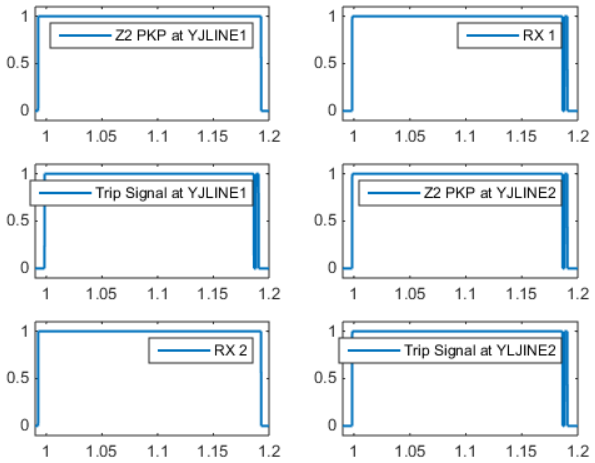
Z2 PKP at YJLINE1
RX 1
Trip Signal at YJLINE1
Z2 PKP at YJLINE2
RX 2
Trip Signal at YLJINE2

(d)

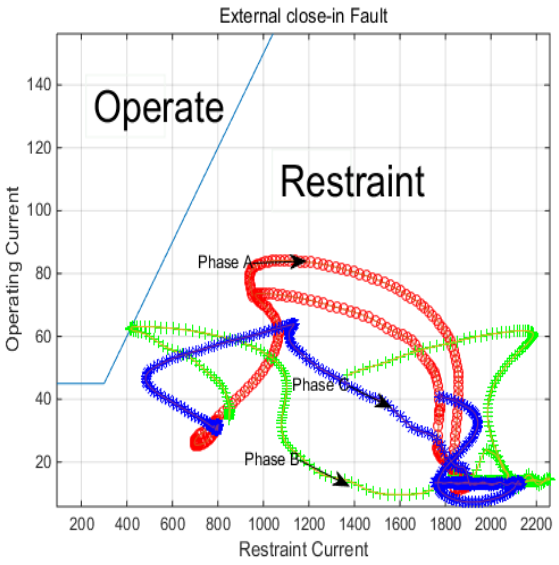

(e)

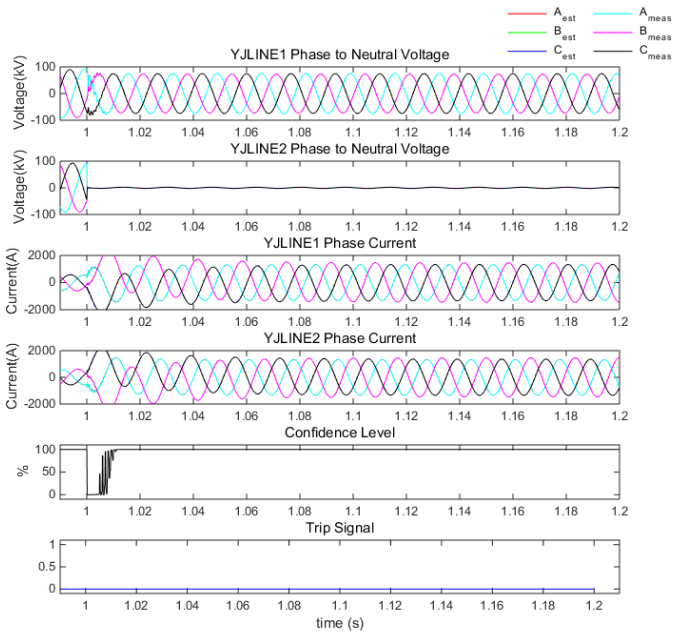

(f)

Figure 7-5 Relay Performance during External fault, a) directional IOC, b) directional TOC, c) stepped distance, d) POTT, e) percentage differential, f) DSE protection

7.5 DSE based protection with instantaneous directional overcurrent protection

7.5.1 Short line protection

Instantaneous directional overcurrent protection usually protects part of the line. It compares the fault current level with its own setting. For long transmission lines (such as 80 miles), the positive sequence impedances are relatively large (such as 50 Ohm), while the source impedance is relatively small (usually under 5 Ohm for strong source), so that the fault current level is largely decided by the location of the fault – the closer the fault to the end of the line, the larger fault current level seen by the relay. That is essentially how protection engineers set up the pickup value: they decide what's the fault current level at 80% of the line, and set that fault current level as the pickup value. Any fault current level higher than the pickup value would indicate the fault happens within the protection zone. Any fault current level lower than the pickup value would indicate either the fault happens outside the protection zone, or within the protection zone but the fault resistance is high.

In short lines however, the fault current level is largely decided by the source-to-line impedance ratio (SLR ratio). With a relatively weak source, or with a relatively short line, the SLR ratio is high (such as 10) and the fault current can be approximated by the source voltage over the source impedance and as a result it doesn't change significantly with the location of the fault. The pickup value is difficult to set up in this case.

On the other hand, the DSE based protection does not rely on the fault current level to trip: even under large fault current if the measurement matches the model it would not trip the line, under small fault current if the measurement does not match the model it would

still trip the line. Consequently, DSE based protection performs better than instantaneous overcurrent directional element when the line is short.

The test case to illustrate the short line protection is in Figure **7-6**. The rest of the system is similar to Section 7.3 except the protection zone is 115 kV, 4km line (short line). The event sequence is as follow: the system is working under normal operation until – **Event 1**, the phase A to neutral fault (0.01 Ohm) happens at 2.5% of the line (from YJLINE1) at t = 0.5s to t=0.7s. **Event 2**, the phase A to neutral fault (0.01 Ohm) happens at 80% of the line (from YJLINE1) at t = 0.9s to t = 1.1s. **Event 3**, the phase A to neutral fault (0.01 Ohm) happens at 100% of the line (right outside the line) at t = 1.3s to t = 1.5s.

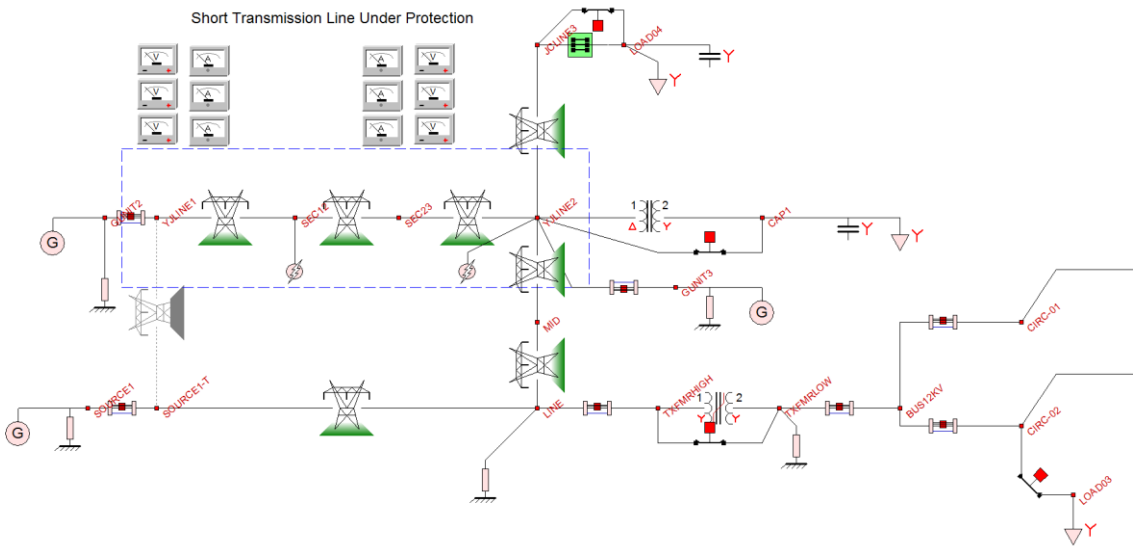

Figure 7-6 Short line test case – a comparison between instantaneous overcurrent protection and DSE based protection

The settings for directional instantaneous overcurrent protection and DSE based protection are listed in Table 7.3. The overcurrent protection is designed to cover 80% of the line.

Table 7.3 Protection Settings for Short Line case

Protection Functions	Settings
Directional Instantaneous Overcurrent	50P PKP: 1510A 67Forward: <0Ohm 67Reverse: > 0Ohm
Dynamic State Estimation Based	Integration Windows Size: 1 cycle Confidence Level Threshold: 50%

The protection results for directional instantaneous overcurrent protection are illustrated next in Figure 7-7. During event 1 the fault currents on both sides are larger than the setting, the protection element would operate correctly. During event 2 the fault currents on YJLINE1 equals to the pickup value, while the fault current on YJLINE2 is larger than the pickup value. In this case both relays would still operate correctly. During event 3 the fault current on YJLINE1 still equals to the pickup value (this is because of the short line), so that the relay at YJLINE1 would trip, or mis-operate. Meanwhile the relay at YJLINE2 would see the fault as reverse fault (check the directional element in the figure).

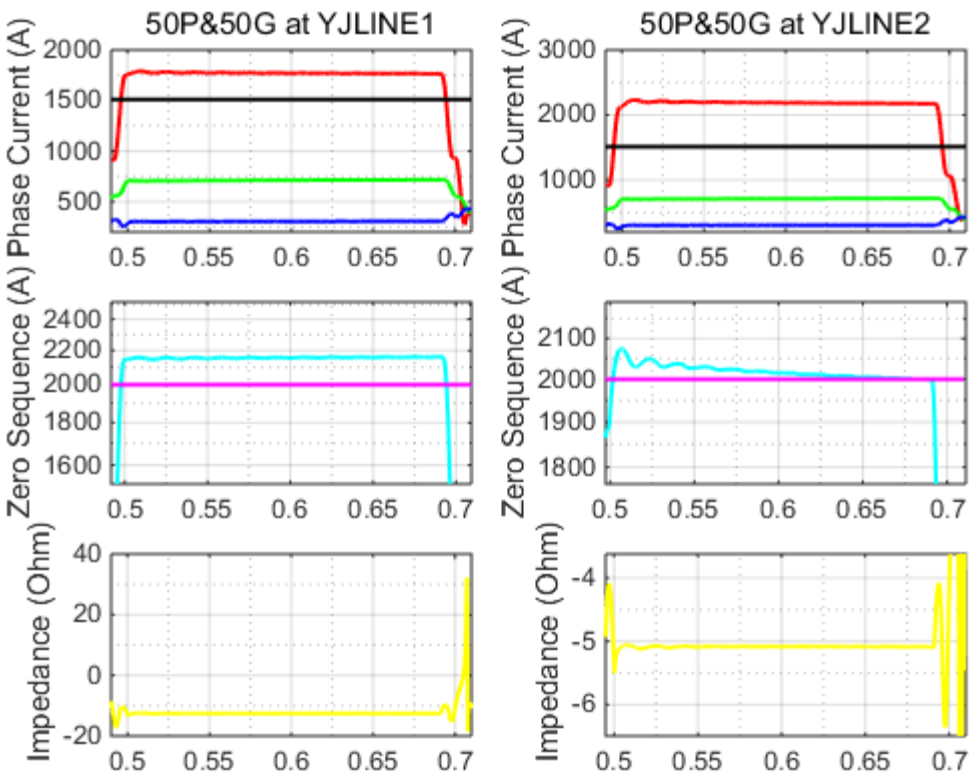
50P&50G at YJLINE1
50P&50G at YJLINE2
Phase Current (A)
Zero Sequence (A)
Impedance (Ohm)
2000
1500
1000
500
3000
2000
1000
2400
2200
2000
1800
1600
2100
2000
1900
1800
40
20
0
-20
-4
-5
-6
0.5
0.55
0.6
0.65
0.7

Event 1

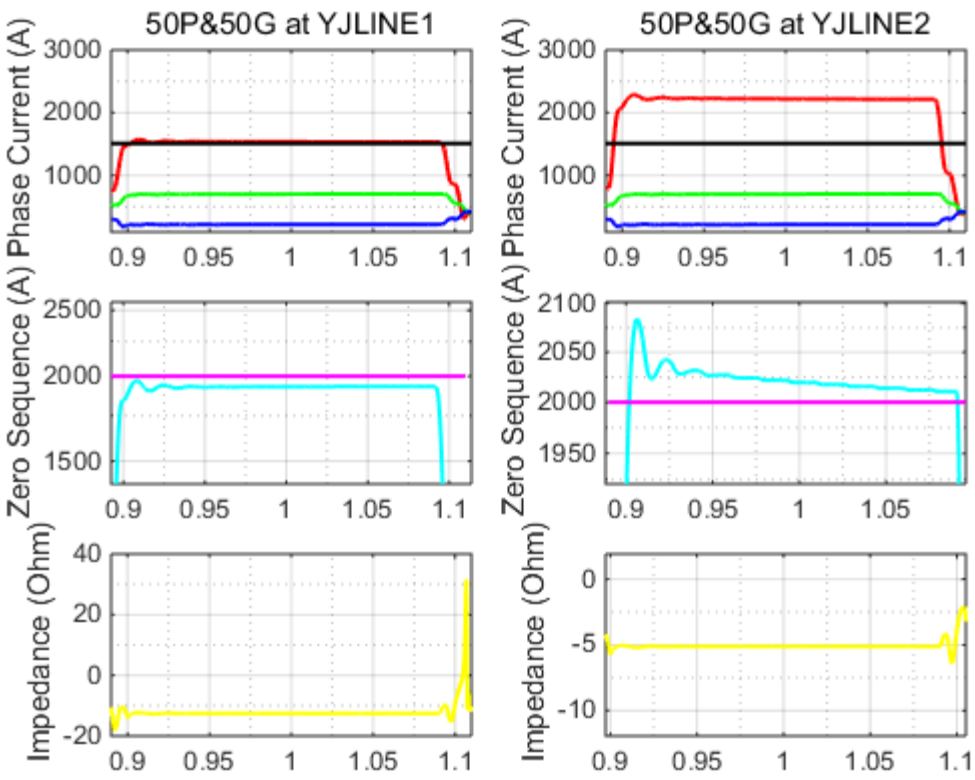
50P&50G at YJLINE1
50P&50G at YJLINE2
Phase Current (A)
Zero Sequence (A)
Impedance (Ohm)
3000
2000
1000
2500
1500
2100
2050
1950
40
20
0
-20
-5
-10
0.9
0.95
1
1.05
1.1

Event 2

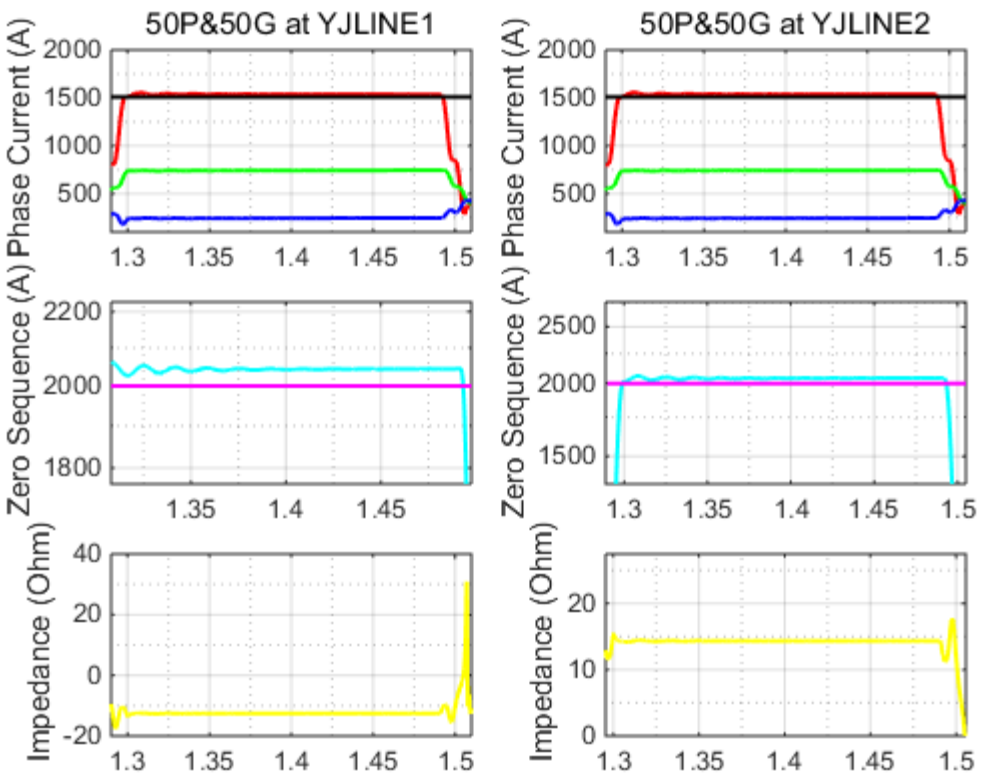

Event 3

Figure 7-7 Short line test case – Protection Results for Instantaneous Overcurrent Protection

By comparison, the results for DSE based protection is included next in Figure **7-8**. During Event 1 and Event 2, the algorithm captures the internal fault and operates correctly. During Event 3 the algorithm provides the required security and would not trip.

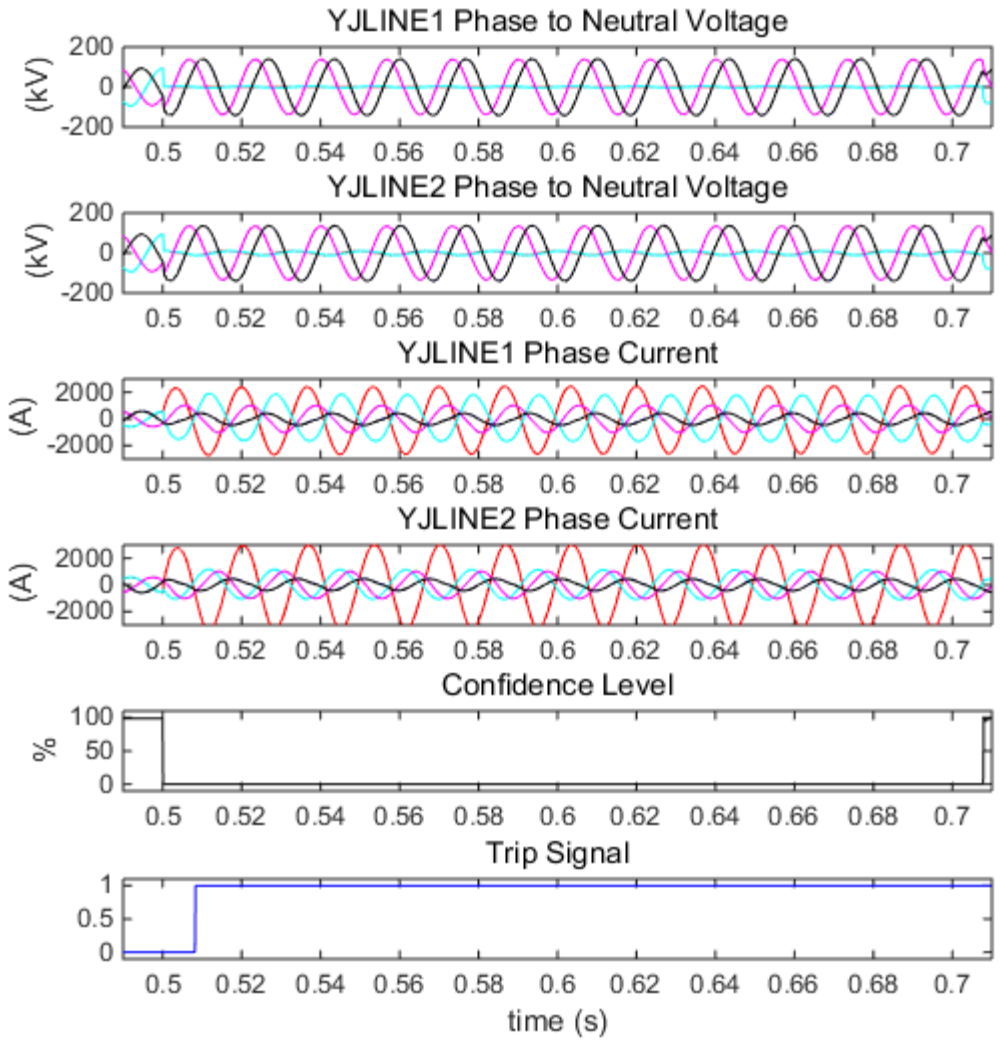
YJLINE1 Phase to Neutral Voltage
(kV)
200
0
-200
YJLINE2 Phase to Neutral Voltage
(kV)
200
0
-200
YJLINE1 Phase Current
(A)
2000
0
-2000
YJLINE2 Phase Current
(A)
2000
0
-2000
Confidence Level
%
100
50
0
Trip Signal
1
0.5
0
0.5 0.52 0.54 0.56 0.58 0.6 0.62 0.64 0.66 0.68 0.7
time (s)

Event 1

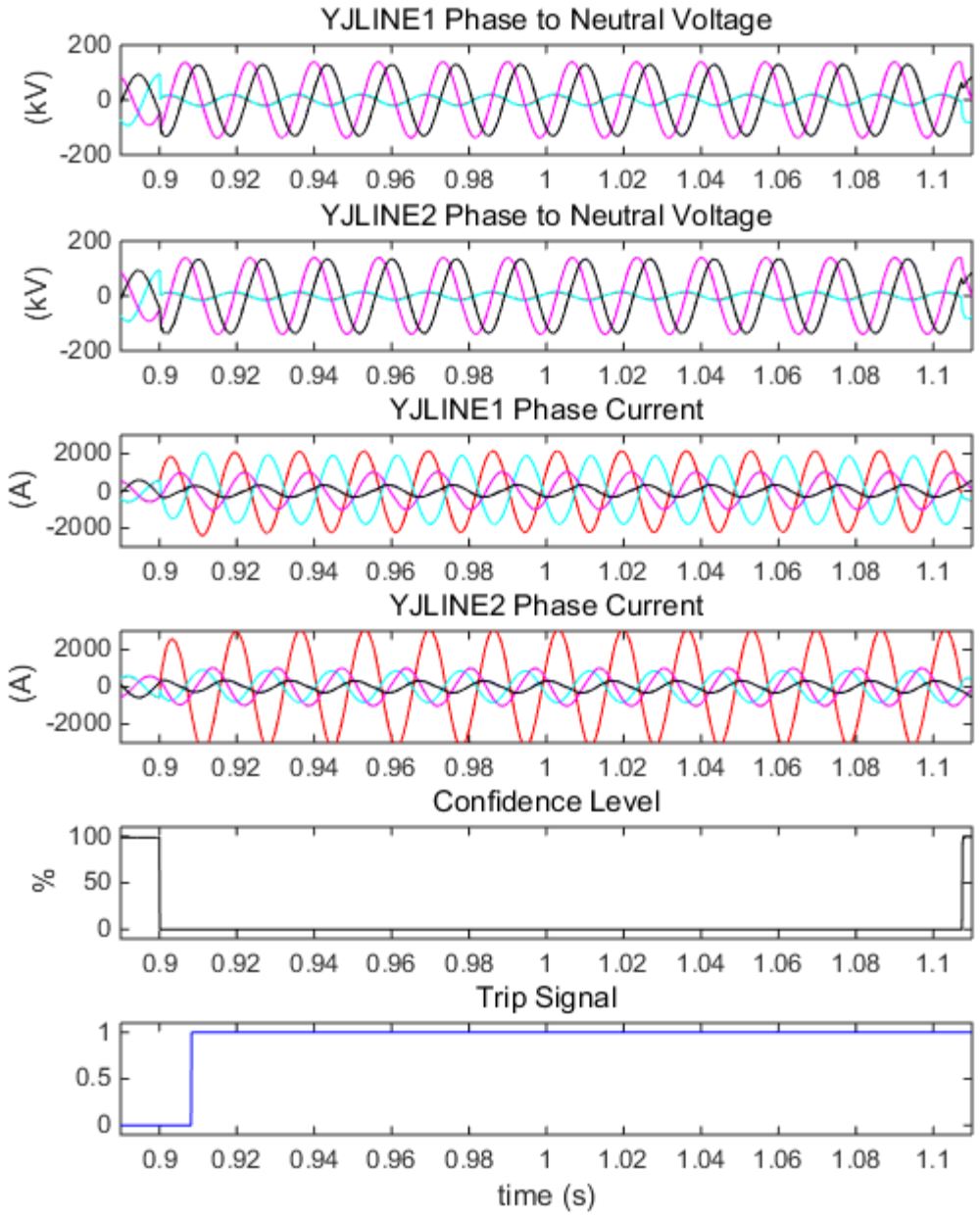
YJLINE1 Phase to Neutral Voltage
(kV)
200
0
-200
YJLINE2 Phase to Neutral Voltage
(kV)
200
0
-200
YJLINE1 Phase Current
(A)
2000
0
-2000
YJLINE2 Phase Current
(A)
2000
0
-2000
Confidence Level
%
100
50
0
Trip Signal
1
0.5
0
0.9 0.92 0.94 0.96 0.98 1 1.02 1.04 1.06 1.08 1.1
time (s)

Event 2

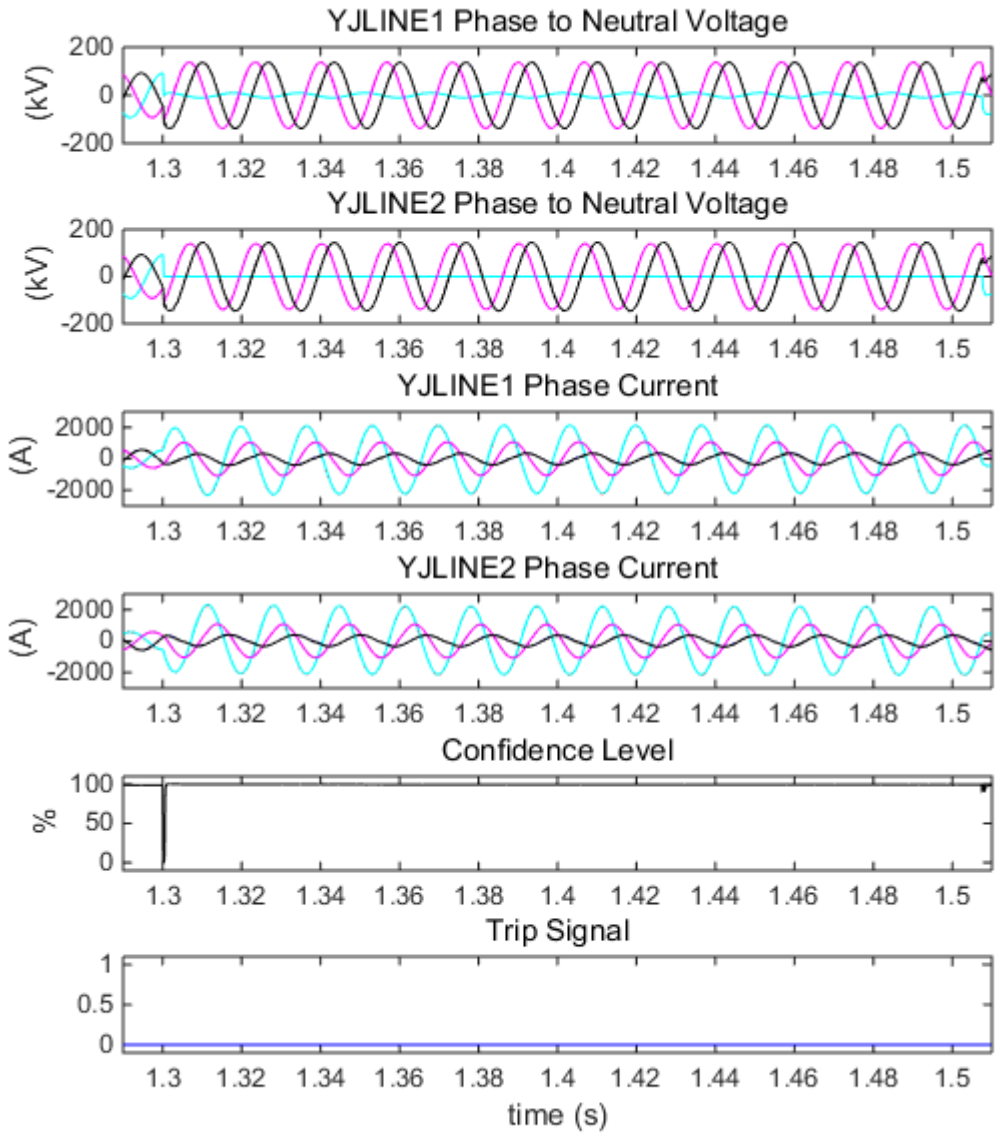

Event 3

Figure 7-8 Short line test case – Protection Results for DSE based protection

7.6 DSE based protection with time directional overcurrent protection

7.6.1 Long line protection

For short transmission line, time overcurrent could be used in a way that relays coordinate with each other along the transmission path. The pickup value for time overcurrent is set relatively lower than the instantaneous overcurrent, and it overreaches the protection zone. If the fault happens within the protection zone, it would trip with a delay (if the instantaneous overcurrent also sees the fault it would trip instantaneously, if it does no see the fault it would rely on the time overcurrent element to trip). If the fault happens outside the protection zone, it would also be delayed to trip the circuit breaker. However, the time coordination between this relay and the relay on the next faulted line is that if they both see the same fault current, then the relay at faulted line would have a delay less than the relay at the protected line. In this case, the relay at the faulted line would trip first (or the instantaneous overcurrent element on the faulted line sees the fault and trip instantaneously), avoiding the mis-operation of the time overcurrent protection.

However, for long transmission lines, the positive sequence impedance is large so that the fault current level would approach heavy loading current level. This is disadvantageous for time overcurrent protection since it would mis-interpret the heavy load as fault current and mis-operate. The DSE based protection, on the other hand, is immune to the fault current level again to provide security.

The test case for long transmission line is illustrated in Figure 7-9. The protected line is 128 km from YJLINE1 to YJLINE2. The line next to the protected line is 40 km with series compensation to increase the power transfer between the generation on the left and the load center on the right. The event sequence is as follow: the system is under normal

operation with loading current at 776A until **Event 1**: the three phase fault happens at time t = 0.5s to t = 0.7s. Then **Event 2**: another load center is connected to the system at t = 1.3s and lasts until the simulation ends. The protection setting is listed in Table 7.4.

The protection results for directional time overcurrent is illustrated in Figure 7-10. For event 1 the time overcurrent protection sees the fault, or the phase fault current equals the phase pickup value, so that it would operate due to a time delay. However, the relay at the next line should also pickup and trip first. For event 2 the heavy loading also triggers the time overcurrent protection to mis-operate.

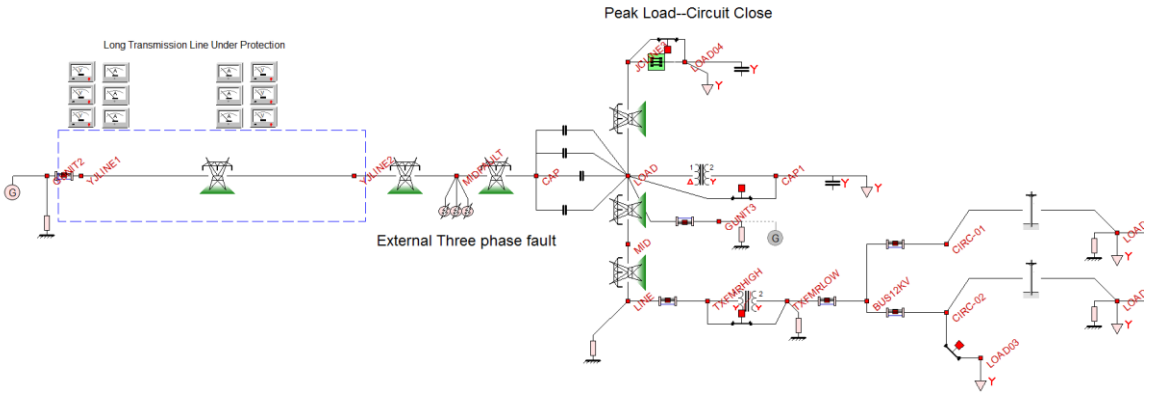

Figure 7-9 Long transmission line test case – a comparison between directional time overcurrent protection and DSE based protection

Table 7.4 Protection Settings for Long Line Case

Protection Functions	Settings
Directional Time Overcurrent	51P PKP: 995A 67Forward: <0Ohm 67Reverse: > 0Ohm Time Dial: 0.1 Moderately Inverse
Dynamic State Estimation Based	Integration Windows Size: 1 cycle Confidence Level Threshold: 50%

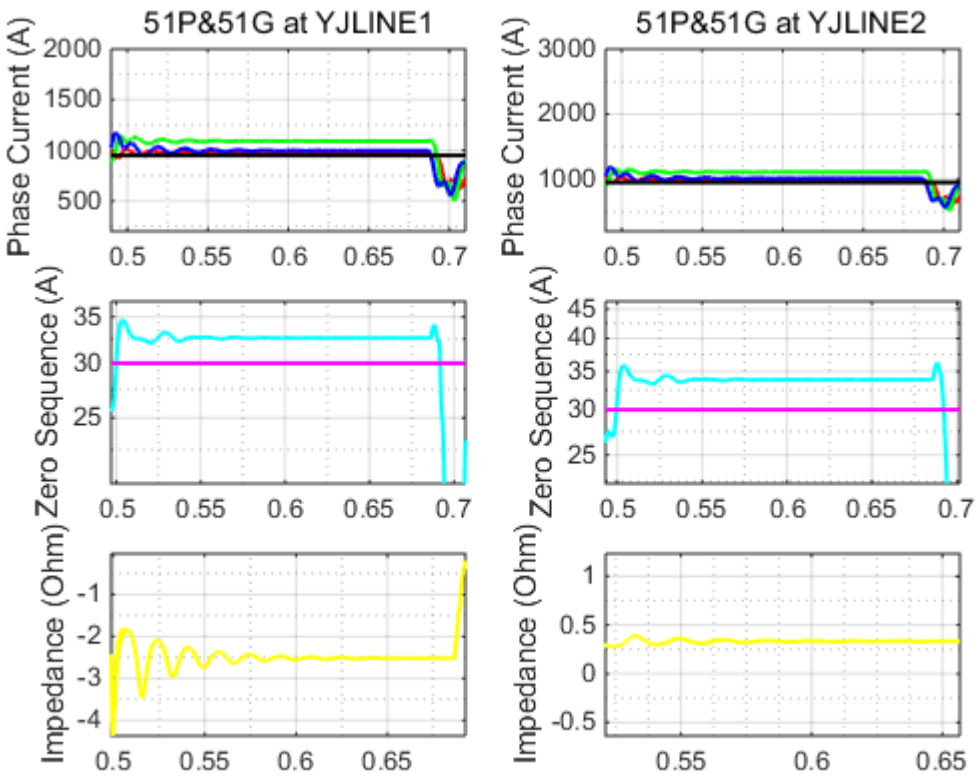
51P&51G at YJLINE1
51P&51G at YJLINE2
Phase Current (A)
Zero Sequence (A)
Impedance (Ohm)

Event 1

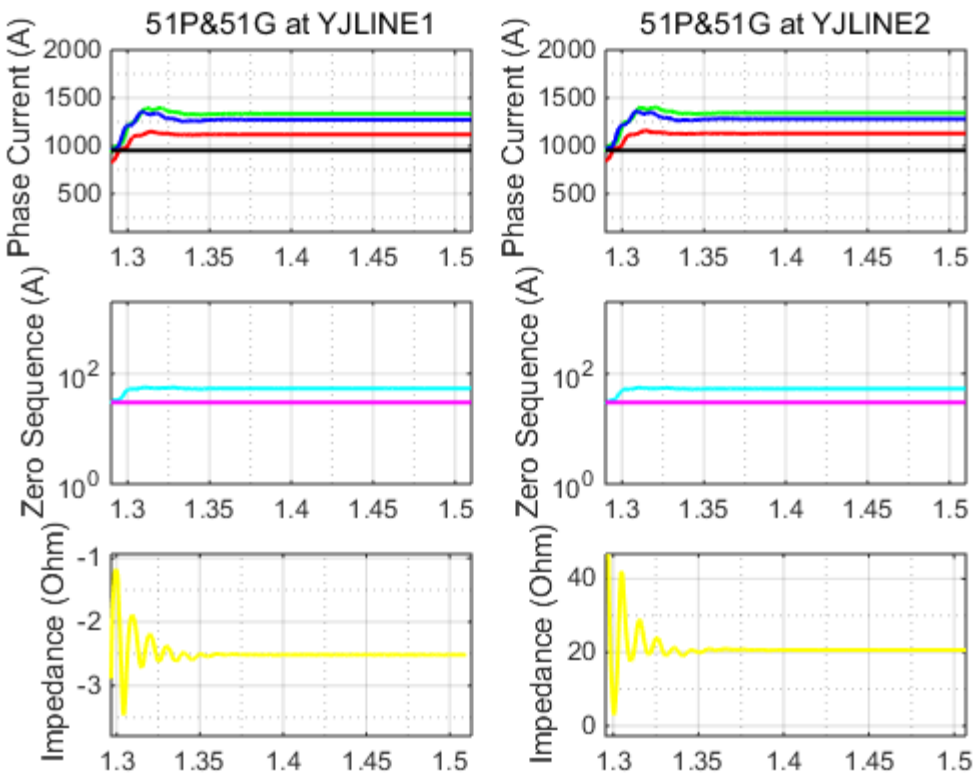

Event 2

Figure 7-10 Long line test case – Protection results for time overcurrent protection

By comparison, the protection results from DSE based protection is illustrated in Figure **7-11**. During Event 1 the fault happens outside the protection zone and the DSE based protection provides security against the fault. During Event 2 the load current increases and the DSE based protection would not mis-operate.

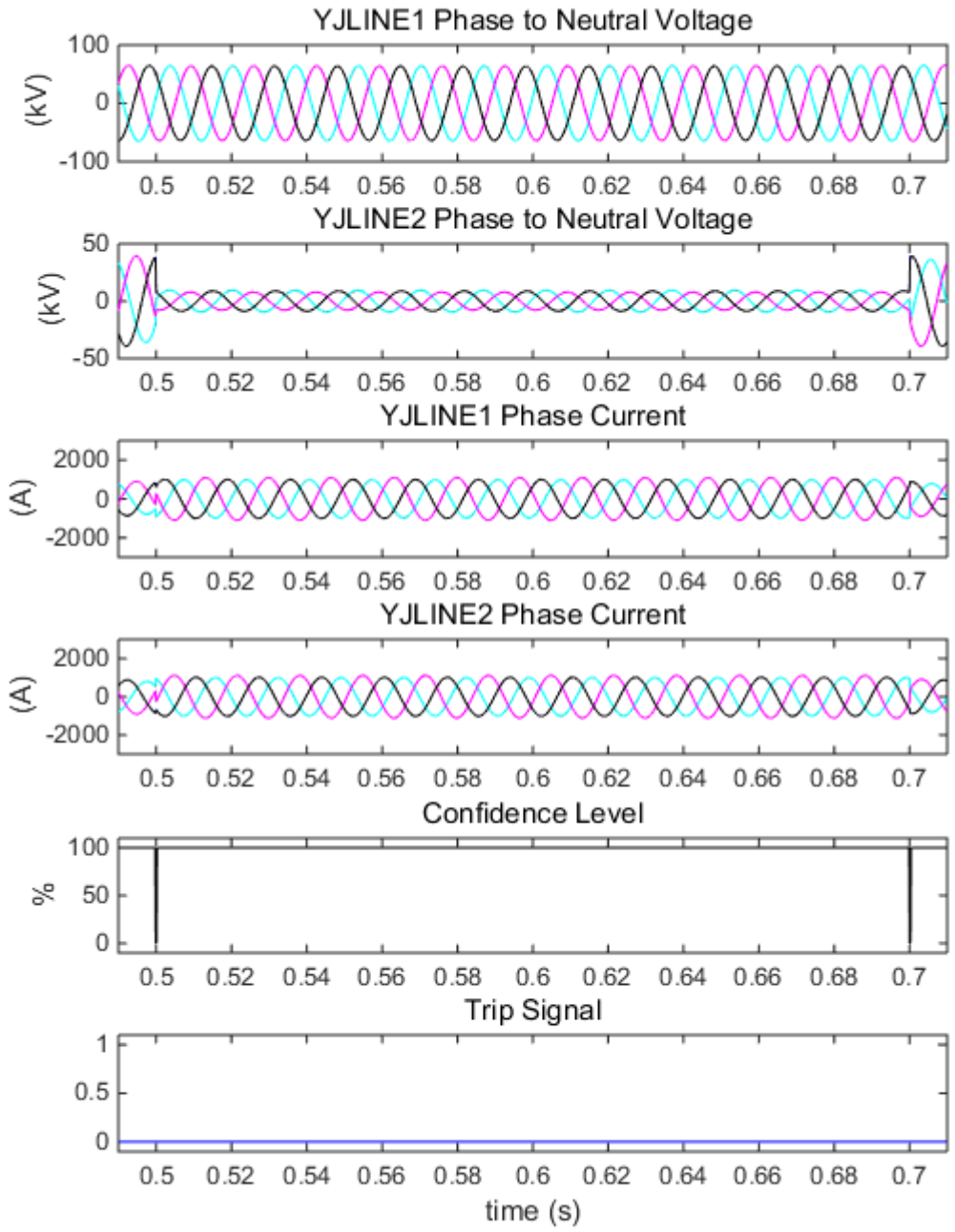
YJLINE1 Phase to Neutral Voltage
100
0
-100
(kV)
0.5 0.52 0.54 0.56 0.58 0.6 0.62 0.64 0.66 0.68 0.7
YJLINE2 Phase to Neutral Voltage
50
0
-50
(kV)
0.5 0.52 0.54 0.56 0.58 0.6 0.62 0.64 0.66 0.68 0.7
YJLINE1 Phase Current
2000
0
-2000
(A)
0.5 0.52 0.54 0.56 0.58 0.6 0.62 0.64 0.66 0.68 0.7
YJLINE2 Phase Current
2000
0
-2000
(A)
0.5 0.52 0.54 0.56 0.58 0.6 0.62 0.64 0.66 0.68 0.7
Confidence Level
100
50
0
%
0.5 0.52 0.54 0.56 0.58 0.6 0.62 0.64 0.66 0.68 0.7
Trip Signal
1
0.5
0
0.5 0.52 0.54 0.56 0.58 0.6 0.62 0.64 0.66 0.68 0.7
time (s)

Event 1

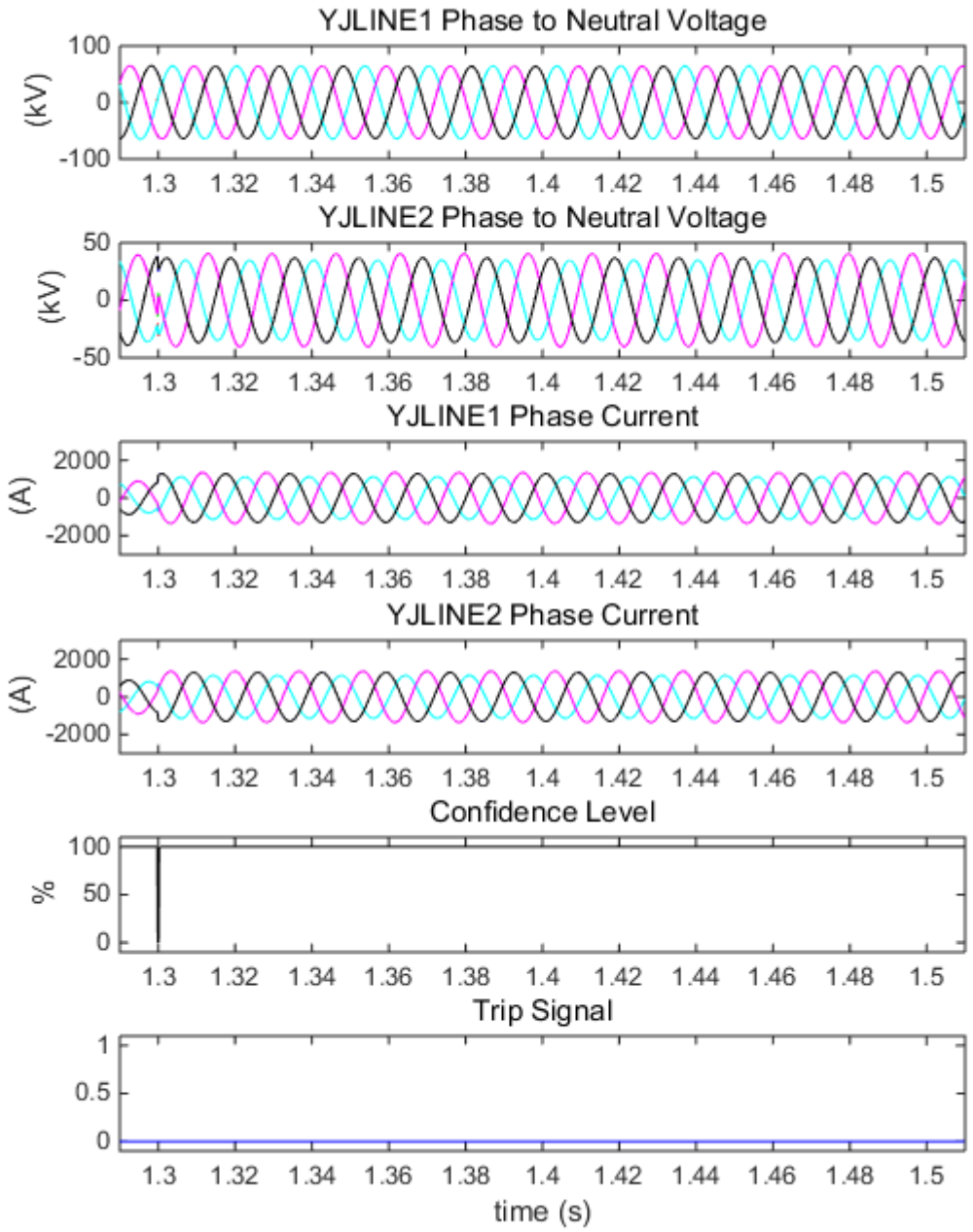

Event 2

Figure 7-11 Long line test case – protection results for DSE based protection

7.7 DSE based protection and Distance protection

7.7.1 Mutual Coupling in Parallel Lines

Utilities often use parallel lines to transport large amount of power through narrow right-of-way (towers and poles) line corridors. Constructing a multiple circuit line is more economic than building separate transmission lines. However magnetic mutual induction occurs in multiple circuit lines and in single circuit lines that run in close proximity with each other using the same right of way. The mutual coupling induces voltages on the faulted lines and unfaulted lines and may alter what the relays "sees" with the possibility of altering the relay decision. If the currents in both lines are in same direction the ground distance element would underreach, if the currents are in opposite direction the ground distance element would overreach. The phase element is not affected by the mutual coupling since the mutual inductance only occurs in zero sequence network (explained below).

To fulfill the statement, a simple test scenario is illustrated in Figure **7-12**. Two 40 parallel lines connect the synchronous generator on the left hand side (node YJLINE1L and node YJLINE1R) with an infinite bus on the right hand side (node YJLINE2L and node YJLINE2R). The base apparent power is 450 MVA, the base voltage is 115kV. The parameters of the sequence network are listed in Figure 7-13, the resistive parts are neglected. The single phase A to ground fault happens at 80% (or 32 miles) of the line from the left hand side at time t=1.0s and lasts for 0.5 second. The fault resistance is 0.1 Ohm.

First of all, a quick fault analysis for the simple test case in frequency domain would illustrates the impact of the mutual coupling on the computed impedance:

1). A fault analysis of this circuit YJLINE1L to YJLINE2L when the parallel circuit YJLINE1R to YJLINE2R is out of service is given by Figure **7-14**, the positive sequence impedance "seen" from the relay is computed by:

$$\frac{\tilde{V}_a}{\tilde{I}_a + m\tilde{I}_0} = \frac{59.92\angle 9.66^\circ kV}{1360\angle -62.77^\circ A + (2.913 + j0.01) \times 469.40\angle -77.31^\circ A} = 4 + j21.8\Omega$$

which corresponds to 80% of the line.

2). A fault analysis of this circuit YJLINE1L to YJLINE2L when the parallel circuit YJLINE1R to YJLINE2R is in service is given by Figure **7-15**, the positive sequence impedance "seen" from the relay is computed by:

$$\frac{\tilde{V}_a}{\tilde{I}_a + m\tilde{I}_0} = \frac{59.67\angle 8.59^\circ kV}{1317\angle -64.46A + (2.913 + j0.01) \times 443.50\angle -76.01^\circ A} = 4.5 + j22.5\Omega$$

which corresponds to more than 80% of the line.

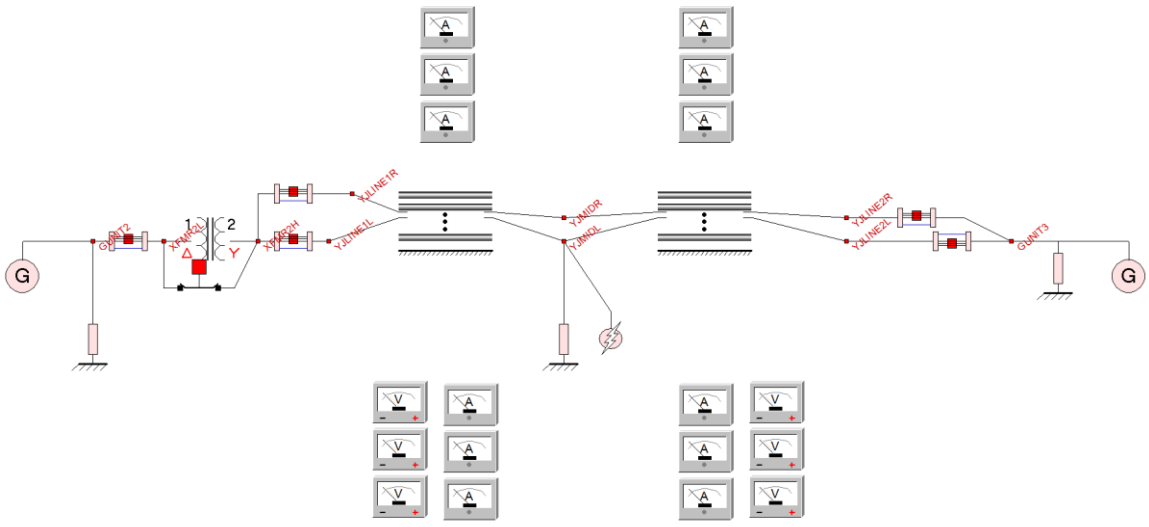

Figure 7-12 Parallel Lines Simple Test Case with single ended generator to infinity bus

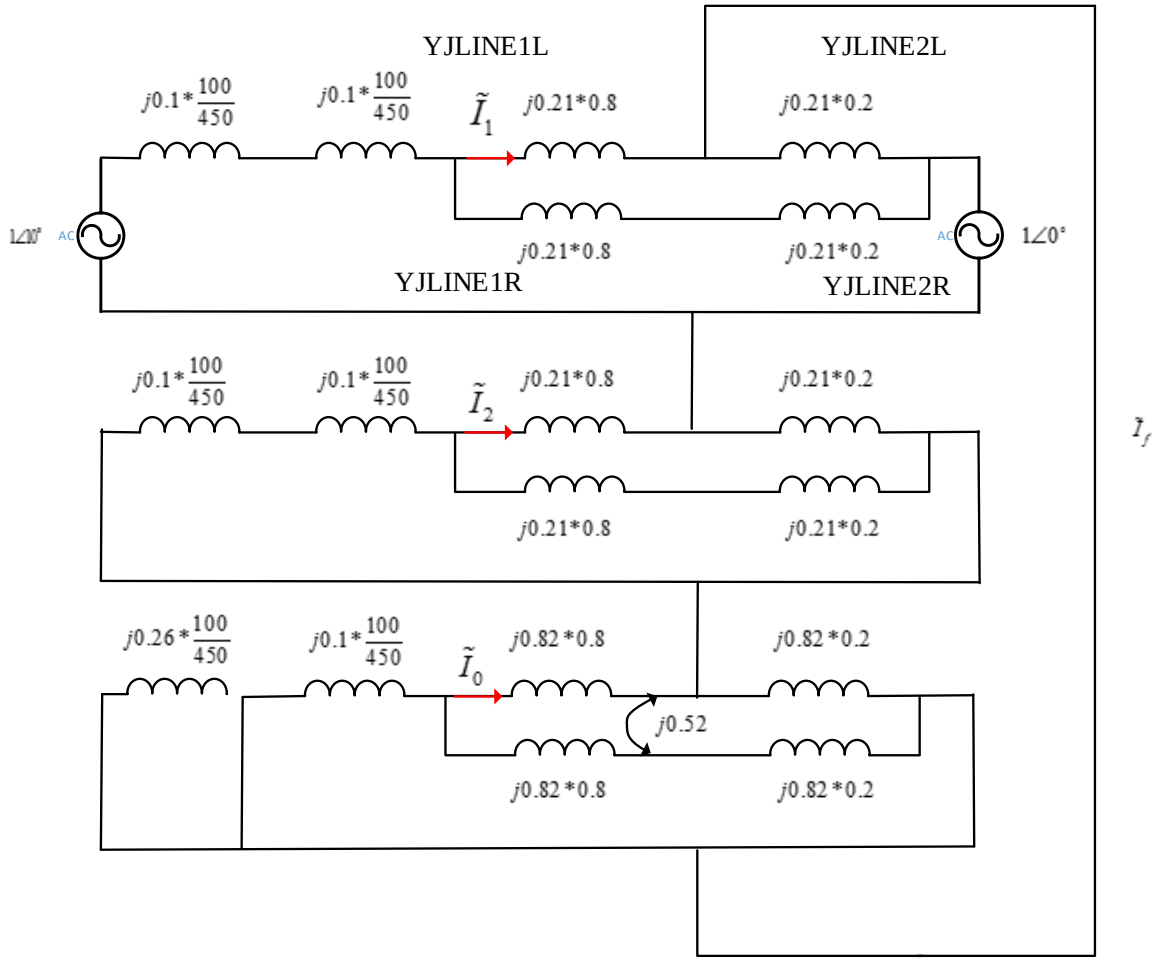

Figure 7-13 Parallel Line Simple Test Case with single ended generator to infinity bus – Parameters for generator, transformer and transmission lines

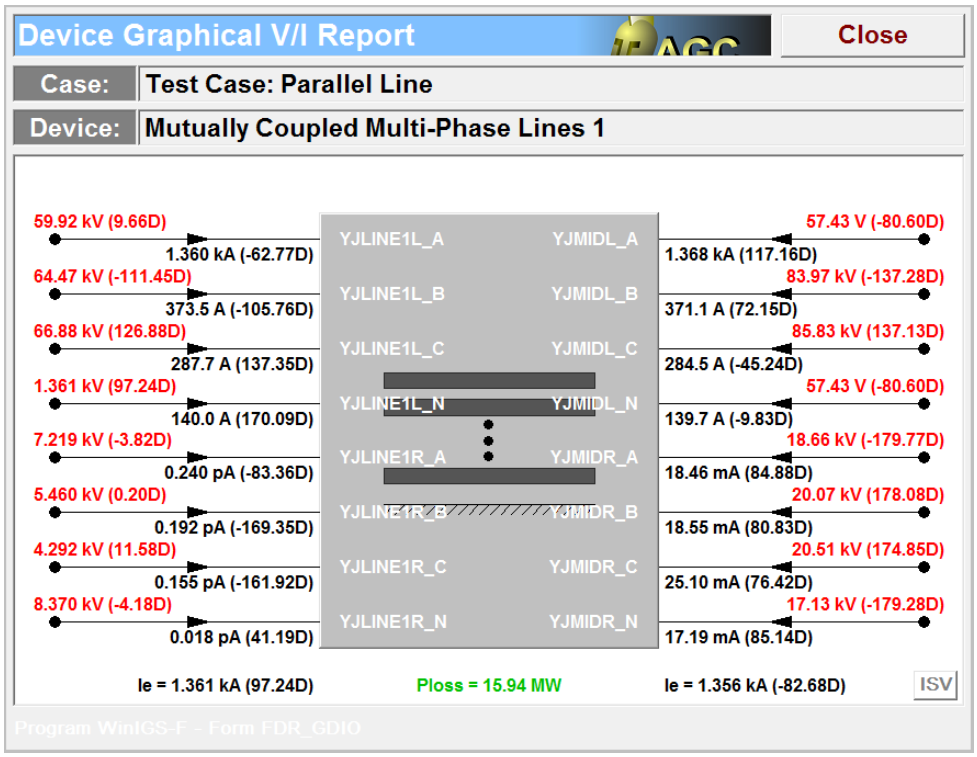

Figure 7-14 Parallel Line Simple Test Case with single ended generator to infinity bus – Fault analysis with parallel line out of service, frequency domain computation

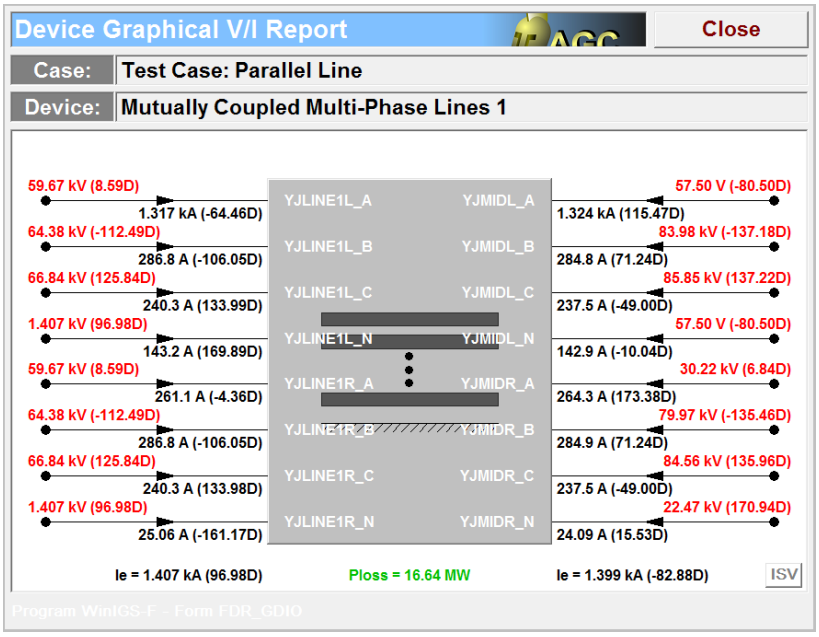

Figure 7-15 Parallel Line Simple Test Case with single ended generator to infinity bus – Fault analysis with parallel line in service, frequency domain computation

Second, a more detailed analysis is provided for the following test scenario illustrated in Figure **7-16**, the system has the same setup with the test system in Section 7.3 except the protected line here is a 40 miles transmission line that mutually couples with another 40 miles transmission line. The node on the left hand side of the protected line YJLINE1 is split into node YJLINE1L and YJLINE1R, the node on the right hand side of the protected line YJLINE2 is split into node YJLINE2L and YJLINE2R. The line from YJLINE1L to YJLINE2L is the line under protection, and the line from YJLINE1R to YJLINE2R is the parallel line that is mutually coupled with the protected line. The geometry parameters for the mutually coupled lines are illustrated in Figure 7-17, the two lines are basically equivalent, phase A conductor for both lines are 24.384 meters high, phase B conductors for both lines are 21.336 meters high, phase C conductors for both lines are 18.288 meters high, and phase N (or shield) conductors for both lines are 27.432 meters high. The lines are 8 meters apart from each other. The parameters for R, L, and C could be referred in Figure 7-18 and Figure 7-19.

There are three events. Event 1: The system is operating in normal condition from time t=0s to t=0.6s. Event 2: The protected line has a phase A to ground fault at 80% of the line from the left hand side, the fault resistance is 0.01 Ohm, from t=0.6s to t=0.8s. Event 3: The parallel line has a phase A to ground fault at 80% of the line from the left hand side, the fault resistance is 0.001 Ohm, from t=1.4s to t=1.6s.

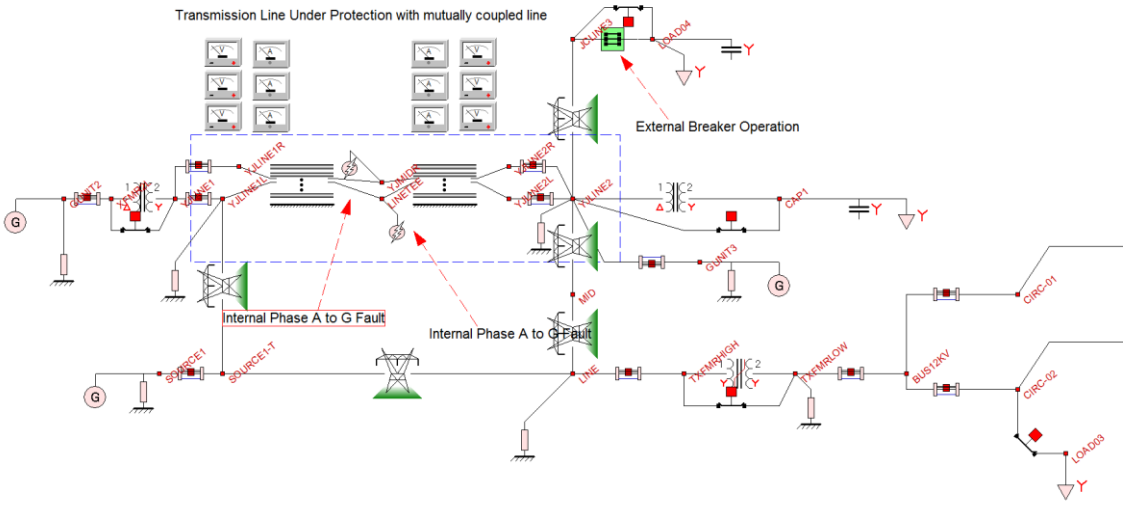

Figure 7-16 Parallel Line Test Case – similar to Section 7.3

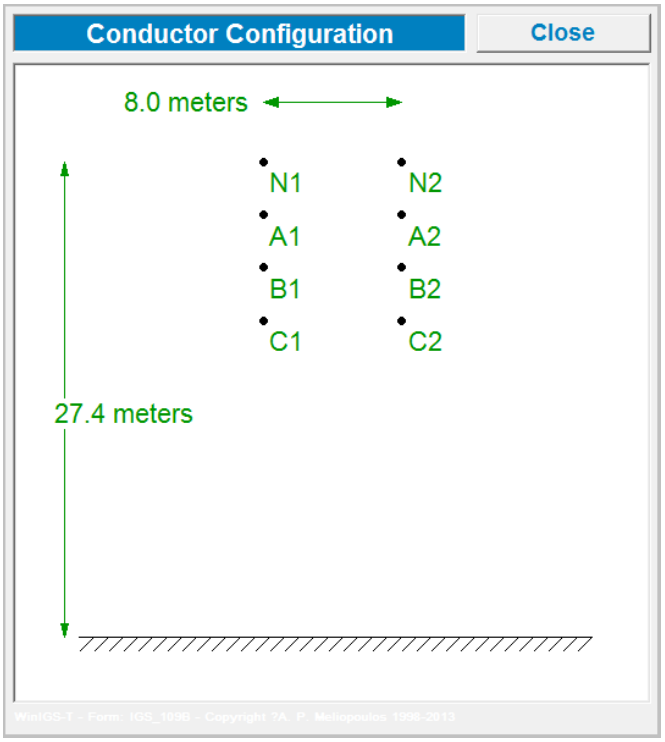

Figure 7-17 Geometry for mutually coupled lines in the test system

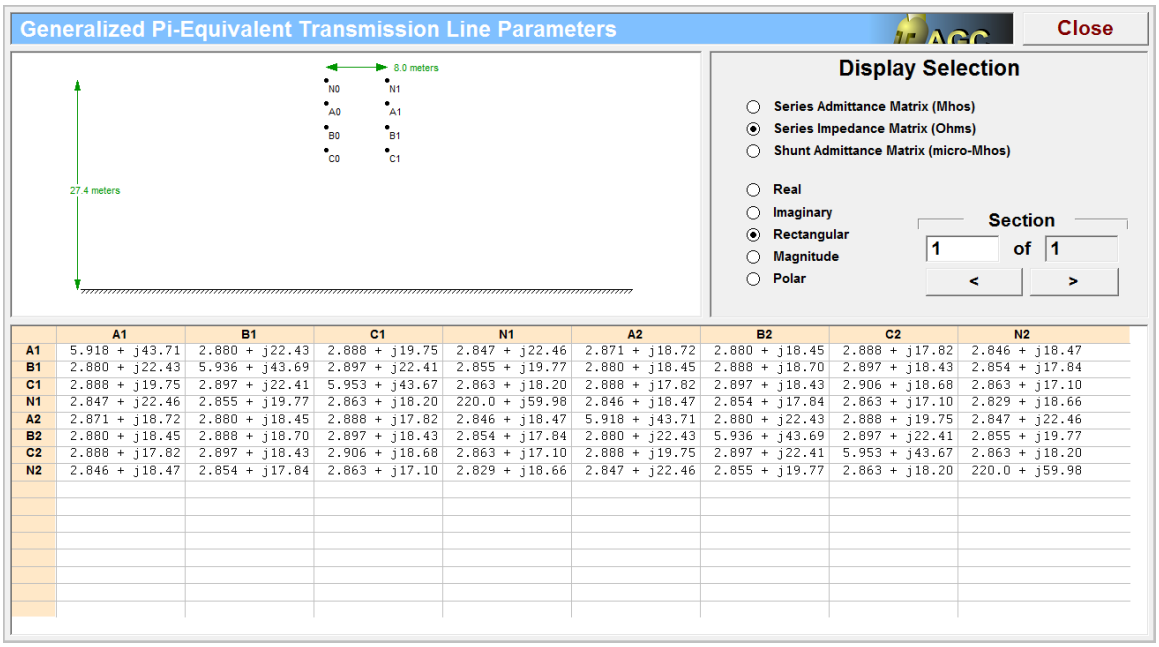

	A1	B1	C1	N1	A2	B2	C2	N2
A1	5.918 + j43.71	2.880 + j22.43	2.888 + j19.75	2.847 + j22.46	2.871 + j18.72	2.880 + j18.45	2.888 + j17.82	2.846 + j18.47
B1	2.880 + j22.43	5.936 + j43.69	2.897 + j22.41	2.855 + j19.77	2.880 + j18.45	2.888 + j18.70	2.897 + j18.43	2.854 + j17.84
C1	2.888 + j19.75	2.897 + j22.41	5.953 + j43.67	2.863 + j18.20	2.888 + j17.82	2.897 + j18.43	2.906 + j18.68	2.863 + j17.10
N1	2.847 + j22.46	2.855 + j19.77	2.863 + j18.20	220.0 + j59.98	2.846 + j18.47	2.854 + j17.84	2.863 + j17.10	2.829 + j18.66
A2	2.871 + j18.72	2.880 + j18.45	2.888 + j17.82	2.846 + j18.47	5.918 + j43.71	2.880 + j22.43	2.888 + j19.75	2.847 + j22.46
B2	2.880 + j18.45	2.888 + j18.70	2.897 + j18.43	2.854 + j17.84	2.880 + j22.43	5.936 + j43.69	2.897 + j22.41	2.855 + j19.77
C2	2.888 + j17.82	2.897 + j18.43	2.906 + j18.68	2.863 + j17.10	2.888 + j19.75	2.897 + j22.41	5.953 + j43.67	2.863 + j18.20
N2	2.846 + j18.47	2.854 + j17.84	2.863 + j17.10	2.829 + j18.66	2.847 + j22.46	2.855 + j19.77	2.863 + j18.20	220.0 + j59.98

Figure 7-18 Series Impedance Matrix for mutually coupled lines in the test system

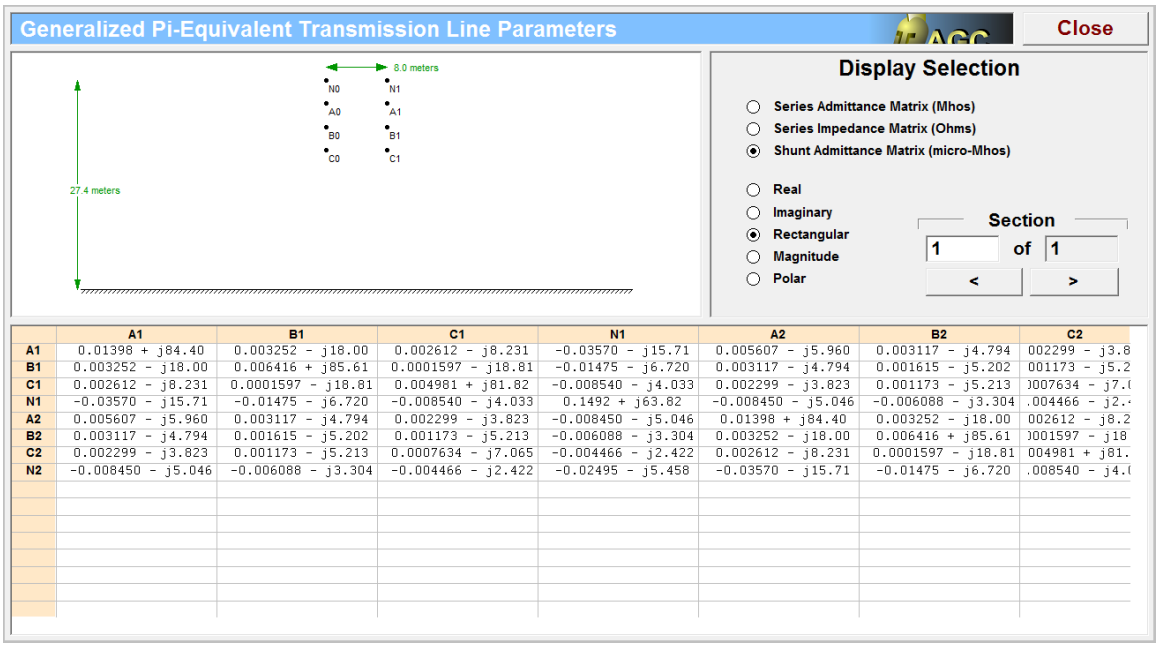

	A1	B1	C1	N1	A2	B2	C2
A1	0.01398 + j84.40	0.003252 - j18.00	0.002612 - j8.231	-0.03570 - j15.71	0.005607 - j5.960	0.003117 - j4.794	002299 - j3.8
B1	0.003252 - j18.00	0.006416 + j85.61	0.0001597 - j18.81	-0.01475 - j6.720	0.003117 - j4.794	0.001615 - j5.202	001173 - j5.2
C1	0.002612 - j8.231	0.0001597 - j18.81	0.004981 + j81.82	-0.008540 - j4.033	0.002299 - j3.823	0.001173 - j5.213	0007634 - j7.(
N1	-0.03570 - j15.71	-0.01475 - j6.720	-0.008540 - j4.033	0.1492 + j63.82	-0.008450 - j5.046	-0.006088 - j3.304	.004466 - j2..
A2	0.005607 - j5.960	0.003117 - j4.794	0.002299 - j3.823	-0.008450 - j5.046	0.01398 + j84.40	0.003252 - j18.00	002612 - j8.2
B2	0.003117 - j4.794	0.001615 - j5.202	0.001173 - j5.213	-0.006088 - j3.304	0.003252 - j18.00	0.006416 + j85.61	001597 - j18
C2	0.002299 - j3.823	0.001173 - j5.213	0.0007634 - j7.065	-0.004466 - j2.422	0.002612 - j8.231	0.0001597 - j18.81	004981 + j81.
N2	-0.008450 - j5.046	-0.006088 - j3.304	-0.004466 - j2.422	-0.02495 - j5.458	-0.03570 - j15.71	-0.01475 - j6.720	.008540 - j4.(

Figure 7-19 Shunt Admittance Matrix for mutually coupled lines in the test system

The protection settings for distance elements is listed in Table **7.5**, the zone 1 element covers 80% of the line, zone 2 element covers 120% of the line, and zone 3 element covers 160% of the line.

The settings for the distance element and the DSE based protection is the following:

Table 7.5 Protection Settings for Parallel Lines Test Case

Protection Functions	Settings
Stepped Distance	Z1PKP: 22.35∠82.17 Z2PKP: 33.53∠82.17, Z2 Delay: 20 cycles Z3PKP: 44.71∠82.17 compensation factor m: 2.91∠0.194 Z3 Delay: 30 cycles
Dynamic State Estimation Based	Integration Windows Size: 1 cycle Confidence Level Threshold: 50%

The protection results in the complex operating plane is illustrated in Figure **7-20**-Figure **7-22**, in event 1 both the operating points computed at both relays are outside the operating zone, in event 2 the operating point computed from the relay at YJLINE1L is inside zone 2 but falls outside zone1, the operating point computed from the relay at YJLINE2L is inside zone 1. As a result, the relay at YJLINE2L would trip instantaneously, whereas the relay at YJLINE1L would not trip instantaneously, but with a 20 cycles delay. Thus the relays at both terminals would not trip simultaneously.

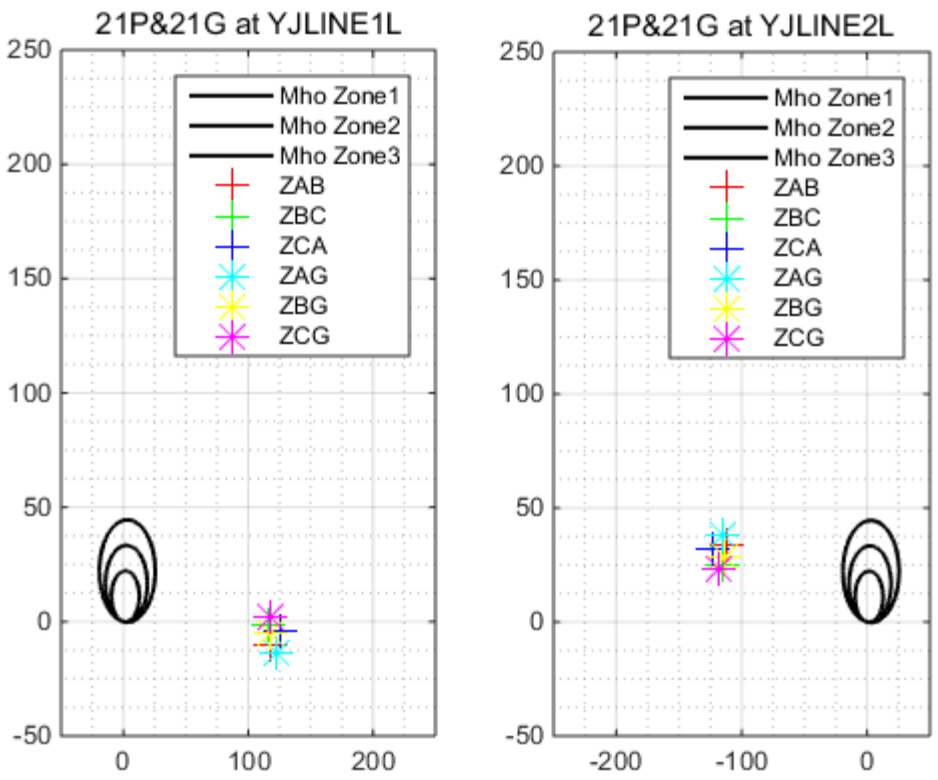

Figure 7-20 Operating points for distance protection in the parallel line test system – Event 1

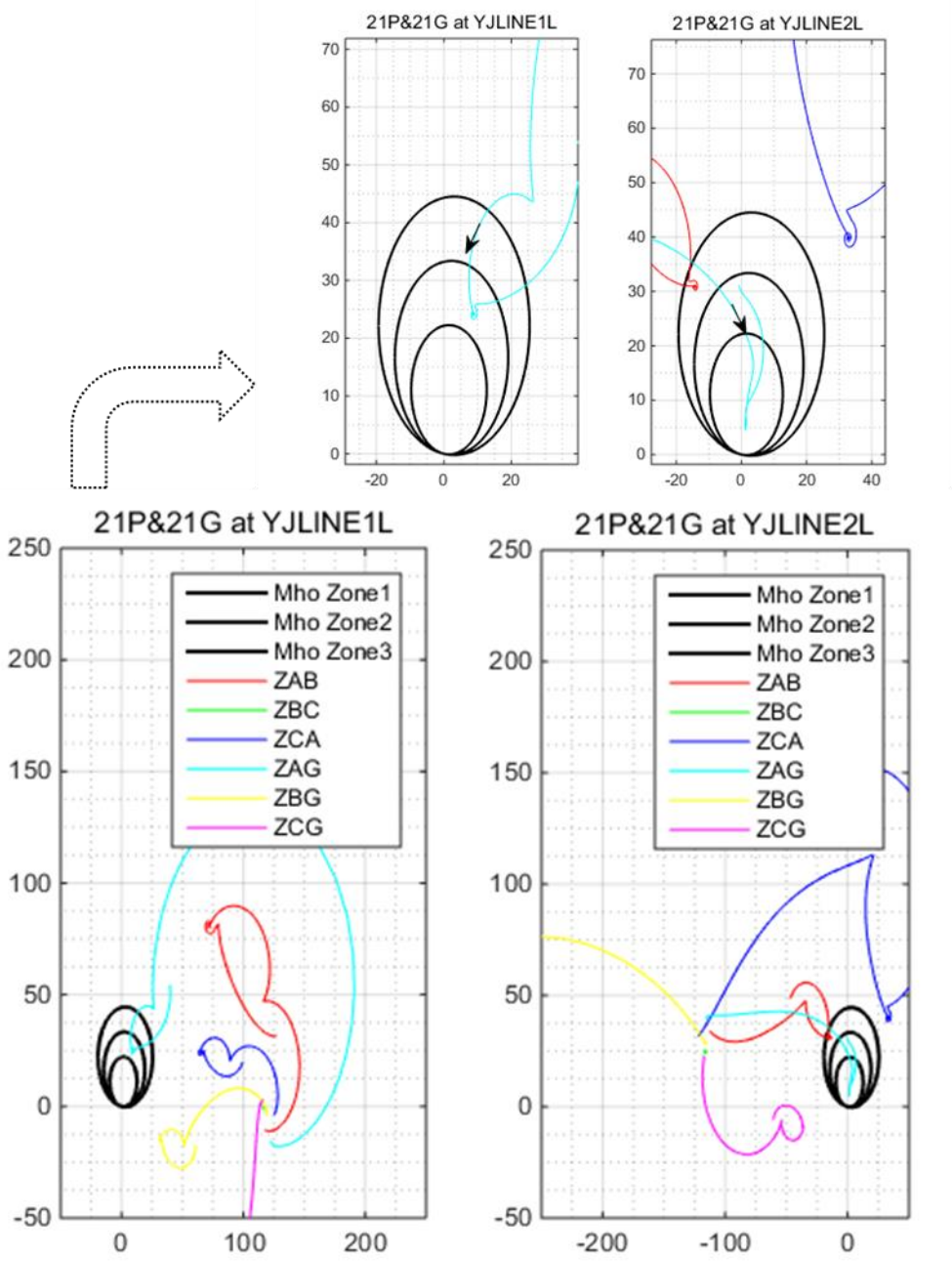

Figure 7-21 Operating points for distance protection in the parallel line test system – Event 2

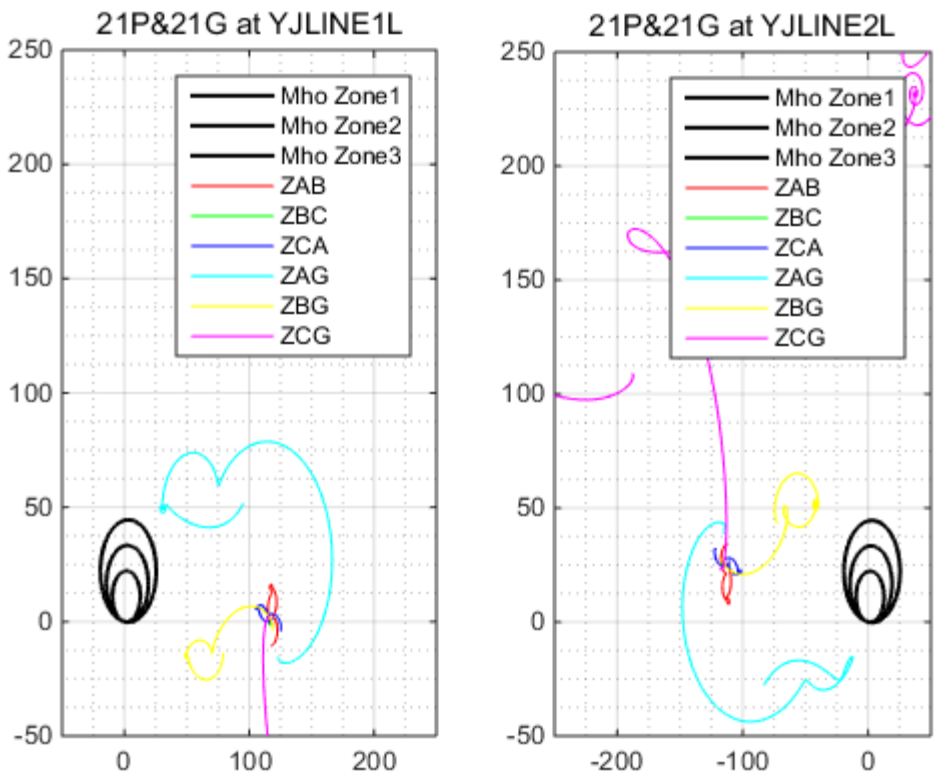

Figure 7-22 Operating points for distance protection in the parallel line test system – Event 3

Third of all, the protection results from the distance elements are compared with that of the DSE based protection. In order for the dynamic state estimation based protection to work properly, the modeling of the mutually coupled lines needs to be justified.

There are three options:

Option 1 –

The first option is to model the entire set of transmission lines including the line that needs to be protected and the lines that has mutual coupling with the protected line, see Figure **7-23**. In this case fault in both lines would be detected. Specifically, the model is similar to the single section model in (4.3), where the difference is that in (4.3) it models

the single four phase transmission line, and in the following equation it models two four phase transmission lines:

$$\begin{aligned} i_1(t) &= C\frac{dv_1(t)}{dt} + i_L(t) \\ i_2(t) &= C\frac{dv_2(t)}{dt} - i_L(t) \\ 0 &= -v_1(t) + v_2(t) + Ri_L(t) + L\frac{di_L(t)}{dt} \end{aligned} \tag{7.6}$$

where,

R, L, C: 8×8 resistance, self inductance, capacitance and matrices.

$i_1(t)$: all through variables on left side of pi equivalent model at time t

$i_2(t)$: all through variables on right side of pi equivalent model at time t

$v_1(t)$: all across variables on left side of pi equivalent model at time t

$v_2(t)$: all across variables on right side of pi equivalent model at time t

$i_L(t)$: the inductance current through the line at time t

$x(t) = [v_1(t) \quad v_2(t) \quad i_L(t)]$

The dimension of the matrices can increase depending on the number of parallel lines being modeled. The problem with the first approach is that since the algorithm is targeted to only protect a single four phase transmission line, if there is a fault in the parallel line (or parallel lines), the DSE based protection would also capture it and categorize it as internal fault. Other mathematical tools can be used to distinguish between the fault in the protected line and the fault in the parallel lines, for example the comparison between the magnitude of residuals by using WLAV in the phasor (frequency) domain, the details are not included in this thesis since the focus lies in the other two options.

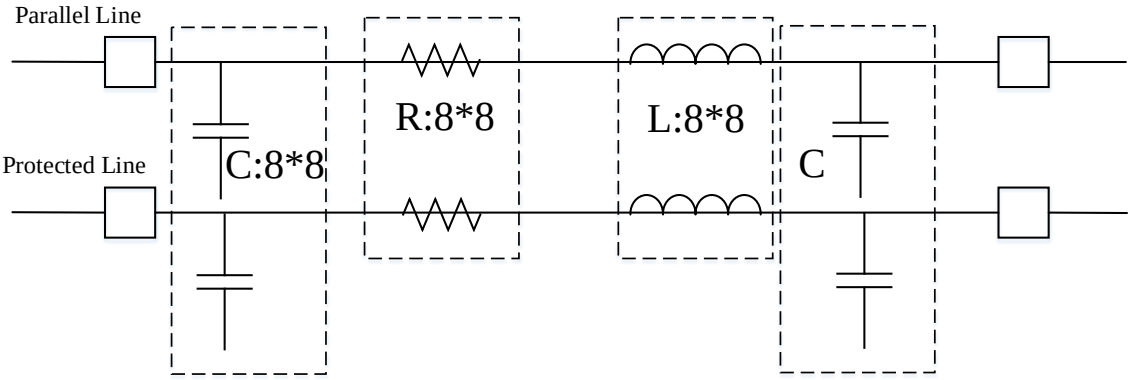

Figure 7-23 Parallel Line Modeling – Option 1

Option 2 –

The second option is to model the single four phase transmission line that needs to be protected, and also models the impact of parallel lines, which is simply a part of (7.6) that only models the KCL and KVL on the protected line. Specifically, the quadratized time domain model is the following:

$$\begin{aligned} i_1(t) &= C_1 \frac{dv_1(t)}{dt} + C_m \frac{dv_{1P}(t)}{dt} + i_{L1}(t) \\ i_2(t) &= C_1 \frac{dv_2(t)}{dt} + C_m \frac{dv_{2P}(t)}{dt} - i_{L1}(t) \\ 0 &= -v_1(t) + v_2(t) + R_1 i_{L1}(t) + L_1 \frac{di_{L1}(t)}{dt} + R_m i_{LP}(t) + L_m \frac{di_{LP}(t)}{dt} \end{aligned} \tag{7.7}$$

where,

R_1, L_1, C_1: 4×4 self resistance, inductance, capacitance matrices for the protected line.

R_m, L_m, C_m : 4×4 mutual resistance, inductance and capacitance matrices that impacts the protected line from the parallel line

$i_1(t)$: all through variables on left side of pi equivalent model for the protected line at time t

$i_2(t)$: all through variables on right side of pi equivalent model for the protected line at time t

$v_1(t)$: all across variables on left side of pi equivalent model for the protected line at time t

$v_2(t)$: all across variables on right side of pi equivalent model for the protected line at time t

$v_{1P}(t)$: all across variables on left side of pi equivalent model for the parallel line at time t

$v_{2P}(t)$: all across variables on right side of pi equivalent model for the parallel line at time t

$i_{L1}(t)$: the inductance current through the protected line at time t

$i_{LP}(t)$: the inductance current through the parallel line at time t

$x(t) = [v_1(t) \quad v_2(t) \quad i_{L1}(t)]$

From this model it could be seen that by comparing the three set of equations in (7.7) with the three set of equations in (4.3), the first equation means the through current on the left hand side of the protected line has an additive term as a charging current contribution from the left hand side of the parallel line, the second equation means the through current on the right hand side of the protected line has an additive term as a charging current contribution from the right hand side of the parallel line, however due to the fact that the contribution of the charging current is very small (the capacitive reactance C_m is a function of the distance between phase conductors and is typically in the order of micro Farads, the change of voltage v_{1P} in normal operating condition is in order of 0kV-100 kV/sample for a 115 kV system, which means that the charging current is in order of 0A - 1A), the

practical way is to model it as noise with a standard deviation of 1A (also note that the change of voltage when the parallel line has a large phase to ground fault can be very high for several samples since the voltage suddenly drops to zero, however this can easily be filtered by the estimation algorithm. The third equation has an additive term as induced voltage contribution from the parallel line. In normal operating condition the currents through the parallel line can be from 0 Amps to several thousand Amps depending on the loading condition, the induced voltage can be from 0 volts to several hundred volts, which depends on how imbalance the parallel line is operating. If the parallel line has an internal fault, its induced voltage on the protected line can be very high (in the order of 10 kV for a 115 kV system), in Option 2 one practical way is to model this additive term as noise with a standard deviation of 10 kV in the virtual measurements, where Option 3 would introduce another way to deal with such high induced voltage.

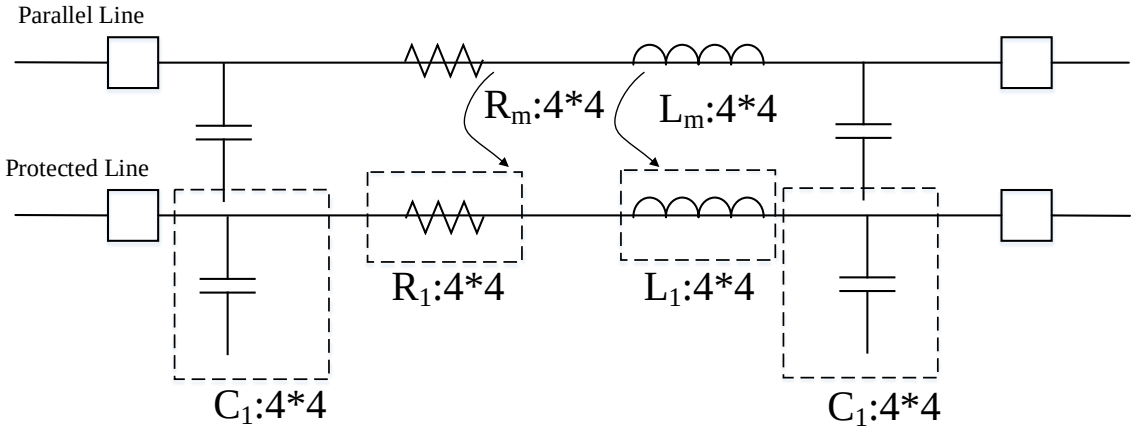

Figure 7-24 Parallel Line Modeling – Option 2 and Option 3

Option 3 –

The third option is to model the single four phase transmission line that needs to be protected, and also models the impact of parallel lines, which is simply a part of (7.6) but due to the large impact of induced voltage the KVL would not be included.

$$\begin{aligned} i_1(t) &= C_1 \frac{dv_1(t)}{dt} + C_m \frac{dv_{1P}(t)}{dt} + i_{L1}(t) \\ i_2(t) &= C_1 \frac{dv_2(t)}{dt} + C_m \frac{dv_{2P}(t)}{dt} - i_{L1}(t) \end{aligned} \tag{7.8}$$

where,

R_1, L_1, C_1: 4×4 self resistance, inductance, capacitance matrices for the protected line.

C_m : 4×4 mutual capacitance matrix that impacts the protected line from the parallel line

$i_1(t)$: all through variables on left side of pi equivalent model for the protected line at time t

$i_2(t)$: all through variables on right side of pi equivalent model for the protected line at time t

$v_1(t)$: all across variables on left side of pi equivalent model for the protected line at time t

$v_2(t)$: all across variables on right side of pi equivalent model for the protected line at time t

$v_{1P}(t)$: all across variables on left side of pi equivalent model for the parallel line at time t

$v_{2P}(t)$: all across variables on right side of pi equivalent model for the parallel line at time t

$i_{L1}(t)$: the inductance current through the protected line at time t

$x(t) = [v_1(t) \quad v_2(t) \quad i_{L1}(t)]$

In this model only the KCL equations are included. The KVL equation is not included if the impact of the induced voltage from parallel line can be very large and difficult to model.

The protection results from the three options are presented in the following.

The protection results from option 1 is illustrated from Figure **7-25**, Figure **7-26**, and Figure **7-27**. The measurements and estimated measurements, confidence level and trip logic is plotted in the same way as in Section 7.3. In event 1 the measurements match the model and the confidence level stays at 100%. In event 2 the algorithm captures the internal fault in the protected line and issues trip signal. In event 3 the algorithm also captures the internal fault in the parallel line and issues trip signal. The distinguish between the internal fault along protected line and internal fault along parallel line requires data processing on the residuals, and since the focus in on the other two options, this technique would not be discussed here.

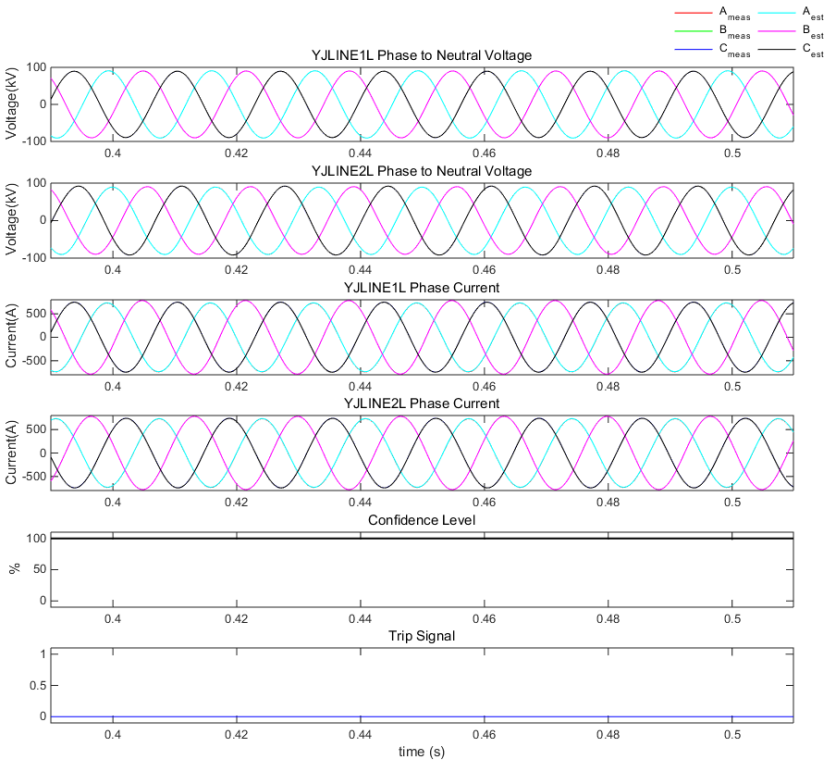

Figure 7-25 DSE dynamic state estimation and protection results, parallel line test system -- Event 1, Option 1

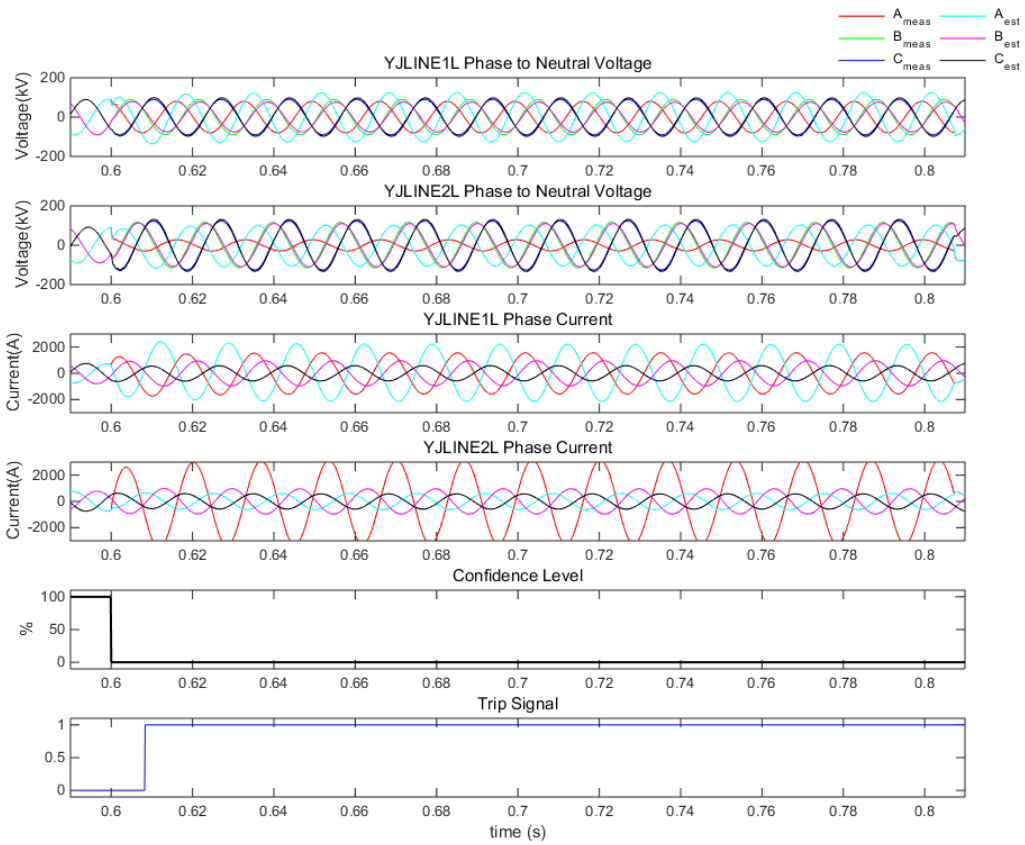

Figure 7-26 DSE dynamic state estimation and protection results, parallel line test system -- Event 2, Option 1

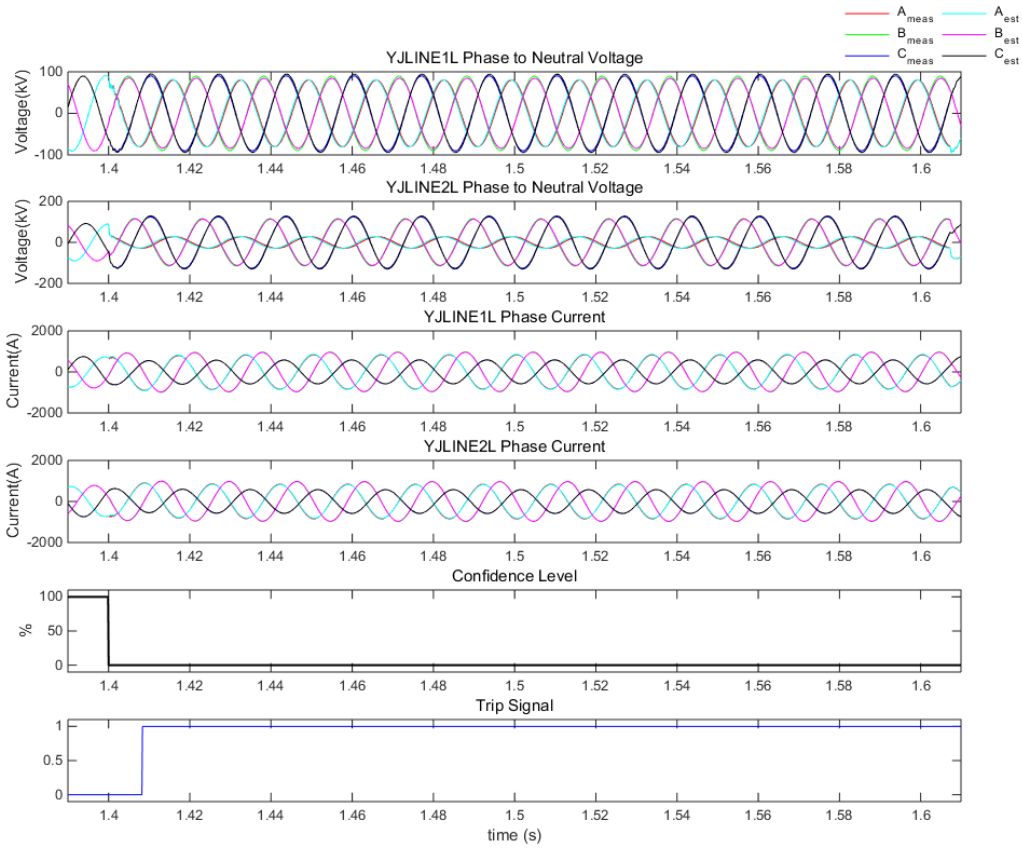

Figure 7-27 DSE dynamic state estimation and protection results, parallel line test system -- Event 3, Option 1

The protection results from option 2 is illustrated from Figure **7-28**, Figure **7-29**, and Figure **7-30**. The measurements and estimated measurements, confidence level and trip logic is plotted in the same way as in Section 7.3. In event 1 the measurements match the model and the confidence level stays at 100%. In event 2 the algorithm captures the internal fault in the protected line and issues trip signal. In event 3 since the algorithm treats the induced voltage as noise the internal fault in the parallel line is not captured. Very interestingly, the mean confidence level during event 3 is 99.5% compared to the 100% during event 1, which means that the induced voltage does impact the estimation algorithm.

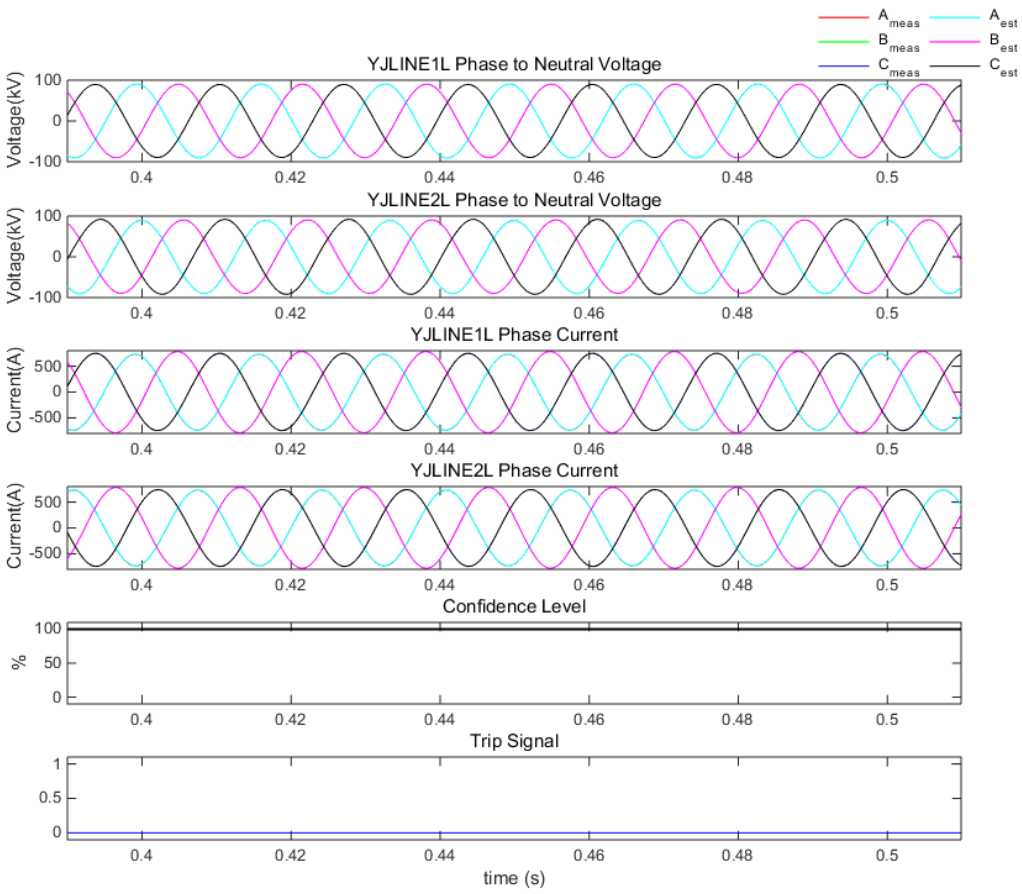

Figure 7-28 DSE dynamic state estimation and protection results, parallel line test system -- Event 1, Option 2

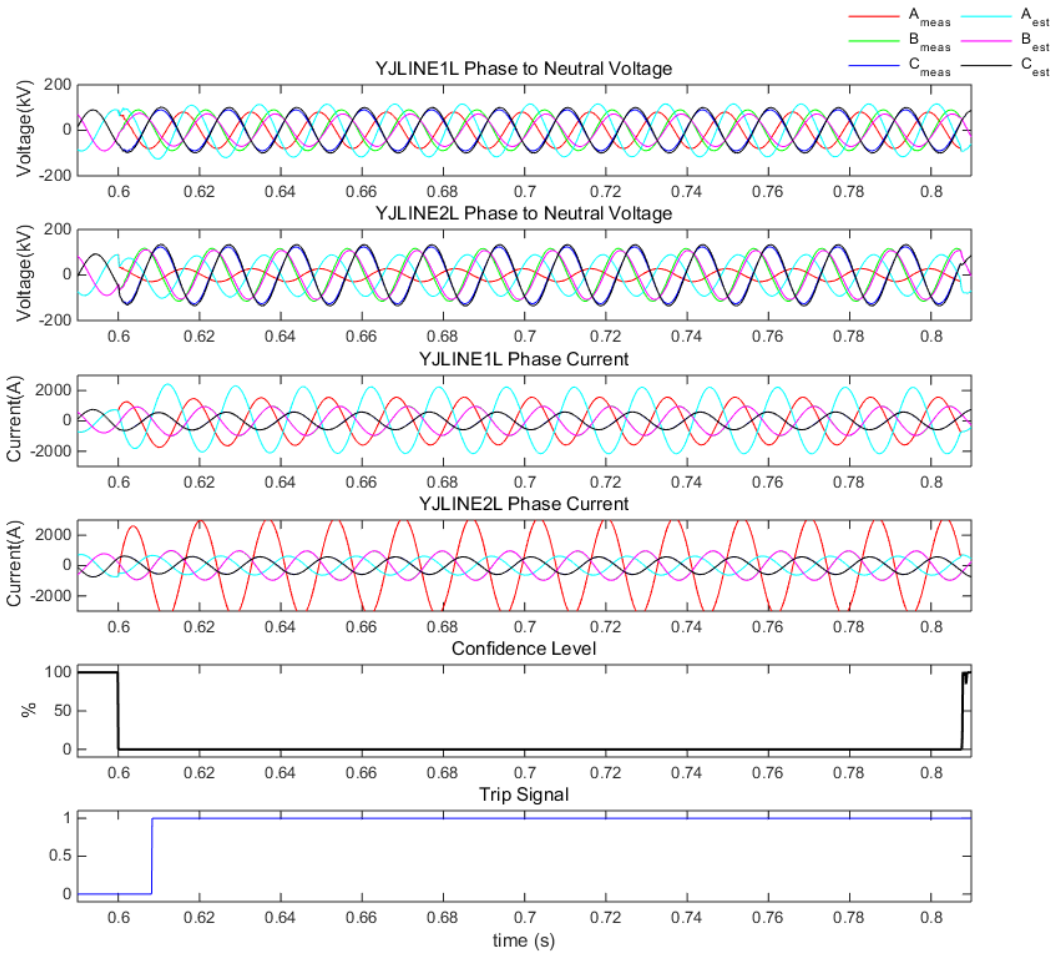

Figure 7-29 DSE dynamic state estimation and protection results, parallel line test system -- Event 2, Option 2

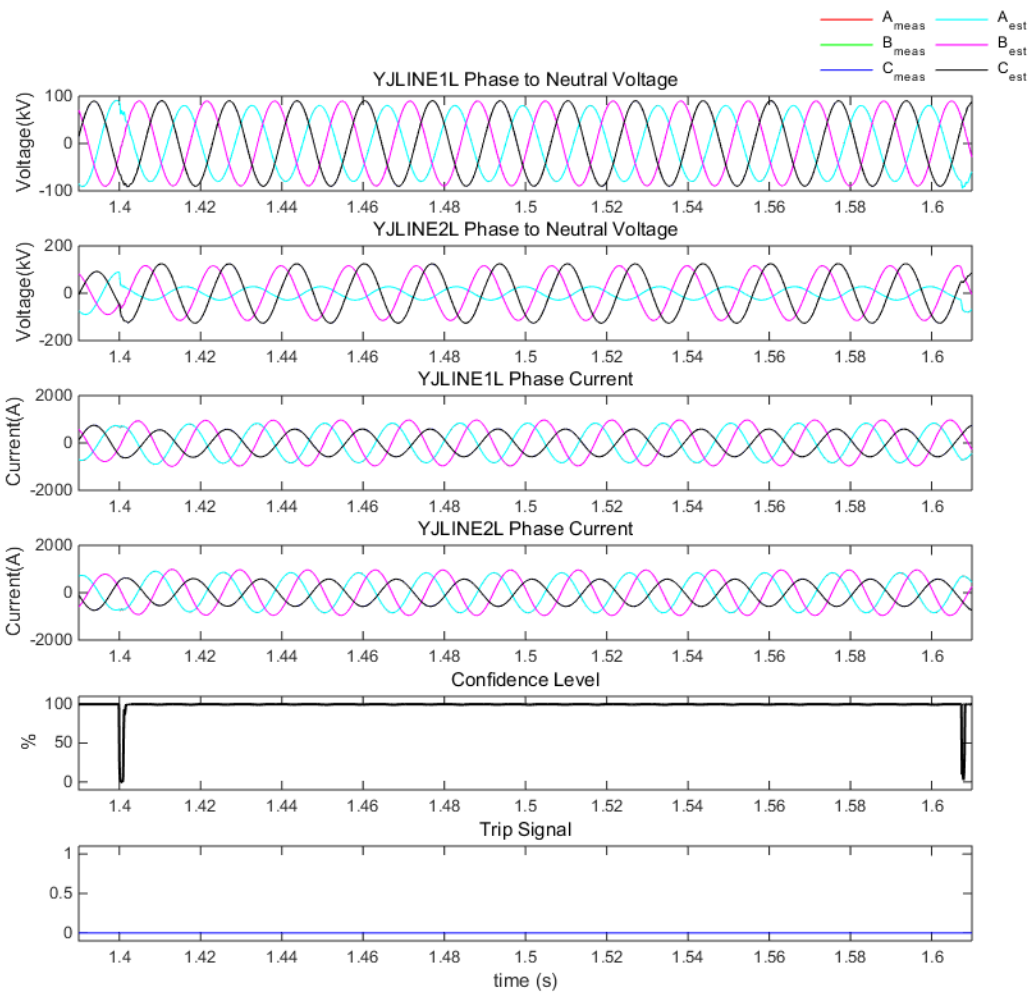

Figure 7-30 DSE dynamic state estimation and protection results, parallel line test system -- Event 3, Option 2

The protection results from option 3 is illustrated from Figure **7-31**, Figure **7-32** and Figure **7-33**. The measurements and estimated measurements, confidence level and trip logic is plotted in the same way as in Section 7.3. In event 1 the measurements match the model and the confidence level stays at 100%. In event 2 the algorithm captures the internal fault in the protected line and issues trip signal. In event 3 the algorithm filters out the internal fault of the parallel line (only transients). The confidence level remains at 100%

compared with that of option 2, which means that the induced voltage does not impact the estimation algorithm.

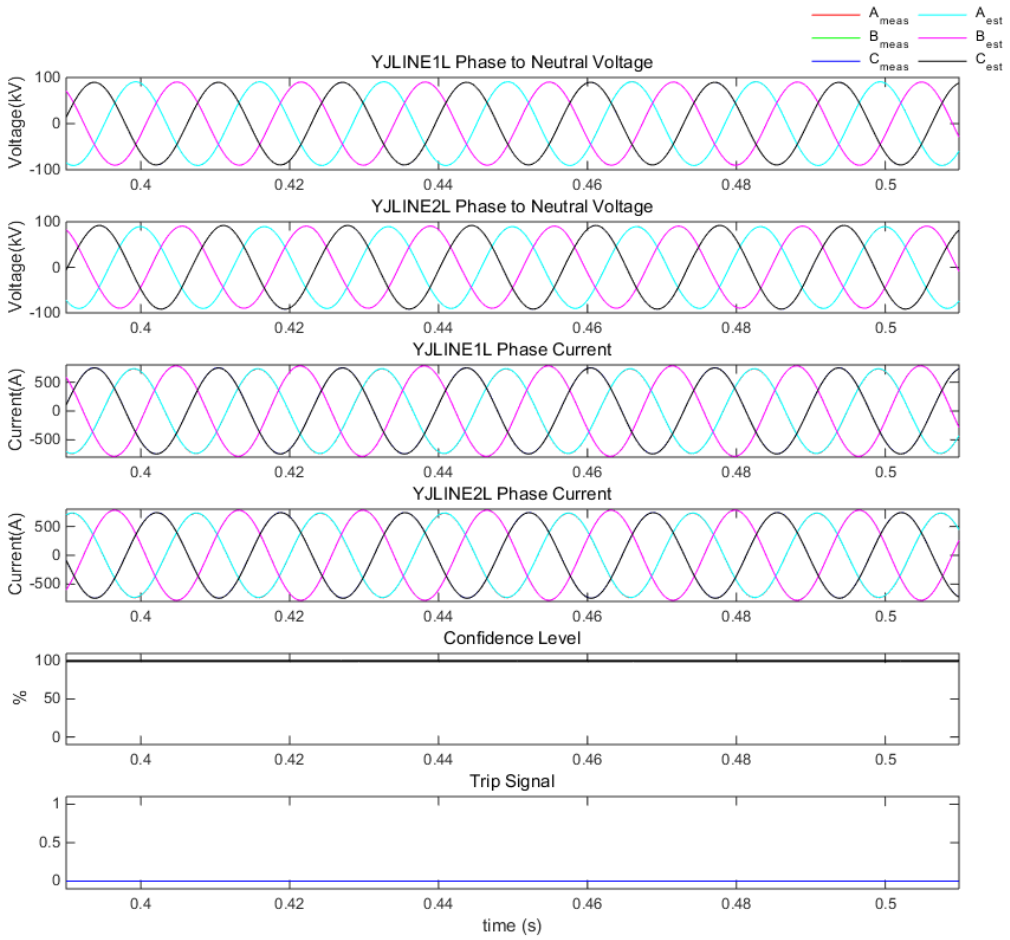

Figure 7-31 DSE dynamic state estimation and protection results, parallel line test system -- Event 1, Option 3

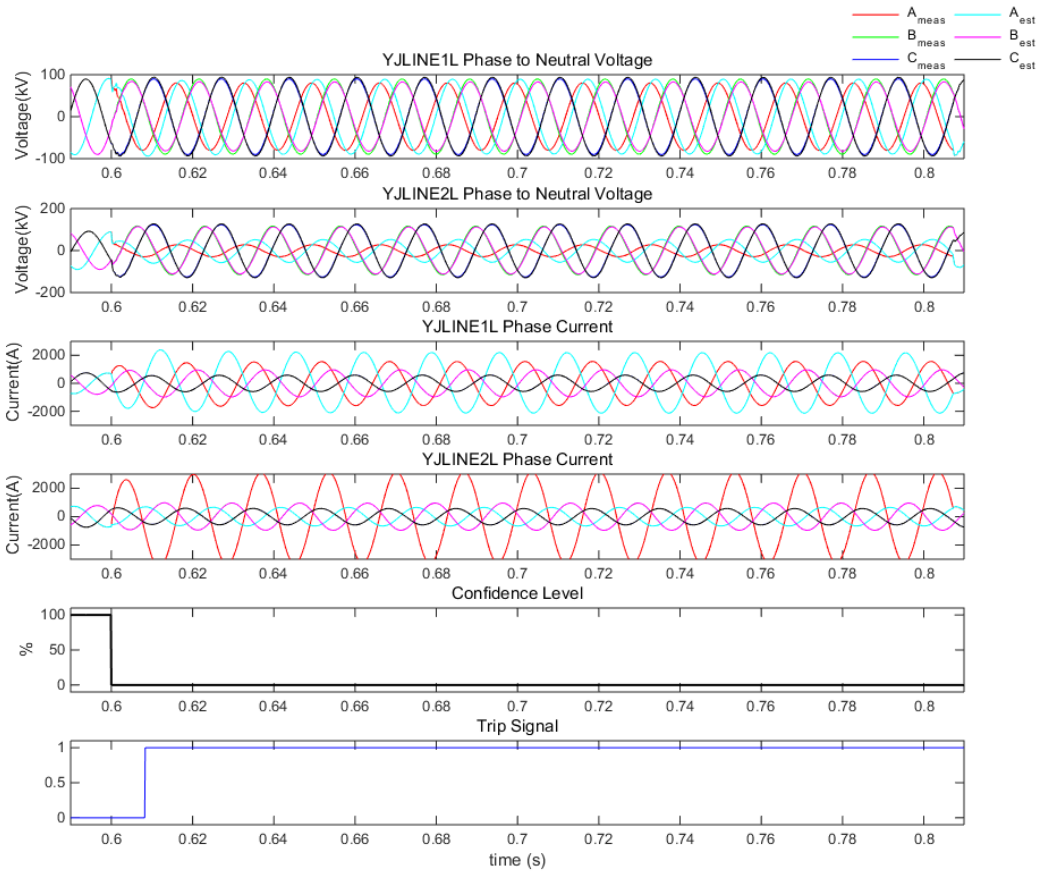

Figure 7-32 DSE dynamic state estimation and protection results, parallel line test system -- Event 2, Option 3

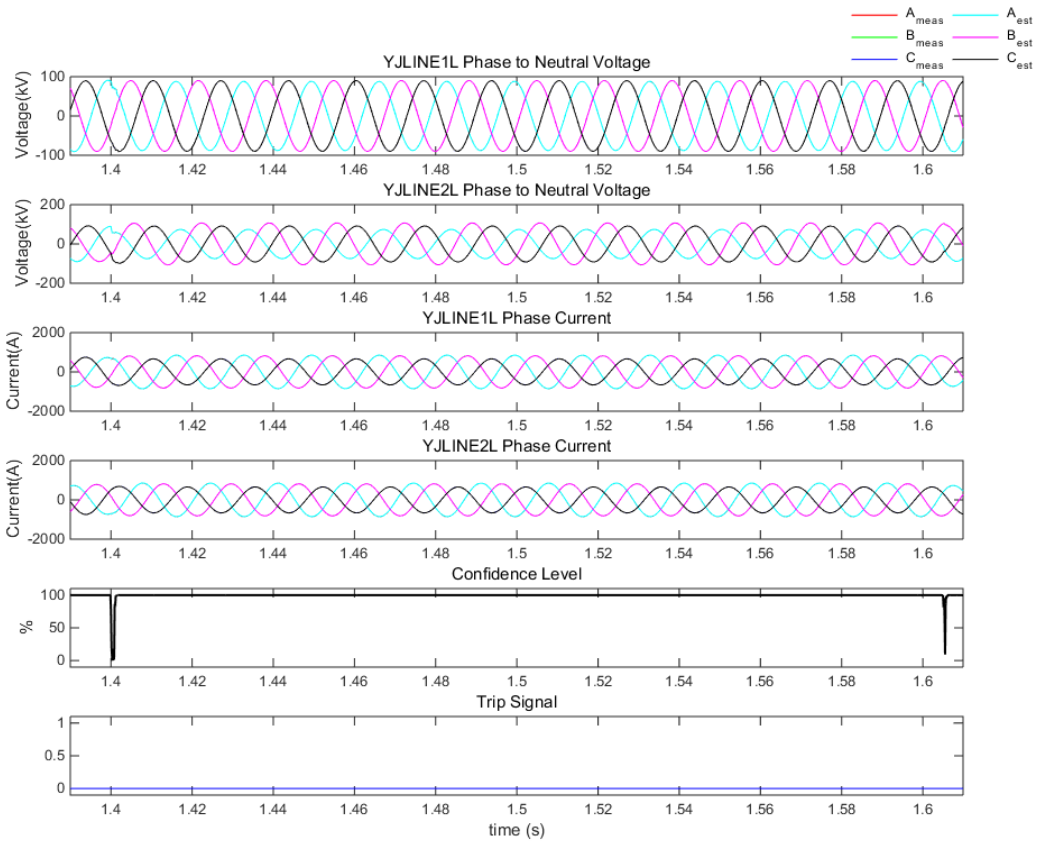

Figure 7-33 DSE dynamic state estimation and protection results, parallel line test system -- Event 3, Option 3

By comparing the protection results from distance protection and DSE based protection, the mutual coupling effect decreases the dependability of the distance protection function, while by correct modeling the effect would not impact the performance of DSE based protection.

7.7.2 Series Compensation for Long lines

Transmission line series compensation increases power transfer capability and improves power system stability. The capacitive reactance usually compensates 30%-70%

of the total line inductive reactance. Series capacitors installed along the transmission line require metal oxide varistors (MOVs) or spark gap to protect the capacitor and reduce the overvoltage across the capacitors. During a severe fault the spark gap would flashover to remove the capacitor from service, in this case the distance protection would not be affected by the series compensation. However, the spark gap would not operate during a low fault current and in this case the apparent impedance would be biased by the capacitor. On the other hand, MOVs clamp the voltage and change the series capacitor reactance in a nonlinear way, the MOV's resistance is a nonlinear function of the across voltage.

The most significant effect is the voltage inversion. A voltage inversion is when the voltage phasor angle changes its direction. When a bolted fault happens, the apparent impedance is computed by the voltage phasor and current phasor measured at the relay end. Without series capacitor this apparent impedance should be equal to the inductive reactance per length multiplied by the length to the fault. In that case voltage phasor and current phasor are approximately 90 degrees apart and the directional element would have maximum torque. However, with series capacitor, if the impedance from the relay to the fault is capacitive rather than inductive, the voltage inversion would occur, and it would make the directional element and distance element mis-operate. Figure **7-34** and Figure **7-35** illustrate the voltage inversion scenario. For a three phase bolted fault, if the capacitive reactance Xc is greater than the inductive reactance mX_L of the faulted line section, voltage V and V' are out of phase with each other. If the relay uses the line side voltage V' the apparent impedance would fall into the first quadrant in the operating plane, or Mho zone, if the relay uses the bus side voltage V the apparent impedance would fall into the third quadrant in the operating plane and the distance protection would declare it

as reverse fault, see Figure **7-34**. On the other hand, if the relay uses the bus side voltage V the directional element and distance element would mis-operate as in Figure **7-35**. The voltage inversion phenomenon would be illustrated in the following test case.

Another phenomenon related to series compensated line is current inversion. During an internal fault, if the equivalent system at one side of the fault is capacitive and the equivalent system at the other side of the fault is inductive, then instead of the currents flowing into the line are in phase, they would be out of phase by 180 degree, which means that there is a current outfeed on the side which sees capacitive reactance. Such phenomenon occurs when the capacitive reactance is larger than the source inductive reactance. The current inversion can affect directional element, distance element, and moreover it can affect differential element. For most bolted, high current faults the protecting spark gap or MOV will bypass series capacitor so that current inversion would not occur, however for high resistance faults and low fault current the bypassing would be prevented, this would be investigated in Section 7.9. This section would only investigate voltage inversion.

The third phenomenon is the subharmonic-frequency transient [17]. The apparent impedance being computed would demonstrate a spiral trajectory, the impedance spiral decreases until it reaches the steady state value after several cycles. During the spiral trajectory if the external fault is close to one of the line side the apparent impedance may temporarily enter the zone and cause the relay to mis-operate. Such phenomenon would be illustrated in the following test case.

The test case is illustrated in Figure **7-36**. The system has the same setup with the test system in Section 7.3 except the protected line here is an 80 miles transmission line that is compensated 30%. The self-inductive reactance for the long line is j67 Ohm, and the series compensation is -j20 Ohm. The line from YJLINE1 to YJLINE2 is the line under protection. The capacitor from node CAPL to node CAPR is the series compensation. The parameters of the line are identical with that of the line in Section 7.3.

There are two events. Event 1: The system is operating in normal condition from time t=0s to t=0.6s. The loading is 425A. Event 2: The protected line has a three phase fault at 25% of the line from the left hand side, the fault resistance is 0.01 Ohm, from t=0.6s to t=0.8s. The fault current on the left hand side goes up to 20 kA, high enough to make the spark gap or MOV to remove the capacitor out of service. However, the series capacitors are assumed to be in service the whole time. The spark gap or MOV is not modeled in this test system and not the focus of this thesis.

The stepped distance protection and DSE based protection are compared. The settings for both of them are listed in Table 7.6. The zone 1 protects 80% of the line since during bolted fault the capacitor would be removed. The zone 2 protects 120% and the zone 3 protects 160% of the line.

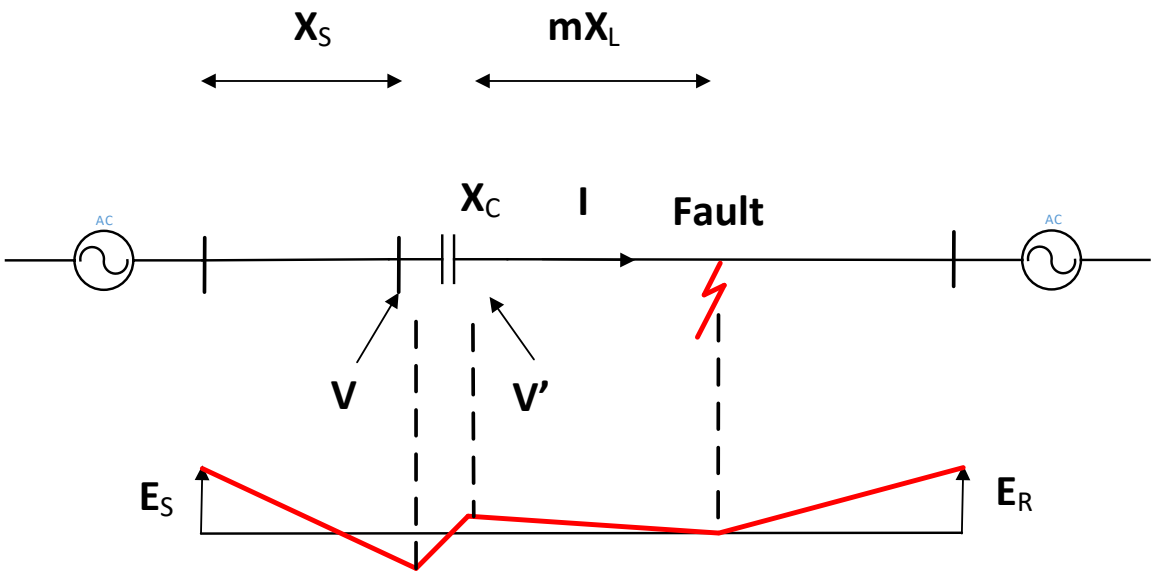

Figure 7-34 Illustration of Voltage Inversion of Series Compensated Line – forward fault [17]

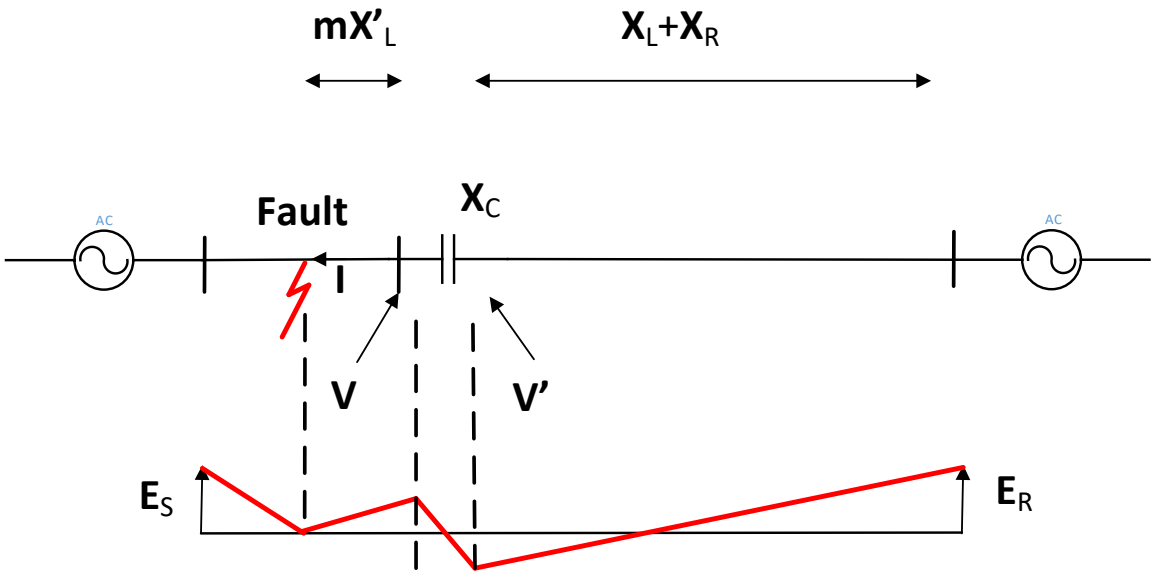

Figure 7-35 Illustration of Voltage Inversion of Series Compensated Line – Reverse fault [17]

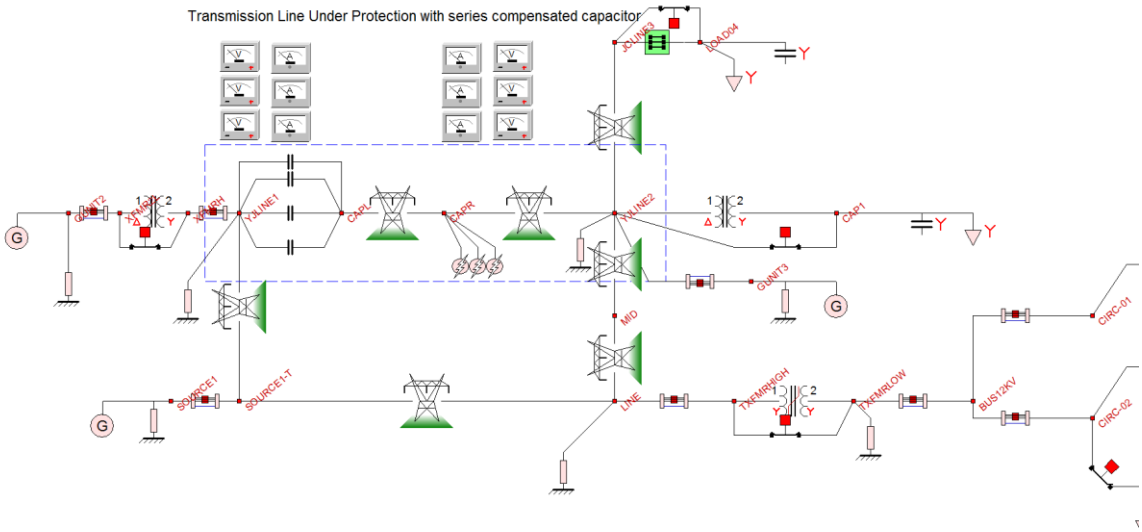

Figure 7-36 Series Compensated Line Test Case – Similar to Section 7.3

Table 7.6 Protection Settings for Compensated Lines Test Case

Protection Functions	Settings
Stepped Distance	Z1PKP: 42.63∠84.42 Z2PKP: 63.95∠84.42 Z2 Delay: 20 cycles Z3PKP: 85.26∠84.42 Z3 Delay: 30 cycles compensation factor m: 3.03∠-6.28
Dynamic State Estimation Based	Integration Windows Size: 1 cycle Confidence Level Threshold: 50%

The protection results for the distance protection are plotted in the operating plane in Figure **7-37** and Figure **7-38**. During event 1, both the operating points computed at both relays are outside the operating zone, in event 2 the operating point computed from the relay at YJLINE1 is in the third quadrant close to the imaginary axis, approximately -10

Ohms, the operating point computed from the relay at YJLINE2 is inside zone 1. As a result, the relay at YJLINE2 would trip instantaneously, whereas the relay at YJLINE1 would not trip.

Also in Figure 7-38 the spiral impedance caused by the sub-harmonic frequency is observed.

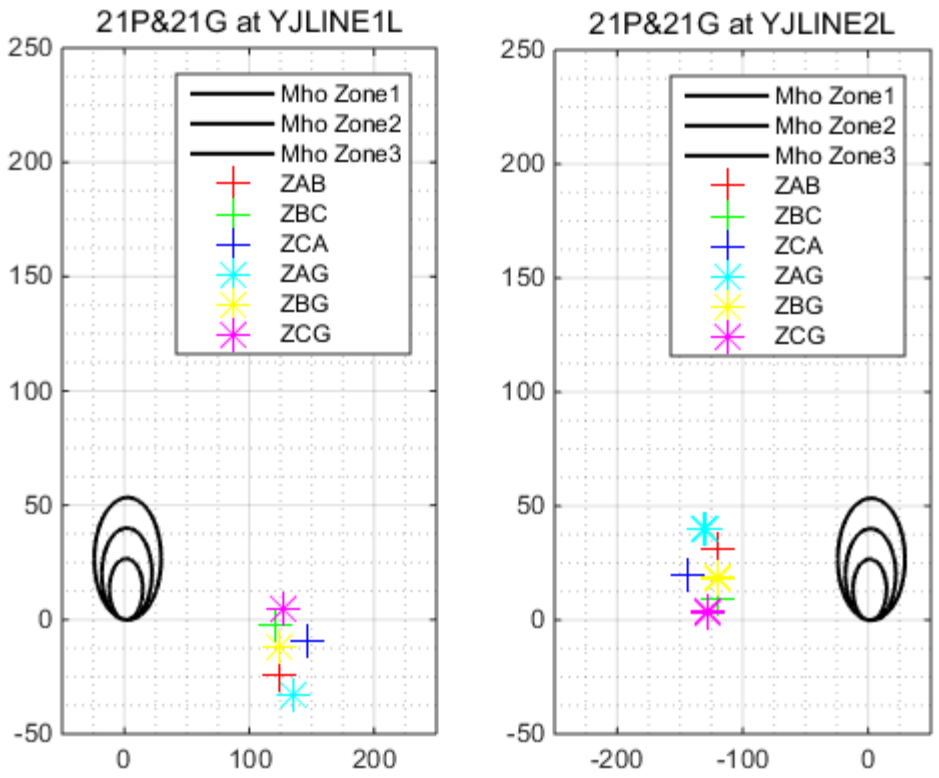

Figure 7-37 Operating points for distance protection in the series compensation test system – Event 1

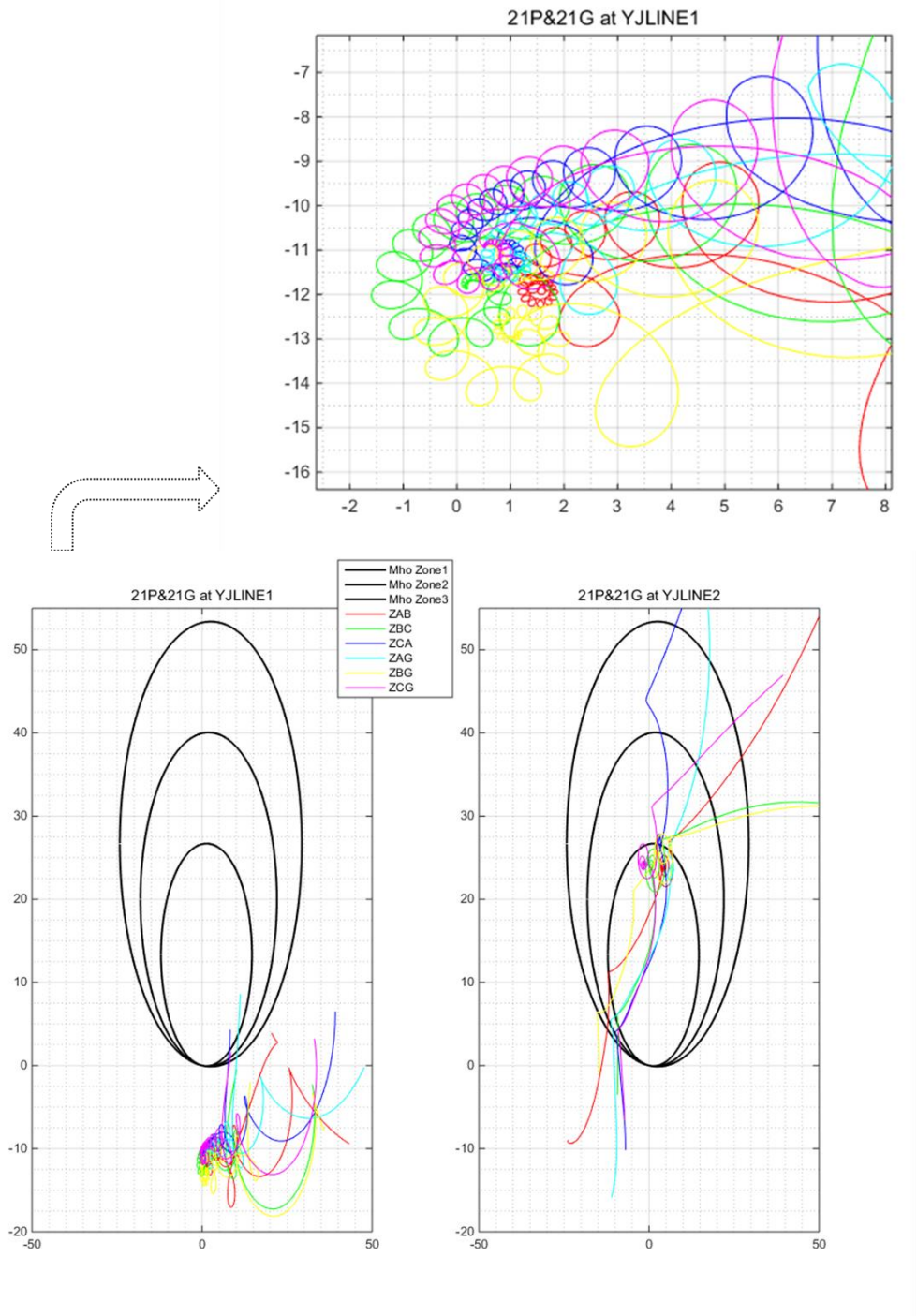

Figure 7-38 Operating points for distance protection in the series compensation test system – Event 2

For DSE based protection, the modeling of the series compensated line also needs to be justified. The reason is that the status of the capacitor, i.e., in service or out of service, affects the modeling of the line. If the capacitor is out of service, the model of the line is same as in (4.3); If the capacitor is in service, then the model of the line is:

$$\begin{aligned} i_1(t) &= C\frac{dv_1(t)}{dt} + i_L(t) \\ i_2(t) &= C\frac{dv_2(t)}{dt} - i_L(t) \\ 0 &= -v_1(t) + v_2(t) + Ri_L(t) + L\frac{di_L(t)}{dt} + v_{cap}(t) \\ 0 &= i_L(t) - C_{cap}\frac{dv_{cap}(t)}{dt} \end{aligned} \tag{7.9}$$

where,

R, L, C: 4×4 self resistance, inductance, capacitance matrices for the line.

C_{cap}: 4×4 series compensated capacitor matrix

$i_1(t)$: all through variables on left side of pi equivalent model for the line at time t

$i_2(t)$: all through variables on right side of pi equivalent model for the line at time t

$v_1(t)$: all across variables on left side of pi equivalent model for the line at time t

$v_2(t)$: all across variables on right side of pi equivalent model for the line at time t

$v_{cap}(t)$: across voltage on the capacitor for the line at time t

$i_L(t)$: the inductance current through the line at time t

$x(t) = \begin{bmatrix} v_1(t) & v_2(t) & i_L(t) & v_{cap}(t) \end{bmatrix}$

From the control perspective, this is a linear hybrid system. Hybrid estimation based on multiple model adaptive estimation and the interacting multiple model algorithm can be applied [54]. Due to the computation time requirement (estimation has to be faster than

sampling), this thesis does not explore the hybrid estimation algorithm. Since the status of the capacitor cannot be updated to the protective relay in real time, two option are provided.

Option 1—

The first option is to observe that the difference between (7.9) and (4.3) is the additional additive term on the KVL equation as the across voltage on the series capacitor. During normal operation the across voltage is in order of 10 kV. Thus if this additive term is treated as noise, which means that the capacitor is assumed to be out of service, then the standard deviation for the virtual measurements (KVL equation) can be set at 0.1 per unit or even higher. In this case only model (4.3) is needed to model this line.

Option 2 –

The second option is similar to the third option in the parallel line modeling. Basically the KVL does not needed to be included, only the KCL laws are included:

$$\begin{aligned} i_1(t) &= C\frac{dv_1(t)}{dt} + i_L(t) \\ i_2(t) &= C\frac{dv_2(t)}{dt} - i_L(t) \end{aligned} \tag{7.10}$$

Where the variables are defined the same as (4.3).

The protection results from the two options are presented in the following.

The protection results from option 1 is illustrated from Figure **7-39** and Figure **7-40**. The standard deviation is chosen at 0.3 per unit. The measurements and estimated measurements, confidence level and trip logic is plotted in the same way as in Section 7.3. In event 1 the measurements match the model and the confidence level stays at 85%-100%. This means that the across voltage does impact the KVL significantly given that the

standard deviation is set at 0.3 per unit which is a large value. In event 2 the algorithm captures the internal fault in the protected line and issues trip signal.

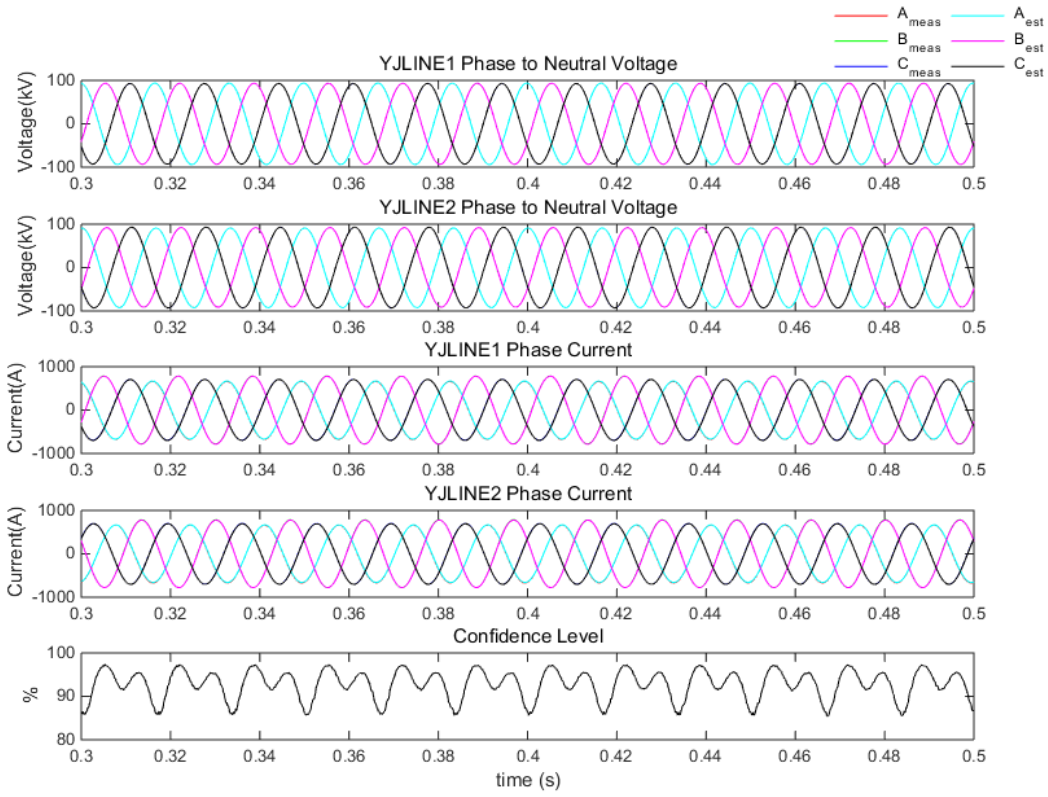

Figure 7-39 DSE dynamic state estimation and protection results, compensated line test system – Event 1, Option 1

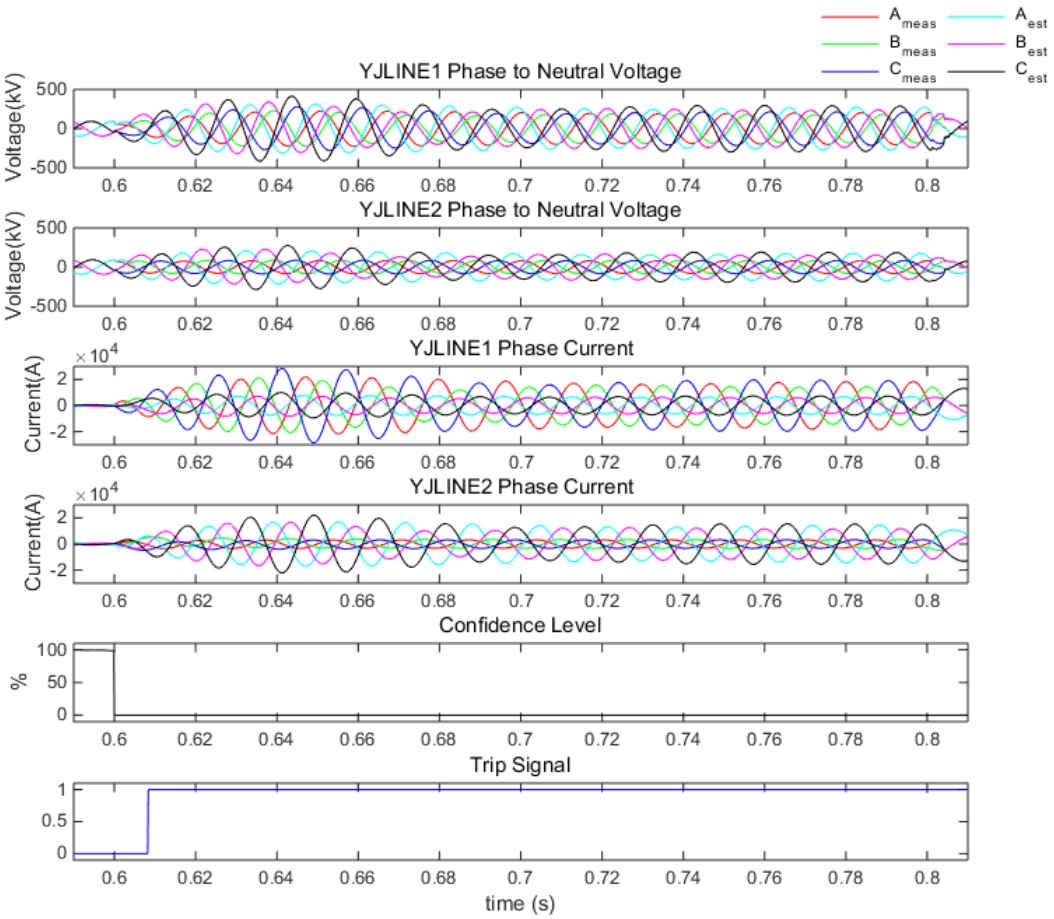

Figure 7-40 DSE dynamic state estimation and protection results, compensated line test system – Event 2, Option 1

The protection results from option 2 is illustrated from Figure 7-41 and Figure 7-42. The measurements and estimated measurements, confidence level and trip logic is plotted in the same way as in Section 7.3. In event 1 the measurements match the model and the confidence level stays at 98%-100%. In event 2 the algorithm captures the internal fault in the protected line and issues trip signal.

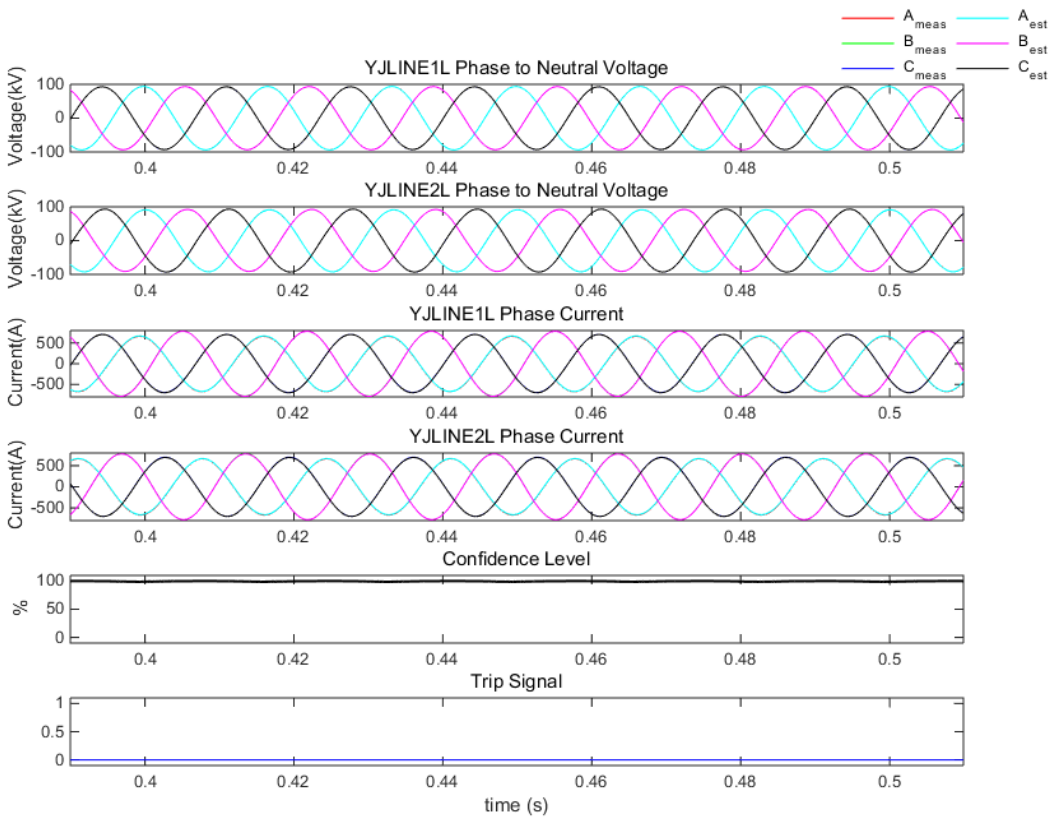

Figure 7-41 DSE dynamic state estimation and protection results, compensated line test system – Event 1, Option 2

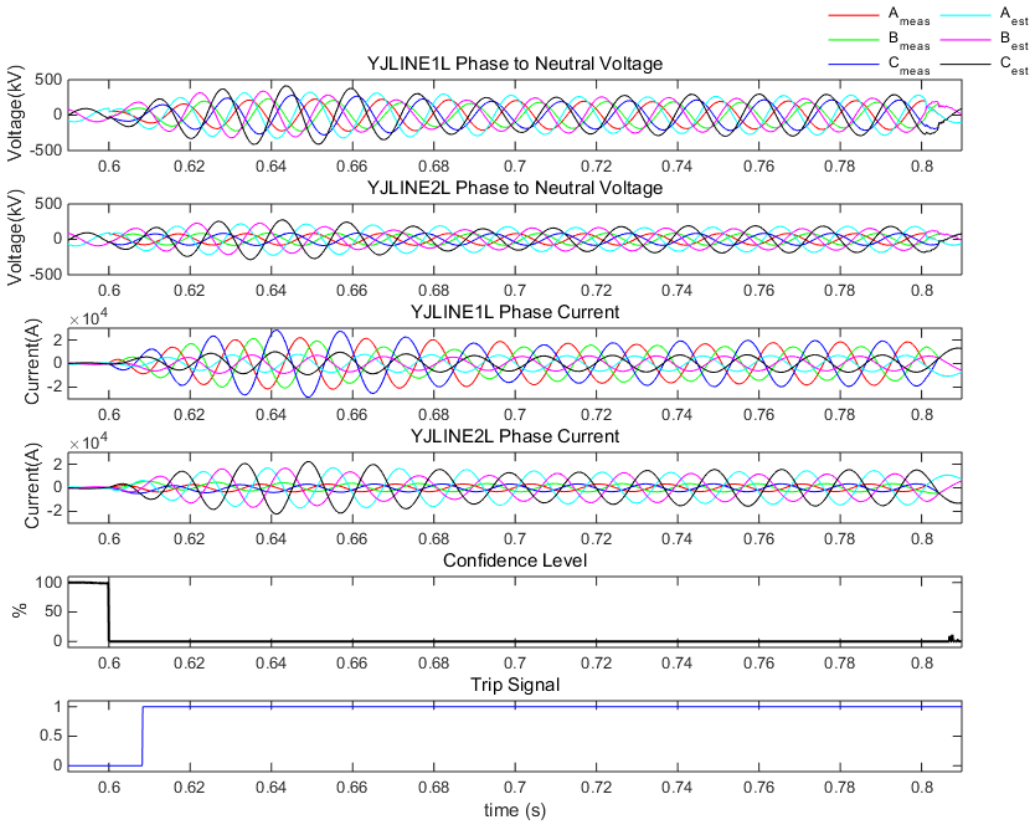

Figure 7-42 DSE dynamic state estimation and protection results, compensated line test system – Event 2, Option 2

In comparison, the distance protection function would fail to operate at one end, while the DSE based protection would provide full dependability.

7.8 DSE based protection and Pilot protection

Directional instantaneous overcurrent, directional time overcurrent, and stepped distance protection are protection functions that only use local information. The pilot protection, on the other hand, is communication-assisted protection that also uses remote

information (on the other end of the line). For local information the protection function often under-reach the protection zone if it operates instantaneously in order to prevent mis-operation upon external fault, or over-reach the protection zone if it operates with a time delay in order to coordinate with the relays on neighboring lines. For either case, the local protection function cannot be certain that the fault happens within the protection zone or outside the protection zone. In order to cover the full protection zone with instantaneous and simultaneous trip from both relays, communication is required. The pilot protection is invented for such purpose.

As introduced in the Literature Review part, there are many pilot protection schemes, each one uses different directional fault detectors, and the protection logic are either based on blocking scheme or permissive scheme. However, with communication assistance, the pilot protection still relies on the fault detector, which are usually directional (instantaneous or time) overcurrent protection or distance protection (zone 1 or zone 2) discussed in previous sections. As such, most disadvantages from these fault detectors discussed in this Chapter would be inherited by the pilot protection scheme.

Moreover, the communication in pilot schemes can also cause issue when sequential tripping on parallel lines and other switching events happen. One such case is current reversal, and it's introduced next.

7.8.1 Current Reversal

The basic concept is this: in parallel line application, faults near one end of a line may result in a sequential trip operation. This sequential trip happens when the instantaneous relay elements trip the breaker nearest to the fault location. Recall that zone 1 element trip independent of the pilot scheme. The breaker farthest from the fault is waiting for a

permissive signal. If one relay trips first (zone 1), and other relay trips sequentially (zone 2), it creates a current reversal in the healthy parallel line, and one terminal of the healthy line may trip incorrectly.

This scenario can easily occur when ground directional overcurrent relays are used because they can often see an end zone fault on an adjacent line. It is less of a factor when ground distance relays are used. The reason is that the phase pickup values are based on fault current analysis however ground pickup values are usually set as 200% of the maximum imbalance of the system. Whereas in transmission systems the imbalance is often very small due to line transposition.

The test case is illustrated in Figure **7-43**. The parallel lines are transferring power from the left hand side to the right hand side. Both transmission lines are 40 km long. The protection zone is the line on the top. For all the 4 relays in the figure (each one of them is associated with one circuit breaker), they use pilot scheme which relies on time ground overcurrent fault detector. Also the instantaneous ground overcurrent protection function is used independent of the pilot scheme. If it sees the fault it would trip instantaneously without knowledge from the pilot scheme. The relays use permissive overreaching transfer trip scheme (POTT).

The event sequence of the current reversal case is as follow: **Event 1** the system is running in normal operation, until **Event 2** – a phase A to ground fault happened along 80% of the parallel line at t = 0.7s. The circuit breaker 2 trips immediately upon seeing the fault at t = 0.76s (60 ms trip time) by directional instantaneous overcurrent protection. Meanwhile the directional time overcurrent ground element at circuit breaker 3 also sees the fault and issues permissive tripping signal to the relay at circuit breaker 4. The fault

current starts to redistribute at circuit breaker 3 and circuit breaker 4. Then the relay at circuit breaker 4 sees the fault by directional time overcurrent protection and since it has been receiving the permission signal from the relay at circuit breaker 3, it would trip the circuit breaker 4. The protection settings are listed in Table 7.7.

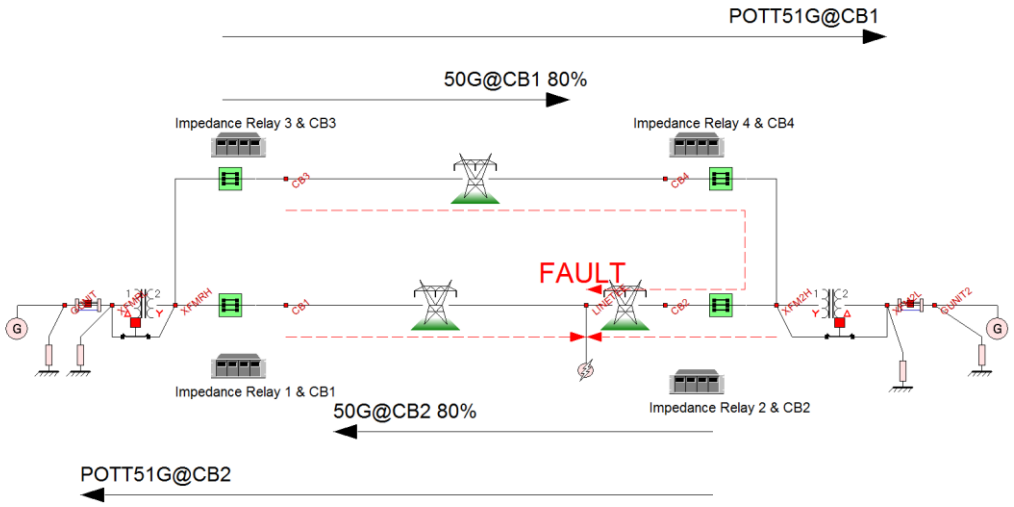

Figure 7-43 Parallel line current reversal test case – a comparison between POTT and DSE based protection

Table 7.7 Protection Settings for Current Reversal Case

Protection Functions	Settings
Directional Instantaneous Overcurrent	50G PKP: 4000A 67Forward: <0Ohm 67Reverse: > 0Ohm
Directional Time Overcurrent	51G PKP: 200A 67 Forward: <0Ohm 67 Reverse: > 0Ohm Delay: 20 cycles
Permissive Overreaching Transfer Trip	Forward Reaching Element: 51G Communication Time Delay: 0ms Reverse Reaching Element: None
Dynamic State Estimation Based	Integration Windows Size: 1 cycle Confidence Level Threshold: 50%

The logical diagram for the POTT pilot scheme using time ground overcurrent element is illustrated in

Figure **7-44** and the details are implemented in MATLAB Simulink module in Figure **7-45**. The computed phasors for the overcurrent elements are presented in Figure **7-46** while the protection logics for all the relays are be presented by the Simulink scope as in Figure **7-47**. With the fault inception, the relay at circuit breaker 2 sees the fault by instantaneous ground overcurrent element so that it trips instantaneously, it also issues the permissive signal. Meanwhile the relay at circuit breaker 1 sees the fault by time ground overcurrent so that it would delay by 20 cycles since it is waiting for the permissive signal from the relay at circuit breaker 2. The relay at circuit breaker 3 sees the fault and sends permissive tripping signal to circuit breaker 4. Since the fault is reverse fault for the relay at circuit breaker 4, it would not operate. Meanwhile the circuit breaker 2 is already open, and the fault current redistributes at circuit breaker 1, 3, and 4. Upon seeing the fault by the relay at circuit breaker 4 and receiving the permissive signal from the relay at circuit breaker 3, then the relay at circuit breaker 4 would mis-operate.

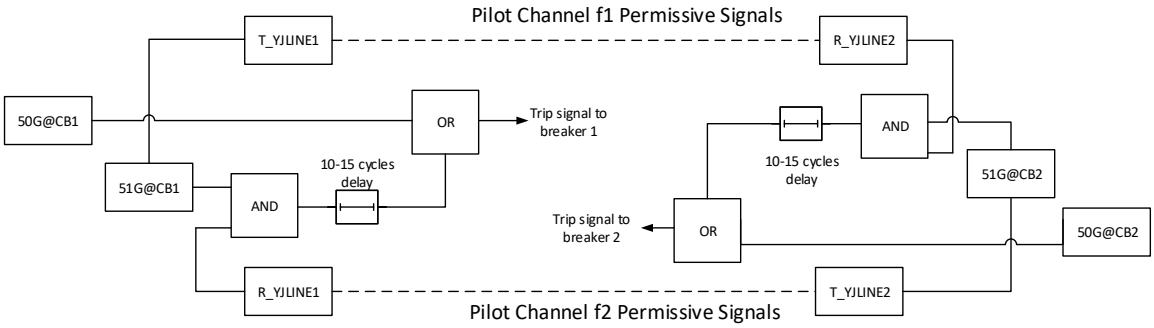

Figure 7-44 POTT logical scheme using time ground overcurrent element

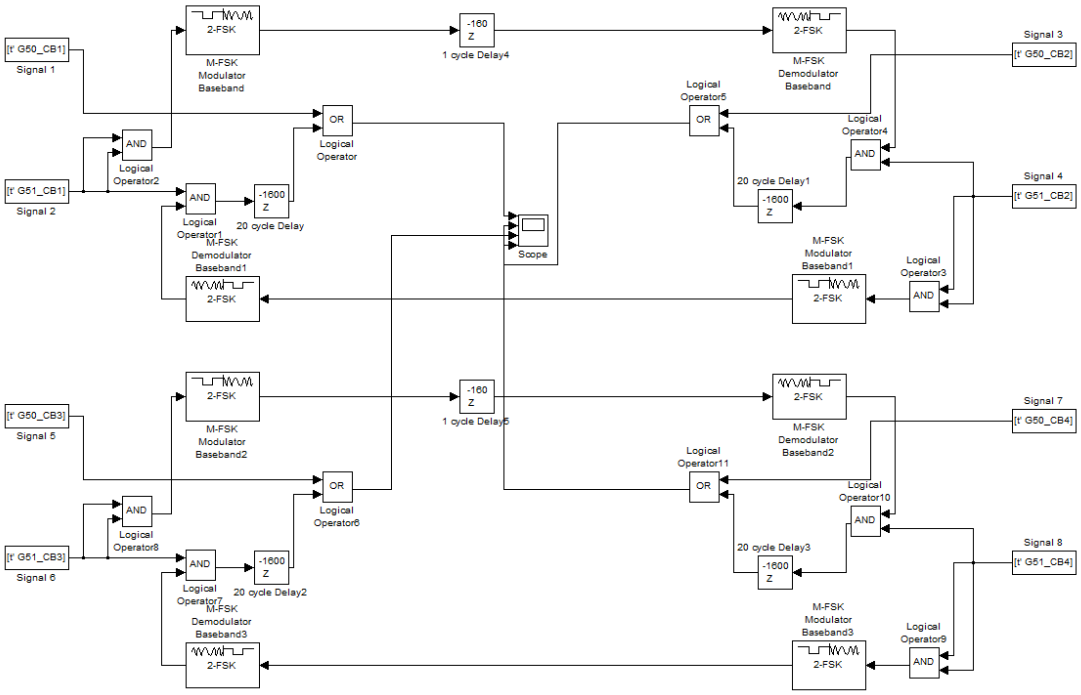

Figure 7-45 MATLAB implementation for POTT pilot scheme

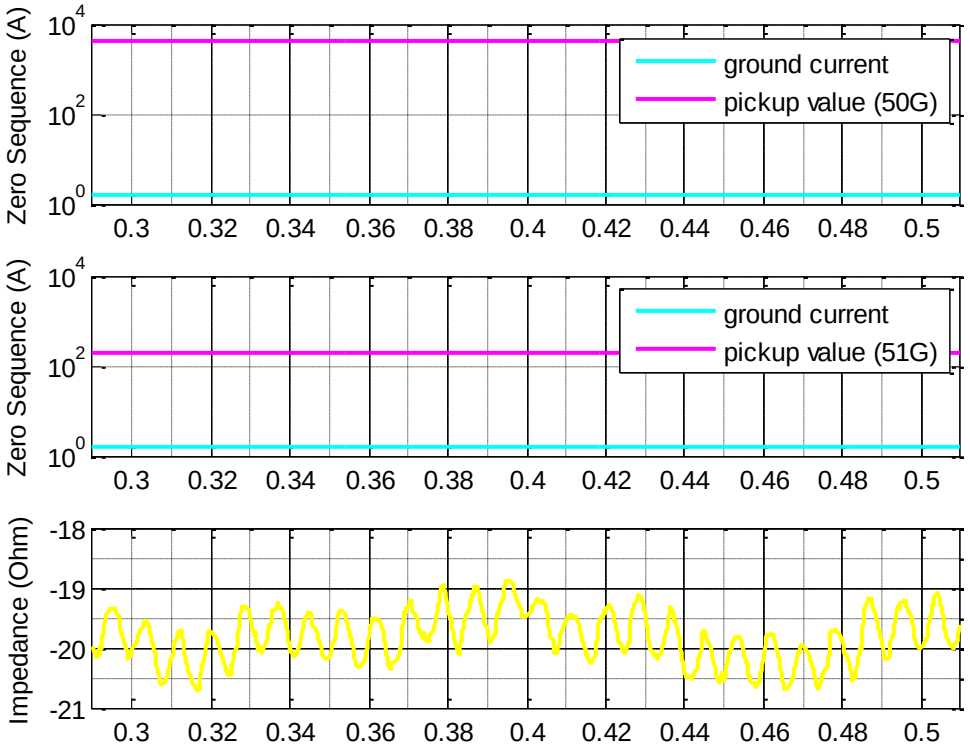
Zero Sequence (A)
10^4
10^2
10^0
ground current
pickup value (50G)
0.3 0.32 0.34 0.36 0.38 0.4 0.42 0.44 0.46 0.48 0.5
Zero Sequence (A)
10^4
10^2
10^0
ground current
pickup value (51G)
0.3 0.32 0.34 0.36 0.38 0.4 0.42 0.44 0.46 0.48 0.5
Impedance (Ohm)
-18
-19
-20
-21
0.3 0.32 0.34 0.36 0.38 0.4 0.42 0.44 0.46 0.48 0.5

Event 1

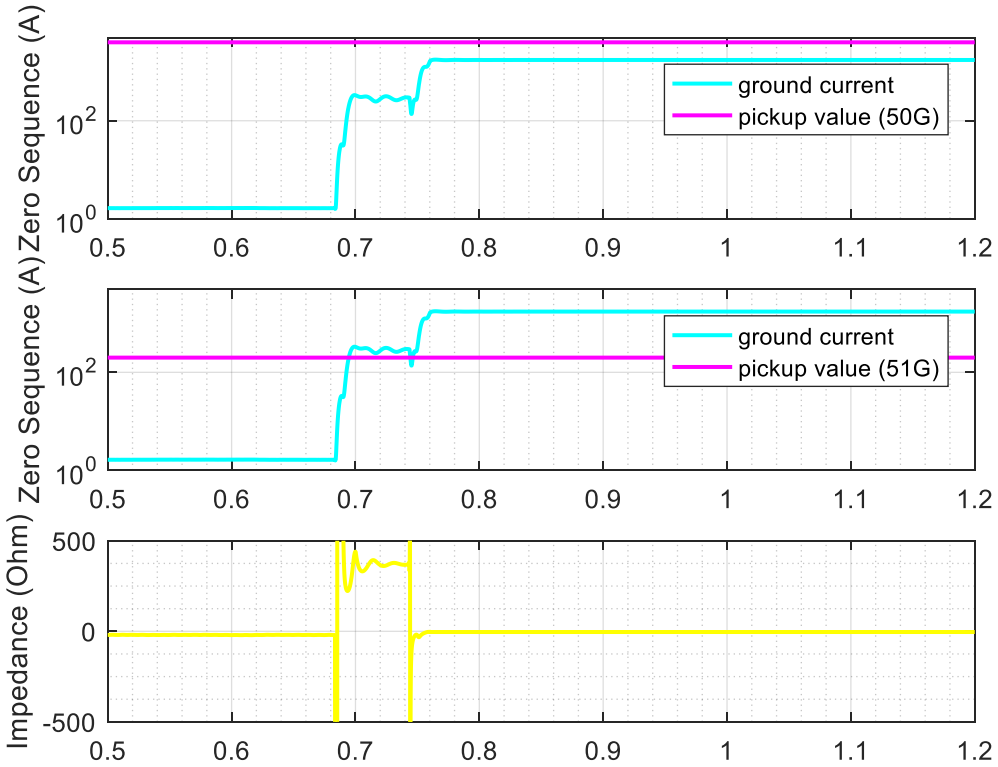

Event 2

Figure 7-46 Current Reversal test case – protection results for directional instantaneous overcurrent and directional time overcurrent as fault detector for pilot scheme (current at circuit breaker 4)

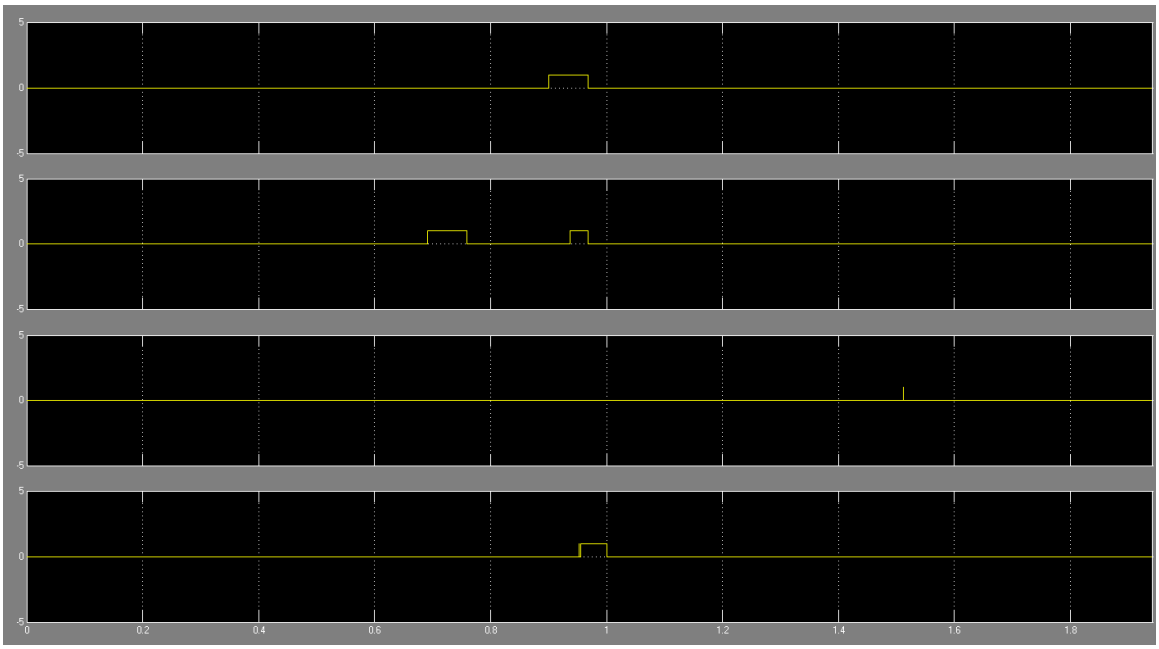

Figure 7-47 Parallel line current reversal test case – Protection Logics from POTT scheme

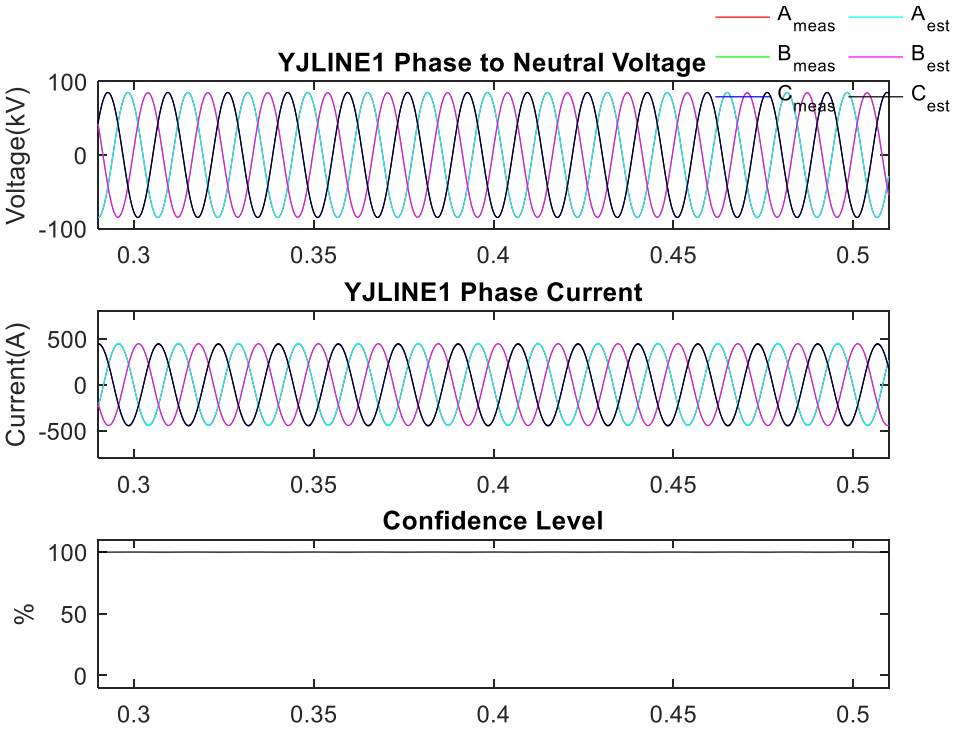

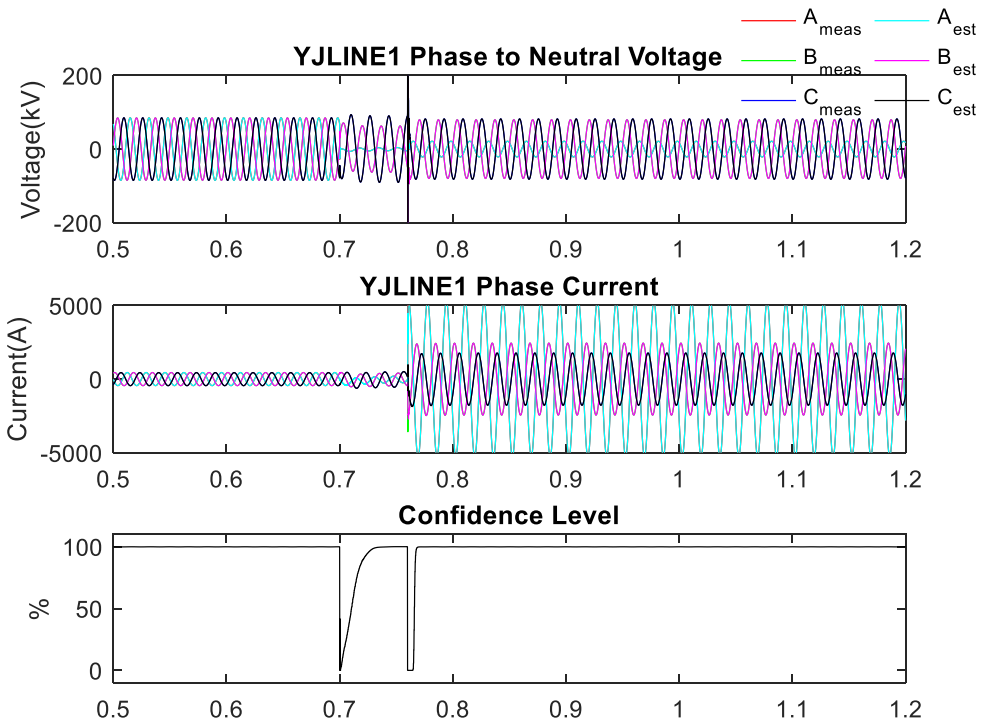

Figure 7-48 Current Reversal test case – Protection results for dynamic state estimation based algorithm (current at circuit breaker 3)

7.9 DSE based protection and current differential protection

The phenomenon of current inversion was introduced in Section 7.7.2. The current inversion affects distance element, directional element and current differential element. In this section the limitation of current differential and limitation of DSE based protection with respect to high impedance fault is first investigated, and then the current inversion case is also investigated.

7.9.1 Limitation to High Impedance Fault

The test system and event sequence is introduced in Section 7.3. An internal high impedance fault between phase A to ground at the middle of the transmission line (Node

LINETEE) is initiated at t=0.6 s and cleared at t=0.8 s. In Section 7.3 the fault resistance is assumed at 1000 Ohm, the current differential does not see the fault and the DSE based protection sees the fault. In this section the sensitivity of both functions are investigated.

Figure **7-49** illustrates the sensitivity of the phase segregated current differential function to high impedance fault. The trajectory is the operating point (differential current versus restraint current) for phase A to ground fault given different fault resistances. When the fault is small (less than 100 Ohms), the operating points lie in the operating region. When the fault approaches 500 Ohms (as in the zoomed in figure), the operating point enters the restraint region. As a result, the current differential is only sensitive to fault resistances less than 500 Ohm.

Figure **7-50** to Figure **7-53** are the DSE based protection results for different fault resistances, it can be concluded that in this test system for the specific fault location the DSE based protection is sensitive to faults up to 3000 Ohm.

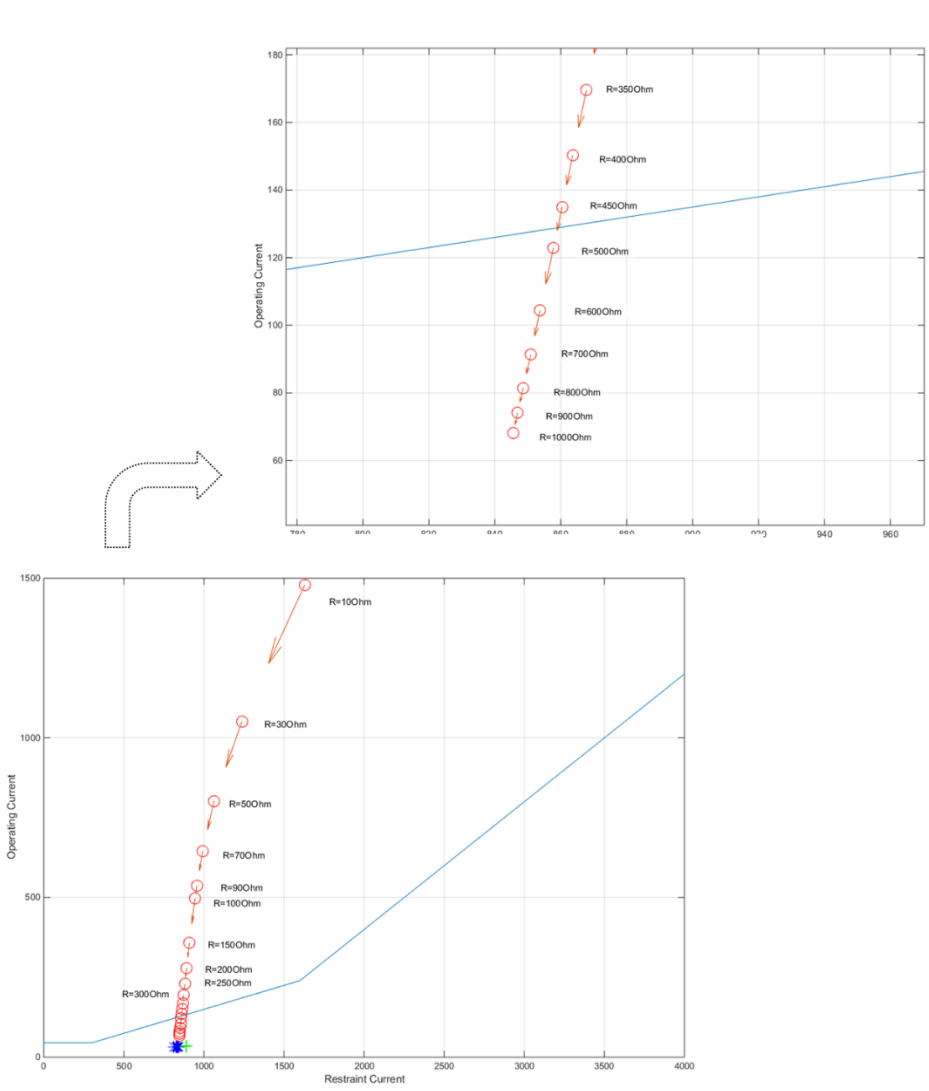

Figure 7-49 Current Differential Protection for High Impedance Fault – Trajectory of Operating Points for Increasing Fault Resistance, phase A to ground fault

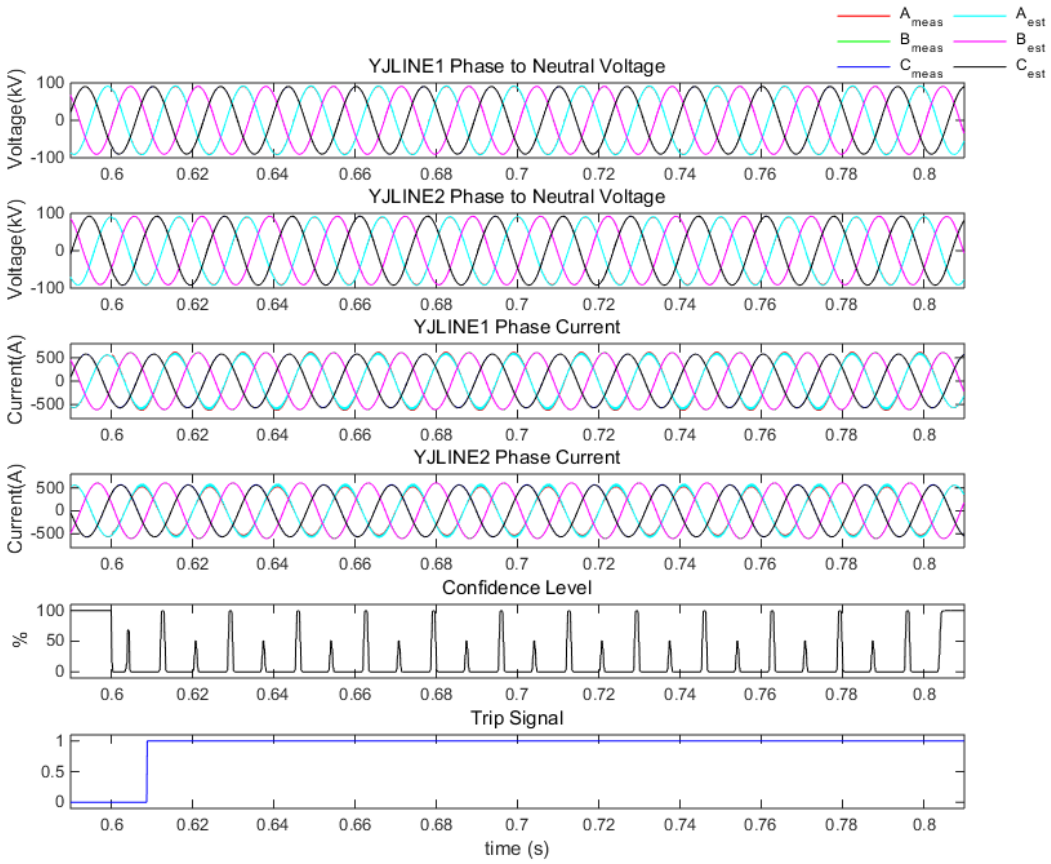

Figure 7-50 DSE Based Protection for High Impedance Fault – Fault Resistance 1000 Ohm.

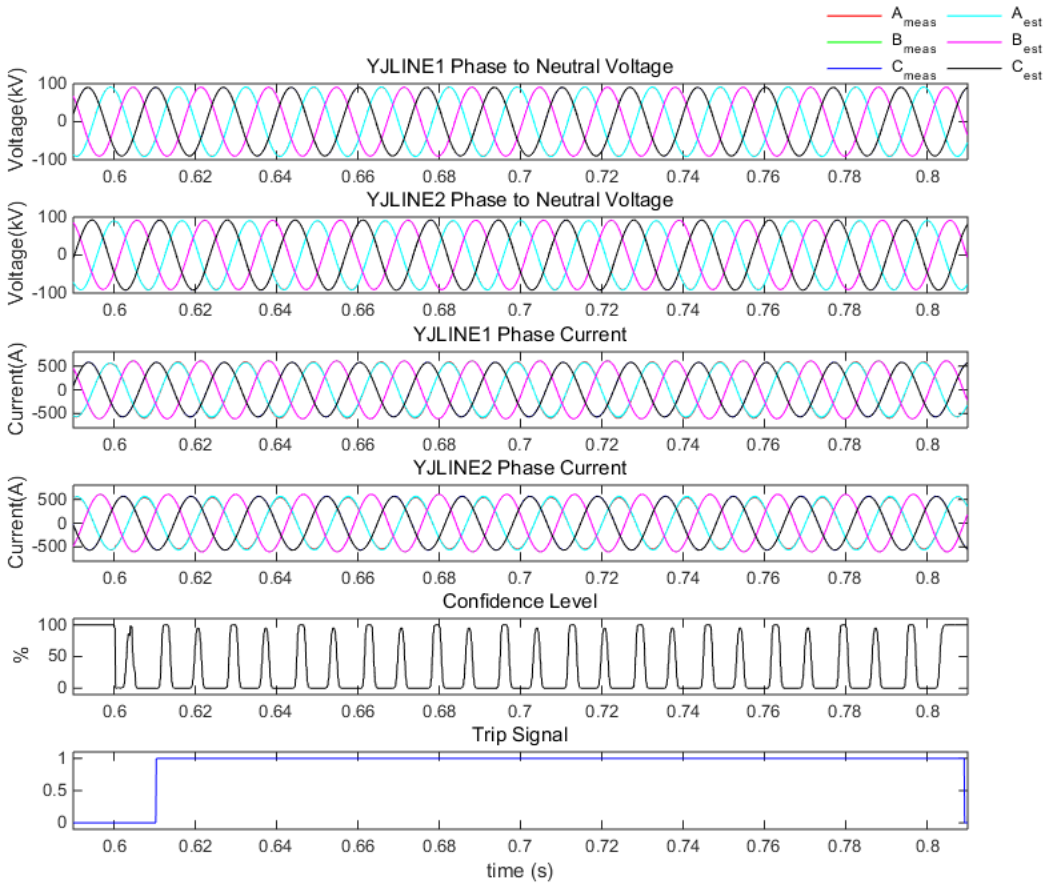

Figure 7-51 DSE Based Protection for High Impedance Fault – Fault Resistance 2000 Ohm

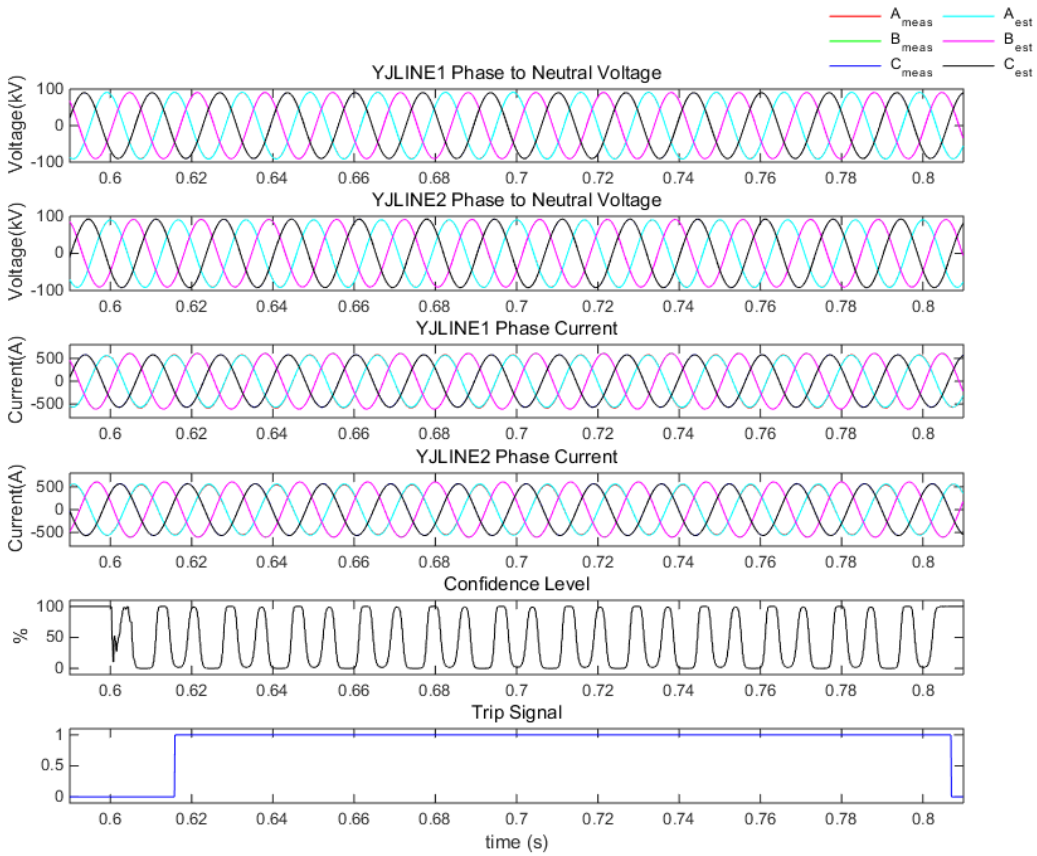

Figure 7-52 DSE Based Protection for High Impedance Fault – Fault Resistance 3000 Ohm

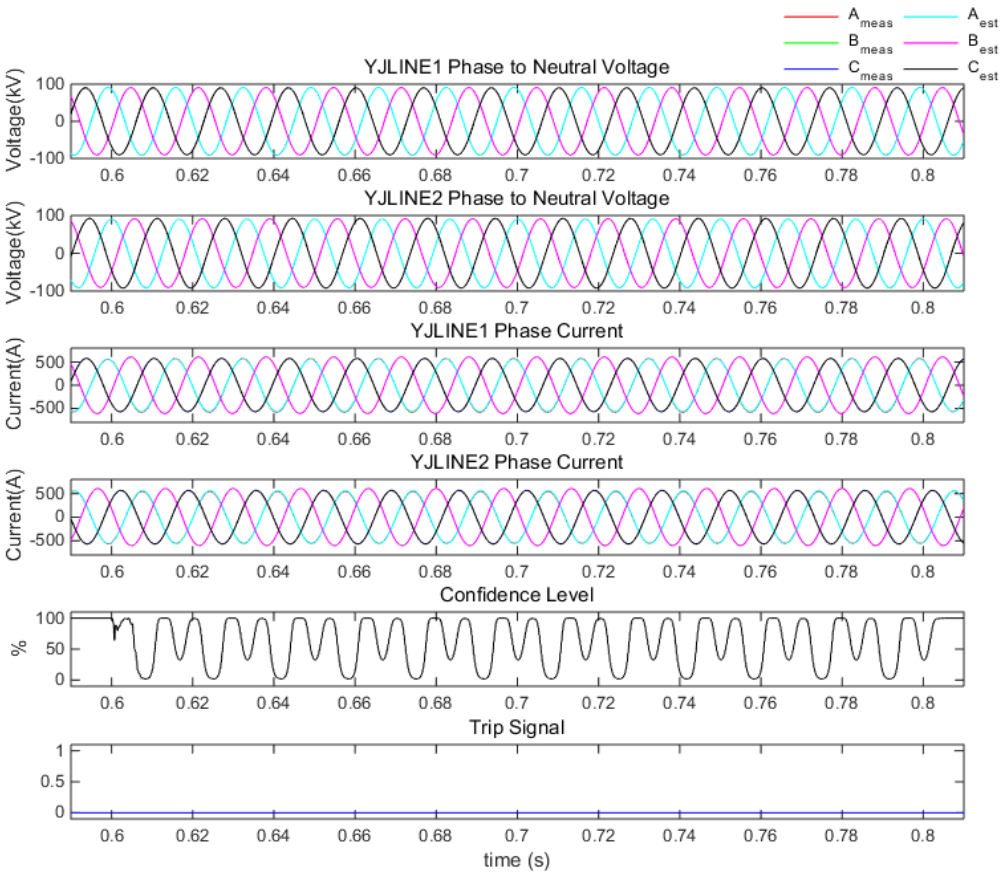

Figure 7-53 DSE Based Protection for High Impedance Fault – Fault Resistance 4000 Ohm

7.9.2 Current Inversion from Series Compensated Lines

The concept of current inversion is explained below in Figure **7-54**. If the left hand side seen from the generator is capacitive (i.e., the capacitive reactance of the capacitor is larger than the inductive reactance of the generator) and the right hand side is inductive, then the current in the left hand side leads the voltage by 90 degrees, and the current on the right hand side lags the voltage by 90 degrees. The two currents are then out of phase. The magnitude of the two currents may not be the same, but if the magnitudes of the two

currents get closer, then the differential current would be small, and restraint current would be large, which makes the operating point stays in the restraint region.

The example test system is illustrated in Figure **7-55**. The series compensated line connects two generations and loads. The line is 80 kilometers long with series impedance of 67 Ohms, and the series capacitor compensates 60% of the line. There is one event: the three phase fault happens at 50% of the line with fault resistance being 0.01 Ohm. The series capacitor is again assumed to be in service and spark gap/MOV is not modeled.

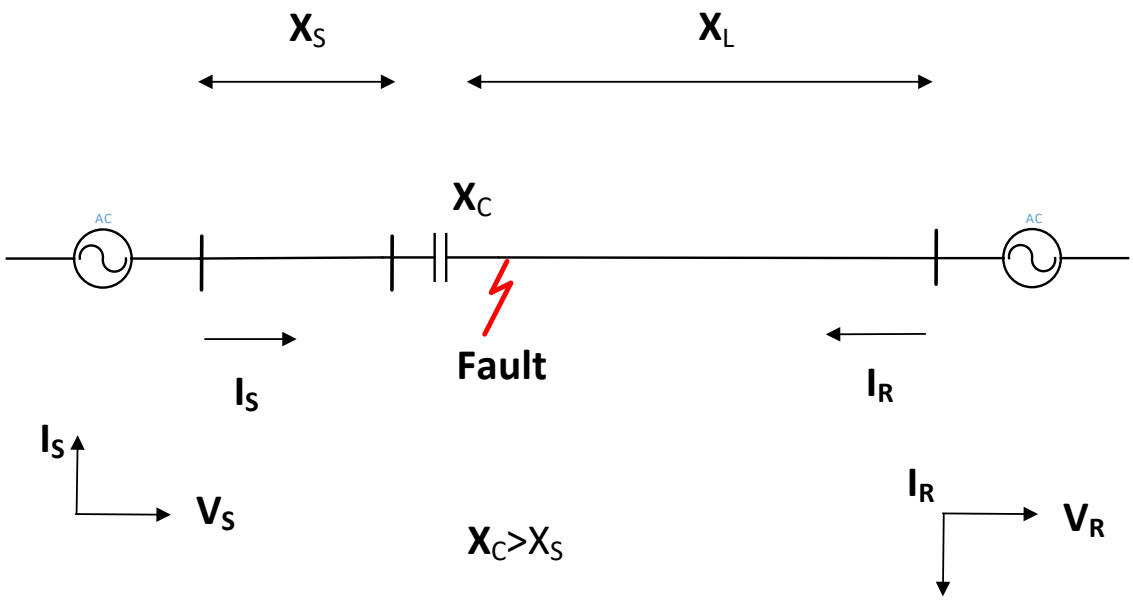

Figure 7-54 Illustration of Current Inversion of Series Compensated Line – forward fault [17]

A quick frequency domain analysis for the current differential protection is presented in Figure **7-56**. It can be seen that the phase currents are out of phase with each other and are of approximately same magnitude for each phase, in that case the differential current as sum of them would be small, while the restraint current would be large. For phase A the

restraint current is 6.5 kA while the differential current is 760A, the operating point clearly resides in the restraint region. The current differential protection results for all the operating points during this event is plotted in Figure 7-57. The trajectory represents the transient behavior of the operating points, it moves from the operating point where the system is operating normally to where the system is under internal fault.

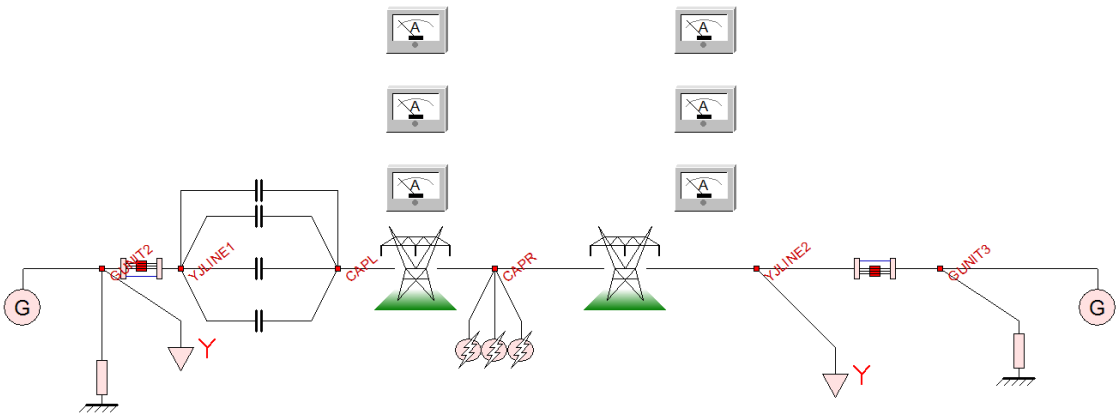

Figure 7-55 Current Inversion for Series Compensated Line Test Case – Current Differential Protection

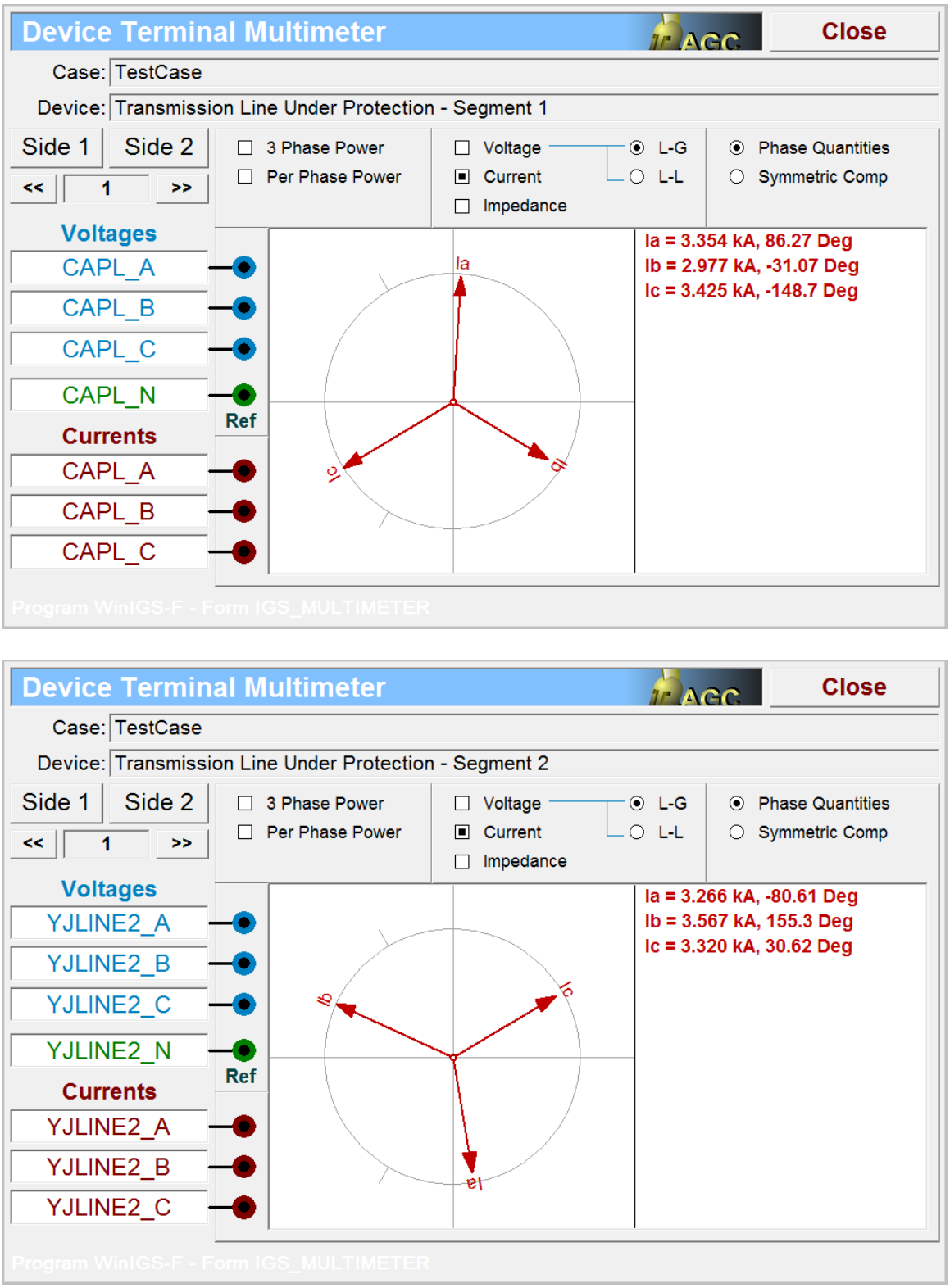

Figure 7-56 Frequency domain analysis for the current differential protection function – current inversion case

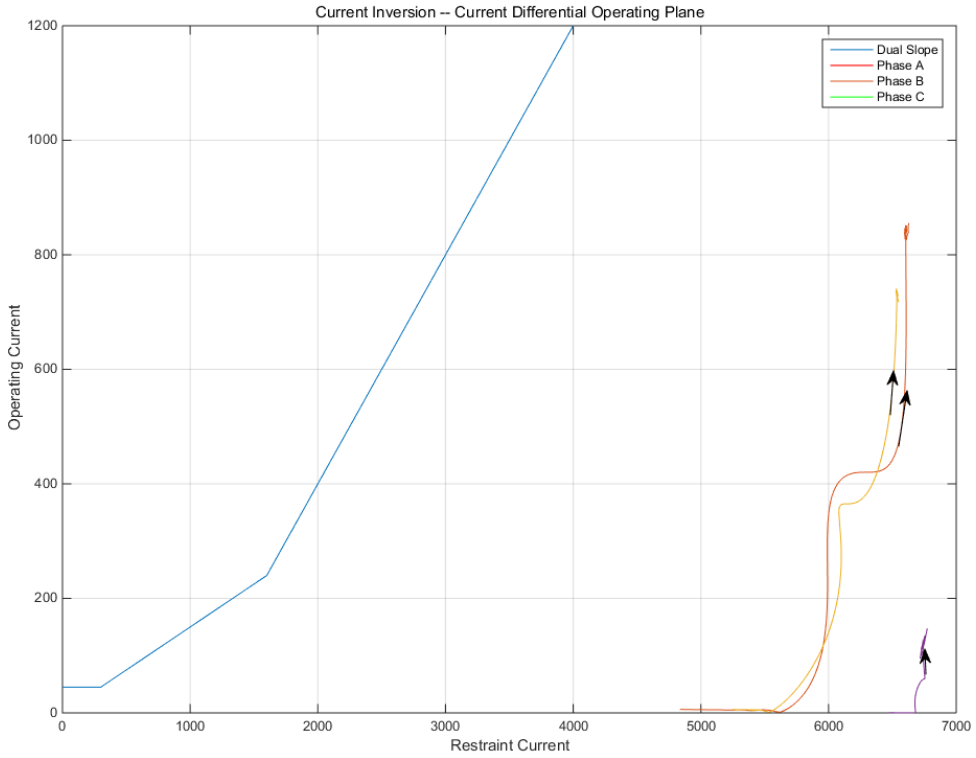

Figure 7-57 Current Differential protection results for current inversion test case

On the other hand, the DSE based protection results for the current inversion case is plotted in Figure **7-58**. As can be seen, the DSE based protection correctly detects the fault and trips the circuit breaker.

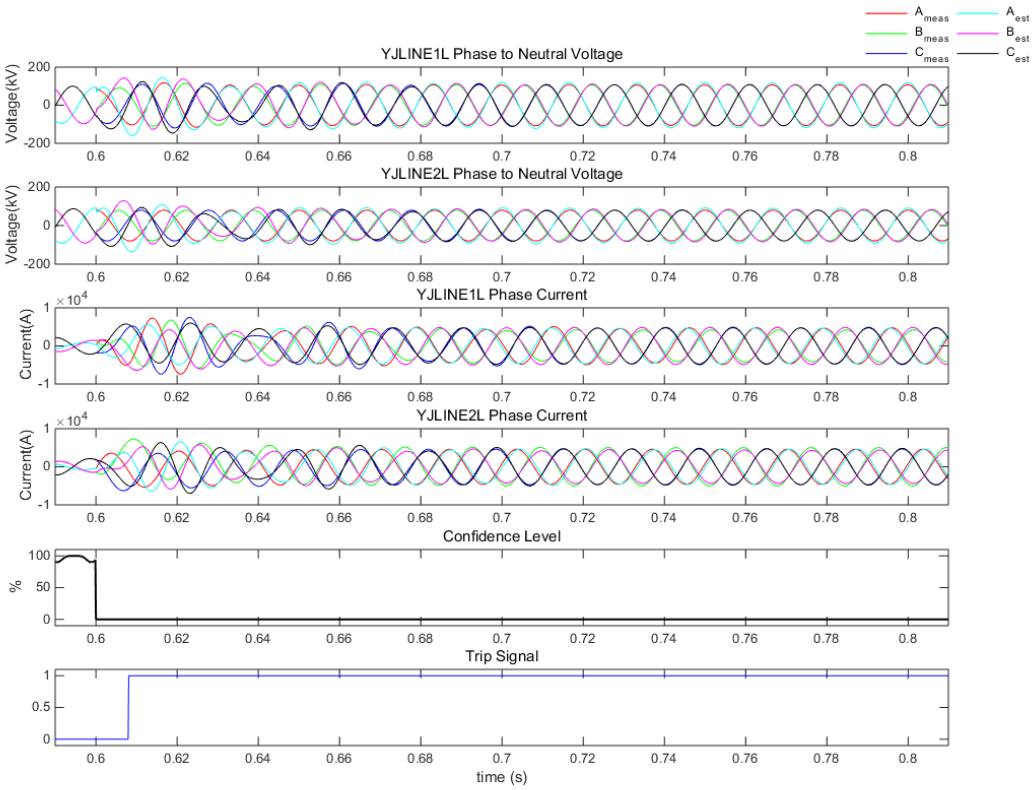

Figure 7-58 DSE based protection results for current inversion test case

Comparing the current differential protection function and the DSE based protection, it is likely even though it's a rare event, that the currents on the terminal where the capacitive reactance is larger than the generator inductive reactance would become outfeed instead of infeed, and the currents on both terminals are out of phase instead of in phase, this would cause the current differential protection function to lose dependability.

7.10 DSE based protection – Practical issues

The DSE based protection would work best when the models are absolutely accurate, and the instrumentation channels have ideal transformation. However, such requirement

cannot be met in practice. In order to investigate the robustness of the algorithm, in this section several practical issues are discussed that affects the performance of the DSE based protection, including 1) modeling error, 2) synchronization error and 3) PT/CT error.

The purpose of this section is not to mathematically formulate the robustness of the algorithm in terms of errors, but to investigate the sensitivity of the algorithm with respect to different errors, i.e., if the confidence level would maintain at high values close to 100% and not to mis-operate the circuit breaker given such errors.

7.10.1 Modeling Error

The parameters for the overhead transmission line modelling in (4.3) are basically three matrices: R (resistance matrix), L (inductance matrix), and C (capacitance matrix). Each matrix is a 4 by 4 matrix with 16 elements, so that the total number of parameters is 48. However, these matrix elements are derived parameters. The fundamental parameters that are used to derive those matrices are the height for each bundled phase conductors, distance between each bundled phase conductors, geometric mean radius of each bundled phase conductors, and finally length of the line. During the process of modeling, the independent parameters can easily be measured, 1) the geometric mean radius can be computed given the radius of the bundled conductors and modified Bessel functions, 2) the horizontal and vertical spacing between conductors, height of conductors can be measured given the tower structure, and 3) the length of the conductors can be measured as distance between connecting towers. And the derived parameters can be computed from the independent parameters given the correct soil resistivity and copper conductivity rate. However, in real life the temperature may change with time, and the height of the conductor may not be equal to the height of the hanging point in the tower due to sag effect. The

transmission line conductors hang downward in a shallow curve between each tower with the lowest point typically being about midway between towers. Sag is a dynamic characteristic, it exists because of the weight of the conductors, and it increases as cables heat up and thus elongate. Heating is caused by both higher ambient air temperature and by heat generated from electricity passing through a line. The greater the sag, the closer a line will be to the ground, and thus the less the height of the line. The actual sag can be determined from the weight of the line and the tension, i.e., ductility of the line under certain temperature.

As discussed, both ambient temperature and line sag alter the parameters of the line in real time. The dc resistance (or resistivity) is linearly dependent on the temperature, while the ac resistance is nonlinearly dependent on the temperature. The impact of the temperature to inductance matrix is more complicated, basically with the increase of the temperature, the geometric mean radius changes (based on the values in the modified Bessel function table), and the mutual inductance would increase (since De=2160sqrt(p/f) increases). On the other hand, the line sag decreases the height of the conductors, but it doesn't change the distance between conductors. Since the self inductance and mutual inductance are functions of both the distance between conductors and the geometric mean radius, the line sag does not change the values of the inductance matrix. However, with the decrease of the height of the conductors, the distance between conductors and its image conductors with respect to the earth decreases, as a result the elements in the capacitance matrix would increase, this could be seen from the fact that the capacitance matrix is the inverse of a matrix:

$$C^{'} = \begin{bmatrix} C_{aa}^{'} & C_{ab}^{'} & C_{ac}^{'} \\ C_{ba}^{'} & C_{bb}^{'} & C_{bc}^{'} \\ C_{ca}^{'} & C_{cb}^{'} & C_{cc}^{'} \end{bmatrix}$$

where

$$C_{ij}^{'} = -\frac{1}{2\pi\varepsilon}\ln\left(\frac{D_{ij}}{D_{ij}^{'}}\right)$$

If the distance between conductor i and j' (as image of j) decreases, such value $C_{ij}^{'}$ would also decrease, and the elements of the inverse of the matrix would increase.

Another modeling error is from frequency. With the modeling in (4.3), the resistance, inductor and capacitor reactance values are based on the fundamental frequency. Such model may not be accurate to describe the system during transients.

The insight of the above discussion suggests that the approach to investigate the modeling error of the transmission line is to assume all elements in each R, L, C matrix is offset by a certain percentage in the same direction, i.e. they both increase or they both decrease. And for the capacitance matrix since the actual height can only be lower than the height of the hanging point, so that elements in the capacitance matrix are assumed to only increase by a certain percentage.

The base test system is the same as in Section 7.3 and also introduced in Figure **7-59**. The parameters for R, jwL, jwC are included in Figure **7-60** and Figure **7-61**.

The sensitivity analysis of the DSE based protection with respect to the capacitance matrix error is illustrated in Figure **7-62**. Without any error the single section modeling generates 100% confidence level during normal operation. The larger the error the lower the average confidence level, and when the capacitance matrix modeling error reaches 50%, the dynamic state estimation can no longer be accurate and thus trip the circuit breaker.

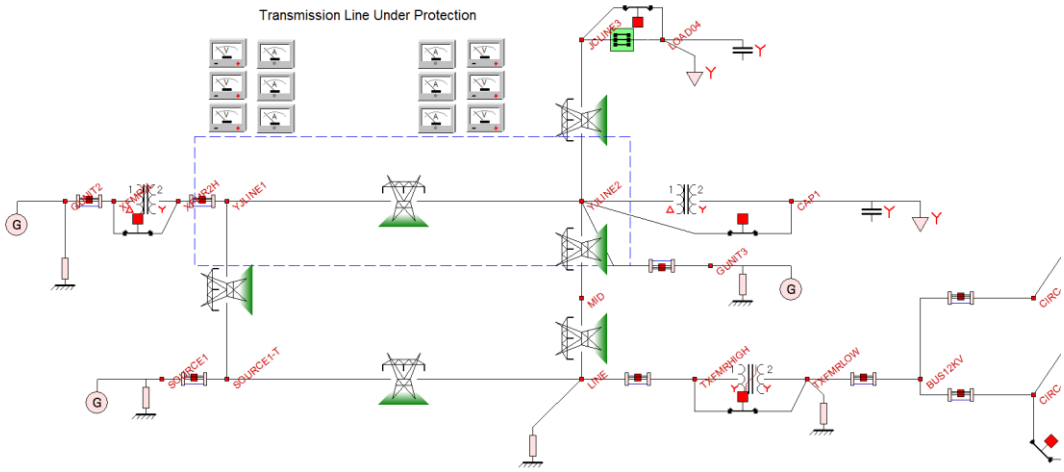

Figure 7-59 Test system for modeling error

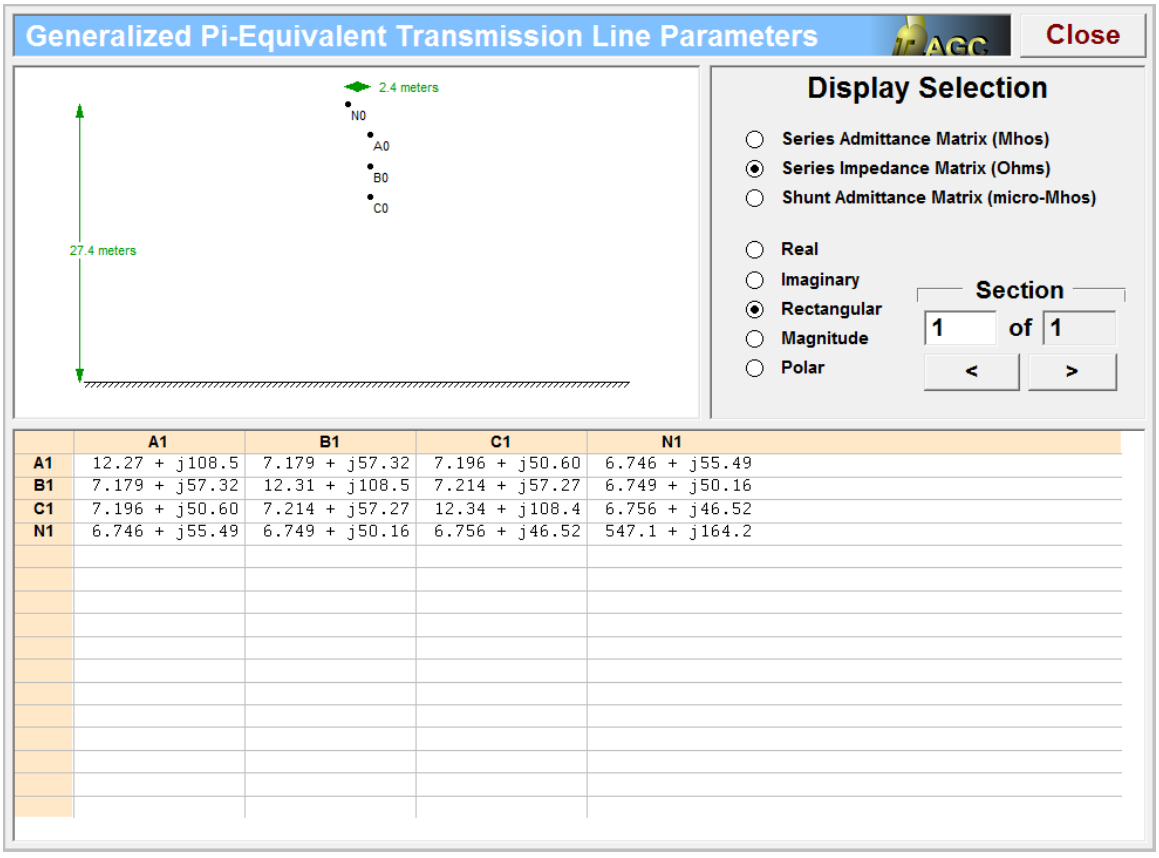

	A1	B1	C1	N1
A1	12.27 + j108.5	7.179 + j57.32	7.196 + j50.60	6.746 + j55.49
B1	7.179 + j57.32	12.31 + j108.5	7.214 + j57.27	6.749 + j50.16
C1	7.196 + j50.60	7.214 + j57.27	12.34 + j108.4	6.756 + j46.52
N1	6.746 + j55.49	6.749 + j50.16	6.756 + j46.52	547.1 + j164.2

Figure 7-60 Test system for modeling error – Impedance matrix

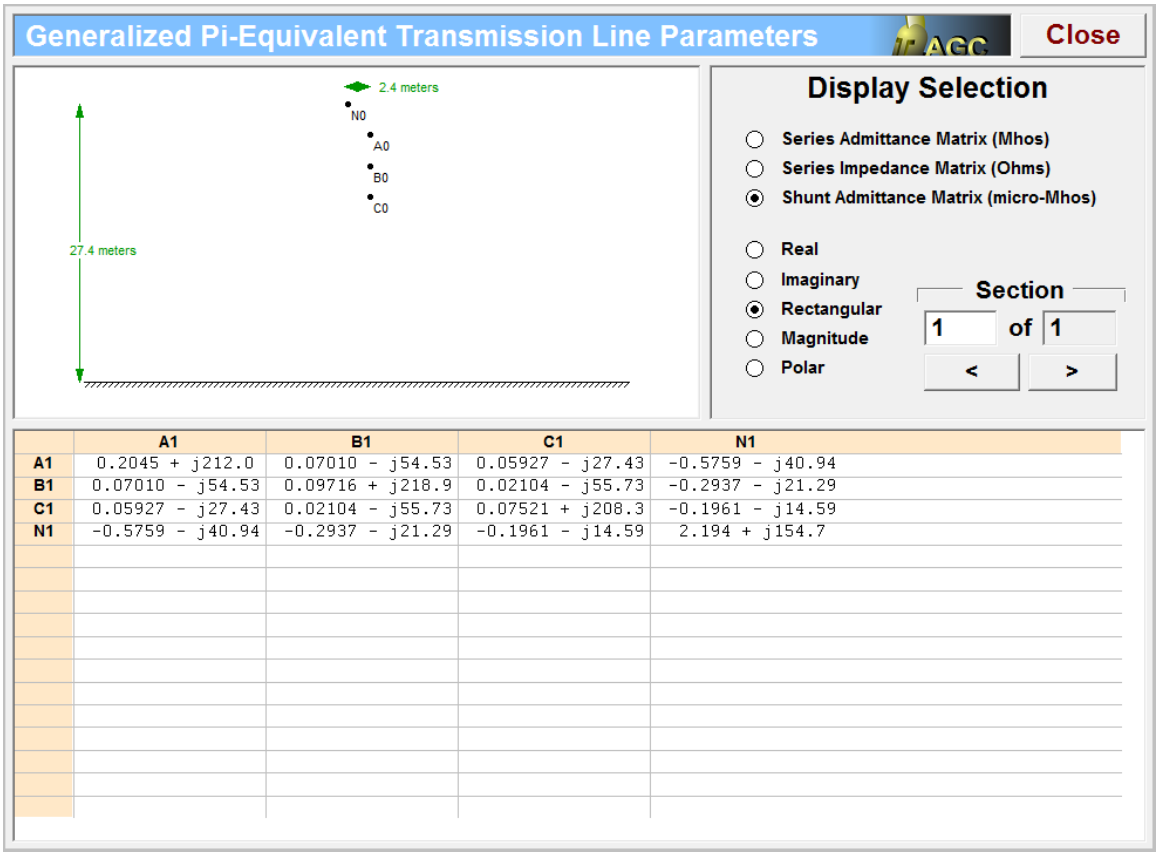

	A1	B1	C1	N1
A1	0.2045 + j212.0	0.07010 - j54.53	0.05927 - j27.43	-0.5759 - j40.94
B1	0.07010 - j54.53	0.09716 + j218.9	0.02104 - j55.73	-0.2937 - j21.29
C1	0.05927 - j27.43	0.02104 - j55.73	0.07521 + j208.3	-0.1961 - j14.59
N1	-0.5759 - j40.94	-0.2937 - j21.29	-0.1961 - j14.59	2.194 + j154.7

Figure 7-61 Test system for modeling error – Shunt Admittance matrix

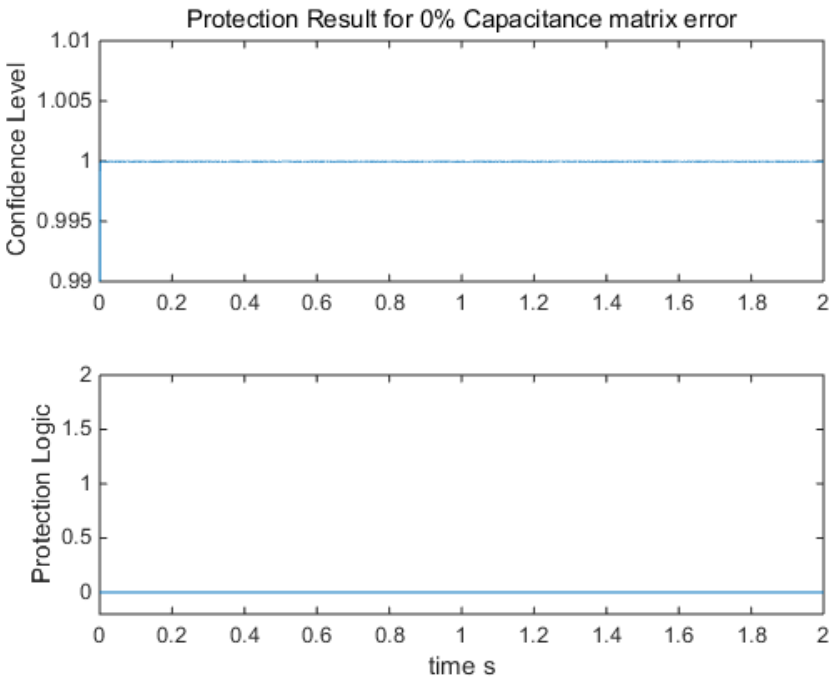
Protection Result for 0% Capacitance matrix error
Confidence Level
1.01
1.005
1
0.995
0.99
0
0.2
0.4
0.6
0.8
1
1.2
1.4
1.6
1.8
2
Protection Logic
2
1.5
1
0.5
0
time s

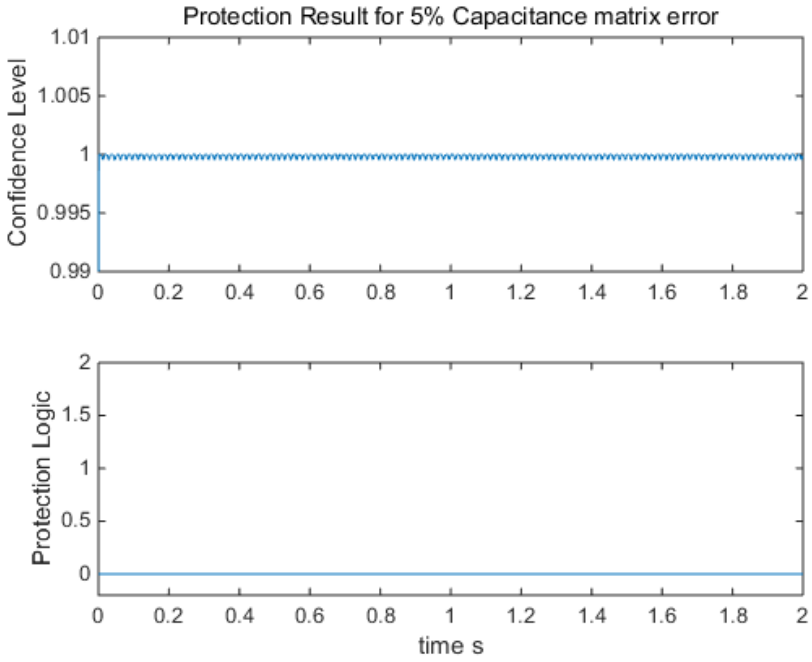
Protection Result for 5% Capacitance matrix error
Confidence Level
1.01
1.005
1
0.995
0.99
0
0.2
0.4
0.6
0.8
1
1.2
1.4
1.6
1.8
2
Protection Logic
2
1.5
1
0.5
0
time s

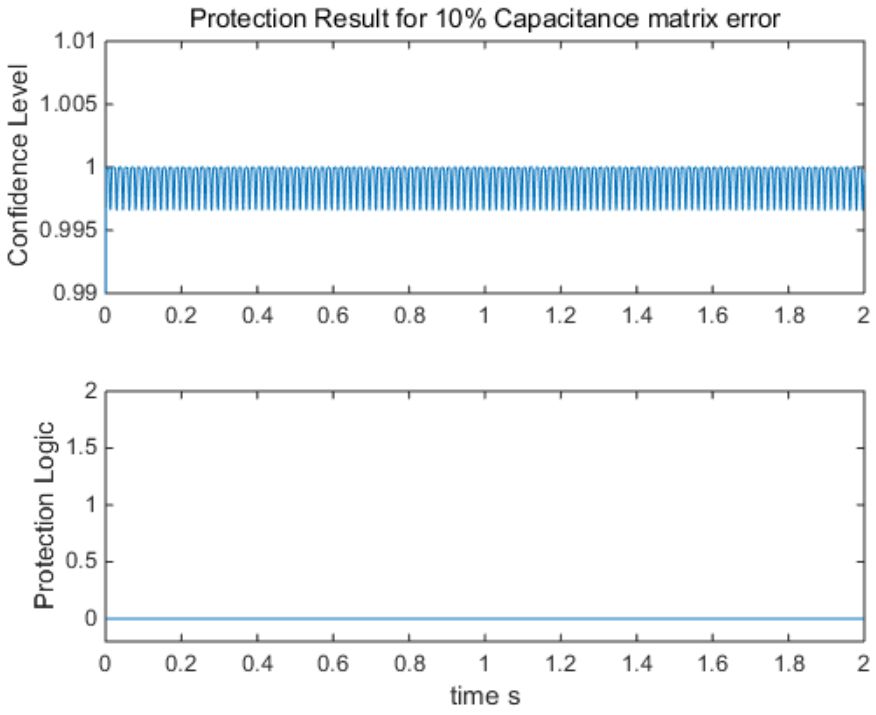
Protection Result for 10% Capacitance matrix error
Confidence Level
1.01
1.005
1
0.995
0.99
0
0.2
0.4
0.6
0.8
1
1.2
1.4
1.6
1.8
2
Protection Logic
2
1.5
1
0.5
0
time s

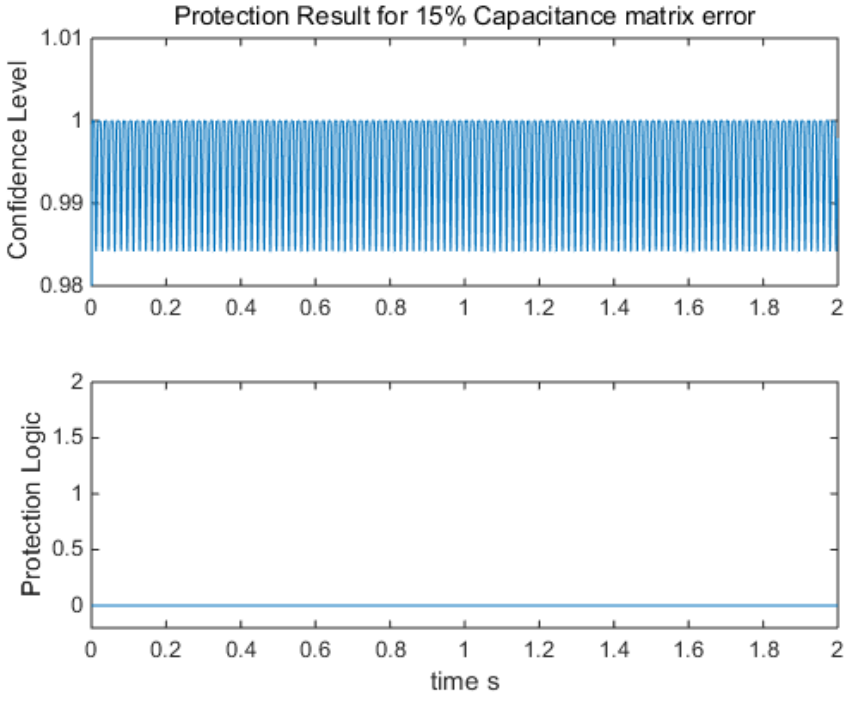
Protection Result for 15% Capacitance matrix error
Confidence Level
1.01
1
0.99
0.98
0
0.2
0.4
0.6
0.8
1
1.2
1.4
1.6
1.8
2
Protection Logic
2
1.5
1
0.5
0
time s

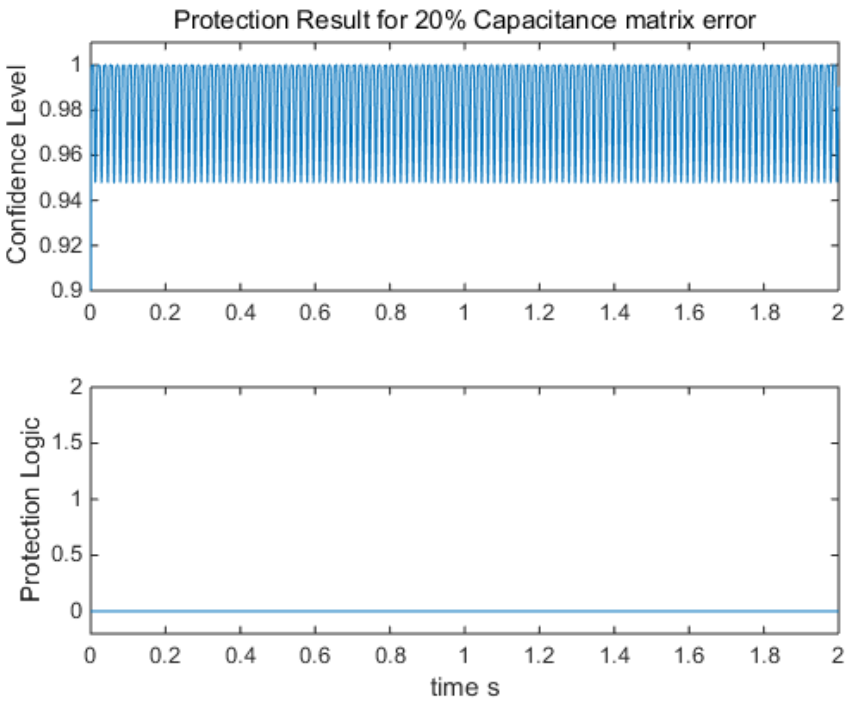
Protection Result for 20% Capacitance matrix error
Confidence Level
1
0.98
0.96
0.94
0.92
0.9
0
0.2
0.4
0.6
0.8
1
1.2
1.4
1.6
1.8
2
Protection Logic
2
1.5
1
0.5
0
time s

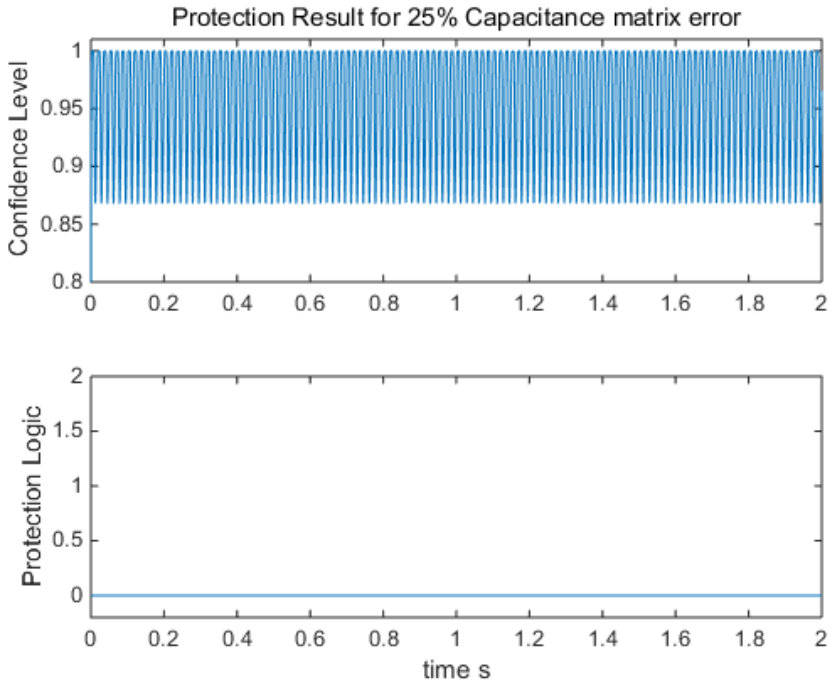
Protection Result for 25% Capacitance matrix error
Confidence Level
1
0.95
0.9
0.85
0.8
0
0.2
0.4
0.6
0.8
1
1.2
1.4
1.6
1.8
2
Protection Logic
2
1.5
1
0.5
0
time s

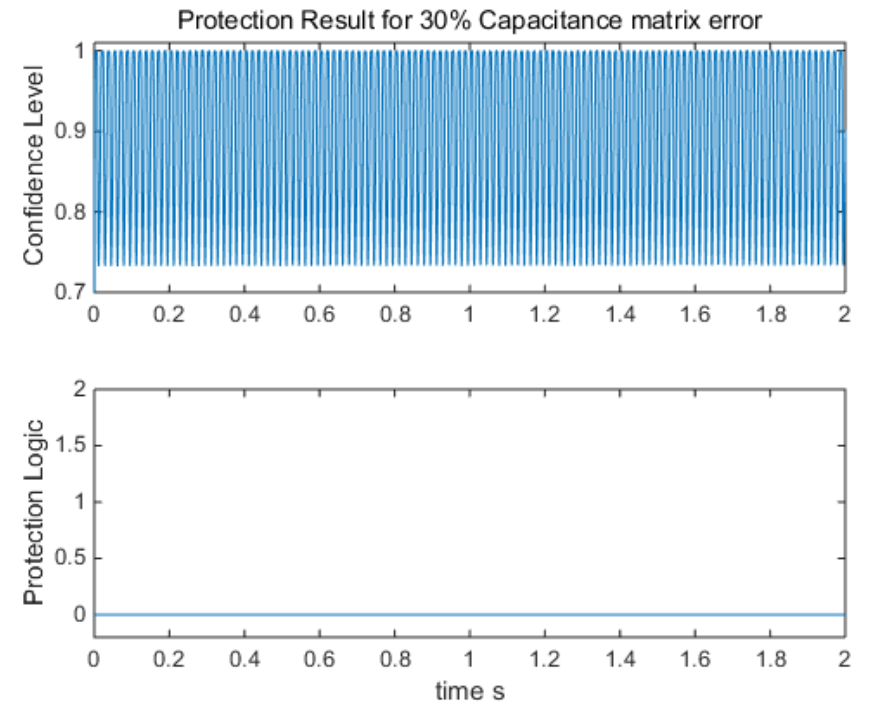
Protection Result for 30% Capacitance matrix error
Confidence Level
1
0.9
0.8
0.7
0
0.2
0.4
0.6
0.8
1
1.2
1.4
1.6
1.8
2
Protection Logic
2
1.5
1
0.5
0
time s

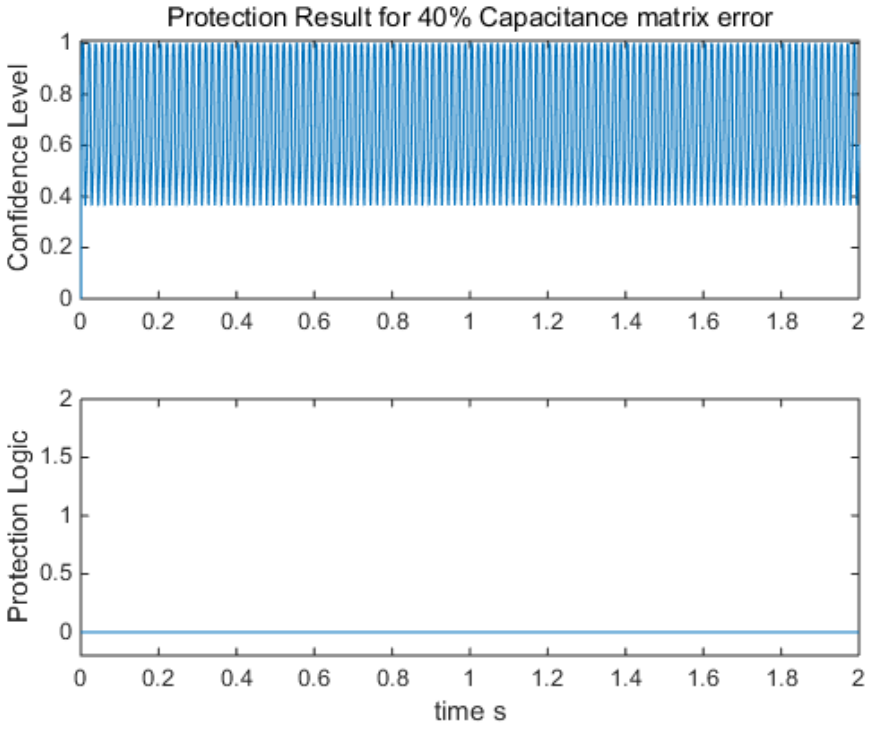
Protection Result for 40% Capacitance matrix error
Confidence Level
1
0.8
0.6
0.4
0.2
0
0.2
0.4
0.6
0.8
1
1.2
1.4
1.6
1.8
2
Protection Logic
2
1.5
1
0.5
0
time s

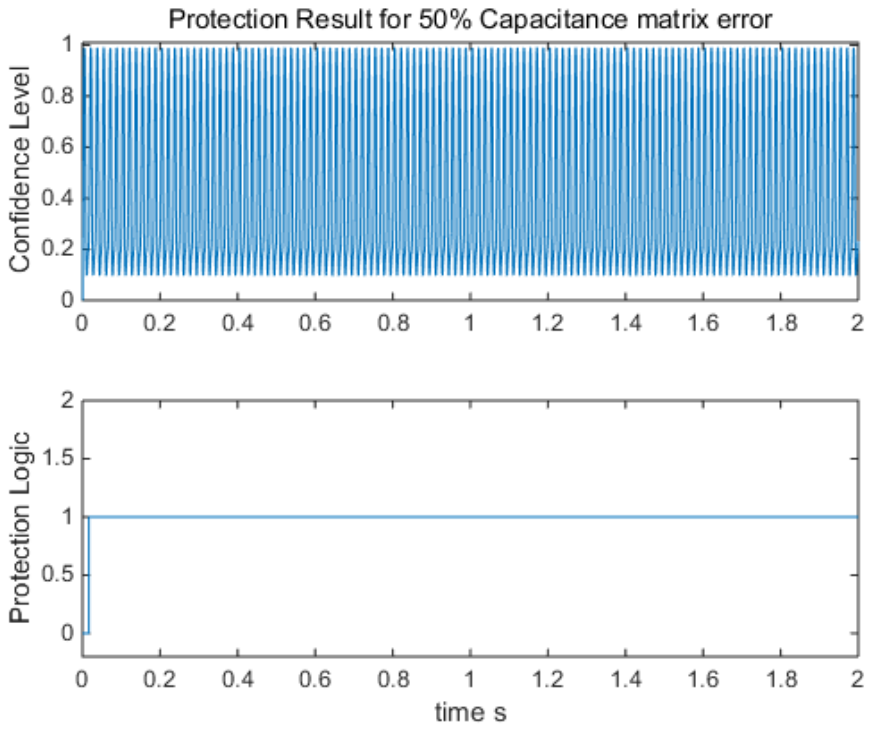

Figure 7-62 Sensitivity analysis of DSE based protection for capacitance modeling error

The sensitivity analysis of the DSE based protection with respect to the inductance matrix error is illustrated in Figure **7-63**. Without any error the single section modeling generates 100% confidence level during normal operation. The larger the error the lower the average confidence level, and when the inductance matrix modeling error reaches 20% or -20%, the dynamic state estimation can no longer be accurate and thus trip the circuit breaker. It can be seen the inductance matrix is more sensitive than the capacitance matrix. This also means that the inductance reactance parameters are easier to estimate.

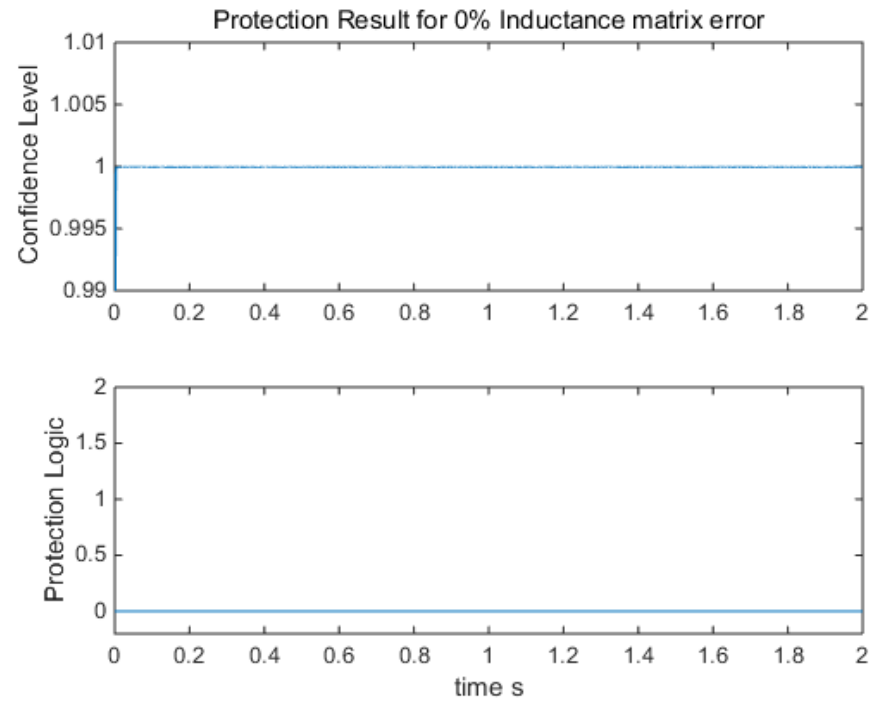
Protection Result for 0% Inductance matrix error
Confidence Level
1.01
1.005
1
0.995
0.99
0
0.2
0.4
0.6
0.8
1
1.2
1.4
1.6
1.8
2
Protection Logic
2
1.5
1
0.5
0
time s

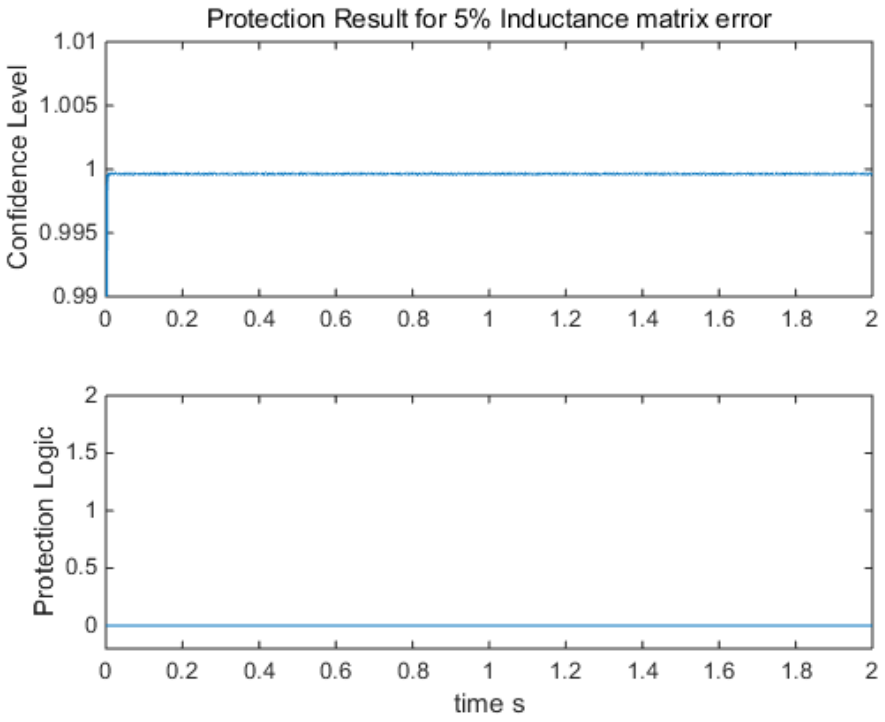
Protection Result for 5% Inductance matrix error
Confidence Level
1.01
1.005
1
0.995
0.99
0
0.2
0.4
0.6
0.8
1
1.2
1.4
1.6
1.8
2
Protection Logic
2
1.5
1
0.5
0
time s

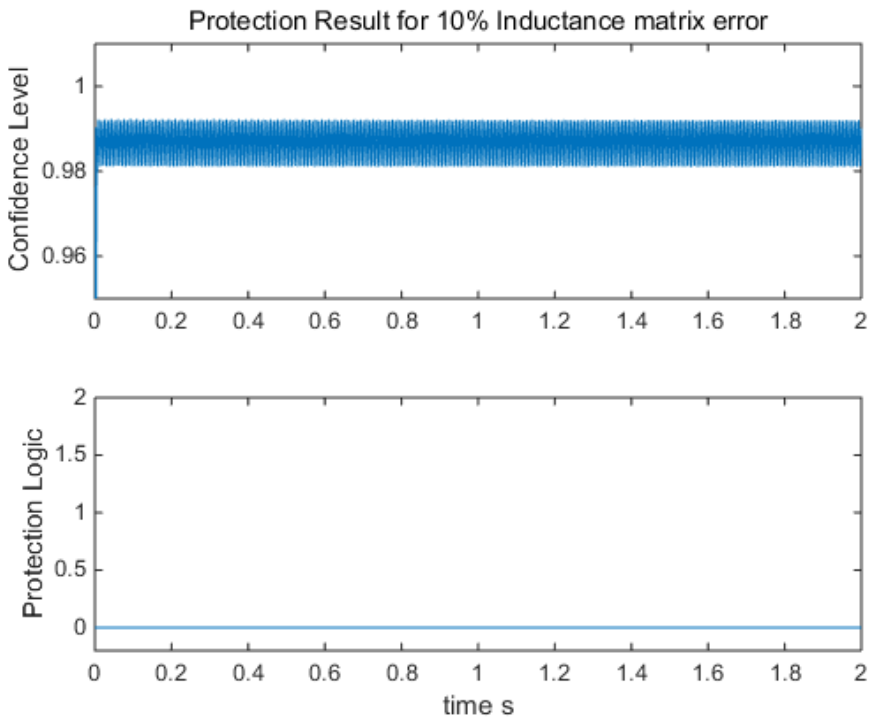
Protection Result for 10% Inductance matrix error
Confidence Level
1
0.98
0.96
0
0.2
0.4
0.6
0.8
1
1.2
1.4
1.6
1.8
2
Protection Logic
2
1.5
1
0.5
0
time s

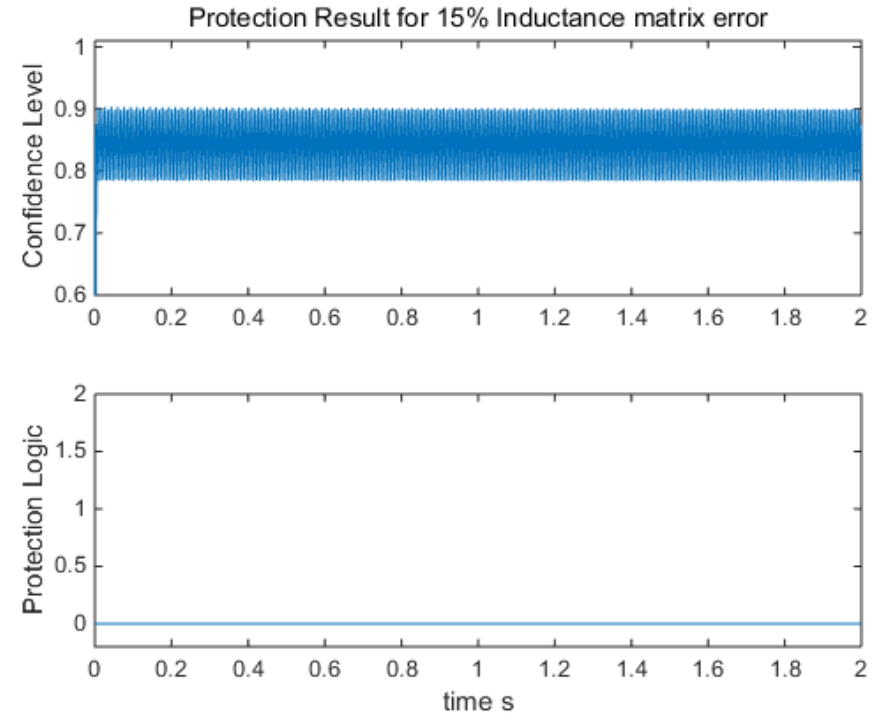
Protection Result for 15% Inductance matrix error
Confidence Level
1
0.9
0.8
0.7
0.6
0
0.2
0.4
0.6
0.8
1
1.2
1.4
1.6
1.8
2
Protection Logic
2
1.5
1
0.5
0
time s

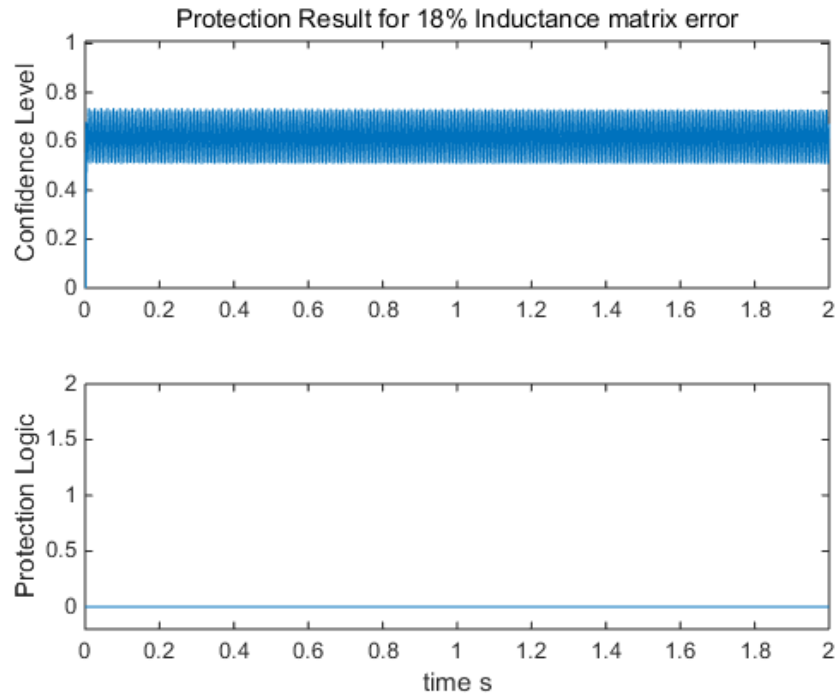
Protection Result for 18% Inductance matrix error
Confidence Level
Protection Logic
time s

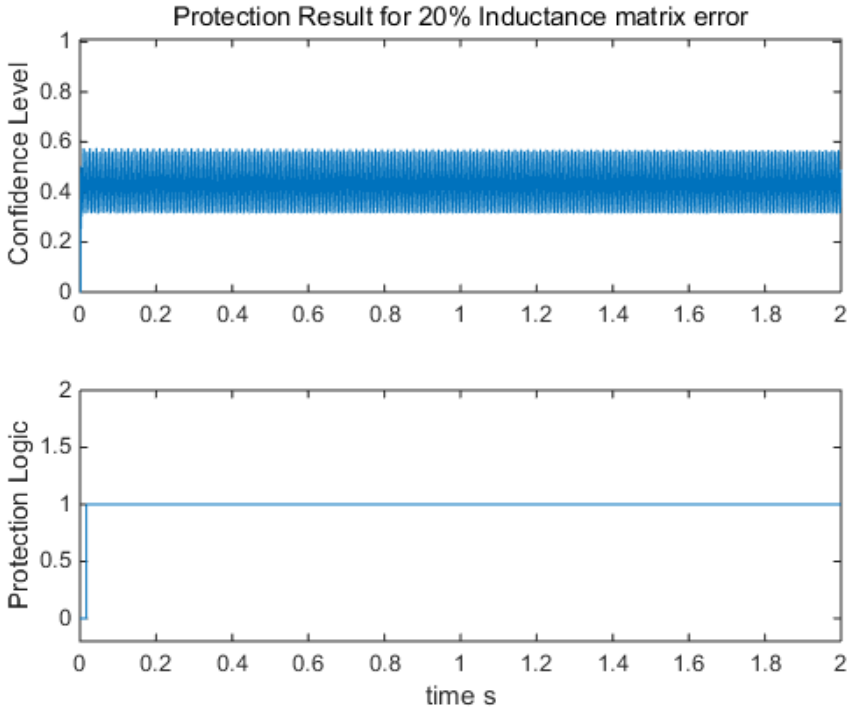
Protection Result for 20% Inductance matrix error
Confidence Level
Protection Logic
time s

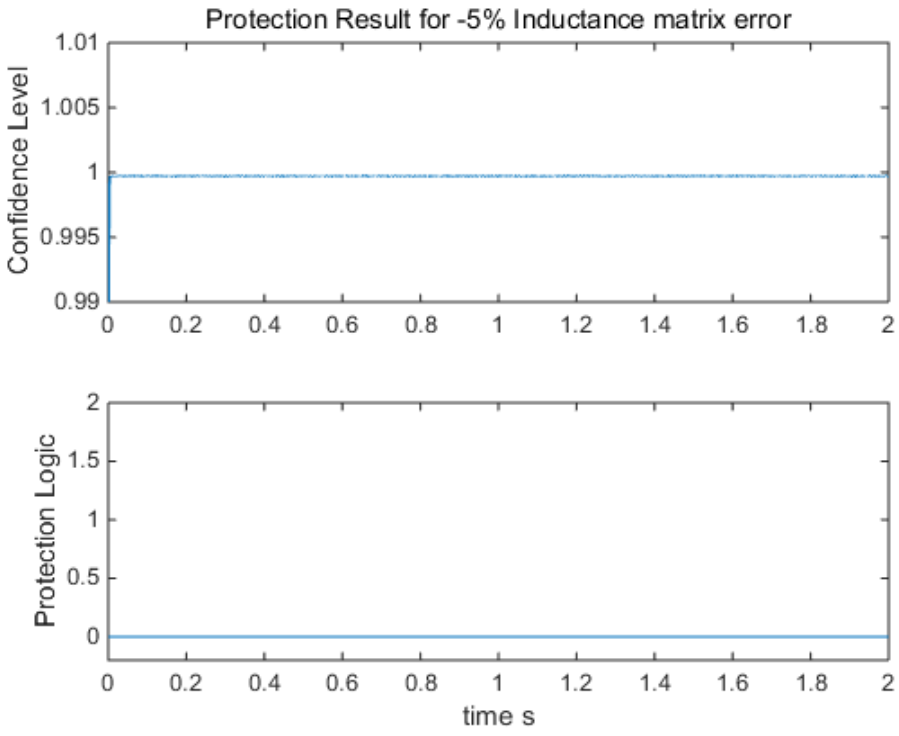
Protection Result for -5% Inductance matrix error
Confidence Level
1.01
1.005
1
0.995
0.99
0 0.2 0.4 0.6 0.8 1 1.2 1.4 1.6 1.8 2
Protection Logic
2
1.5
1
0.5
0
0 0.2 0.4 0.6 0.8 1 1.2 1.4 1.6 1.8 2
time s

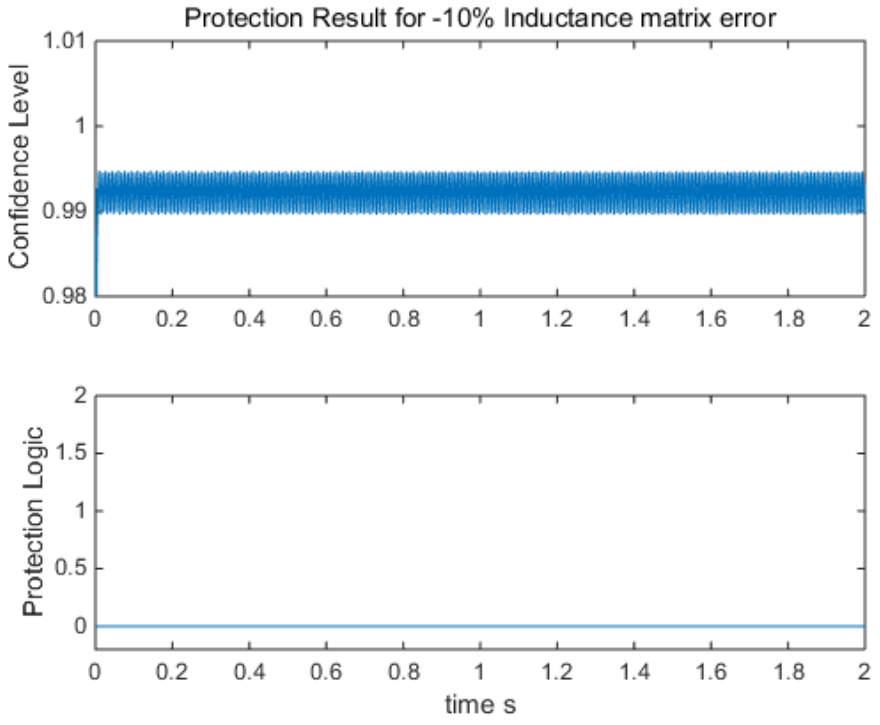
Protection Result for -10% Inductance matrix error
Confidence Level
1.01
1
0.99
0.98
0 0.2 0.4 0.6 0.8 1 1.2 1.4 1.6 1.8 2
Protection Logic
2
1.5
1
0.5
0
0 0.2 0.4 0.6 0.8 1 1.2 1.4 1.6 1.8 2
time s

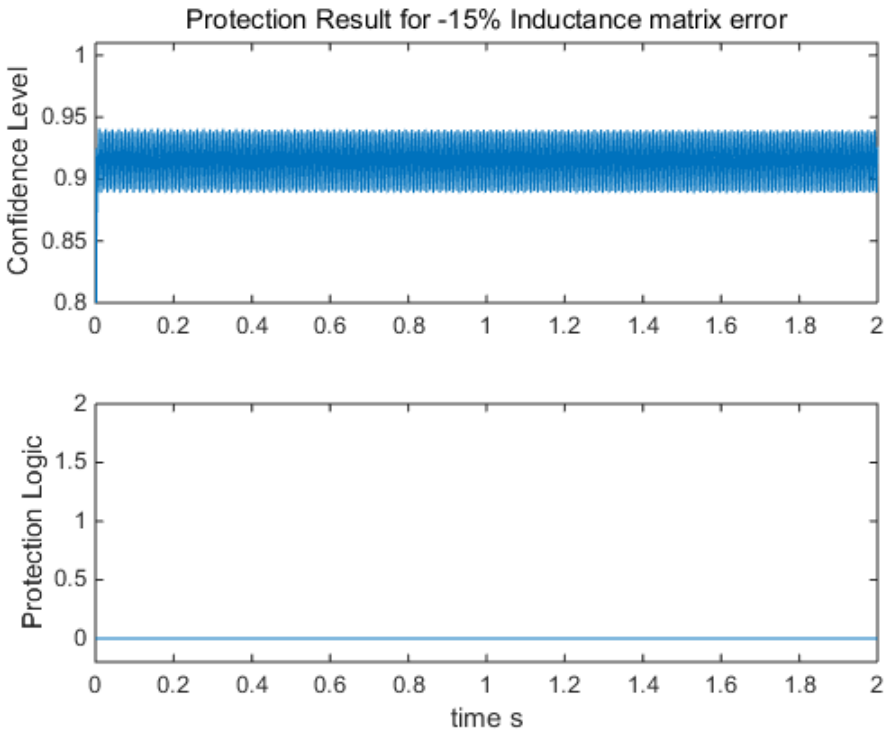
Protection Result for -15% Inductance matrix error
Confidence Level
1
0.95
0.9
0.85
0.8
0 0.2 0.4 0.6 0.8 1 1.2 1.4 1.6 1.8 2
Protection Logic
2
1.5
1
0.5
0
0 0.2 0.4 0.6 0.8 1 1.2 1.4 1.6 1.8 2
time s

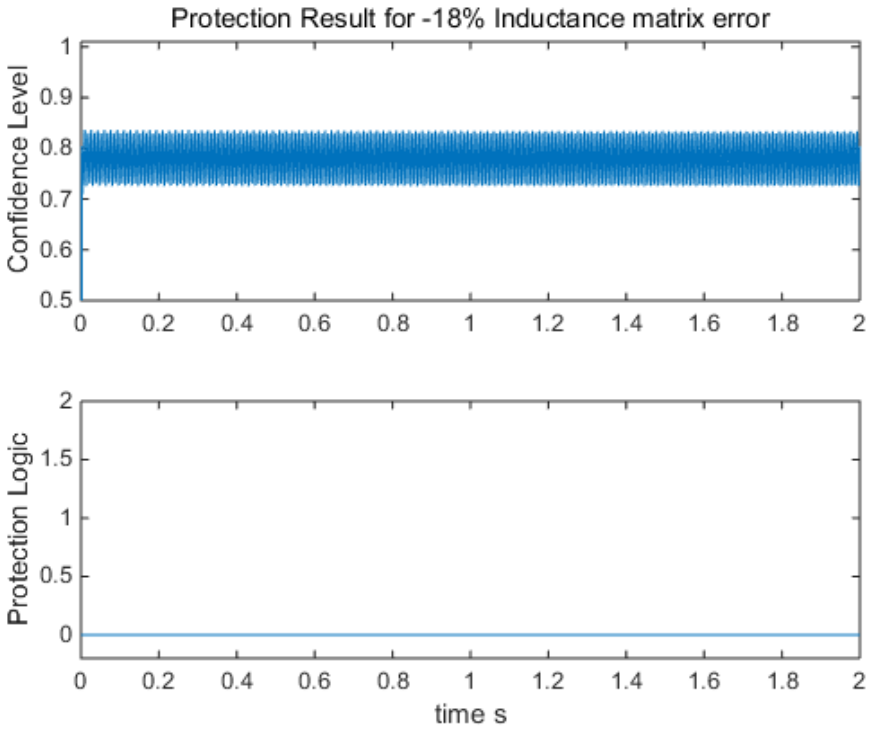
Protection Result for -18% Inductance matrix error
Confidence Level
1
0.9
0.8
0.7
0.6
0.5
0 0.2 0.4 0.6 0.8 1 1.2 1.4 1.6 1.8 2
Protection Logic
2
1.5
1
0.5
0
0 0.2 0.4 0.6 0.8 1 1.2 1.4 1.6 1.8 2
time s

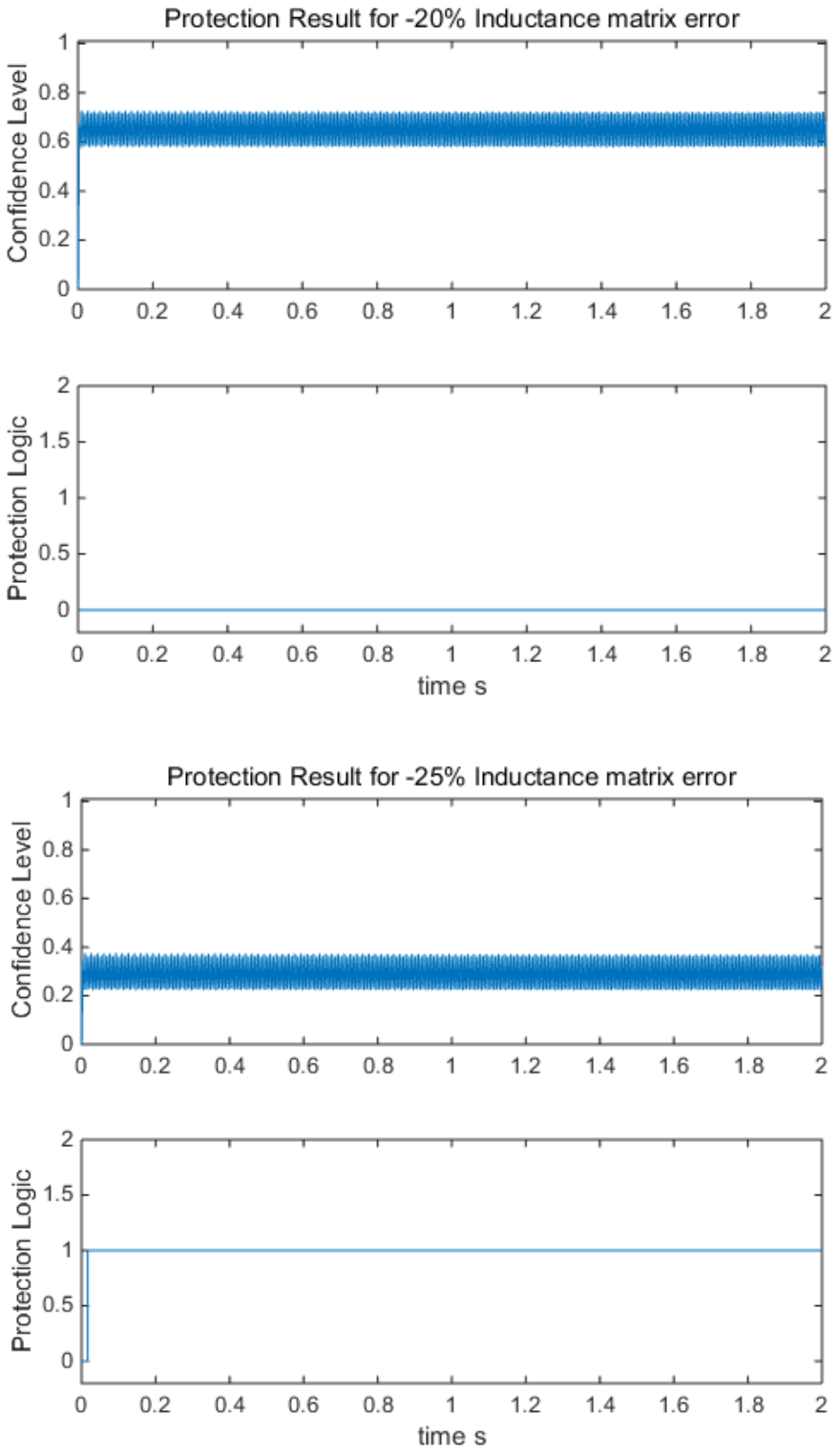

Figure 7-63 Sensitivity analysis of DSE based protection for inductance matrix modeling error

The sensitivity analysis of the DSE based protection with respect to the resistance matrix error is illustrated in Figure **7-64**. Without any error the single section modeling generates 100% confidence level during normal operation. The larger the error the lower the average confidence level, and when the inductance matrix modeling error reaches 250%, the dynamic state estimation can no longer be accurate and thus trip the circuit breaker. Meanwhile even if the resistance matrix elements are all initialized to be 0 (as -100% error), the protection results are good enough. It can be seen the resistance matrix is much less sensitive than the other two matrices. This also means that the resistive parameters are difficult to estimate.

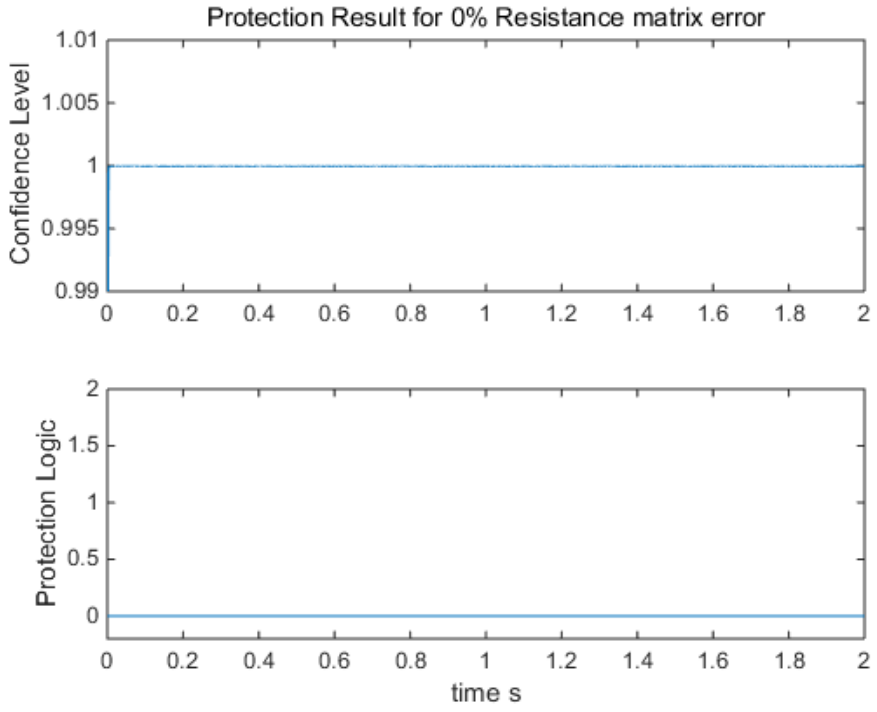

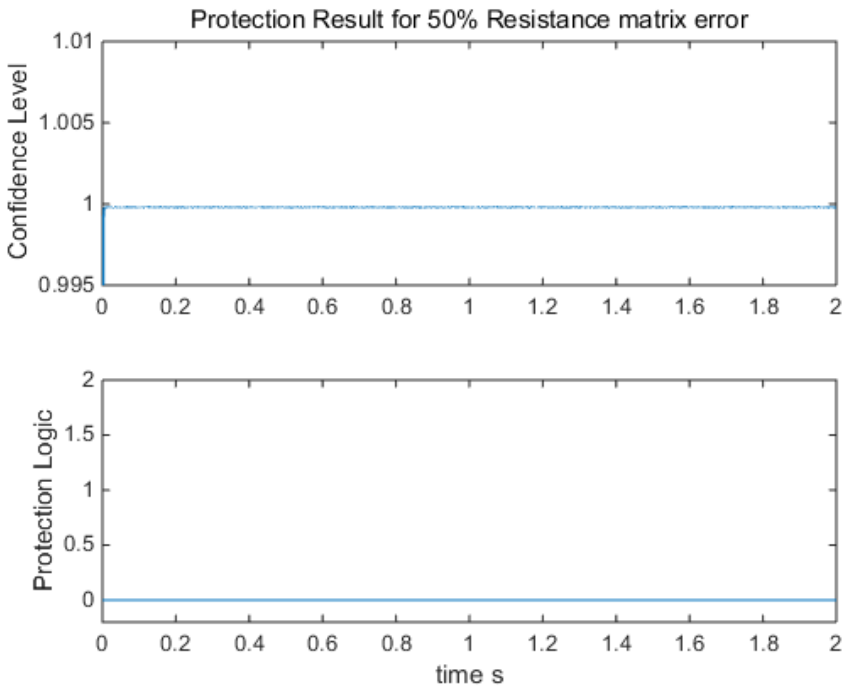
Protection Result for 50% Resistance matrix error
Confidence Level
1.01
1.005
1
0.995
0 0.2 0.4 0.6 0.8 1 1.2 1.4 1.6 1.8 2
Protection Logic
2
1.5
1
0.5
0
0 0.2 0.4 0.6 0.8 1 1.2 1.4 1.6 1.8 2
time s

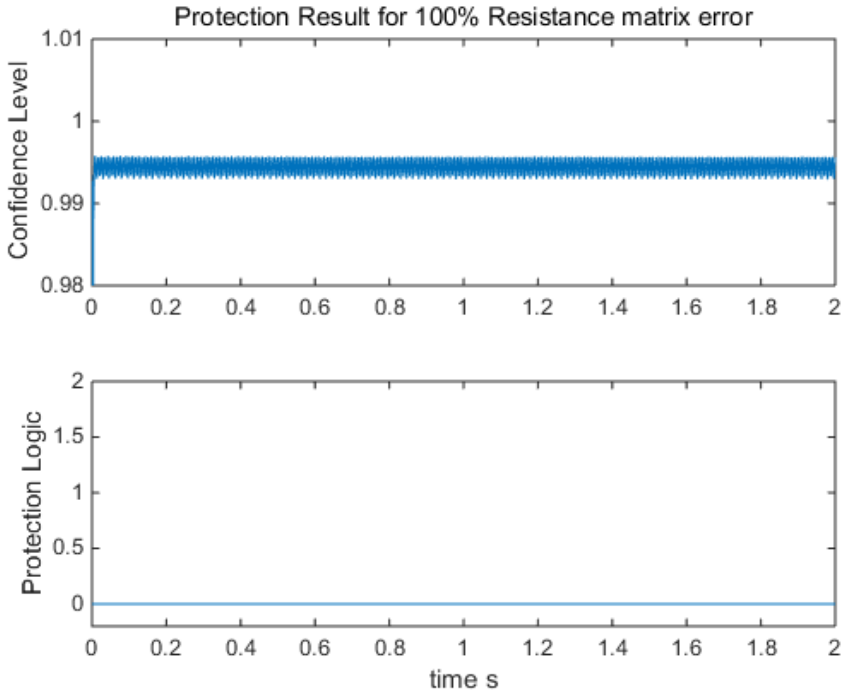
Protection Result for 100% Resistance matrix error
Confidence Level
1.01
1
0.99
0.98
0 0.2 0.4 0.6 0.8 1 1.2 1.4 1.6 1.8 2
Protection Logic
2
1.5
1
0.5
0
0 0.2 0.4 0.6 0.8 1 1.2 1.4 1.6 1.8 2
time s

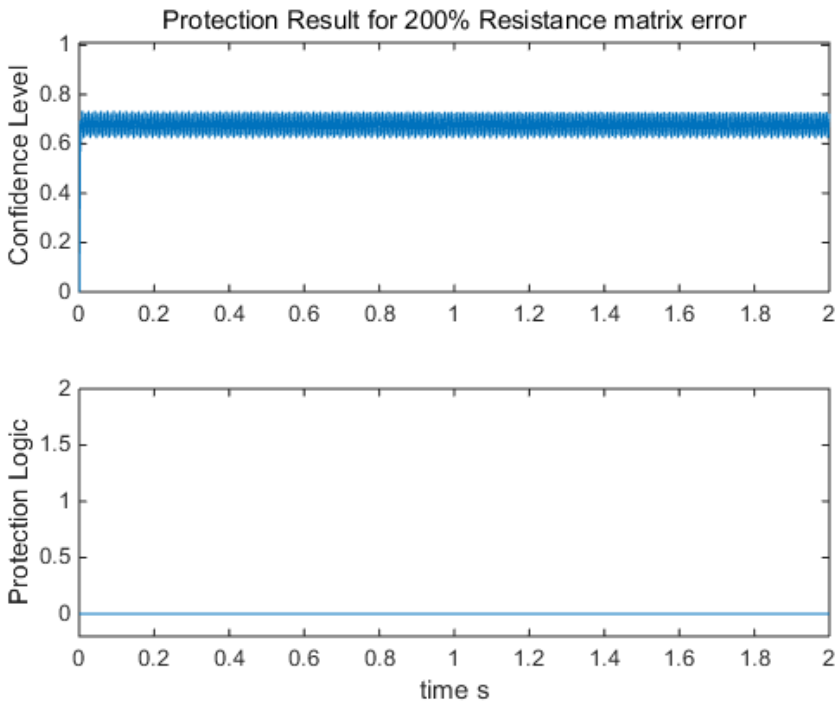
Protection Result for 200% Resistance matrix error
Confidence Level
Protection Logic
time s

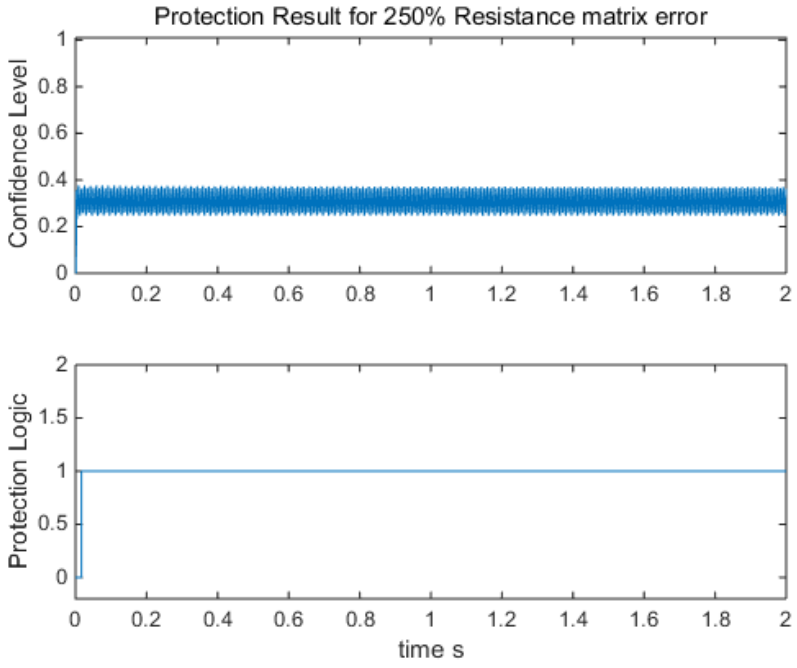
Protection Result for 250% Resistance matrix error
Confidence Level
Protection Logic
time s

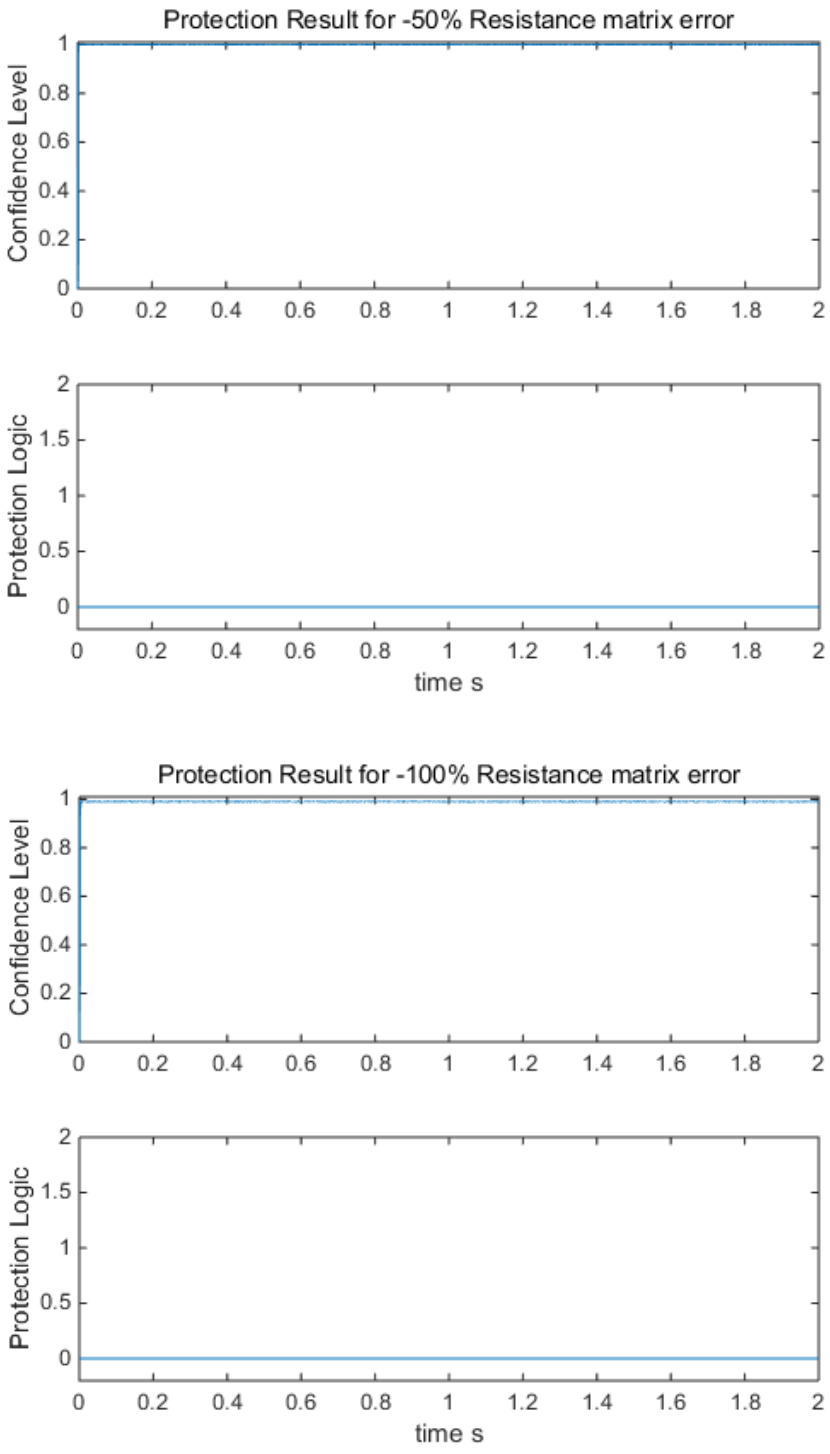

Figure 7-64 Sensitivity analysis of DSE based protection for resistance matrix modeling error

7.10.2 Synchronization Error

Most merging units are GPS or IRIG-B synchronized, each device measures the time difference between the output of its own sampling oscillator and the 1PPS GPS signal providing a 1us order of precision suitable for protection relay applications. Each device then corrects the oscillation frequency of its sampling oscillator so that the time difference becomes zero. The devices continuously update the correction factor and stores it as the absolute accuracy of the oscillator. The samples from the merging units could be time aligned by data concentrators. However, synchronization error can still occur due to several reasons: 1) reception of the GPS signal by the GPS antenna may be interrupted during the course of a day, and the oscillator may start drifting away. 2) during synchronization the maximum alignment inaccuracy between measurements on both sides of the line could still be 2 microseconds, and 3) the analog filter, sampling and hold, and digital processing (including time stamping) for the analog waveform would have time delay. In order to guarantee the dependability and security of the DSE based protection, synchronization error needs to be investigated.

The approach to investigate this issue is as follow: in the simulation software the simulating time step is set at 0.5 microsecond. Then 0.5 microsecond synchronization error is obtained by shifting the measurements on the right hand side (three voltage measurements and three current measurements) by 1 samples away.

Figure **7-65** illustrates the sensitivity of the DSE based protection from sync error. With 1 or 2 microsecond the confidence level and protection logic would not be affected by the sync error, which means that if both merging units are time synchronized by GPS or IRIG-B, the DSE based algorithm would provide reliable protection. However, if GPS

is lost temporarily and the sync error increases to 5 microseconds, then the protection logic would be compromised.

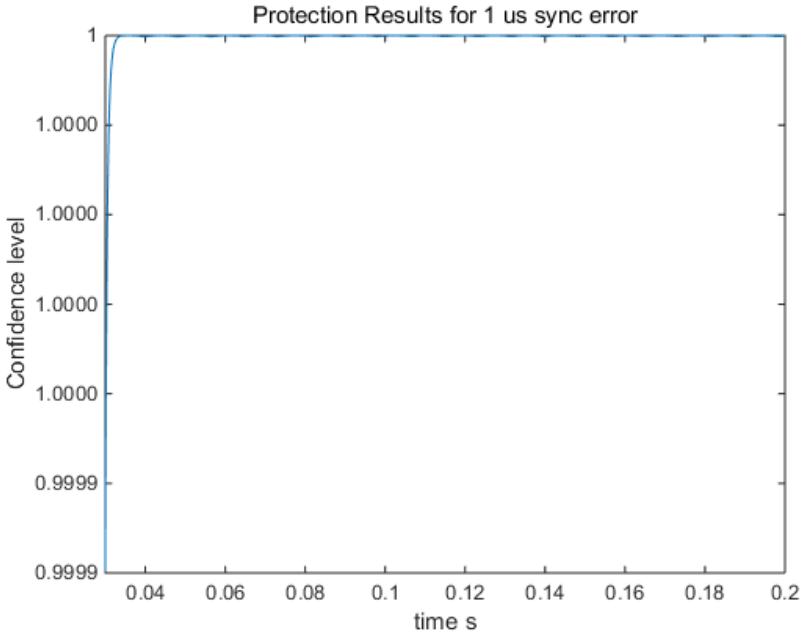

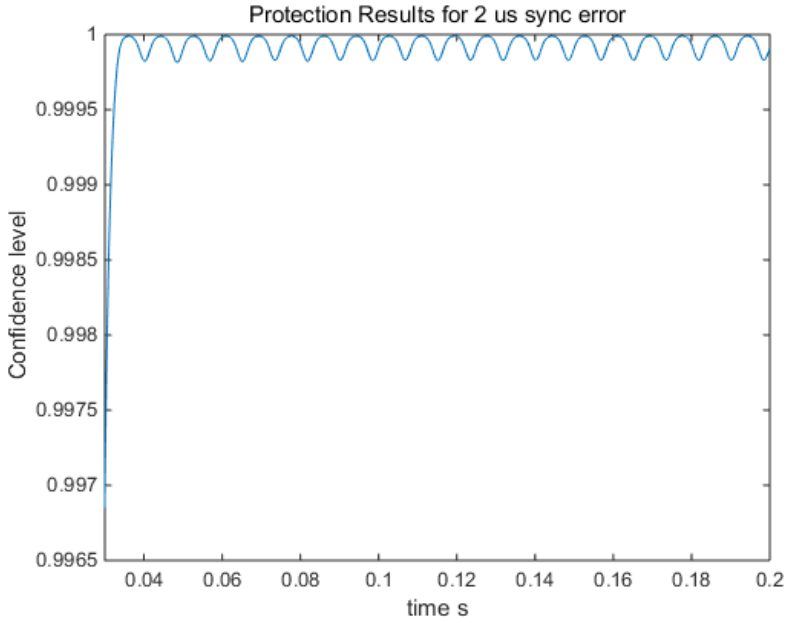

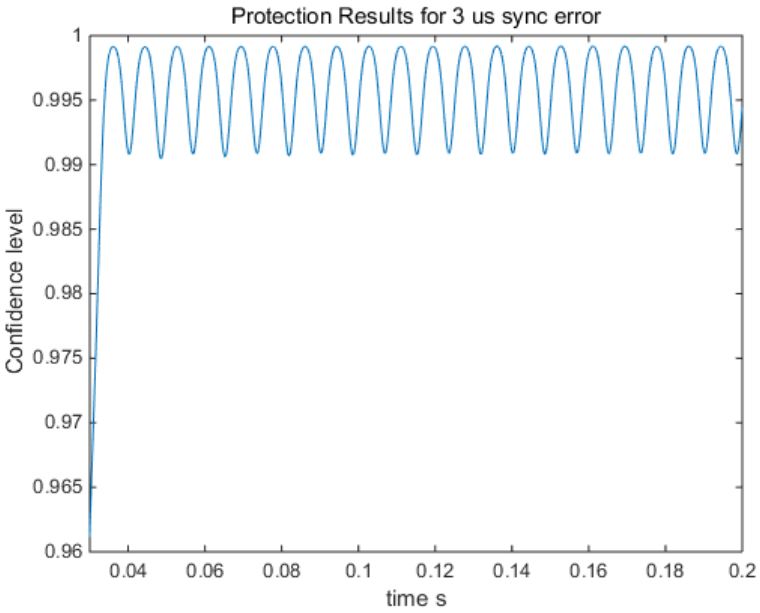
Protection Results for 3 us sync error
Confidence level
time s
1
0.995
0.99
0.985
0.98
0.975
0.97
0.965
0.96
0.04
0.06
0.08
0.1
0.12
0.14
0.16
0.18
0.2

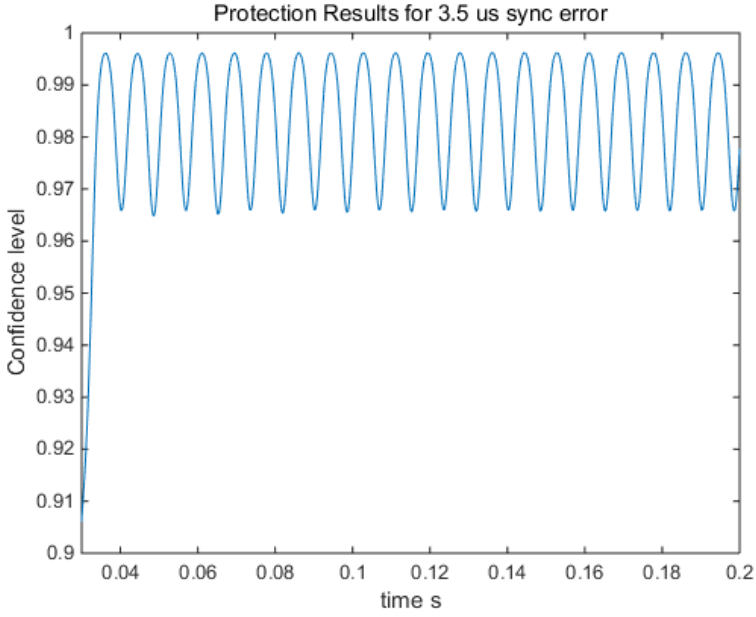
Protection Results for 3.5 us sync error
Confidence level
time s
1
0.99
0.98
0.97
0.96
0.95
0.94
0.93
0.92
0.91
0.9
0.04
0.06
0.08
0.1
0.12
0.14
0.16
0.18
0.2

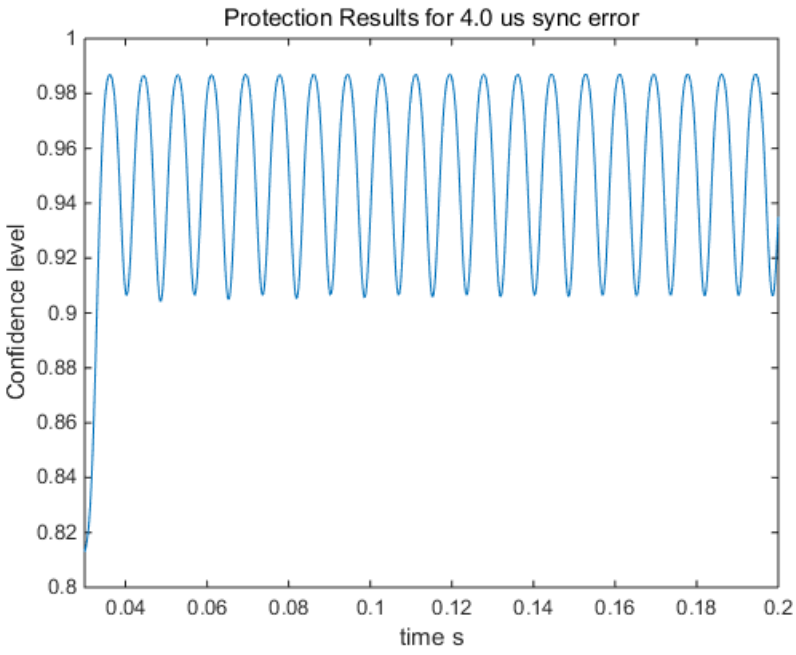
Protection Results for 4.0 us sync error
Confidence level
time s
1
0.98
0.96
0.94
0.92
0.9
0.88
0.86
0.84
0.82
0.8
0.04
0.06
0.08
0.1
0.12
0.14
0.16
0.18
0.2

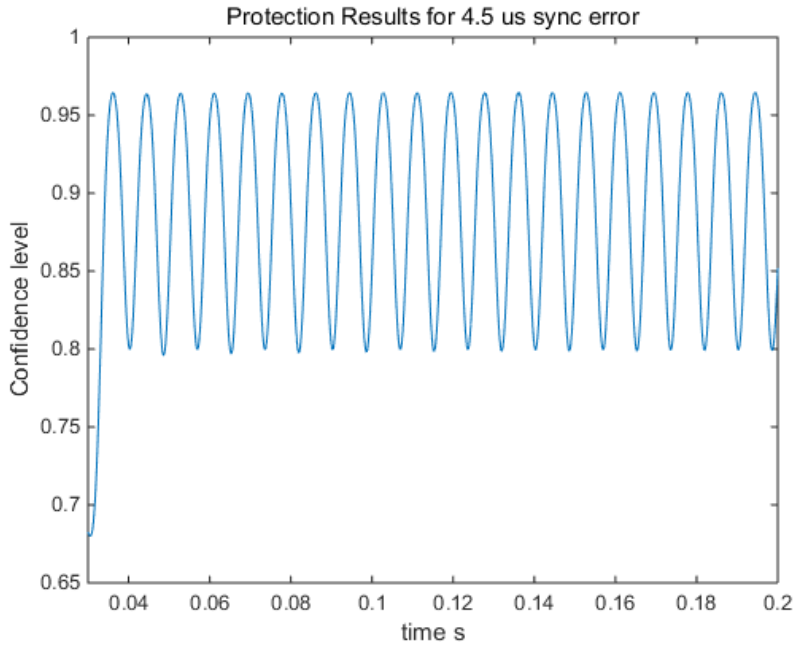
Protection Results for 4.5 us sync error
Confidence level
time s
1
0.95
0.9
0.85
0.8
0.75
0.7
0.65
0.04
0.06
0.08
0.1
0.12
0.14
0.16
0.18
0.2

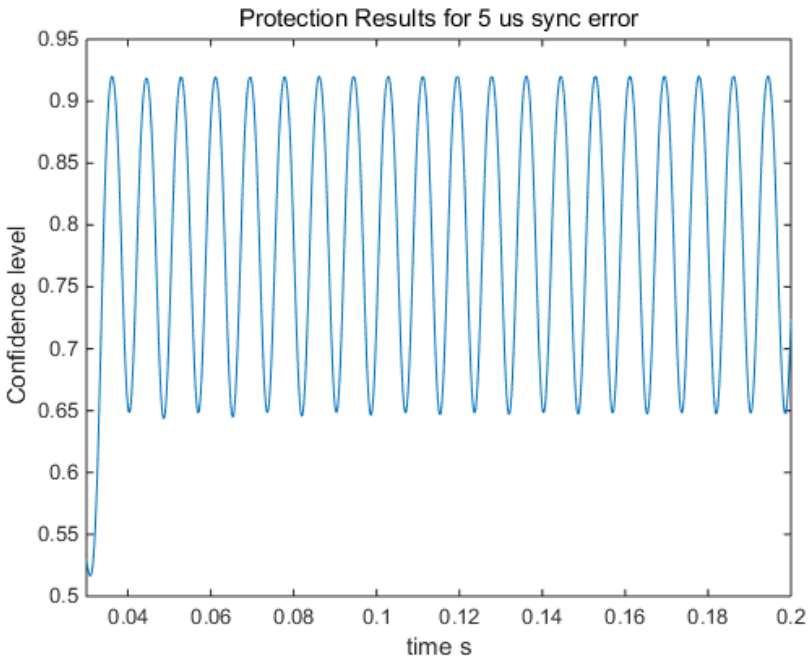

Figure 7-65 Sensitivity analysis of DSE based protection for synchronization error

7.10.3 Instrumentation Error

The chain of measurement instrumentation equipment starts from high voltage and current measurement point and ends with analog or digital signal. Figure **7-66** [55] illustrates the instrumentation channel. The purpose is to bring down the high voltage level (potential transformer) and high current level (current transformer) to the relaying level that can be measured by electronic devices. The control cable extends the analog signal at the field back to the relay house where the relays samples the analog waveform.

The first task is to investigate the measurement error on the secondary side of the instrument transformer when no ratio correction factor is involved during normal operation. The reason is simple: the ratio correction factor is generally a complex quantity, implying that there is both a phase shift and a magnitude error for time domain waveform, so that

it's easy to correct the data in phasor domain, but it would be very difficult to correct that in time domain.

Other than that, two phenomena are investigated in this section. The first one is CT saturation. CT saturation occurs when the electric current through the CT results in CT magnetic flux linkage above the level for which the CT has been designed. When saturation occurs, the secondary current is not a scaled replica of the primary current. In case of internal faults this is not a problem as the current in the secondary will cause the DSE based protection function to operate as expected. However, when saturation occurs during external faults it is likely that the saturation would cause the DSE based protection to mis-operate.

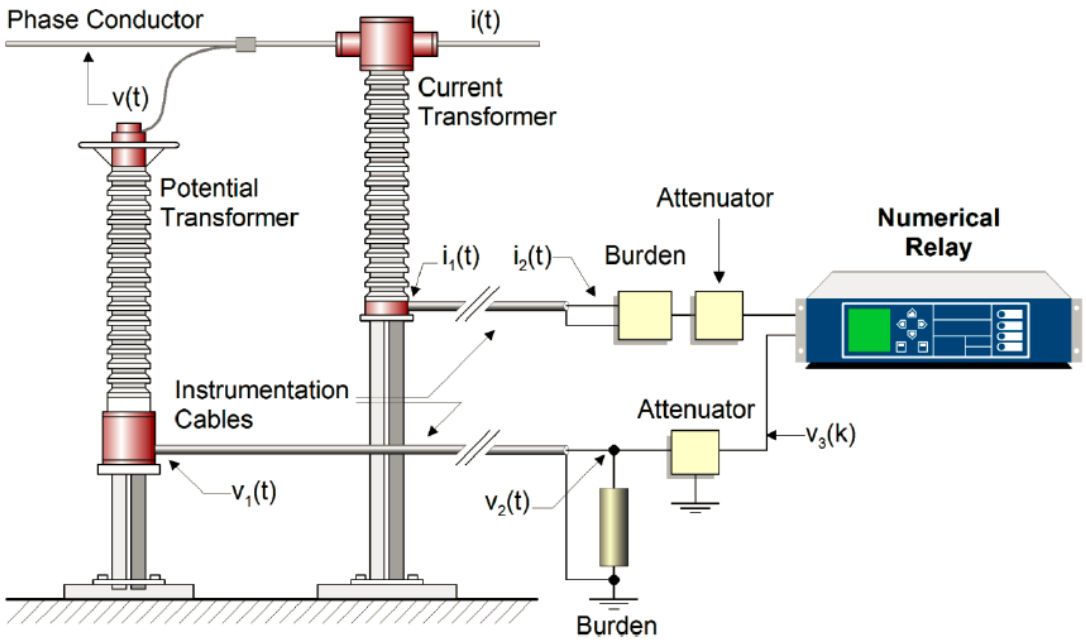

Figure 7-66 Illustration of instrumentation channel – potential transformer, current transformer, control cable, and burden [55]

Another phenomenon is the PT transient response. When the transmission line is energized or when the line has a close fault to the bus, the voltage drops immediately, and the potential transformer may have transient response, and again in this case the secondary voltage is not a scaled replica of the primary voltage.

The ratio correction factor (RCF) is neglected in this section, i.e., to always assume the actual transformation ratio equals to the ideal transformation ratio. For current transformers the RCF approaches unity as the burden and cable and winding impedances are reduced and the magnetizing impedance is relatively large if the CT core is not saturated, or the flux density is generally smaller than 0.5 Tesla.

The short conclusion for this section is that while potential transformer measurement error does not have a large impact on the DSE protection results and confidence level computation, the current transformer can have a large impact during CT saturation. And as a result, the option is to model both the transmission line and instrumentation channel in the same time.

Potential Transformer Measurement Error:

The first test case is illustrated in Figure **7-67**. The protected zone is 80 miles from YJLINE1 to YJLINE2. The only event is that the system is running in normal operation until **Event 1** – a three phase fault close to YJLINE1 (0.6 mile away) from t = 0.804s to t = 1.004s. The three phase fault causes the voltage measurements on node YJLINE1 to drop immediately, and as a result the transient response of the potential transformer can be observed. The potential transformer, control cable and burden is also illustrated in the figure below.

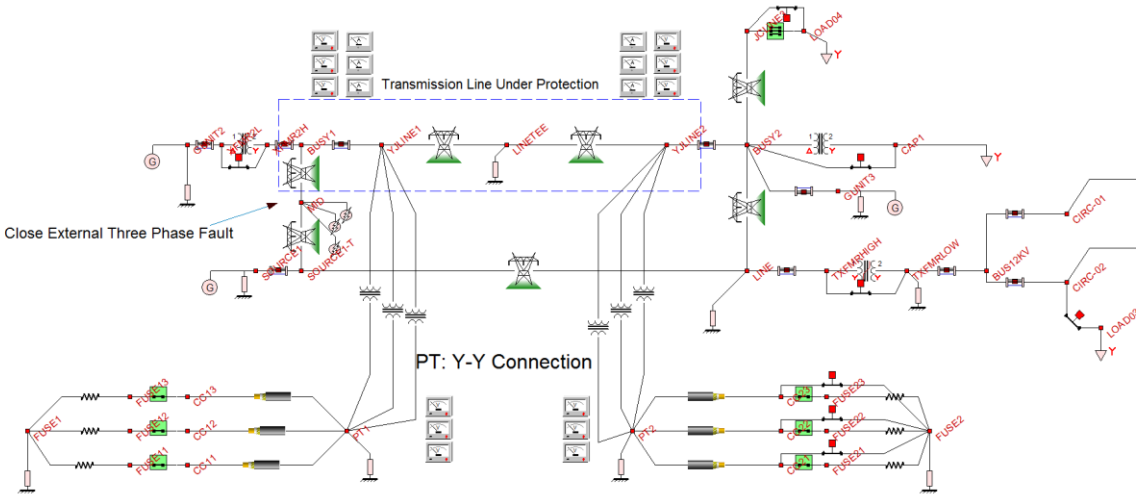

Figure 7-67 Test case for Potential Transformer Error

Figure **7-68** illustrates the voltage measurement for phase A at primary side versus the voltage measurement for phase A at secondary side (on the burden) scaled back to the primary side by ideal transformation. Clearly from this figure, during normal operation there is a biased magnitude error and also a phase shift between the original and the replica. This is caused by the leakage reactance and winding resistance. The zoom-in figure during normal operation and external fault is also included. During transients when the phase A voltage drops immediately, it can also be observed from this figure that while the primary voltage drops immediately, the secondary voltage oscillates for several cycles. This is the transient response, the oscillation is caused by the resonance between leakage reactance and parasitic capacitance at high frequency, such that the potential transformer does not have uniform frequency response. Typically, the resonance is around 1 kHZ. In this case the resonance frequency is computed as 1250Hz.

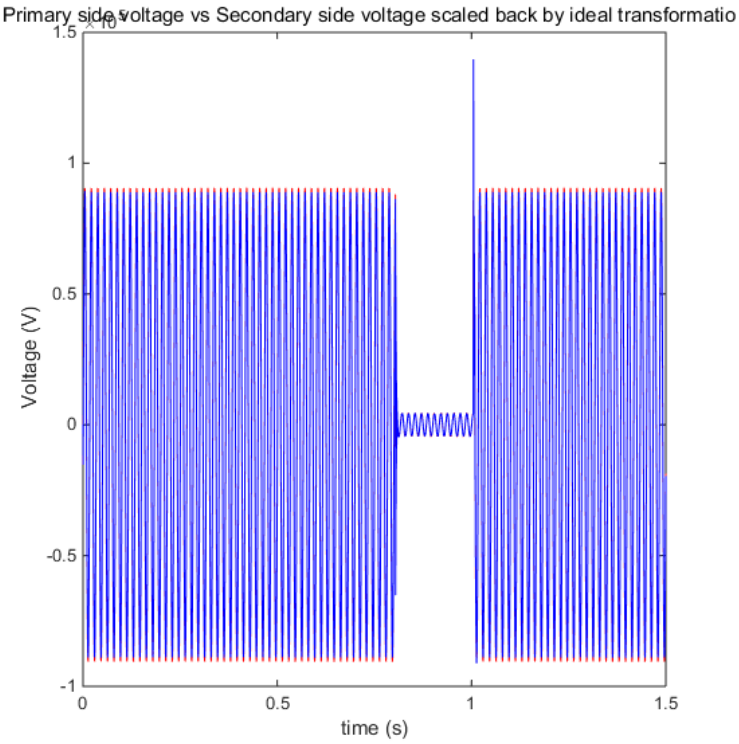

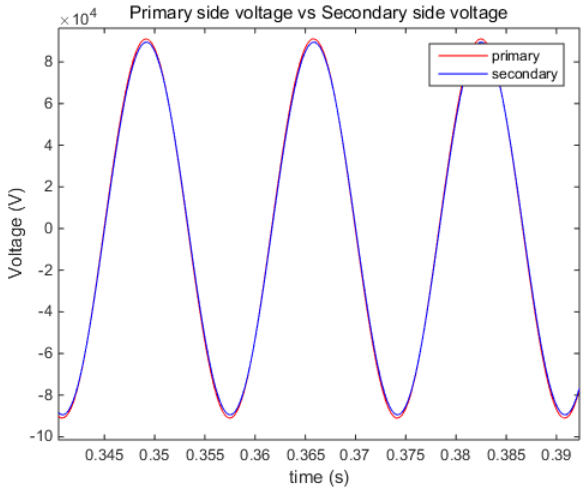

Zoomed in during normal operation

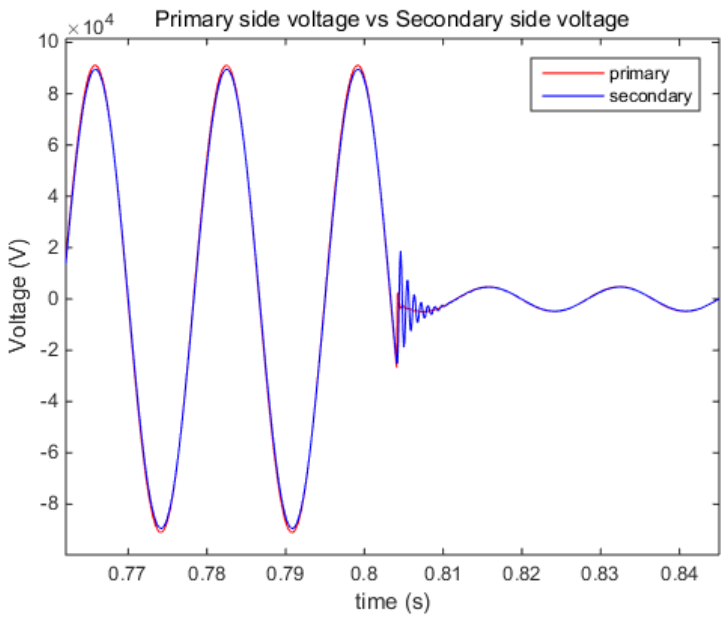

Zoomed in during external fault

Figure 7-68 Primary side voltage versus Secondary side voltage

The DSE based protection results based on the primary side voltage measurements is presented in Figure 7-70 while the DSE based protection results with secondary side voltage scaled back to primary side by ideal transformation, i.e., without ratio correction factor at fundamental frequency is presented in Figure 7-71. Note that the PT error with no ratio correction factor during normal operation does not impact the protection results, and the PT transient response does not impact the protection results as well.

The magnetizing currents for the potential transformer is neglected in this modeling, the equivalent circuit for the potential transformer on the secondary side is illustrated in Figure 7-69.

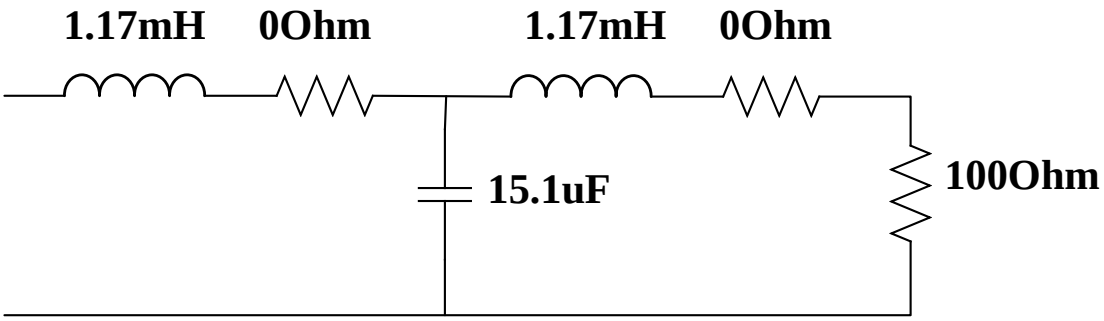

Figure 7-69 Equivalent Circuit for Potential Transformer and Relay Burden

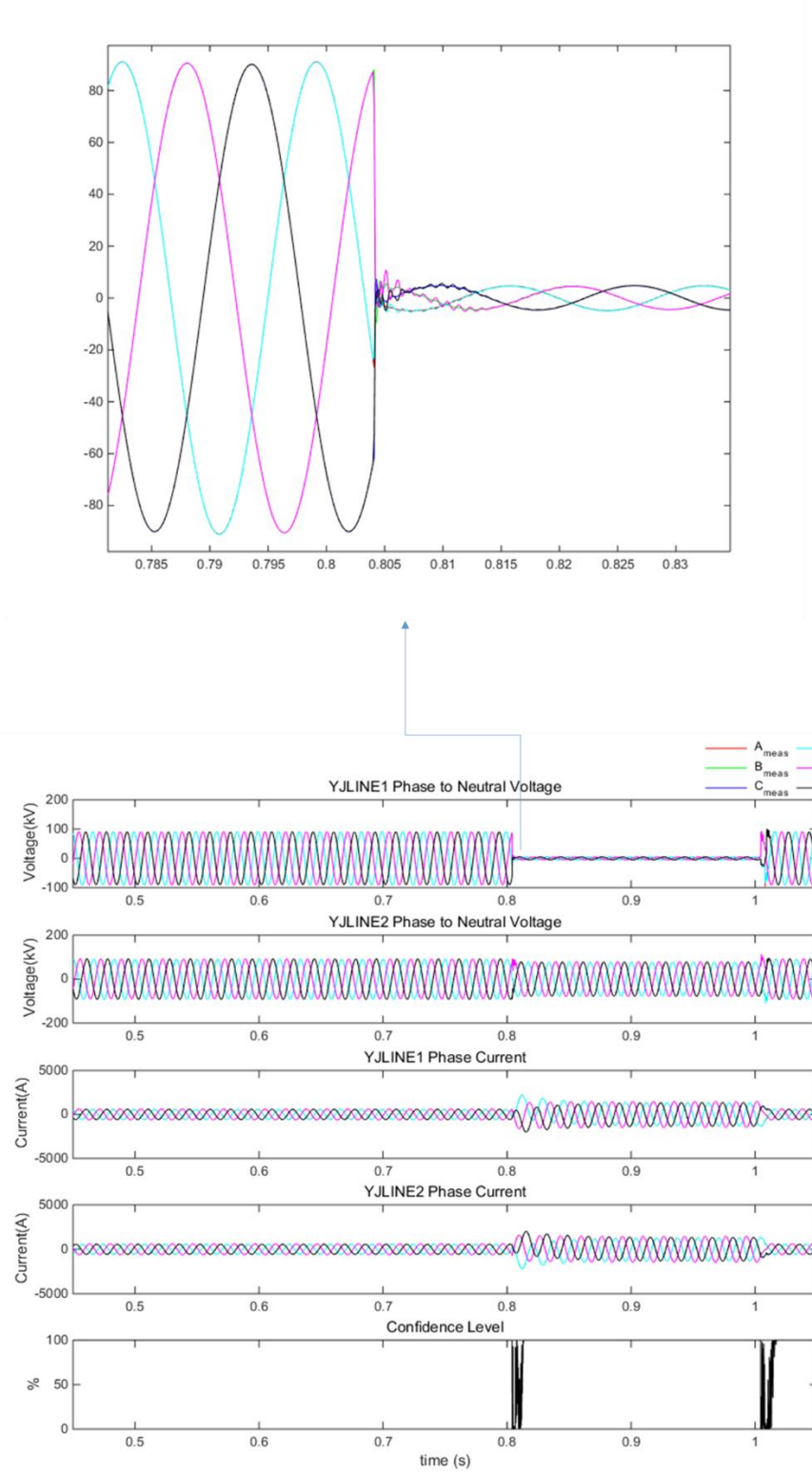
A meas
B meas
C meas
A est
B est
C est
YJLINE1 Phase to Neutral Voltage
Voltage(kV)
YJLINE2 Phase to Neutral Voltage
Voltage(kV)
YJLINE1 Phase Current
Current(A)
YJLINE2 Phase Current
Current(A)
Confidence Level
%
time (s)

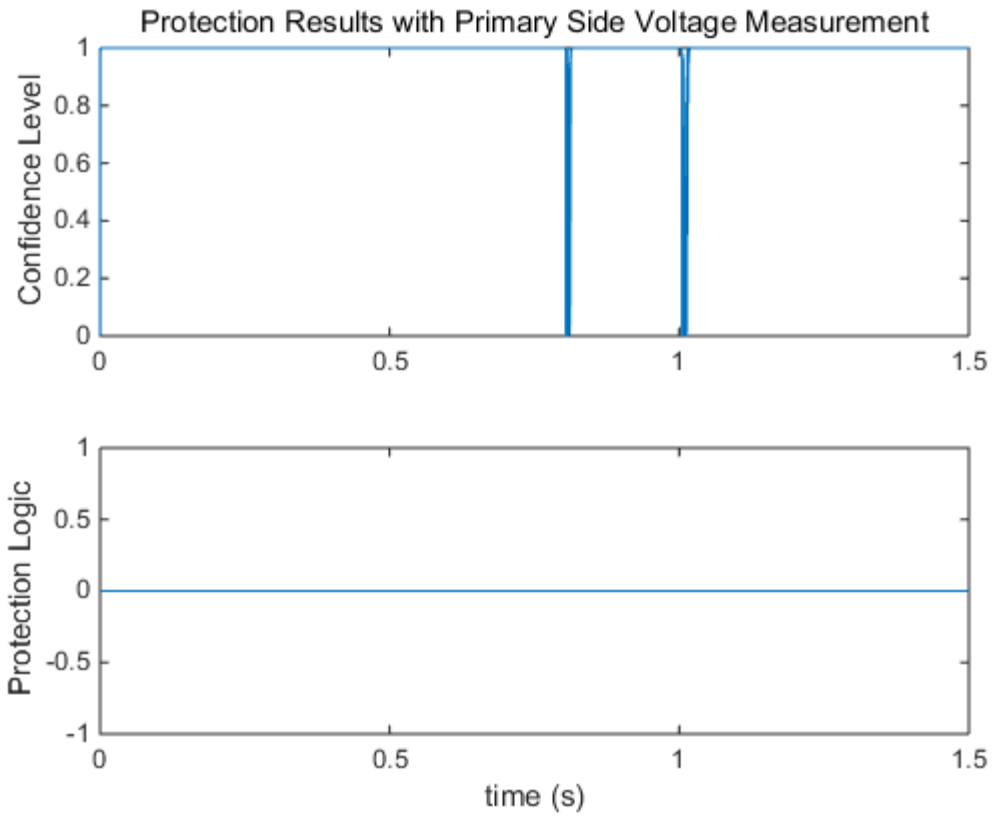

Figure 7-70 DSE based protection with primary side voltage measurements

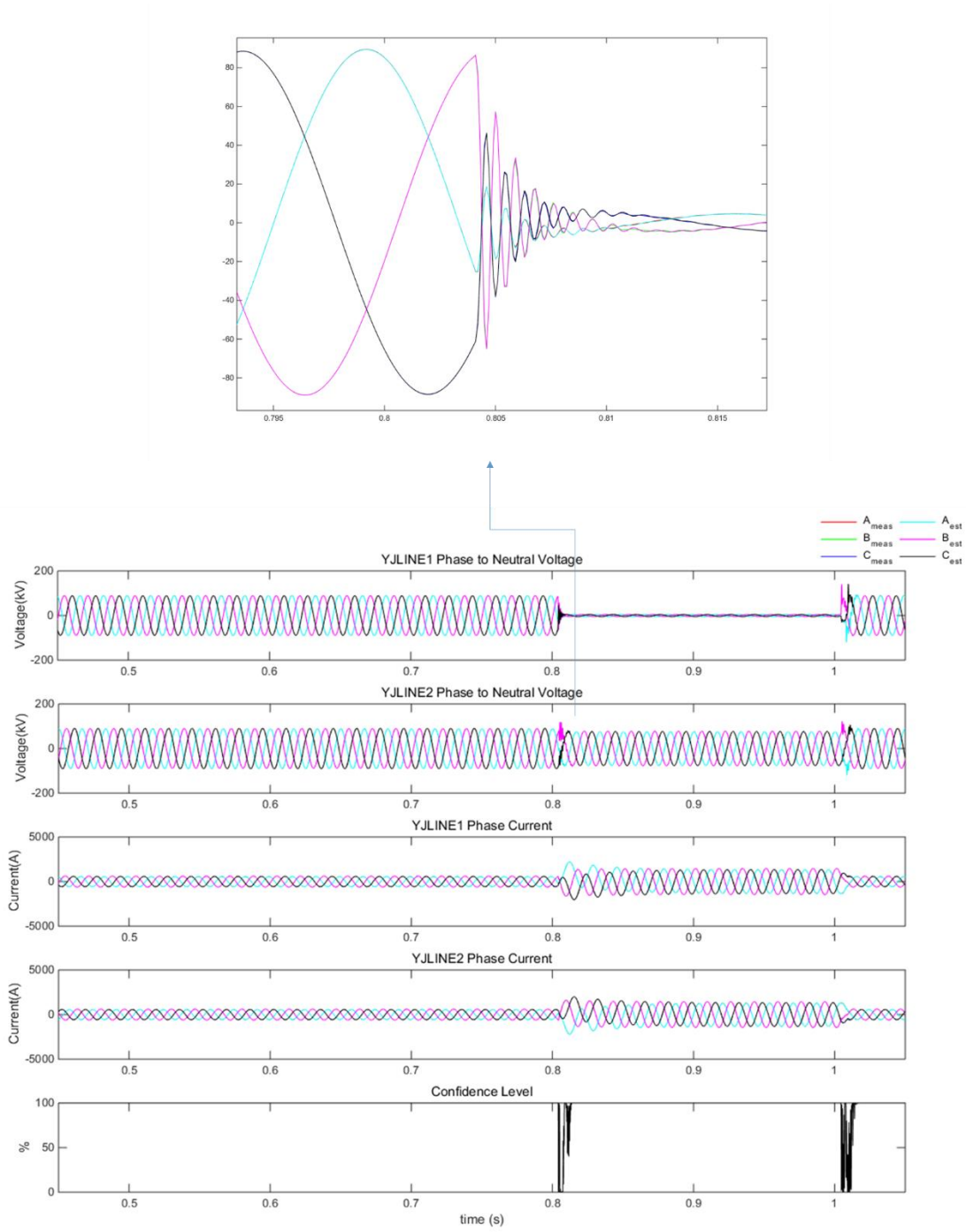
A meas
A est
B meas
B est
C meas
C est
YJLINE1 Phase to Neutral Voltage
Voltage(kV)
YJLINE2 Phase to Neutral Voltage
Voltage(kV)
YJLINE1 Phase Current
Current(A)
YJLINE2 Phase Current
Current(A)
Confidence Level
%
time (s)

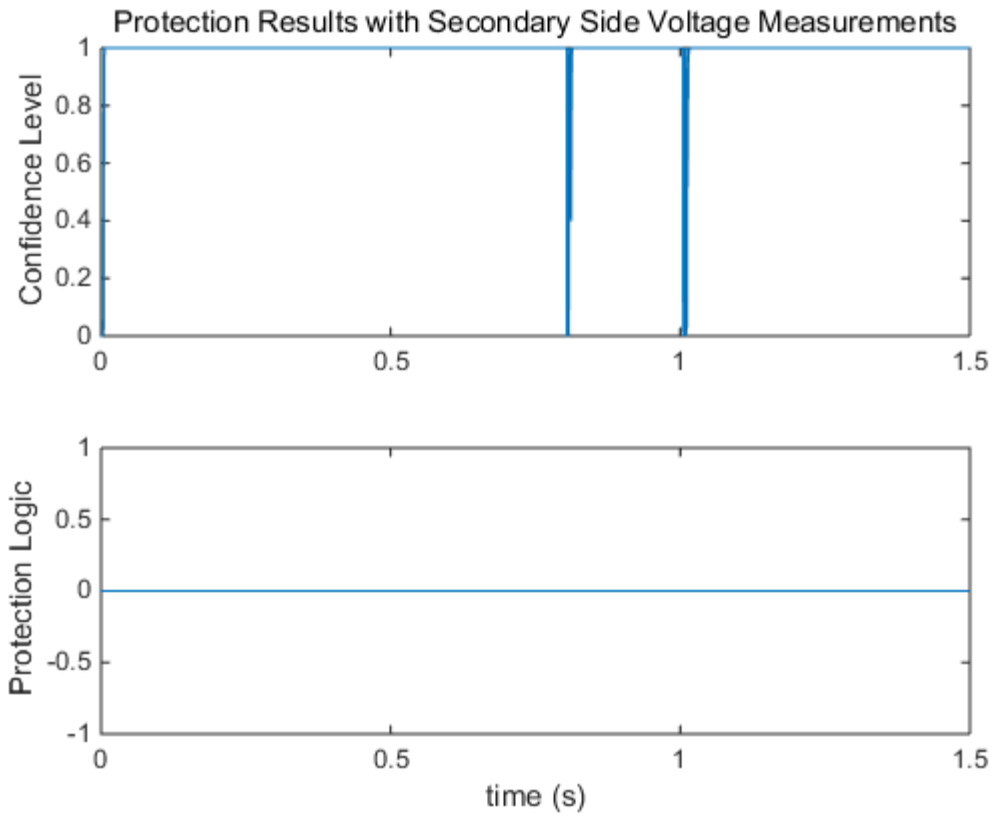

Figure 7-71 DSE based protection result with secondary side voltage measurements

Since the measurement error caused by potential transformer does not impact the estimation results and protection logic significantly, the DSE based protection by modeling the transmission line only is acceptable. It is to be found out that such is not the case for current transformer.

Current Transformer Measurement Error:

In an ideal current transformer, the primary to secondary current ratio is independent of primary current magnitude, frequency, and burden resistor value. However actual devices deviate from this behavior due to several causes, namely: 1) winding resistance, 2)

leakage impedance, 3) magnetizing impedance, 4) core hysteresis and saturation, 5) parasitic capacitance.

The CT magnetic core exhibits a nonlinear relationship between the magnetic field intensity and the magnetic flux density. This results into a nonlinear relationship between the magnetizing current and the flux linkage (or the induced voltage). When saturation occurs, the CT secondary current is severely distorted. When the saturation is associated with an internal fault, the DSE based protection would trip correctly. However, it is to be investigated that when the saturation is associated with an external fault would the DSE based protection behave correctly.

The test system is illustrated in Figure **7-72**. To demonstrate the severe CT saturation, the protection zone is a 1 km line spanning from node YJLINE1 to YJLINE2. The system is working under normal operation until the **Event 1** (and only event) occurs at t=1.2s to t=1.8s as a three phase fault close to bus YJLINE2. The operating current through the line increases from 850 A (loading current) to 26 kA (fault current). This fault is very severe since the line is very short. Only one current transformer is modeled to measure the secondary side current of phase A at left terminal of the protection zone.

The model of the current transformer is illustrated in Figure **7-73**.

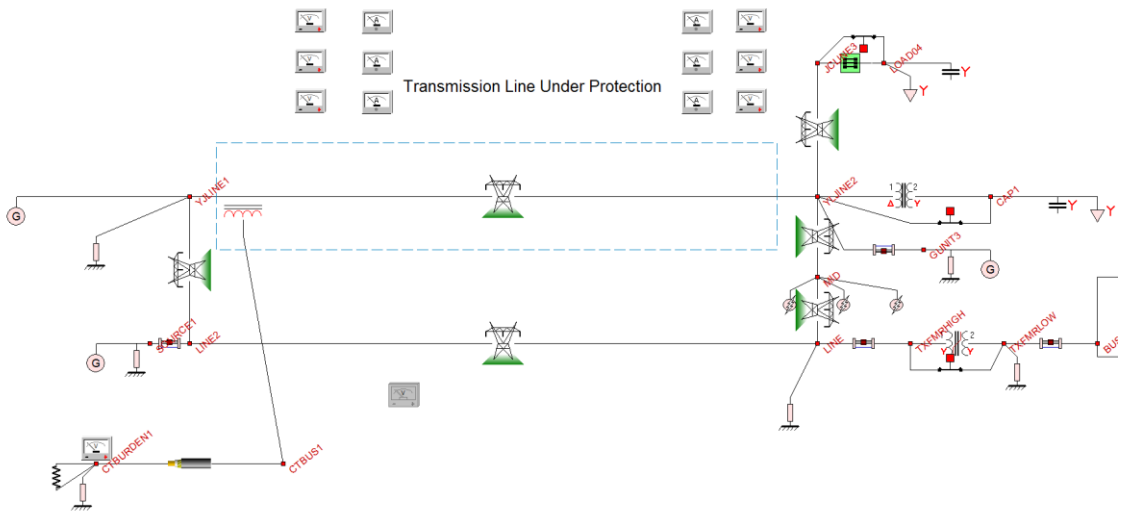

Figure 7-72 Test system for CT Saturation – short line

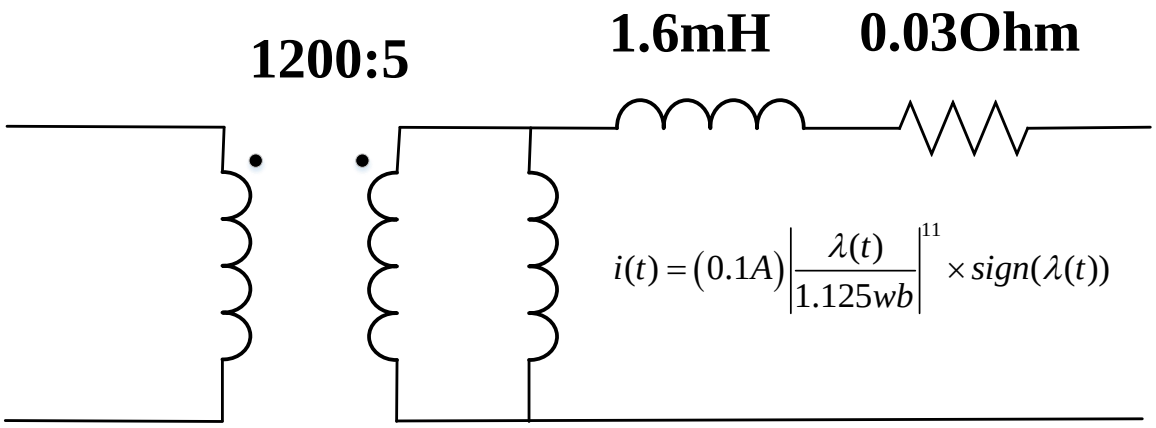

Figure 7-73 Current Transformer equivalent circuit for test case

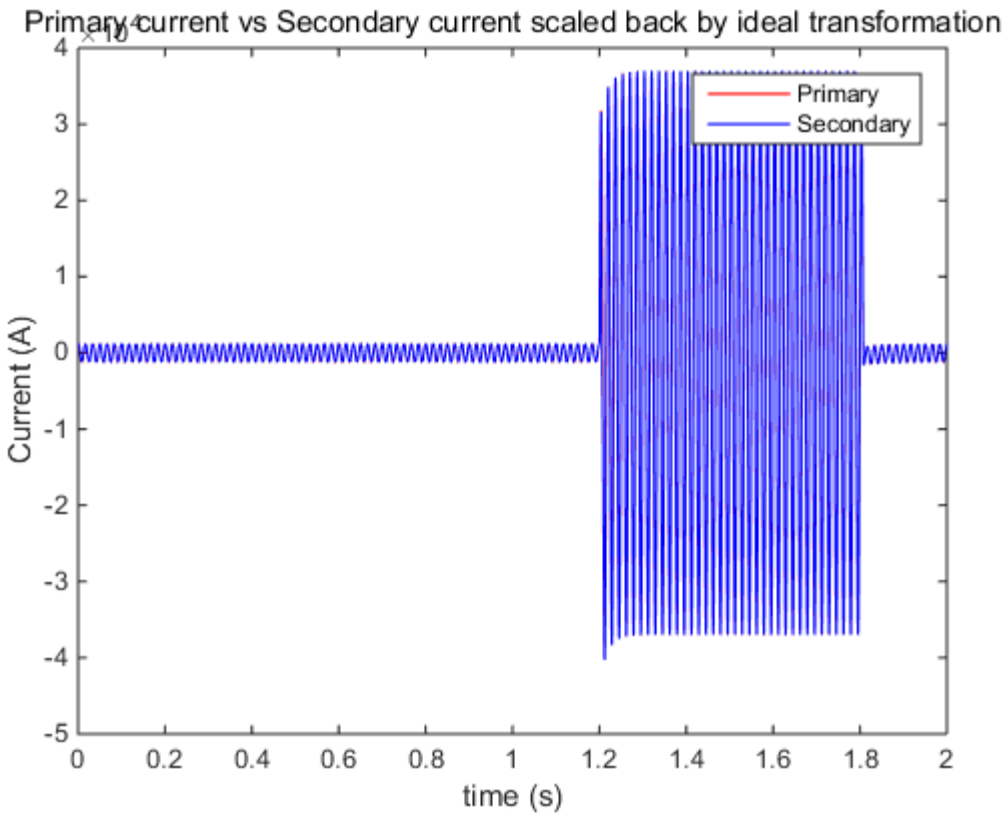

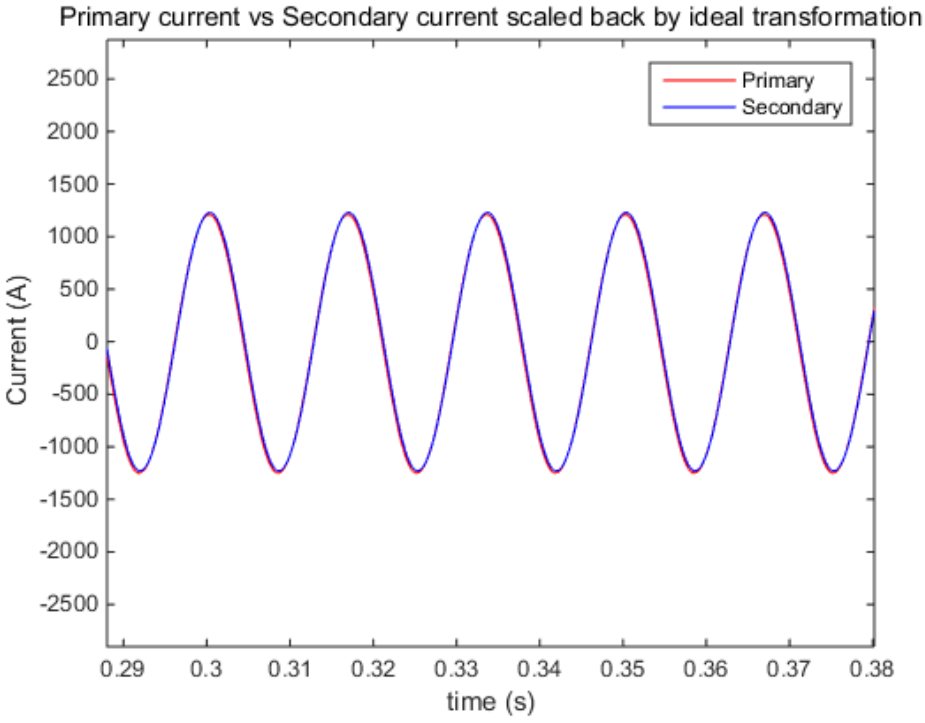

Zoomed in during Normal Operation

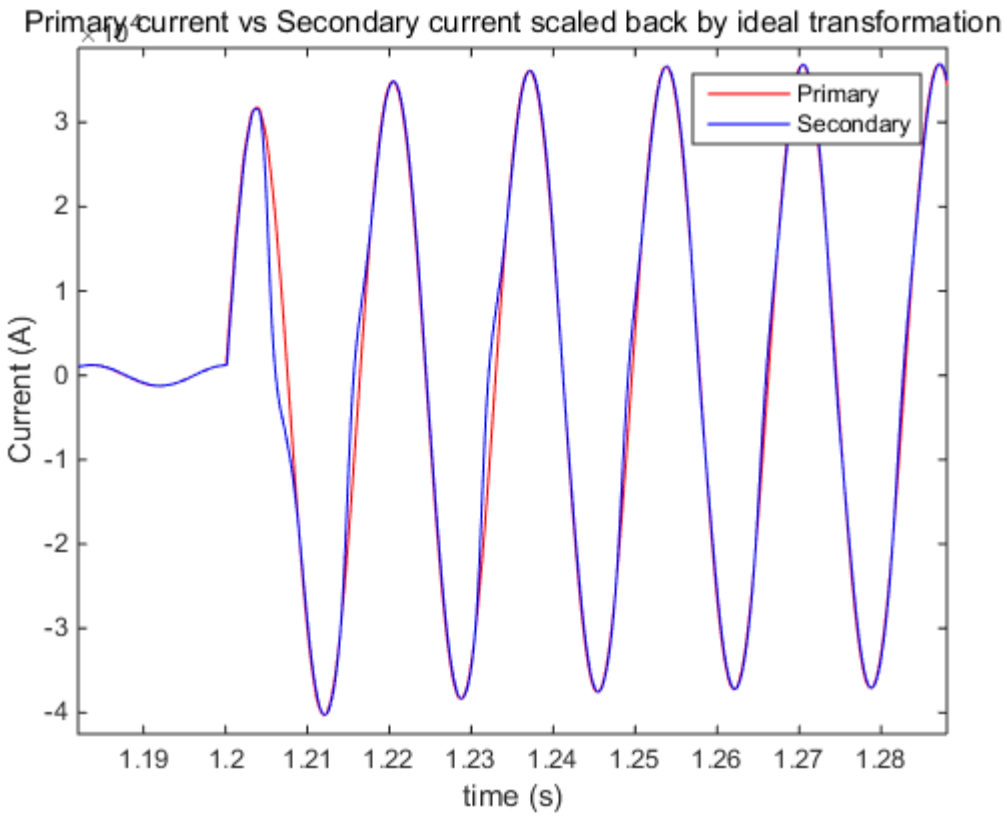

Zoomed in during Event 1

Figure 7-74 Primary Side Current vs Secondary Side Current by ideal transformation

Figure 7-74 illustrates the comparison between the primary side current of phase A and the secondary side current of phase A scaled back by ideal transformation. During normal operation without ratio correction factor there is a phase shift between the two, and the magnitude of both are slightly different. The difference between the two currents are as high as 30A. During external fault the secondary side current is highly distorted and the difference between the two currents increases up to 2000A (10% of the primary current).

The DSE based protection results using either primary side current measurements or secondary side current measurements (by multiplying ideal transformation ratio) are illustrated in Figure **7-75** and Figure **7-76**. The current measurement error is set at 30A. As

can be observed, when the primary side current is used, the protection results are correct. However, when the secondary side current is used, the DSE based protection would mis-operate during a severe external fault. A conclusion is arrived that the DSE based protection is more sensitive to current measurement errors than voltage measurement errors.

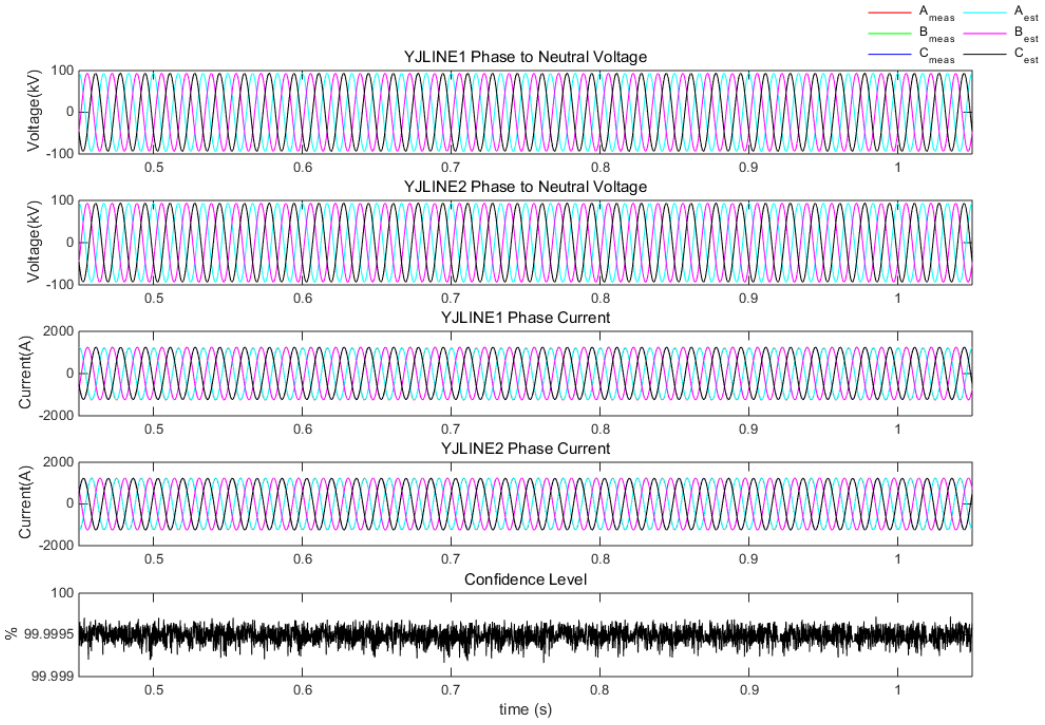

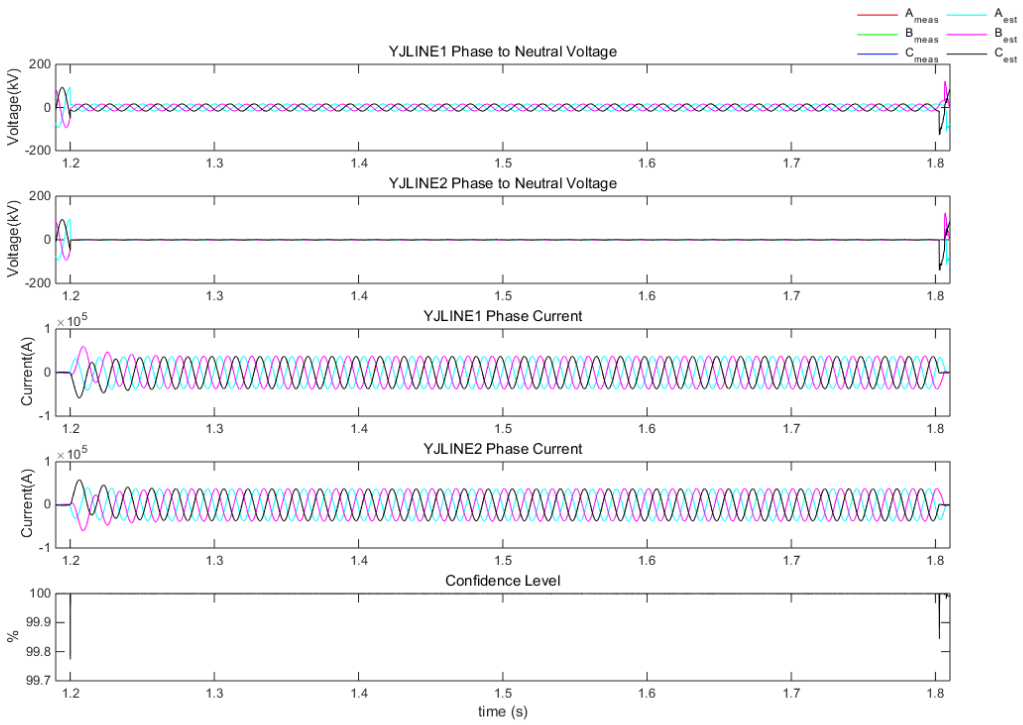

Figure 7-75 DSE based protection results using Primary side current measurements

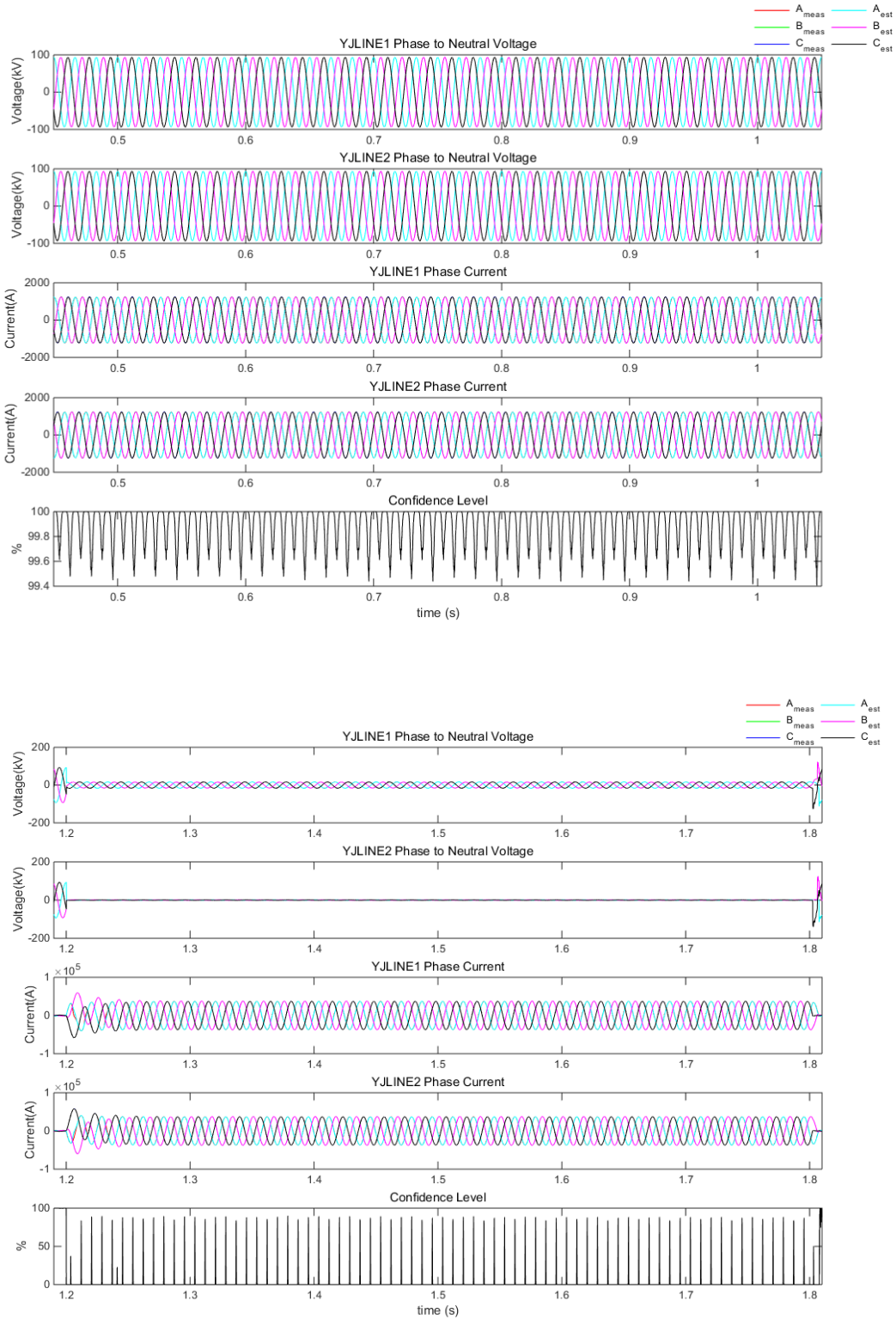

Figure 7-76 DSE based protection results with Secondary side current measurements

To address this issue, one option is to model the transmission line and the current transformer (also the instrumentation channel) together. In this section only a single phase transformer for phase A at YJLINE1 is modeled. See Figure **7-77**. The model is mathematically written in the following way:

$$i_1(t) = C\frac{dv_1(t)}{dt} + i_L(t)$$
$$i_2(t) = C\frac{dv_2(t)}{dt} - i_L(t)$$
$$0 = -v_1(t) + v_2(t) + L\frac{di_L(t)}{dt} + Ri_L(t)$$
$$0 = -\frac{i_{La}(t)}{N} + i_m(t) + i_{Lct}(t)$$
$$0 = \frac{d\lambda(t)}{dt} - e(t)$$
$$0 = (L_w + L_c)\frac{di_{Lct}(t)}{dt} + (r_w + r_c + r_b)i_{Lct}(t) - e(t)$$
$$0 = i_m(t) - i_0\left(\frac{\lambda(t)}{\lambda_0}\right)^n \text{sgn}(\lambda(t))$$

where definitions of R, L ,C, $i_L(t)$, $v_1(t)$, $v_2(t)$ are still the same as in (4.3) for transmission line, and,

$\lambda(t)$: the flux linkage of the current transformer at time t

N : N1/N2 the transformation ratio of the current transformer at time t

$i_m(t)$: magnetizing current of the current transformer at time t

$i_{Lct}(t)$: secondary current of the current transformer that flows through the burden

L_w: leakage reactance

L_c: control cable reactance

r_w: winding resistance

r_c: control cable resistance

r_b: burden resistance

i_0 : magnetizing current constant

λ_0 : flux linkage constant

Sgn: sign function, it's 1 when flux is positive, it's -1 when flux is negative.

n: exponent of the current transformer

Since this model is highly nonlinear because of its relationship between magnetizing current and flux linkage, the quadratization is needed to transform the model into:

$$i_1(t) = C\frac{dv_1(t)}{dt} + i_L(t)$$
$$i_2(t) = C\frac{dv_2(t)}{dt} - i_L(t)$$
$$0 = -v_1(t) + v_2(t) + L\frac{di_L(t)}{dt} + Ri_L(t)$$
$$0 = -\frac{i_{La}(t)}{N} + i_m(t) + i_{Lct}(t)$$
$$0 = \frac{d\lambda(t)}{dt} - e(t)$$
$$0 = (L_w + L_c)\frac{di_{Lct}(t)}{dt} + (r_w + r_c + r_b)i_{Lct}(t) - e(t)$$
$$0 = \frac{1}{\lambda_0}i_m(t)\lambda(t) - y_2(t)y_3(t)$$
$$0 = y_1(t) - \frac{1}{\lambda_0^2}\lambda^2(t)$$
$$0 = y_2(t) - y_1^2(t)$$
$$0 = y_3(t) - y_2^2(t)$$
$$0 = i_m(t) - y_4^2$$

where the states are defined as:

$$x(t) = \begin{bmatrix} v_{a1}(t) \\ v_{b1}(t) \\ v_{c1}(t) \\ v_{n1}(t) \\ v_{a2}(t) \\ v_{b2}(t) \\ v_{c2}(t) \\ v_{n2}(t) \\ i_{La}(t) \\ i_{Lb}(t) \\ i_{Lc}(t) \\ i_{Ln}(t) \\ \lambda(t) \\ e(t) \\ i_{m}(t) \\ i_{Lct}(t) \\ y_1(t) \\ y_2(t) \\ y_3(t) \\ y_4(t) \end{bmatrix}$$

And quadratic integration can be applied to this model to obtain the SCAQCF discretized model.

After the combined model of the transmission line, current transformer (single phase), control cable and burden is built, the DSE based protection can be applied to this model, and the primary current of phase A would not be an actual measurement anymore, instead the secondary voltage on the burden would be an actual measurement. This would not decrease the degree of freedom of the model. There are 40 states (for both time t and time tm), and 52 measurements (for both time t and tm).

The DSE protection results for the same test system is again illustrated in Figure 7-78. During normal operation when there is no CT saturation, the estimated measurements perfectly align with the actual measurements and the confidence level is around 99.99%.

During event 1 external fault the estimated measurements still perfectly align with the actual measurements. Specifically, Figure **7-79** is a comparison between the measured CT secondary voltage and estimated CT secondary voltage, observe the saturated effect here, and also the estimated voltage has no difference with the measured voltage.

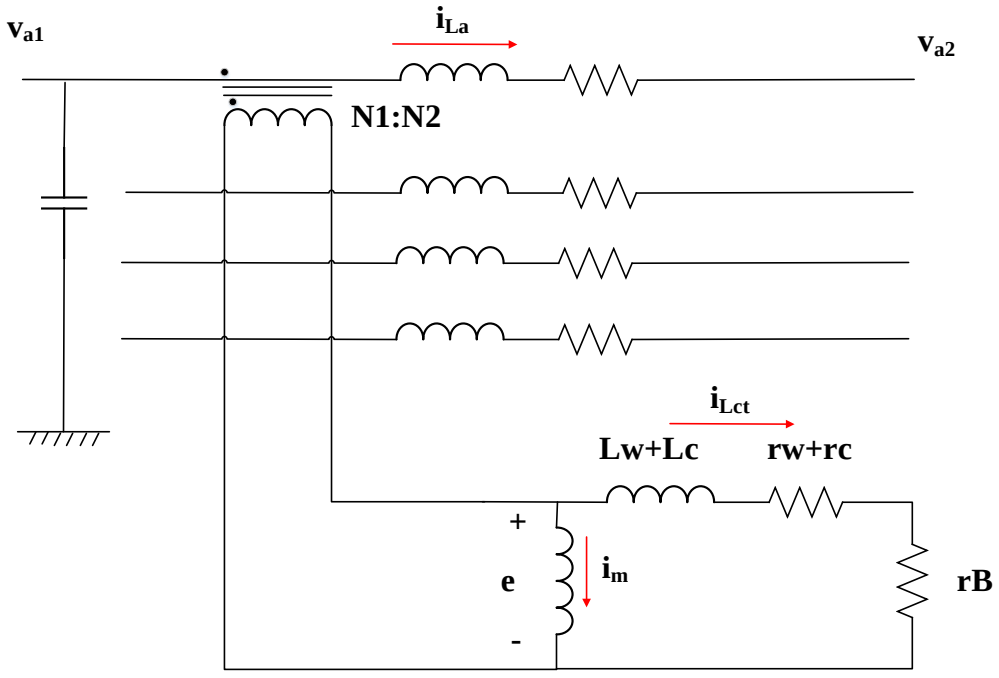

Figure 7-77 Modeling of transmission line, current transformer, and instrumentation channel for CT saturation analysis

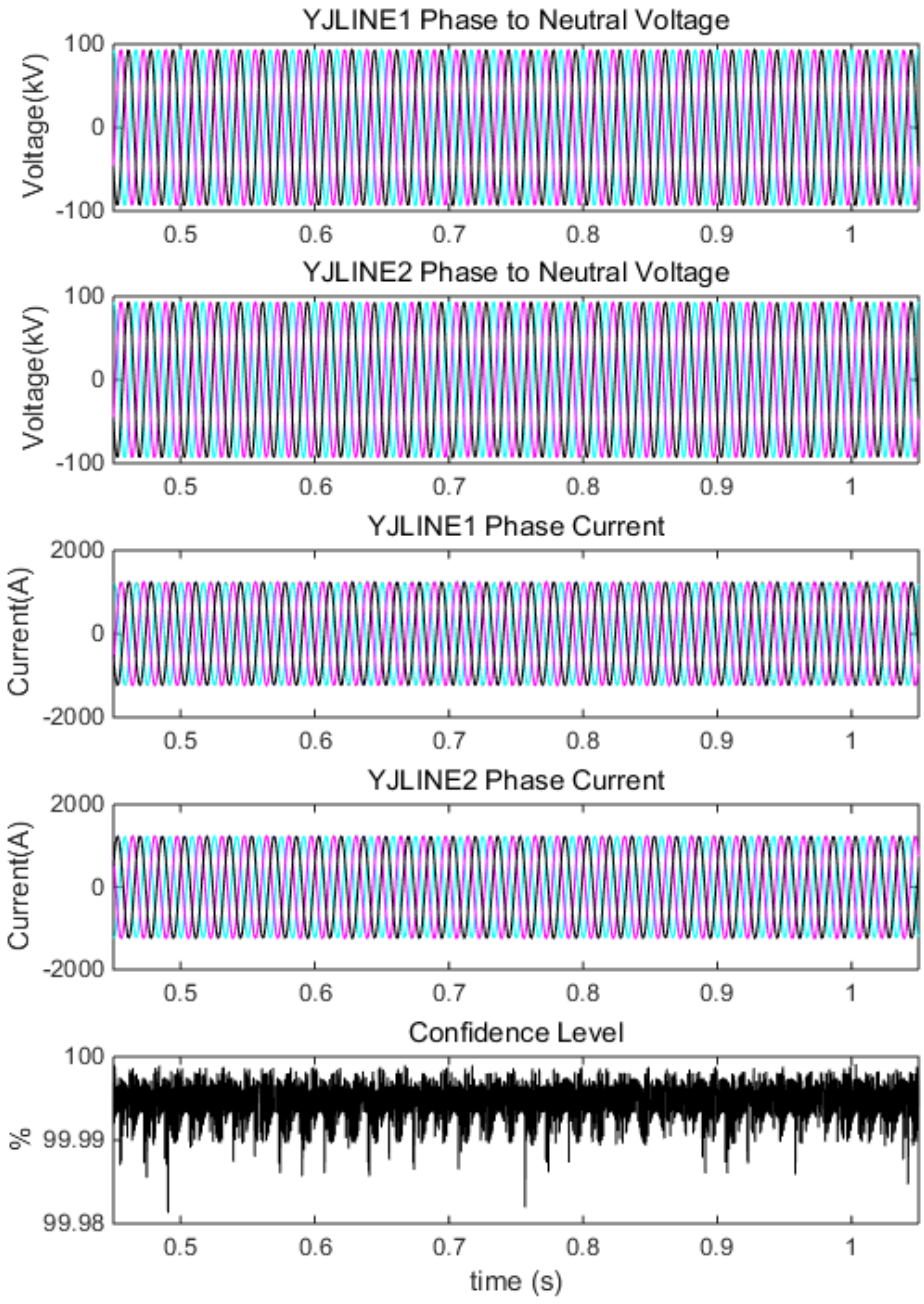

Normal Operation

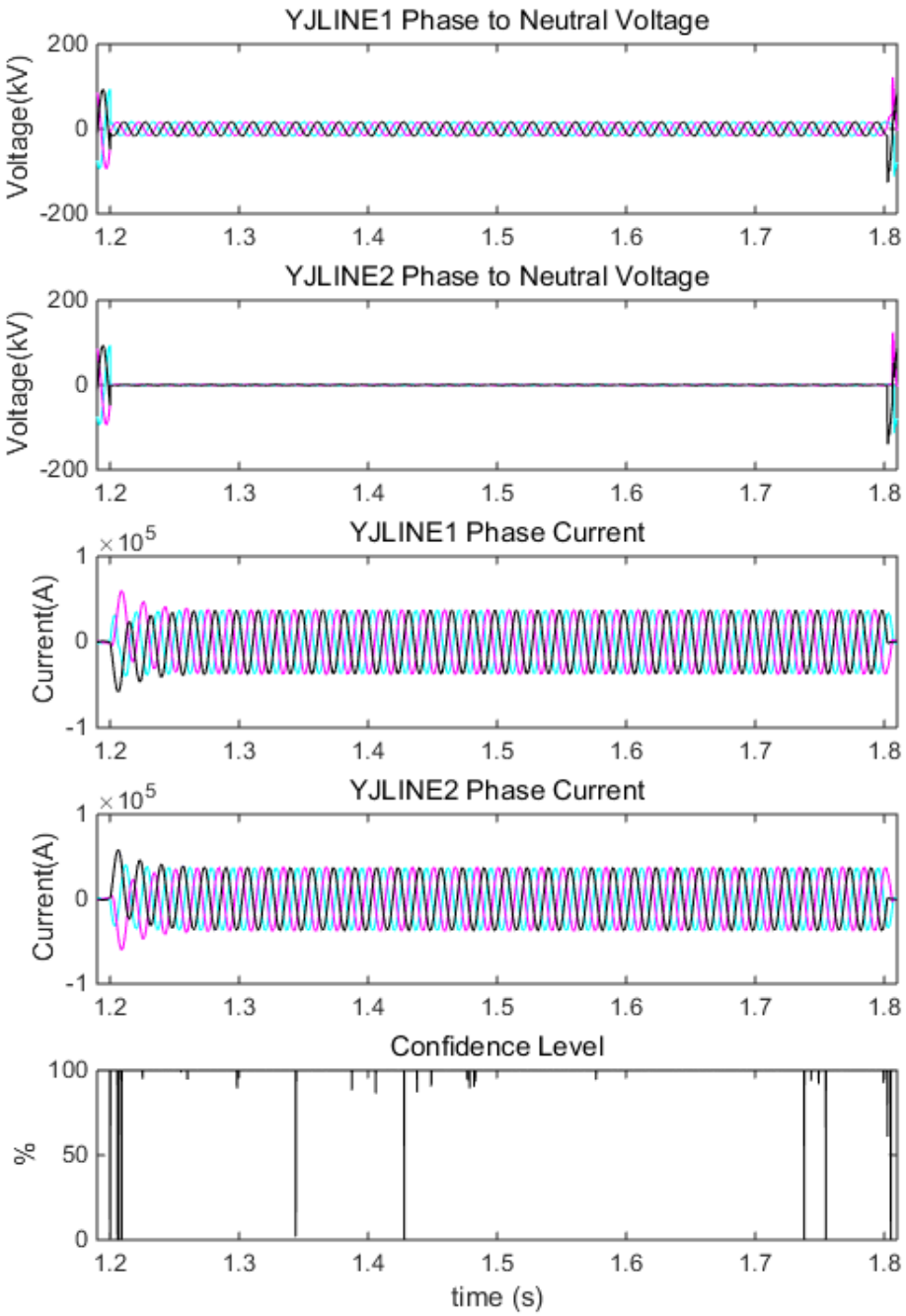

External Fault

Figure 7-78 DSE based protection results by modeling both the transmission line and instrumentation channel

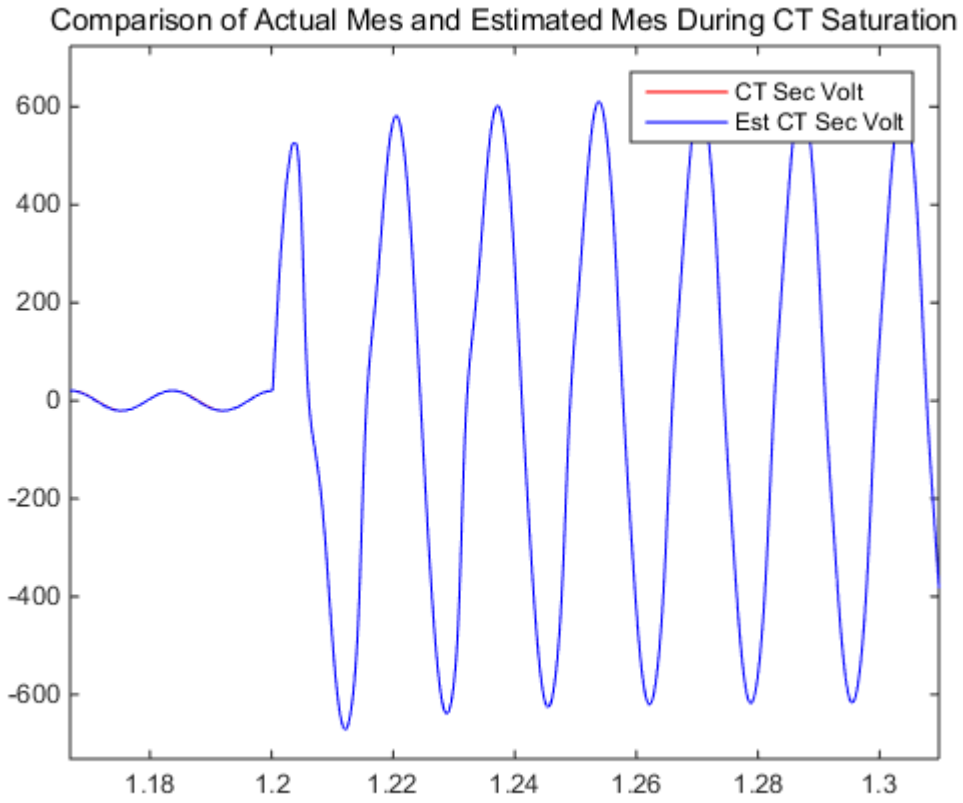

Figure 7-79 Comparison of saturated CT secondary voltage and estimated CT secondary voltage

7.11 Summary

This chapter started with comparing the three different dynamic state estimation algorithms, then it provided two test cases to compare the performance of legacy protection algorithms with proposed algorithm in terms of security, dependability and sensitivity. It also explored the disadvantages from each individual protection algorithm. Finally, it investigated the modeling error, synchronization error and instrumentation error that would affect the performance of the algorithm.

CHAPTER 8 CONCLUSION AND FUTURE WORK DIRECTION

8.1 Conclusions

The main advantage of the DSE based protection with respect to the combination of the legacy protections is its sensitivity during high impedance fault when the fault current is small compared to the load current, and its security during close external fault when the directional element could be easily compromised. The DSE based protection was compared with legacy protection functions. The conclusions are: 1) the DSE based protection can distinguish an internal fault with an external fault while the directional instantaneous overcurrent protection cannot in a short line case (Section 7.5.1), 2) the DSE based protection can distinguish an internal fault with a heavy load while the directional time overcurrent protection cannot in a long line case (Section 7.6.1), 3) the DSE based protection is insensitive to induced voltage while the stepped distance protection may see the fault in another zone (see Section 7.7.1), 4) the DSE based protection is insensitive to the status of the series compensated capacitor while the stepped distance protection may see the fault in another quadrant (see Section 7.7.2), 5) the DSE based protection would not mis-operate when there is a sequential tripping on parallel line while the pilot protection would mis-operate when the fault current reverses its direction (see Section 7.8.1), 6) the DSE based protection is more sensitive on high impedance fault than current differential (see Section 7.9.1), 7) the DSE based protection would not be affected by current inversion problems while the current differential would see it as through current instead of internal fault (see Section 7.9.2).

The performance of the three dynamic state estimation algorithms is investigated in Section 7.2 by comparing the diagonal elements of the covariance matrices and by comparing the estimation results during normal operation. It can be seen that all three algorithms perform well and there is no one algorithm that outperforms other algorithms significantly.

Practical implementation issues were partially investigated. Some of these issues are: 1) modeling error: it can be seen that the protection results would only be compromised when the modeling error for inductance matrix is over 20%, and as a matter of fact this also means that using confidence level as an indicator for modeling error would not be proper if high accuracy for parameter is required (see Section 7.10.1), 2) synchronization error: it can be seen that the protection results would only be compromised when the sync error exceeds 5 microseconds, while IRIG-B usually provides 1 microsecond accuracy (see Section 7.10.2), 3) measurement error from potential transformer does not impact the protection results significantly, while measurement error from current transformer does impact the protection results significantly during CT saturation. However, if both line and CT is modeled then the estimated measurements can track the actual measurement perfectly (see Section 7.10.3).

8.2 Contributions

The main contributions of this dissertation are: 1) proposed a new protection algorithm for transmission lines to avoid settings and coordination errors, and to fulfill several protection gaps [47], [56], 2) proposed the infrastructure for data acquisition systems for

the dynamic state estimation based relay [48], 3) developed object-oriented model for transmission line, applied and investigated several dynamic state estimation algorithms performance for the proposed method, 4) demonstrated the advantage of the proposed method with respect to legacy protection methods in numerous cases, and 5) investigated practical issues for the application of the proposed method.

8.3 Future Work Directions

Fault diagnosis in transmission lines is a complex task. Meanwhile fault detection is only part of it. This thesis is focused on the fault detection for transmission lines. Other than that, the fault diagnosis also should include bad data, fault identification, fault location, and fault resistance estimation. Modern protective relays often include the functionality of single-pole-tripping, to trip only the faulted phase while maintaining the operation of the un-faulted phase. This can only be realized when the fault identification method is also included. Modern protective relays also include the functionality of fault location, to send out crews to the faulted scene. However currently this can only be achieved when the fault resistance is very small. Lastly the loss of potential for the potential transformer would make the voltage measurement be zero values, the impact to the DSE based protection should also be investigated.

APPENDICES

Appendix A: The General Physically Based Transmission Line Model

This section is heavily referred from "Power System Grounding and Transients: An Introduction" by Dr. A. P. Meliopoulos. In this appendix the general physically based transmission line model that provides the basis for all other simplified version (including the single section and multi section model used in this thesis for protection purpose) is described. Figure A.1 illustrates a three-phase transmission line. It comprises of five paths of electric current flow: the three phase conductors, shield or neutral conductors, and the earth.

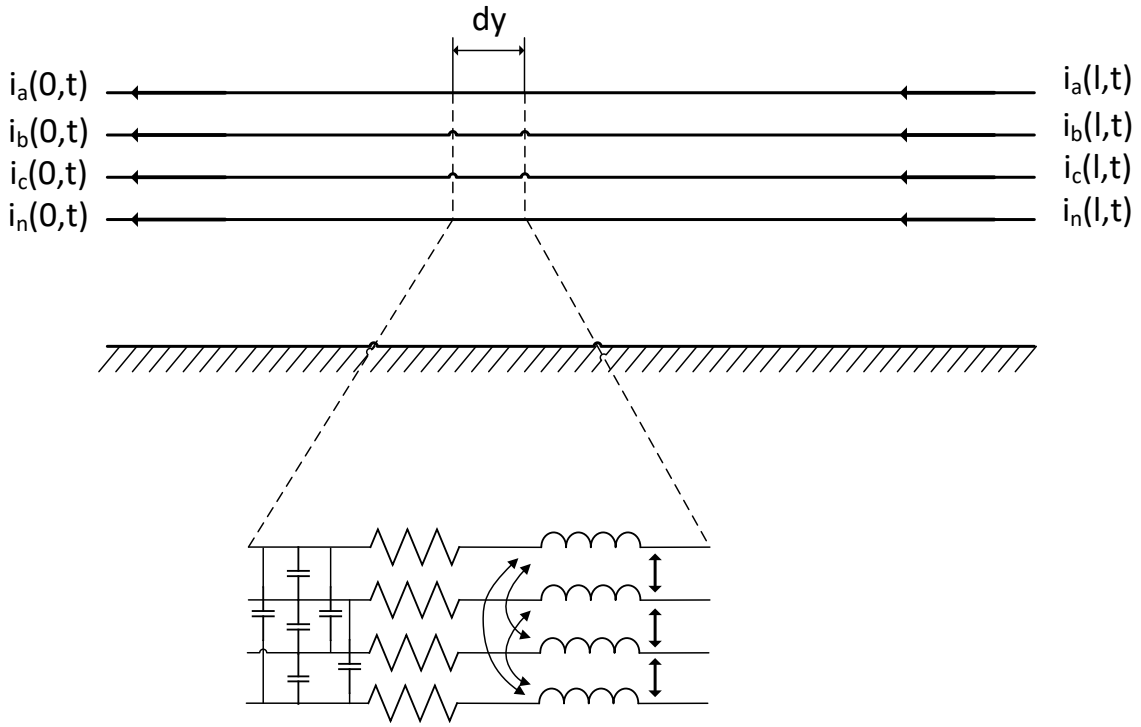

FigureA.1. The general transmission line model.

Each conductor i is characterized with a series self-resistance r_{ii}, series mutual resistance to any other conductor j r_{ij}, series self-inductance L_{iie}, series mutual inductance

to any conductor j L_{ije}, self capacitance C_{ii}, and mutual capacitance to any other conductor j C_{ij}. The series self and mutual resistance and inductance can be computed using Carson's method or approximate solutions. According to [50], the series parameters for R and L are:

$$r_{ii} = r_i + r_e$$
$$r_{ij} = r_e$$
$$L_{iie} = \frac{\mu}{2\pi} \ln \frac{D_e}{D_i}$$
$$L_{ije} = \frac{\mu}{2\pi} \ln \frac{D_e}{D_{ij}}$$

where

$$r_e = \frac{w\mu}{8}$$

r_i: conductor i resistance, ohms per meter

d_i: conductor i geometric mean radius

D_e: $2160\sqrt{\rho / f}$

ρ : soil resistivity

f: frequency of currents

D_{ij} : distance between conductors i and j

The self and mutual capacitances are computed according to [50] as:

$$C' = \begin{bmatrix} C'_{aa} & C'_{ab} & C'_{ac} & C'_{an} \\ C'_{ba} & C'_{bb} & C'_{bc} & C'_{bn} \\ C'_{ca} & C'_{cb} & C'_{cc} & C'_{cn} \\ C'_{na} & C'_{nb} & C'_{nc} & C'_{nn} \end{bmatrix}$$

where

$$C'_{ij} = -\frac{1}{2\pi\varepsilon}\ln\frac{D_{ij}}{D_{ij'}}$$

D'_{ij} : distance between conductor i and image of conductor j with respect to ground

Then the matrix C' is inverted to get the capacitance matrix C.

Here R, L and C are per length.

Assume there is self and mutual conductance between the phase conductors. Thus the KVL and KCL for Figure A.1 gives:

$$\frac{\partial v(y,t)}{\partial y} = Ri(y,t) + L\frac{\partial i(y,t)}{\partial t}$$

$$\frac{\partial i(y,t)}{\partial y} = Gv(y,t) + C\frac{\partial v(y,t)}{\partial t}$$

The coupled first order differential equations are then translated into second-order decoupled differential equations:

$$\frac{\partial^2 i(y,t)}{\partial y^2} = CL\frac{\partial^2 i(y,t)}{\partial t^2} + (GL + CR)\frac{\partial i(y,t)}{\partial t} + GRi(y,t)$$

$$\frac{\partial^2 v(y,t)}{\partial y^2} = LC\frac{\partial^2 v(y,t)}{\partial t^2} + (LG + RC)\frac{\partial v(y,t)}{\partial t} + RGv(y,t)$$

Solutions to the partial differential equations are mostly numerical. In order to obtain a graphical understanding of the general model, an equivalent circuit must be presented.

Consider the sinusoidal steady state where currents and voltages are in phasors, the problem becomes

$$\frac{d^2\tilde{V}(y)}{dy^2} = (R + jwL)(G + jwC)\tilde{V}(y)$$

$$\frac{d\tilde{V}(y)}{dy} = (R + jwL)\tilde{I}(y)$$

By decomposition of the above equation into sequence networks, the solutions for sequence quantities are:

$$\begin{bmatrix} \tilde{V}_{s1} \\ \tilde{I}_{s1} \end{bmatrix} = \begin{bmatrix} \cosh(p_1 l) & Z_1 \sinh(p_1 l) \\ \frac{1}{Z_1}\sinh(p_1 h) & \cosh(p_1 l) \end{bmatrix} \begin{bmatrix} \tilde{V}_{R1} \\ \tilde{I}_{R1} \end{bmatrix}$$

$$\begin{bmatrix} \tilde{V}_{s2} \\ \tilde{I}_{s2} \end{bmatrix} = \begin{bmatrix} \cosh(p_2 l) & Z_1 \sinh(p_2 l) \\ \frac{1}{Z_2}\sinh(p_2 h) & \cosh(p_2 l) \end{bmatrix} \begin{bmatrix} \tilde{V}_{R2} \\ \tilde{I}_{R2} \end{bmatrix}$$

$$\begin{bmatrix} \tilde{V}_{s0} \\ \tilde{I}_{s0} \end{bmatrix} = \begin{bmatrix} \cosh(p_0 l) & Z_1 \sinh(p_0 l) \\ \frac{1}{Z_0}\sinh(p_0 h) & \cosh(p_0 l) \end{bmatrix} \begin{bmatrix} \tilde{V}_{R0} \\ \tilde{I}_{R0} \end{bmatrix}$$

where:

p_1: propagation constant for positive sequence network

Z_1: characteristic impedance for positive sequence network

p_2: propagation constant for negative sequence network

Z_2: characteristic impedance for negative sequence network

p_0: propagation constant for zero sequence network

Z_0: characteristic impedance for zero sequence network

The analytical solution is equivalent to the following circuit:

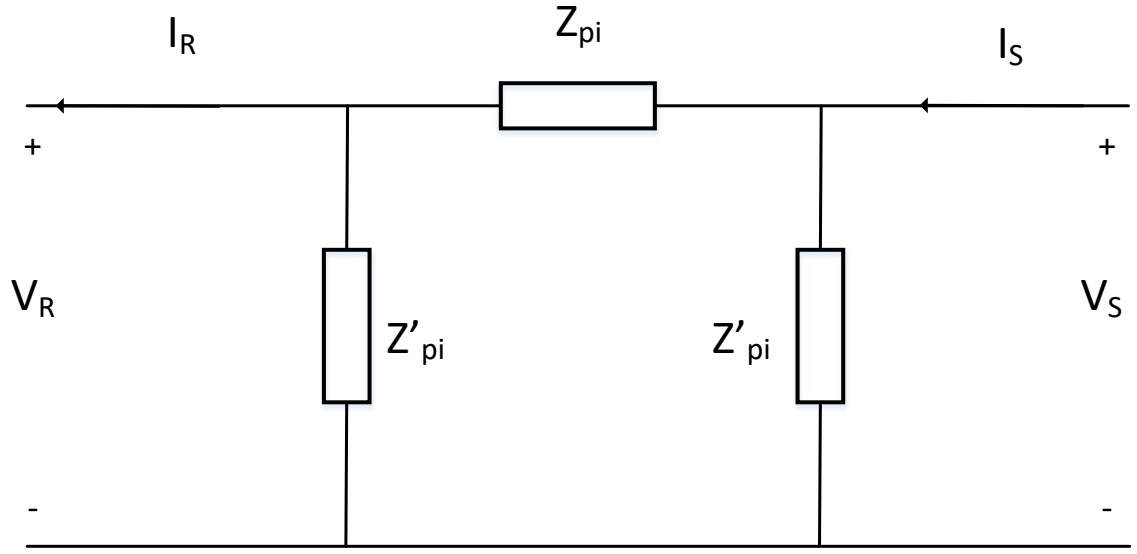

Figure A.2 Transmission Line Equivalent Circuit – Sequence Network

where,

$$Z_{\pi} = Z_0 \sinh(pl)$$

$$Z_{\pi}^{'} = \frac{Z_0 \sinh(pl)}{\cosh(pl) - 1}$$

When the transmission line is short, i.e., pl is much smaller than 1.0, the above quantities are approximate:

$$Z_{\pi} = Z_0 \sinh(pl) = \sqrt{\frac{(R + jwL)}{(G + jwC)}} \frac{e^{\sqrt{(R+jwL)(G+jwC)}l} - e^{-\sqrt{(R+jwL)(G+jwC)}l}}{2} \approx \sqrt{\frac{(R + jwL)}{(G + jwC)}} \sqrt{(R + jwL)(G + jwC)}l = (R + jwL)l$$

$$Z_{\pi}^{'} = \frac{\sqrt{\frac{R + jwL}{G + jwC}} \frac{e^{\sqrt{(R+jwL)(G+jwC)}l} - e^{-\sqrt{(R+jwL)(G+jwC)}l}}{2}}{\frac{e^{\sqrt{(R+jwL)(G+jwC)}l} + e^{-\sqrt{(R+jwL)(G+jwC)}l}}{2} - 1} \approx \sqrt{\frac{R + jwL}{G + jwC}} \frac{\sqrt{(R+jwL)(G+jwC)}l}{\left(\sqrt{(R+jwL)(G+jwC)}l\right)^2} = \frac{1}{(G + jwC)l}$$

Which means that the equivalent circuit series parameters are proportional to the length with the resistance or inductance per length, and the shunt parameters are reversely proportional to the length with the capacitance per length, regardless of the frequency.

The above simplification provides basis for the single section modeling.

Appendix B: Example for Computed Chi Square Value in Fault Condition

Even though the DSE based protection allows fast fault detection in only 2 or 3 samples, the confidence level in a single time step cannot be used as indicator for the protection logic, i.e., it is not appropriate to issue trip command based on one single confidence level at a certain time step. There are several reasons: 1) during external fault or transients, the confidence level may also drop temporarily since the quadratic integration may not be able to track a sudden voltage or current change, 2) during internal fault the confidence level may oscillates if the fault is very small, 3) the measurement noise at a certain sample may be large to cause a low confidence level.

In this appendix an example is provided to illustrate the second point, it provides the analytical form of the chi square value when the device under protection has an internal fault, and investigate the behavior of the computed chi square value under the fault. Assume the device under protection is a pure resistor and the measurements are the across voltage and the through current:

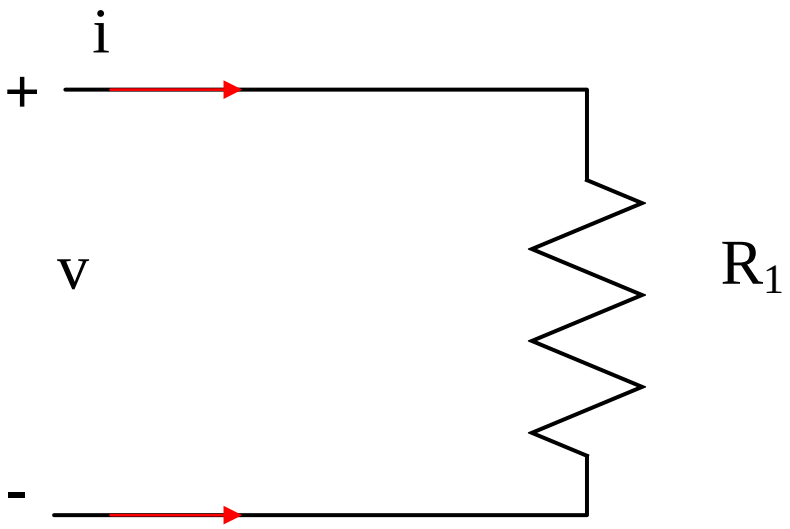

The state is defined as the current through the resistor. This is the simplest device under protection. The measurement model is as follow:

$$z(t) = Hx(t)$$

Where,

$$z(t) = \begin{bmatrix} v(t) \\ i(t) \end{bmatrix}$$

$$x(t) = i(t)$$

$$H = \begin{bmatrix} R_1 \\ 1 \end{bmatrix}$$

$$W = \begin{bmatrix} \frac{1}{\sigma_v^2} & 0 \\ 0 & \frac{1}{\sigma_i^2} \end{bmatrix}$$

The standard deviations for the voltage and current are defined as σ_v and σ_i. The estimate state at each time step can be computed directly by:

$$\hat{x}(t) = \left(H^T W H\right)^{-1} H^T W z(t)$$

If during an internal fault, the resistance changes from R1 to R2, then

If somehow there is a fault and the resistance changes from R1 to R2, and assume that the current measurement through the resistor at time t is i(t), the voltage measurement across the resistor at time t is v(t)=R2*i(t), i.e., there is no measurement error. Or,

$$z(t) = \begin{bmatrix} i(t) \\ R_2 i(t) \end{bmatrix}$$

Then the estimated state x(t) at time t is:

$$\hat{x}(t) = \left(H^T W H\right)^{-1} H^T W \times z(t) = i(t) * \frac{\sigma_i^2 + R_1 R_2 \sigma_v^2}{\sigma_i^2 + R_1^2 \sigma_v^2}$$

The estimated measurement z(t) at time t is:

$$\hat{z}(t) = H\hat{x}(t) = \begin{bmatrix} R_1 i(t) * \frac{\sigma_i^2 + R_1 R_2 \sigma_v^2}{\sigma_i^2 + R_1^2 \sigma_v^2} \\ i(t) * \frac{\sigma_i^2 + R_1 R_2 \sigma_v^2}{\sigma_i^2 + R_1^2 \sigma_v^2} \end{bmatrix}$$

The residual is computed as the difference between the actual measurement and the estimated measurement:

$$r(t) = \hat{z}(t) - z(t) = \begin{bmatrix} i(t) \frac{\sigma_i^2 (R_1 - R_2)}{\sigma_i^2 + R_1^2 \sigma_v^2} \\ i(t) \frac{\sigma_v^2 R_1 (R_2 - R_1)}{\sigma_i^2 + R_1^2 \sigma_v^2} \end{bmatrix}$$

And the chi square value is:

$$chi(t) = r(t)^T W r(t) = \frac{\sigma_i^2 \sigma_v^2 (R_2 - R_1)^2}{\sigma_i^2 + R_1^2 \sigma_v^2} i^2(t)$$

The analytical form of the chi square value shows that it is always larger than or equal to 0, however it would be a periodic wave when a fault occurs (when R2=R1 this value is always 0) with the minimum value being 0, and the frequency of the chi square value is double of the fundamental frequency of the power system. If the protection logic relies on only the current computed chi square value, then the protection logic would be 1 (trip)

when the periodic chi square value is larger than a threshold, and 0 (not to trip) when the periodic chi square value is less than a threshold. Specifically, when the chi square value is 0 (every half cycle of the power system frequency) the confidence level would be 100%. In order to prevent that, this thesis computes the average confidence level and the protection logic is to trip when the average confidence level is less than a threshold.

Appendix C: HardFiber System and MU320 Description

C.1 HardFiber System

The hardfiber system receives GOOSE control message and transmits SMV message. The format for the GOOSE message header follows IEC 61850-8-1, and illustrated in the following figure:

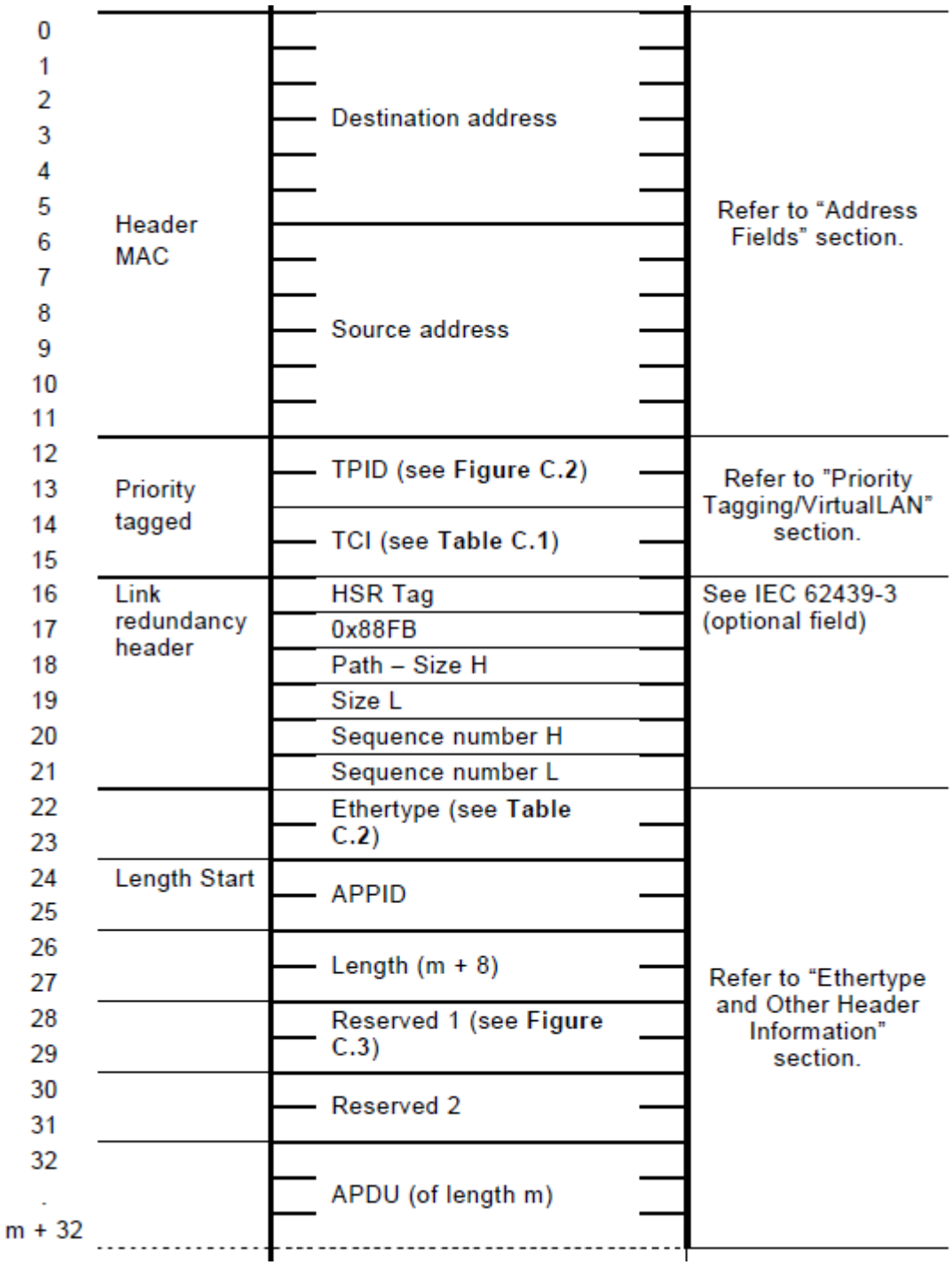

Each field of the data packet header is explained as follow. The HardFiber system does not check the source MAC address of the relay since this is dedicated communication. The destination MAC address should be multicast, broadcast or unicast, such address is set to

01-0C-CD-01-00-00 for multicast. The priority tag is used for poll frames, the TPID is 0x8100 and the TCI is 0x0000. The link redundancy header is omitted since it's only optional. The Ethertype for GOOSE is 0x88B8 while the Ethertype for SMV is 0x88BA. The APPID for GOOSE is 0x00 while the APPID for SMV is 0x01. The length of the remaining data is 277 bytes. The reserved field are filled with 0x0000.

The protocol also defined the APDU (GOOSEPDU) format as the following:

Abstract Buffer Format according to IEC61850-8-1		ASN.1 Tag for Data	ASN.1 Length	Comments
Attribute name	Attribute type			
goCBRef	Visible-string	0x80		Length determined by SCL configuration
timeAllowedToLive	INT32U	0x81	5	32 Bit Big Endian; unsigned; see **Table A.3**
datSet	Visible-string	0x82		Length determined by SCL configuration
goID	Visible-string	0x83		Length determined by SCL configuration
t	UtcTime	0x84	8	64 Bit timestamp as defined in ...
stNum	INT32U	0x85	5	32 Bit Big Endian; unsigned; see **Table A.3**
sqNum	INT32U	0x86	5	32 Bit Big Endian; unsigned; see **Table A.3**
Test	Boolean	0x87	4	8 Bit set to 0 FALSE; anything else = TRUE
confRev	INT32U	0x88	3	32 Bit Big Endian; unsigned; see **Table A.3**
ndsCom	Boolean	0x89	2	8 Bit set to 0 FALSE; anything else = TRUE
numDatSetEntries	INT32U	0x8a	20	32 Bit Big Endian; unsigned; see **Table A.3**

The gocbRef is the GOOSE control block reference, GE designed it to be a fixed length of 24 in octets. Any examples is "M81A99000000 /LLN0GOC" where the first part is the serial number for the device, LLN0 means the device's logical node 0, GO is short for GOOSE, and C stands for "C" dataset. The length of this field can either be determined by reading the substation configuration language (SCL) configuration file, or it can be determined since the GOOSE data packet uses ASN.1 Basic Encoding Rule so that it also records the tag of this field and length of this field. The timeAllowedtoLive is a 32 bits integer and the unit is in milliseconds. The dataset is 21 octets set. The goID (GOOSE ID) is optional so not implemented here. The field t is the UTC time of when this GOOSE

message is generated. The status number (stNum) and sequence number (sqNum) records the event sequence. The test field means if this GOOSE message is only for test purpose. The confRev is for configuration revision, any relay attempting to revise the format of the GOOSE. The ndsCom means if the GOOSE need commissioning and it's a Boolean. The numDatSetEntries means how many data sets the relay is expected to read after this field. In the GOOSE message transmitted by GE relay, the number of data sets is 17.

The allData field is user defined by GE. It contains 17 data in total. The first data is the sample number, it is a sample sequence number and must be incremented by the relay each successive sample. The value of sampNum sent here will be attached to the sample data returned to the relay by each Brick, allowing the correlation of samples from different Brick, and detection of missing sample data. All Bricks use this value, whether or not their serial numbers match a serNum attribute. The sample number starts with zero and increments by one each successive sample, and it rolls over from 2^{32}-1 to 0. The second and third data is the Brick's serial number and digital outputs. This two datum are repeated for 8 times (in together 17 data including the sample number). This design allows each relay to control eight Bricks by one GOOSE message. The digital outputs contain the commands from the relay. Upon receiving the GOOSE message, if the serial number attribute of a data object matches a Brick serial number appended with the core number, that core accepts the outputs attribute of the same data as its commands. This design allows the circuit breaker to receive tripping commands from the relay.

Member Offset	Data Set Member	Attribute type	Description

1	<LDName>/IBRK.U1.SmpNum	INT32	Sequence Number of Sample Data
2	<LDName>/IBRK.U1.serNum	STRING 13	Brick 1's serial number
3	<LDName>/IBRK.U1.outputs	Outputs	All Brick 1's commanded states for contact outputs, latching output, and shared outputs
4	<LDName>/IBRK.U2.serNum	STRING 13	
5	<LDName>/IBRK.U2.outputs	Outputs	
6	<LDName>/IBRK.U3.serNum	STRING 13	
7	<LDName>/IBRK.U3.outputs	Outputs	
8	<LDName>/IBRK.U4.serNum	STRING 13	
9	<LDName>/IBRK.U4.outputs	Outputs	
10	<LDName>/IBRK.U5.serNum	STRING 13	
11	<LDName>/IBRK.U5.outputs	Outputs	
12	<LDName>/IBRK.U6.serNum	STRING 13	
13	<LDName>/IBRK.U6.outputs	Outputs	
14	<LDName>/IBRK.U7.serNum	STRING 13	
15	<LDName>/IBRK.U7.outputs	Outputs	
16	<LDName>/IBRK.U8.serNum	STRING 13	
17	<LDName>/IBRK.U8.outputs	Outputs	

The sampled value message on the other hand, is defined by IEC 61850-9-2 for its header and self-defined by GE for its content, and the model of that data set can also be determined by reading the SCL configuration file. The header is defined as the following:

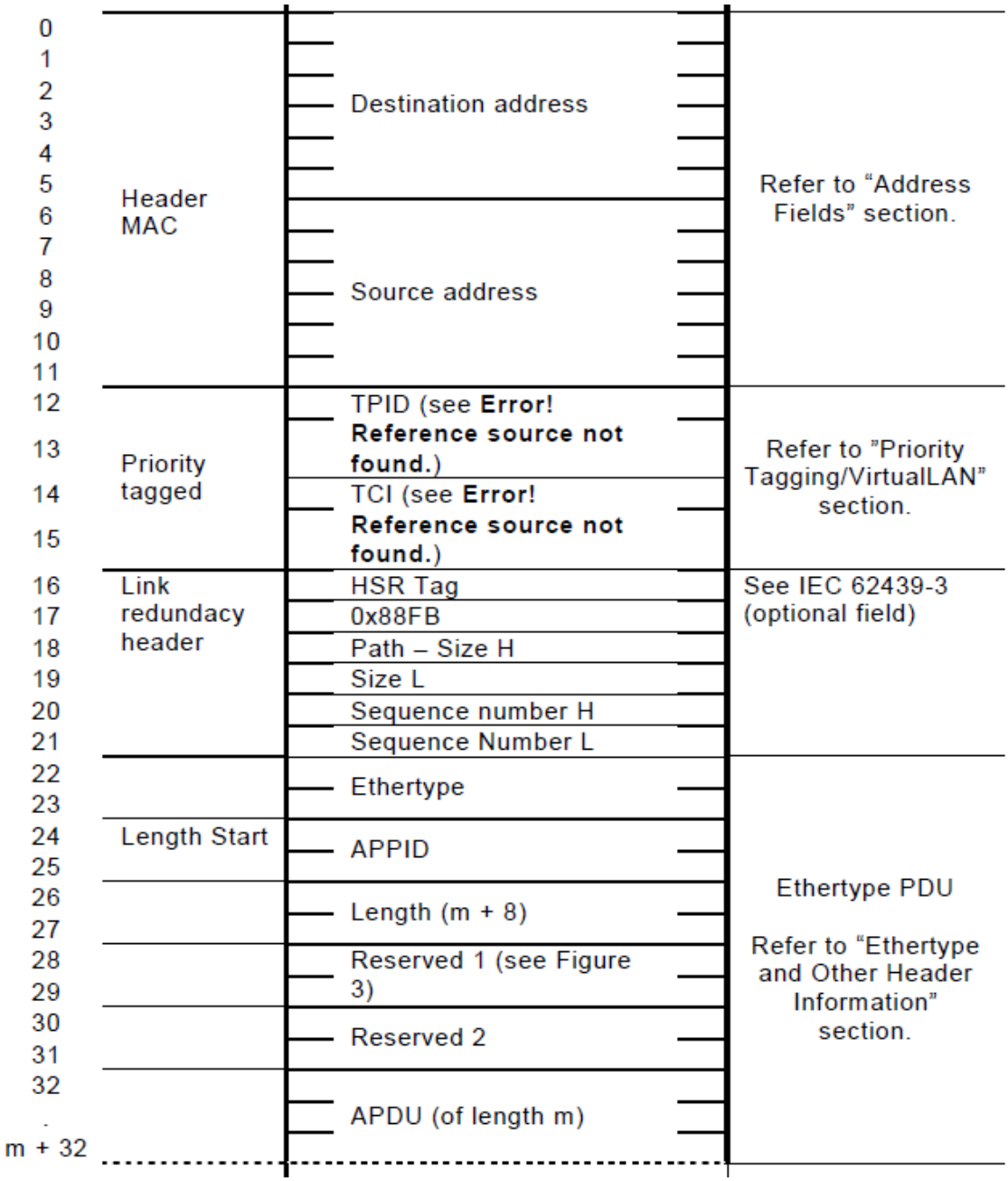

The multicast MAC destination address for SMV is 01-0C-CD-04-00-00, the source address is the Brick MAC address and it's unique for each Brick. The priority tag and link

redundancy header is omitted. The Ethertype for SMV is 0x88BA. The APPID is 0x01. The length field records how many bytes after this field. Both reserved 1 and 2 are 0x0000.

The protocol also defined the APDU (SAVPDU) format as the following:

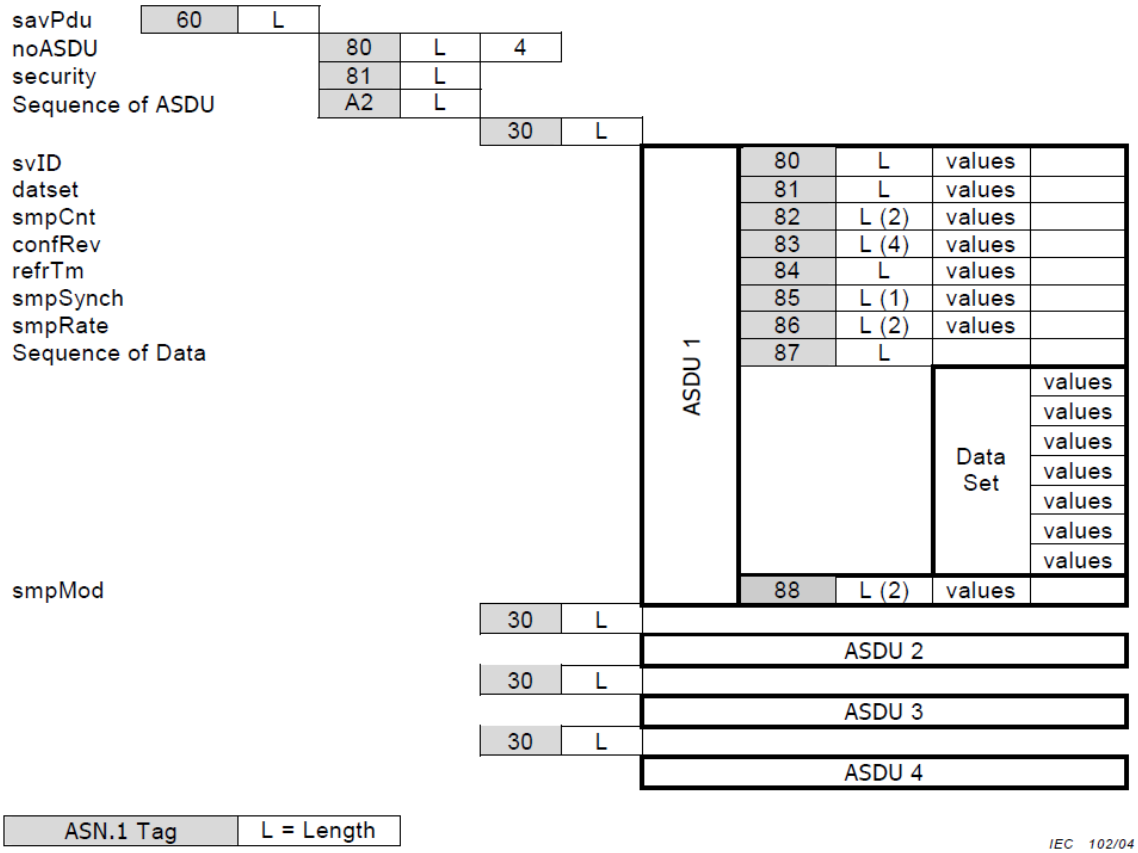

The noASDU means how many ASDUs are included in this packet, for the Brick this number is 9. The security field is optional and not included. The sequence of ASDU (seqASDU) contains the svID field, for the Brick an example would be "M84A090000753/F", which includes the serial number and core number. The dataset field is omitted. The smpCnt field is always 0 for the Brick. The configuration revision (confRev) means which version is this dataset. The refresh time is omitted. The smpSynch is always

false since it's not the Brick's responsibility to get synchronized. The smpRate field is omitted. The sequence of data (seqData) is then self-defined by GE.

The sequence of data contains the model field, which represents the product name, order code and product version, sample number field, which is the replicated sequence number of sampled data in the GOOSE message, and diagnostics field, which includes the information about the sync error, loss of supply, transceiver troubleshooting, etc. Also the data set contains the analog input that is need for the DSE based protection, digital input, contact inputs, etc. See the table that follows:

Member Offset	Data Set Member	Attribute type	Description
1	<LDName>/IBRK.U.analogs.ac1	INT32	AC1 – Ia
2	<LDName>/IBRK.U.analogs.ac2	INT32	AC2 – Ib
3	<LDName>/IBRK.U.analogs.ac3	INT32	AC3 – Ic
4	<LDName>/IBRK.U.analogs.ac4	INT32	AC4 – Ix
5	<LDName>/IBRK.U.analogs.ac5	INT32	AC5 – Va
6	<LDName>/IBRK.U.analogs.ac6	INT32	AC6 – Vb
7	<LDName>/IBRK.U.analogs.ac7	INT32	AC7 – Vc
8	<LDName>/IBRK.U.analogs.ac8	INT32	AC8 – Vx
9	<LDName>/IBRK.U.analogs.dc1	INT32	DC1
10	<LDName>/IBRK.U.analogs.dc2	INT32	DC2
11	<LDName>/IBRK.U.analogs.dc3	INT32	DC3
12	<LDName>/IBRK.U.analogs.contactinputs	ContactInputs	
13	<LDName>/IBRK.U.analogs.sharedinputs	SharedInputs	

14	<LDName>/IBRK.U.analogs.outputMonitors	OutputMonitors	
15	<LDName>/IBRK.U.analogs.model	STRING35	Product name
16	<LDName>/IBRK.U.analogs.SmpNum	INT32U	Sequence number
17	<LDName>/IBRK.U.analogs.diagnostics	Diagnostics	

The ICD file for the Brick is also attached below.

```
<?xml version="1.0" encoding="UTF-8" ?>
<!-- Created by GE Multilin Mon Jun 30, 2008 -->
<SCL xmlns="http://www.iec.ch/61850/2003/SCL"
xmlns:xsi="http://www.w3.org/2001/XMLSchema-instance"
xsi:schemaLocation="http://www.iec.ch/61850/2003/SCL SCL.xsd">
<Header id="Brick" version="5.601" revision="1" toolID="ICDGenerator"
nameStructure="IEDName"/>
<Communication>
<SubNetwork name="NONE">
<ConnectedAP iedName="IEDName" apName="P1">
<Address>
<P type="IP" xsi:type="tP_IP">192.168.37.199</P>
<P type="IP-SUBNET" xsi:type="tP_IP-SUBNET">255.255.255.0</P>
<P type="IP-GATEWAY" xsi:type="tP_IP-GATEWAY">0.0.0.0</P>
<P type="S-Profile">1</P>
</Address>
<SMV ldInst="LDInst" cbName="MSVCB01">
<Address>
<P type="MAC-Address" xsi:type="tP_MAC-Address">
01-0C-CD-04-00-00</P>
<P type="APPID" xsi:type="tP_APPID">0000</P>
<P type="VLAN-ID" xsi:type="tP_VLAN-ID">007</P>
<P type="VLAN-PRIORITY" xsi:type="tP_VLAN-PRIORITY">0</P>
</Address>
</SMV>
        <SMV ldInst="LDInst" cbName="MSVCB02">

<Address>
<P type="MAC-Address" xsi:type="tP_MAC-Address">
01-0C-CD-04-00-00</P>
<P type="APPID" xsi:type="tP_APPID">0000</P>
<P type="VLAN-ID" xsi:type="tP_VLAN-ID">007</P>
<P type="VLAN-PRIORITY" xsi:type="tP_VLAN-PRIORITY">0</P>
</Address>
</SMV>
</ConnectedAP>
</SubNetwork>
</Communication>
<IED type="GE Brick Merging Unit" configVersion="1.0" desc="Brick"
name="IEDName" manufacturer="GE Multilin">
<Services>
<ConfLNs fixPrefix="true" fixLnInst="true"/>
<ConfDataSet max="2" maxAttributes="14"/>
<GOOSE max="0"/>
<GSESettings cbName="Fix" appID="Dyn"/>
<SMVSettings cbName="Fix" datSet="Fix" svID="Fix" optFields="Fix"
```

```
smpRate="Fix">
<SmpRate>128</SmpRate>
<SmpRate>16</SmpRate>
</SMVSettings>
</Services>
<AccessPoint name="P1">
<Server>
<Authentication none="true"/>
<LDevice inst="LDInst">
<LN0 lnType="IEDName/LDInst/LLN0_0" lnClass="LLN0" inst="">
<DataSet name="F" desc="Fast Data Set of Brick's Sampled Values
Transmitted via Multicast SV Service">
<FCDA ldInst="LDInst" prefix="" lnInst="1" lnClass="IBRK"
fc="MX" doName="U" daName="analogs.ac1"/>
<FCDA ldInst="LDInst" prefix="" lnInst="1" lnClass="IBRK"
fc="MX" doName="U" daName="analogs.ac2"/>
<FCDA ldInst="LDInst" prefix="" lnInst="1" lnClass="IBRK"
fc="MX" doName="U" daName="analogs.ac3"/>
<FCDA ldInst="LDInst" prefix="" lnInst="1" lnClass="IBRK"
fc="MX" doName="U" daName="analogs.ac4"/>
<FCDA ldInst="LDInst" prefix="" lnInst="1" lnClass="IBRK"
fc="MX" doName="U" daName="analogs.ac5"/>
<FCDA ldInst="LDInst" prefix="" lnInst="1" lnClass="IBRK"
fc="MX" doName="U" daName="analogs.ac6"/>
<FCDA ldInst="LDInst" prefix="" lnInst="1" lnClass="IBRK"
fc="MX" doName="U" daName="analogs.ac7"/>
<FCDA ldInst="LDInst" prefix="" lnInst="1" lnClass="IBRK"
fc="MX" doName="U" daName="analogs.ac8"/>
<FCDA ldInst="LDInst" prefix="" lnInst="1" lnClass="IBRK"
fc="MX" doName="U" daName="analogs.dc1"/>
<FCDA ldInst="LDInst" prefix="" lnInst="1" lnClass="IBRK"
fc="MX" doName="U" daName="analogs.dc2"/>
<FCDA ldInst="LDInst" prefix="" lnInst="1" lnClass="IBRK"
fc="MX" doName="U" daName="analogs.dc3"/>
<FCDA ldInst="LDInst" prefix="" lnInst="1" lnClass="IBRK"
fc="ST" doName="U" daName="contactInputs"/>
<FCDA ldInst="LDInst" prefix="" lnInst="1" lnClass="IBRK"
fc="ST" doName="U" daName="sharedInputs"/>
<FCDA ldInst="LDInst" prefix="" lnInst="1" lnClass="IBRK"
fc="ST" doName="U" daName="outputMonitors"/>
</DataSet>
<DataSet name="S" desc="Slow Data Set of Brick's Sampled Values
Transmitted via Multicast SV Service">
<FCDA ldInst="LDInst" prefix="" lnInst="1" lnClass="IBRK"
        fc="CF" doName="U" daName="model"/>

<FCDA ldInst="LDInst" prefix="" lnInst="1" lnClass="IBRK"
fc="ST" doName="U" daName="smpNum"/>
<FCDA ldInst="LDInst" prefix="" lnInst="1" lnClass="IBRK"
fc="ST" doName="U" daName="diagnostics"/>
</DataSet>
<SampledValueControl name="MSVCB01" smvID="0022040080141/F"
smpRate="128" nofASDU="8" confRev="1"
datSet="F">
<SmvOpts refreshTime="false" sampleSynchronized="true"
sampleRate="false" security="false" dataRef="false"/>
</SampledValueControl>
<SampledValueControl name="MSVCB02" smvID="0022040080141/S"
smpRate="16" nofASDU="1" confRev="1"
datSet="S">
<SmvOpts refreshTime="false" sampleSynchronized="true"
sampleRate="false" security="false" dataRef="false"/>
</SampledValueControl>
</LN0>
<LN lnType="IEDName/LDInst/LPHD_0" lnClass="LPHD" inst="1"/>
<LN lnType="IEDName/LDInst/IBRK_0" lnClass="IBRK" inst="1"
prefix=""/>
</LDevice>
</Server>
</AccessPoint>
```

```
</IED>
<DataTypeTemplates>
<LNodeType id="IEDName/LDInst/LLN0_0" lnClass="LLN0">
<DO name="Mod" type="INC_0"/>
<DO name="Beh" type="INS_0"/>
<DO name="Health" type="INS_1"/>
<DO name="NamPlt" type="LPL_0"/>
</LNodeType>
<LNodeType id="IEDName/LDInst/LPHD_0" lnClass="LPHD">
<DO name="PhyHealth" type="INS_1" />
<DO name="Proxy" type="SPS_1"/>
<DO name="PhyNam" type="DPL_0"/>
</LNodeType>
<LNodeType id="IEDName/LDInst/IBRK_0" lnClass="IBRK">
<DO name="Mod" type="INC_0"/>
<DO name="Beh" type="INS_0"/>
<DO name="Health" type="INS_1"/>
<DO name="NamPlt" type="LPL_0"/>
<DO name="U" type="BRICK_0"/>
</LNodeType>
<DOType id="INC_0" cdc="INC">
<DA name="stVal" fc="ST" dchg="true" bType="Enum" type="Mod"/>
<DA name="q" fc="ST" qchg="true" bType="Quality"/>
<DA name="t" fc="ST" bType="Timestamp"/>
<DA name="ctlModel" fc="CF" bType="Enum" type="ctlModel"/>
</DOType>
<DOType id="INS_0" cdc="INS">
<DA name="stVal" fc="ST" bType="Enum" type="Beh"/>
<DA name="q" fc="ST" bType="Quality"/>
<DA name="t" fc="ST" bType="Timestamp"/>
</DOType>
<DOType id="INS_1" cdc="INS">
<DA name="stVal" fc="ST" bType="Enum" type="Health"/>
<DA name="q" fc="ST" bType="Quality"/>
<DA name="t" fc="ST" bType="Timestamp"/>
</DOType>
<DOType id="LPL_0" cdc="LPL">
<DA name="vendor" fc="DC" bType="VisString255"/>
<DA name="swRev" fc="DC" bType="VisString255"/>
<DA name="d" fc="DC" bType="VisString255"/>
        <DA name="configRev" fc="DC" bType="VisString255"/>

</DOType>
<DOType id="DPL_0" cdc="DPL">
<DA name="vendor" fc="DC" bType="VisString255">
<Val>GE Multilin</Val>
</DA>
<DA name="swRev" fc="DC" bType="VisString255">
<Val>5.601</Val>
</DA>
<DA name="serNum" fc="DC" bType="VisString255"/>
<DA name="model" fc="DC" bType="VisString255"/>
<DA name="location" fc="DC" bType="VisString255"/>
</DOType>
<DOType id="SPS_1" cdc="SPS">
<DA name="stVal" fc="ST" dchg="true" bType="BOOLEAN"/>
<DA name="q" fc="ST" qchg="true" bType="Quality"/>
<DA name="t" fc="ST" bType="Timestamp"/>
</DOType>
<DOType id="BRICK_0" cdc="BRICK">
<DA name="smpNum" fc="ST" bType="INT32U" dchg="true"/>
<DA name="model" fc="CF" bType="VisString35"/>
<DA name="serNum" fc="CF" bType="VisString13"/>
<DA name="outputs" fc="CO" bType="BitString32" dchg="true"/>
<DA name="analogs" fc="MX" bType="Struct" type="Analogs_0"/>
<DA name="contactInputs" fc="ST" bType="BitString32" dchg="true"/>
<DA name="sharedInputs" fc="ST" bType="BitString32" dchg="true"/>
<DA name="outputMonitors" fc="ST" bType="BitString32" dchg="true"/>
<DA name="diagnostics" fc="ST" bType="Struct" type="Diagnostics_0"/>
<DA name="lnNs" fc="EX" bType="VisString255"/>
```

```
</DOType>
<DAType id="Analogs_0">
<BDA name="ac1" bType="INT32U"/>
<BDA name="ac2" bType="INT32U"/>
<BDA name="ac3" bType="INT32U"/>
<BDA name="ac4" bType="INT32U"/>
<BDA name="ac5" bType="INT32U"/>
<BDA name="ac6" bType="INT32U"/>
<BDA name="ac7" bType="INT32U"/>
<BDA name="ac8" bType="INT32U"/>
<BDA name="dc1" bType="INT32U"/>
<BDA name="dc2" bType="INT32U"/>
<BDA name="dc3" bType="INT32U"/>
</DAType>
<DAType id="Diagnostics_0">
<BDA name="diagnosticFlags" bType="BitString32"/>
<BDA name="adcTemp" bType="INT16"/>
<BDA name="transceiverTemp" bType="INT16"/>
<BDA name="transceiverVolts" bType="INT16"/>
<BDA name="transceiverCurrent" bType="INT16"/>
<BDA name="transceiverTxPower" bType="INT16"/>
<BDA name="transceiverRxPower" bType="INT16"/>
</DAType>
<EnumType id="Mod">
<EnumVal ord="1">on</EnumVal>
<EnumVal ord="2">blocked</EnumVal>
<EnumVal ord="3">test</EnumVal>
<EnumVal ord="4">test/blocked</EnumVal>
<EnumVal ord="5">off</EnumVal>
</EnumType>
<EnumType id="ctlModel">
<EnumVal ord="0">status-only</EnumVal>
<EnumVal ord="1">direct-with-normal-security</EnumVal>
<EnumVal ord="2">sbo-with-normal-security</EnumVal>
<EnumVal ord="3">direct-with-enhanced-security</EnumVal>
<EnumVal ord="4">sbo-with-enhanced-security</EnumVal>
        </EnumType>

<EnumType id="Beh">
<EnumVal ord="1">on</EnumVal>
<EnumVal ord="2">blocked</EnumVal>
<EnumVal ord="3">test</EnumVal>
<EnumVal ord="4">test/blocked</EnumVal>
<EnumVal ord="5">off</EnumVal>
</EnumType>
<EnumType id="Health">
<EnumVal ord="1">Ok</EnumVal>
<EnumVal ord="2">Warning</EnumVal>
<EnumVal ord="3">Alarm</EnumVal>
</EnumType>
</DataTypeTemplates>
        </SCL>
```

C.2 MU320

The MU320 and Siemens 7SC805 follows the IEC 61850-9-2 light edition, which defines explicitly the data set members that would be transmitted through sampled value messages, see below:

Member Offset	Data Set Member	Attribute type	Description
1	InnATCTR1.Amp.instMag.i	INT32	Ia value
2	InnATCTR1.Amp.instMag.q	INT32	Ia quality
3	InnBTCTR2.Amp.instMag.i	INT32	Ib value
4	InnBTCTR2.Amp.instMag.q	INT32	Ib quality
5	InnCTCTR3.Amp.instMag.i	INT32	Ic value
6	InnCTCTR3.Amp.instMag.q	INT32	Ic quality
7	InnNmTCTR4.Amp.instMag.i	INT32	In value
8	InnNmTCTR4.Amp.instMag.q	INT32	In quality
9	UnnATVTR1.Vol.instMag.i	INT32	Va value
10	UnnATVTR1.Vol.instMag.q	INT32	Va quality
11	UnnBTVTR2.Vol.instMag.i	INT32	Vb value
12	UnnBTVTR2.Vol.instMag.q	INT32	Vb quality
13	UnnCTVTR3.Vol.instMag.i	INT32	Vc value
14	UnnCTVTR3.Vol.instMag.q	INT32	Vc quality
15	UnnNmTVTR4.Vol.instMag.i	INT32	Vn value
16	UnnNmTVTR4.Vol.instMag.q	INT32	Vn quality

Same as the naming convention from the data set member for the Brick, the name for each data object goes with Logical Node.Data Object.Data Attribute. Different from the data set member defined for the Brick, the light edition defined both instantaneous value and quality for each measurement.

The ICD file for the MU320 is as follow:

```
<?xml version="1.0" encoding="UTF-8"?>
<!-- edited with XMLSPY v5 rel. 4 U (http://www.xmlspy.com) by Christoph Brunner (ABB Switzerland Ltd) -->
<SCL xmlns="http://www.iec.ch/61850/2003/SCL" xmlns:xsi="http://www.w3.org/2001/XMLSchema-instance"
xsi:schemaLocation="http://www.iec.ch/61850/2003/SCL
SCL.xsd">
    <Header id="9-2LE-Spec" nameStructure="FuncName" version="0.7" revision="1"/>
    <Substation name="">
        <VoltageLevel name="">
            <Bay name="">
                <ConductingEquipment name="Inn" type="CTR">
                    <SubEquipment name="A" phase="A">
                        <LNode lnClass="TCTR" lnInst="1"/>
                    </SubEquipment>
                    <SubEquipment name="B" phase="B">
                        <LNode lnClass="TCTR" lnInst="2"/>
                    </SubEquipment>
                    <SubEquipment name="C" phase="C">
                        <LNode lnClass="TCTR" lnInst="3"/>
                    </SubEquipment>
                    <SubEquipment name="N" phase="N">
                        <LNode lnClass="TCTR" lnInst="4"/>
                    </SubEquipment>
                </ConductingEquipment>
                <ConductingEquipment name="Unn" type="VTR">
                    <SubEquipment name="A" phase="A">
                        <LNode lnClass="TVTR" lnInst="1"/>
                    </SubEquipment>
                    <SubEquipment name="B" phase="B">
                        <LNode lnClass="TVTR" lnInst="2"/>
                    </SubEquipment>
                    <SubEquipment name="C" phase="C">
                        <LNode lnClass="TVTR" lnInst="3"/>
                    </SubEquipment>
                    <SubEquipment name="N" phase="N">
                        <LNode lnClass="TVTR" lnInst="4"/>
                    </SubEquipment>
                </ConductingEquipment>
            </Bay>
        </VoltageLevel>
    </Substation>

    <IED name="TEMPLATE">
        <AccessPoint name="">
            <Server>
                <Authentication/>
                <LDevice inst="MUnn">
                    <LN0 lnType="9-2LELLN0" lnClass="LLN0" inst="">
                        <DataSet name="PhsMeas1">
                            <FCDA lnClass="TCTR" ldInst="1" fc="MX" doName="Amp"/>
                            <FCDA lnClass="TCTR" ldInst="2" fc="MX" doName="Amp"/>
                            <FCDA lnClass="TCTR" ldInst="3" fc="MX" doName="Amp"/>
                            <FCDA lnClass="TCTR" ldInst="4" fc="MX" doName="Amp"/>
                            <FCDA lnClass="TVTR" ldInst="1" fc="MX" doName="Vol"/>
                            <FCDA lnClass="TVTR" ldInst="2" fc="MX" doName="Vol"/>
                            <FCDA lnClass="TVTR" ldInst="3" fc="MX" doName="Vol"/>
                            <FCDA lnClass="TVTR" ldInst="4" fc="MX" doName="Vol"/>
                        </DataSet>
                        <SampledValueControl name="MSVCB01" datSet="PhsMeas1" smvID="xxxxMUnn01"
smpRate="80" nofASDU="1" confRev="1">
```

```
                        <SmvOpts    refreshTime="false"    sampleSynchronized="true"    sampleRate="false"
security="false" dataRef="false"/>
                    </SampledValueControl>
                </LN0>
                <LN lnType="9-2LETCTR" lnClass="TCTR" inst="1"/>
                <LN lnType="9-2LETCTR" lnClass="TCTR" inst="2"/>
                <LN lnType="9-2LETCTR" lnClass="TCTR" inst="3"/>
                <LN lnType="9-2LETCTR" lnClass="TCTR" inst="4"/>
                <LN lnType="9-2LETVTR" lnClass="TVTR" inst="1"/>
                <LN lnType="9-2LETVTR" lnClass="TVTR" inst="2"/>
                <LN lnType="9-2LETVTR" lnClass="TVTR" inst="3"/>
                <LN lnType="9-2LETVTR" lnClass="TVTR" inst="4"/>
            </LDevice>
        </Server>
    </AccessPoint>
</IED>
<DataTypeTemplates>
    <LNodeType id="9-2LELLN0" lnClass="LLN0">
        <DO name="Mod" type="9-2LEINC"/>
    </LNodeType>
    <LNodeType id="9-2LETCTR" lnClass="TCTR">
        <DO name="Amp" type="9-2LESAVAmp"/>
    </LNodeType>
    <LNodeType id="9-2LETVTR" lnClass="TVTR">
        <DO name="Vol" type="9-2LESAVVol"/>
    </LNodeType>
    <DOType id="9-2LESAVAmp" cdc="SAV">
        <DA name="instMag" bType="Struct" type="9-2LEAV" fc="MX"/>
        <DA name="q" bType="Quality" fc="MX"/>
        <DA name="sVC" bType="Struct" type="9-2LEsVCAmp" fc="CF"/>
    </DOType>
    <DOType id="9-2LESAVVol" cdc="SAV">
        <DA name="instMag" bType="Struct" type="9-2LEAV" fc="MX"/>
        <DA name="q" bType="Quality" fc="MX"/>
        <DA name="sVC" bType="Struct" type="9-2LEsVCVol" fc="CF"/>
    </DOType>
    <DOType id="9-2LEINC" cdc="INC">
        <DA name="ctlVal" fc="CO" bType="INT32"/>
        <DA name="stVal" fc="ST" bType="INT32" dchg="true"/>
        <DA name="q" fc="ST" bType="Quality" dchg="true"/>


        <DA name="t" fc="ST" bType="Timestamp" dchg="true"/>
    </DOType>
    <DAType id="9-2LEAV">
        <BDA name="i" bType="INT32"/>
    </DAType>
    <DAType id="9-2LEsVCAmp">
        <BDA name="scaleFactor" bType="FLOAT32">
            <Val>0.001</Val>
        </BDA>
        <BDA name="offset" bType="FLOAT32">
            <Val>0</Val>
        </BDA>
    </DAType>
    <DAType id="9-2LEsVCVol">
        <BDA name="scaleFactor" bType="FLOAT32">
            <Val>0.01</Val>
        </BDA>
        <BDA name="offset" bType="FLOAT32">
            <Val>0</Val>
        </BDA>
    </DAType>
</DataTypeTemplates>
```

REFERENCES

[1] NERC, NERC Presidents Top Priority Issues for Bulk Power System Reliability, [Online]. Available at:

http://www.nerc.com/newsHeadlines%20DL/NERC%20President%20Top%20Priority%20BPS%20Reliability%20Issues%201-7-11.pdf

[2] NERC Planning Committee, Misoperations Report Prepared by: Protection System Misoperations Task Force, [Online]. Available: http://www.nerc.com/docs/pc/psmtf/PSMTF_Report.pdf

[3] NERC, Protection System Response to Power Swings, Prepared by System Protection and Control Subcommittee. [Online]. Available:

http://www.nerc.com/comm/PC/System%20Protection%20and%20Control%20Subcommittee%20SPCS%2020/SPCS%20Power%20Swing%20Report_Final_20131015.pdf

[4] PSRC, "Understanding Microprocessor-based Technology Applied to Relaying," *Report of Working Group I-01*. [Online]. Available:

http://www.pes-psrc.org/Reports/UNTAR-Ed2.pdf

[5] General Electric, L90 Instruction Manual, GEK-119616. [Online]. Available: https://www.gedigitalenergy.com/app/ViewFiles.aspx?prod=l90&type=3

[6] J. Blackburn, *Protective Relaying: Principles and Applications*, 3rd ed, CRC Press, 2006.

[7] K. Zimmerman, D. Costello, "Fundamentals and Improvements for Directional Relays", *37th Annual Western Protective Relay Conference*, 2010.

[8] Jeff Roberts and Armando Guzman, "Directional Element Design and Evaluation", *49th Annual Georgia Tech Protective Relaying Conference,* 1995.

[9] Line Protection Subcommittee of Power System Relay Committee WG D23 report, "Transmission Line Applications of Directional Ground Overcurrent Relays" [Online]. Available: http://www.pes-psrc.org/Reports

[10] Line Protection Subcommittee of Power System Relay Committee WG D3 report, "Considerations in Choosing Directional Polarizing Methods for Ground Overcurrent Elements in Line Protection Applications", [Online]. Available: http://www.pes-psrc.org/Reports/Apublications_new_format.htm

[11] Fernando Calero, Daqing Hou, "Practical Considerations for Single Pole Trip Line-Protection Schemes", *68th Annual Conference for Protective Relay Engineers, 2005*

[12] IEEE Power System Relaying Committee, “IEEE Guide for Protective Relay Applications to Transmission Lines,” 1999

[13] ABB, REL670 Technical Reference Manual version 1.2, [Online]. Available: https://library.e.abb.com/public/850dd24dbf264d2b9754a6e13ed0c4cd/1MRK506312-UEN_D_en_Technical_reference_manual__REL670_1.2.pdf

[14] Schweitzer Engineeirng Laboratories, SEL-321, [Online]. Available: https://www.selinc.com/SEL-321/

[15] General Electric, D60 Instruction Manual for 7.3x product version, GEK-119616. [Online]. Available: https://www.gedigitalenergy.com/app/ViewFiles.aspx?prod=d60&type=3

[16] J. Andrichak, George Alexander, "Distance Relay Fundamentals", General Electric, [Online]. Available: https://www.gedigitalenergy.com/smartgrid/Mar07/article7.pdf

[17] Hector Altuve, Joseph Mooney, and George Alexdander, "Advances in Series-Compensated Line Protection", *2009 63rd Annual Georgia Tech Protective Relaying Conference*, 2009

[18] Demetrios Tziouvaras, Hector Altuve, and Fernando Calero, "Protecting Mutually Coupled Transmission Lines: Challenges and Solutions", *2014 67th Annual Conference for Protective Relay Engineers*, 2014

[19] NERC, System Protection and Control Task Force, "The Complexity of Protecting Three-Terminal Transmission Lines", [Online]. Available: http://www.nerc.com/comm/PC/System%20Protection%20and%20Control%20Subcommittee%20SPCS%20DL/SPCTF-3TerminalLines091906.pdf

[20] Gerhard Ziegler, *Numerical Distance Protection: Principles and A pplications*, Erlangen, Germany: Publicis Corporate Publishing, 2006

[21] Andre Filomena, Rodrigo Salim, Mariana Resener, and Arturo Bretas, “Ground Distance Relaying With Fault-Resistance Compensation for Unbalanced Systems”, *IEEE Trans. Power Delivery*, vol. 23, no.3, pp.1319-1326, Jul. 2008

[22] Hector Altuve, Gabriel Benmouyal, Jeff Roberts, and Demetrios Tziouvaras, " Transmission Line Differential Protection with an Advanced Characteristic ", *2004 8th IEE International Conference on Developments in Power System Protection*, 2004

[23] Stanley Horowitz, Arun Phadke, *Power System Relaying*, 2nd ed, Research Studies Press, 1995

[24] SEL, Transmission Line Protection Review of Communications-Assisted Tripping Schemes, [Online]. Available:

https://selinc.cachefly.net/GHRC/1_Tuesday/Transmission/2539_TransmissionLineProt_DC_20120709.pdf

[25] Demetrios Tziouvaras, Jeff Roberts, Gabriel Benmouyal, and Daqing Hou, "The Effect of Conventional Instrument Transformer Transients on Numerical Relay Elements", *28th Annual Western Protective Relay Conference*, Spokane, WA, 2001

[26] Demetrios Tziouvaras, Hector Altuve, Gabriel Benmouyal, and Jeff Roberts, "Line Differential Protection with an Enhanced Characteristic", *63th Annual Conference for Protective Relay Engineers*, 2010

[27] Bogdan Kasztenny, Ilia Voloh, and Eric Udren, "Rebirth of the Phase Comparison Line Protection Principle", *59th Annual Conference for Protective Relay Engineers*, 2006

[28] Leonard Ernst, Walter Hinman, David Quam, and James Thorp, "Charge Comparison Protection of Transmission Lines - Relaying Concepts", *IEEE Trans. Power Delivery*, vol. 7, no.4, pp.1834-1852, Oct. 1992

[29] ABB, RED670 Technical Reference Manual version 1.2, [Online]. Available: https://library.e.abb.com/public/d28f6dc6b4683e96c1257b0c00445ad7/1MRK505222-UEN_C_en_Technical_reference_manual__RED670_1.2.pdf

[30] Alstom Grid, MiCOM Alstom P54x ver41_51K Manual GB, [Online]. Available: ftp://ftp.alstom.com/Alstom_Manuals/P54x_EN_M_K74.pdf

[31] Swhweitzer Engineeirng Laboratories, SEL-387L, [Online]. Available: https://www.selinc.com/sel-387l/

[32] Siemens, 7SD610x Manual A6 V4.70, [Online]. Available: http://w3.siemens.com/smartgrid/global/en/products-systems-solutions/protection/line-differential/pages/7sd61.aspx

[33] Hank Miller, John Burger, Normann Fischer, and Bogdan Kasztenny, "Modern Line Current Differential Protection Solutions", *2010 63rd Annual Conference for Protective Relay Engineers,* 2010.

[34] IEEE Instrumentation and Measurement Society, "IEEE Standard for a Precision Clock Synchronization Protocol for Networked Measurement and Control Systems", 2008.

[35] Roff Isermann, "Process Fault Detection based on Modeling and Estimation Methods—A Survey," *Automatica*, Vol. 20, no. 4, pp. 387-404, 1984.

[36] A. S. Willsky, "A Survey of Design Methods for Failure Detection in Dynamic Systems," *Automatica*, Vol. 12, pp 601-611, 1976.

[37] R. V. Beard: Failure Accomodation in Linear Systems Through Self-Reorganization, Rept. MVT-71-1, Man Vehicle Laboratory, Cambridge, Mass., Feb, 1971

[38] H. L. Jones, Failure Detection in linear systems, Ph.D Thesis, Department of Aeronautics and Astronautics, M.I.T, Cambridge, Mass., Sept, 1973

[39] A. S. Willsky, "Failure detection in dynamic systems," *AGARD*, no.109, 1980

[40] A. S. Willsky, H. L. Jones, "A generalized likelihood ratio approach to state estimation in linear systems subject to abrupt changes," *Proc. IEEE Conf. on Decision and Control*, Phoenix, Arizone, 1974.

[41] I. Hwang, S. Kim, "A Survey of Fault Detection, Isolation, and Reconfiguration Methods", *IEEE Trans. Control Systems Technology*, vol. 18, no. 3, pp 636-653, May. 2010.

[42] J. E. White and J. L. Speyer, "Detection filter design: Spectral theory and algorithm," *IEEE Trans. Autom. Control*, vol. 32, no. 7, pp. 593–603, Jul. 1987.

[43] J. H. Park, Y. Halevi, and G. Rizzoni, "A new interpretation of the fault-detection filter 1: Closed-form algorithm," *Int. J. Control*, vol. 60, no. 5, pp. 767–787, 1994.

[44] J. H. Park, Y. Halevi, and G. Rizzoni, "A new interpretation of the fault-detection filter 2: The optimal detection filter," *Int. J. Control*, vol. 60, no. 5, pp. 767–787, 1994.

[45] K. Watanabe and D. M. Himmelblau, "Instrument fault detection insystem with uncertainties," *Int. J. Syst. Sci.*, vol. 13, no. 2, pp. 137–158, 1982.

[46] Stoustrup and Niemann, "Fault estimation—A standard problem approach," *Int. J. Robust Nonlinear Control*, vol. 12, pp. 649–673, 2002.

[47] A.P. Meliopoulos., George J. Cokkinides, Zhenyu Tan, Sungyun Choi, Yonghee Lee, Paul Myrda. "Setting-less protection: Feasibility study.", *2013 46th Hawaii International Conference on System Sciences (HICSS)*, pp. 2345-2353. IEEE, 2013

[48] A.P. Meliopoulos. "Setting-less Protection: Laboratory Testing", June 2014. [Online]. Available: http://www.pserc.wisc.edu/documents

[49] A. P. Meliopoulos, G. J. Cokkinides, and G. Stefopoulos, "Quadratic Integration Method," in *Proceedings of the International Power System Transients Conference*, Montreal, Jun. 2005

[50] A. P. Meliopoulos, *Power System Grounding and Transients*, Marcel Dekker, 1988.

[51] R. E. Kalman, "A New Approach to Linear Filtering and Prediction Problems", *Journal of Basic Engineering*, vol. 82, no. 1, pp. 35-45, March, 1960

[52] M. Bockarjova, G. Andersson, “Transmission Line Conductor Temperature Impact on State Estimation Accuracy”, *Power Tech, IEEE Lausanne,* 2007

[53] IEC 61850 Suite.

[54] I. Hwang, H. Balakrishnan, and C. Tomlin. "State estimation for hybrid systems: applications to aircraft tracking." IEE Proceedings Control Theory and Applications 153.5 (2006): 556.

[55] A. Meliopoulos, G. Cokkinides, “Power System Relaying, an Introduction”, copyright 1996-2014

[56] A. P. Meliopoulos; G. J. Cokkinides; P. Myrda; Y. Liu; R. Fan; L. Sun; R. Huang; Z. Tan, "Dynamic State Estimation Based Protection: Status and Promise," in IEEE Transactions on Power Delivery, vol.PP, no.99 (accepted)